Investigation of pharmacokinetics and thioether metabolites to assess bioactivation and toxicity of drugs

Thesis submitted in accordance with the requirements of the University of Liverpool for the degree of Doctor of Philosophy

By

Hayley Margaret Webb

June 2011

DECLARATION

This thesis is the result of my own work. The material contained within this thesis has not been presented, nor is it currently being presented, either wholly or in part for any degree or other qualification

Hayley Margaret Webb

This research was carried out in the Department of Molecular and Clinical Pharmacology, The University of Liverpool.

CONTENTS

ACKNOWLEDGEMENTS

I would like to thank my PhD supervisors Dr. Dominic Williams, Dr. Iain Gardner and Prof. Kevin Park for their continual advice, support and encouragement throughout the PhD and beyond.

I would like to express my thanks to the BBSRC and Pfizer for their sponsorship. For their constant help and friendliness during my time spent at Pfizer, I would like to say a massive thank you to Katie, JD, Paul, Russell and Mark. Thanks to Dr. James Maggs for his MS advice and assistance.

A huge thank you goes to all the PhD students, post-docs and staff within the drug safety research group at the University of Liverpool, who have made working in the department a pleasure. I would like to say a special thank you to Sophie Regan who has given me (and everyone else) so much of her time, help, advice and friendship.

Thank you to my amazing friends, Craig, Swale and Rach for providing perspective, understanding and a whole lot of laughs; they have truly kept me sane. A massive thank you goes to my family for their love and encouragement during my PhD. I would especially like to thank Mum and Dave for their love, friendship and support. Finally, I would like to thank Christopher, for providing unlimited motivation, encouragement and love throughout the PhD and always.

PUBLICATIONS

Papers

HM Webb, J Duckworth, P Turnpenny, M Savage, I Gardner, D Smith, BK Park and DP Williams. Influence of chemical structure on mechanisms of toxicity: Studies with furosemide and its thiophene analogue, Drug Metabolism and Disposition. *Manuscript in preparation*

Book Chapters

HM Webb, S Regan, DJ Antoine, N Lane, R J Walsh, A Srivastava, P Starkey-Lewis, C Benson, DP Williams, H Laverty, C Goldring and BK Park. Encyclopedia of Drug Metabolism and Interactions Volume III, Chapter 9: Drug Bioactivation and Oxidative Stress. *Wiley-Blackwell, publish date; 15 Jun 2012.*

Abstracts

HM Webb, J Duckworth, P Turnpenny, I Gardner, D Smith; BK Park; DP Williams. Pharmacokinetic investigation into the mechanism of toxicity of Furosemide and its thiophene analogue. (2009). BTS Annual Congress. *Toxicology* 262 (1), pg. 23-24.

ABBREVIATIONS

α	alpha
ABT	1-aminobenzotriazole
ACN	acetonitrile
ADME	absorption, disposition, metabolism and excretion
ADR	adverse drug reaction
ALT	alanine amino transferase
AP	alkaline phosphatase
APAP	acetaminophen; paracetamol
AST	aspartate amino transferase
AUC	area under a curve
BMI	body mass index
Bq	becquerel
BSEP	bile salt export pump
BSP	sulfobromophthalein
°C	degrees centigrade
^{14}C	carbon 14
C_{24}	drug concentration at 24 hours post dose
Ci	curie
Cl	clearance
Cl_u	unbound clearance
C_{max}	maximum drug concentration
CO_2	carbon dioxide
CRM	chemically reactive metabolite
CTRL	control
CYP	cytochrome P450
Da	dalton
DCNP	2, 6-dichloro-4-nitrophenol
dH_2O	distilled water
DILI	drug induced liver injury
DMSO	dimethyl sulphoxide
DNA	deoxyribonucleic acid
DTNB	5,5'-dithio-bis(2-nitrobenzoicacid)
ELISA	enzyme-linked immunosorbent assay
EC_{50}	half maximal effective concentration
EtOH	ethanol
EDTA	ethylenediaminetetraacetic acid
F	bioavailability
FA	formic acid
FDA	food and drug administration
FMO	flavin monoxygenase
FS	furosemide

γ	gamma
γ-GCL	gamma-glutamyl cysteinly ligase
GGT	gamma-glutamyl transpeptidase
GSH	glutathione
GSSG	oxidised glutathione
GST	glutathione S-transferase
H&E	hematoxylin and eosin
H_2O	water
H_2O_2	hydrogen peroxide
HCl	hydrochloric acid
HEPES	4-(2-hydroxyethyl)-1-piperazineethansulphonic acid
HIV	human immunodeficiency virus
HLA	human leukocyte antigen
HLB	hydrophilic-lipophilic-balanced
HLM	human liver microsomes
HMGB1	high mobility group box 1 protein
HPLC	high performance liquid chromatography
i.m.	intramuscular
i.p.	intraperitoneal
i.v.	intravenous
IC_{50}	half maximal inhibitory concentration
IFNγ	
IL	interleukin
K18	keratin 18
LC	liquid chromatography
LC-MS/MS	liquid chromatography tandem mass spectrometry
LPB	liver protein binding
m/z	mass to charge ratio
MDR1	multidrug resistance 1 gene
MeOH	methanol
MHC	major histocompatilibility complex
MIST	metabolites in safety testing
MLM	mouse liver microsomes
MRM	multiple reaction monitoring
MS	mass spectrometry
MTS	3-(4,5-dimethylthiazol-2-yl)-2,5- diphenyl tetrazolium bromide
NAC	n-acetyl cysteine
NADPH	nicotinamide adenine dinucleotide phosphate (reduced)
NaOH	sodium hydroxide
NAPQI	n-acetyl-*p*-benzoquinone imine
NCE	new chemical entity
NK	natural killer

NMR	nuclear magnetic reasonance
NNRTI	non-nucleoside reverse transcriptase inhibitor
NSAID	non-steroidal anti-inflammatory
NVP	nevirapine
OH	hydroxy
p.o.	oral administration
P450	cytochrome P450
PEG	polyethylene glycol
PK	pharmacokinetics
PPB	plasma protein binding
RAGE	receptor for advanced glycation endproducts
RED	rapid equilibrium dialysis
RLM	rat liver microsomes
RNA	ribonucleic acid
ROA	route of administration
ROS	reactive oxidative species
rpm	rotations per minute
SAR	structure activity relationship
SD	standard deviation
SEM	standard error of the mean
SJS	Stevens-Johnson syndrome
SPE	solid phase extraction
SSA	5-sulphosalicyclic acid
SULT	sulphotransferase
$T_{1/2}$	half life
TA	tienilic acid
TEN	toxic epidermal necrolysis
TIC	total ion chromatogram
TK	toxicokinetics
TLR	toll-like receptor
TNF-α	tumor necrosis factor-alpha
UDPGA	uridine 5'-diphospho-glucuronic acid
UGT	uridine 5'-diphospho-glucuronosyltransferase
ULN	upper limit of normal
UV	ultraviolet
v/v	volume/volume
Vd	volume of distribution
w/v	weight/volume
XIC	extracted ion chromatogram

ABSTRACT

ADRs are a major complication of drug therapy and are one of the main causes of attrition in drug development. Bioactivation of drugs to CRMs is believed to be a crucial step in the development of many direct and immune-mediated ADRs. FS, a furan containing diuretic drug, has been shown to produce massive hepatic necrosis in mice through bioactivation of the furan ring to a reactive epoxide intermediate. A thiophene analogue of FS (TPA) has been synthesized in order to compare the heterocyclic moieties in the same biological environment. NVP, used for the treatment of HIV-1 infection, can cause skin reactions and hepatotoxicity, which are thought to be mediated through CRM formation and subsequent induction of the immune system. FS, TPA and NVP can be used to assess current systems used to investigate the potential hazard of a drug.

Substitution of the furan ring in FS to a thiophene ring (TPA) improved the potency towards the pharmacological target; the $Na^+/2Cl^-/K^+$ co-transport system in the thick ascending limb of the loop of Henle. It was found that TPA was three times more potent than FS, with IC_{50} values of 17 μM and 50 μM respectively. TPA displayed an improved safety profile *in vivo* in terms of serum ALT activity levels compared to FS (237.3 and 4441.4 U/L respectively, 1.21 mmol/kg *i.p.* for 24 hours). Evidence for the bioactivation of TPA, was provided through studies in rat and mouse liver microsomes. Neither FS nor TPA elicited hepatotoxicity or depleted hepatic GSH levels in the rat *in vivo*.

The disposition of FS and TPA were found to be similar in the mouse; however, the plasma AUC increased supraproportionally (≈240-fold to 4300-fold) as the dose was increased from 3/5 to 400 mg/kg orally in the mouse and rat suggesting that, in both species, clearance for both compounds becomes saturated at high oral doses. The toxicokinetic studies reported highlight that the liver exposure in the mouse was twice that in the rat (1.12 mmol/kg *i.p.*), with free liver AUC values at 243 and 128 μg.h/ml respectively. It was also observed, an *i.p.* dose of FS induced hepatotoxicity in male mice, yet, at the same dose, orally administered FS failed to do so. Oral administration of FS in the mouse resulted in significantly reduced plasma and liver exposure compared to *i.p.* administration.

NVP was tested in *in vitro* and *in vivo* systems for a toxicological end-point; NVP failed to induce cytotoxicity in both male Wistar and female Brown Norway rat hepatocytes, however, a NVP-induced skin rash developed over 3 weeks of daily NVP treatment in female Brown Norway rats. Urinary metabolites were quantified by mass spectrometry on day 7, 14 and 21 of the study; however, no time-dependant trend in any NVP metabolite was observed. No evidence of liver injury or elevation in serum HMGB-1 was observed. It is shown, in the work presented, that 12-OH NVP is a substrate for bioactivation; 12-OH NVP was administered to male Wistar rats and only M1 was identified in the bile. Following administration of NVP to male Wistar rats, both M1 and M2 were identified in the bile.

The work presented here has shown that the development of an assessment framework that encompasses all aspects of drug disposition and metabolism, and their relationship with bioactivation and toxicity, would be a valuable tool in drug development. The construction of a decision tree that can be populated with quantitative data could be used in the assessment of NCEs and highlight properties that require optimisation. Outcomes of changes or interventions to a new therapy could then be measured quantitatively and mechanisms defined. A caveat to this

framework would stipulate that the model systems employed would have to be carefully selected to best represent the clinical situation. This work highlights the need for improved preclinical hazard assessment and understanding of animal models. Development of more informative and translational biomarkers would allow better clinical hazard identification, as well as improving survivability of NCE during the drug development process.

CHAPTER 1

GENERAL INTRODUCTION

CONTENTS

1.1 INTRODUCTION

Adverse drugs reactions (ADRs) are a major cause of drug attrition and are a huge burden on healthcare systems. In the US, ADRs rank between the 4th and 6th leading cause of death (Lazarou *et al.*, 1998). The majority of ADRs are predictable, and become apparent during preclinical and clinical toxicity assessment (Olson *et al.*, 2000), and those that manifest in the human population, are commonly as a result of a prescribing error or through drug-drug interactions (Winterstein *et al.*, 2002). Unlike these 'predictable' types of ADRs, idiosyncratic ADRs are rarer but are more likely to be fatal (Edwards and Aronson, 2000). Idiosyncratic ADRs are often detected only when the offending drug has been released into the wider population following regulatory approval. Idiosyncratic ADRs are generally immune mediated (Uetrecht, 2009) and include hepatotoxicity, severe cutaneous reactions, anaphylaxis and blood dyscrasias (Park *et al.*, 2000).

The work of James and Elizabeth Miller provided the first evidence of drug metabolism leading to the formation of reactive metabolites that can bind covalently to protein and ultimately result in toxicity (Miller, 1970, Miller, 1994). This concept is now well established, and there is a wealth of evidence to suggest that drug metabolism to a reactive metabolite (bioactivation) is the initiating step in a number of direct and immune-mediated toxicities (Park *et al.*, 2005, Kalgutkar and Soglia, 2005). A common mechanism for the detoxification of reactive metabolites occurs via glutathione (GSH) conjugation (Williams *et al.*, 2002). The identification of drug metabolite-GSH adducts in a preclinical setting is sometimes treated as a hazard signal as it is indicative of reactive metabolite formation (Gan *et al.*, 2009, Reese *et al.*, 2010), conversely it could be argued that identification of a GSH adduct is an indication of an effective detoxification system. Idiosyncratic ADRs are not reproducible in preclinical species, and so, much focus has been on the development of surrogate endpoints of toxicity (biomarkers; either biological or chemical), animal models and improved understanding of structure-activity relationships of drugs.

A list of chemical moieties frequently associated with drug bioactivation and subsequent toxicity (structural alerts) has been compiled (Kalgutkar *et al.*, 2005). One approach to improving a drugs safety profile would be to avoid incorporating these structural alerts altogether; however, these moieties often are key to the

pharmacology of the drug. In addition, the presence of a structural alert does not automatically result in a toxic compound; not all drugs that contain a structural alert are bioactivated and not all bioactivated drugs are toxic (Kalgutkar and Soglia, 2005). The structure-activity relationships are, therefore, not straight forward.

Five-membered aromatic heterocyclic rings are widely distributed in nature and they are often incorporated into new chemical entities during drug design to increase pharmacological selectivity and potency (Dalvie *et al.*, 2002). Furan and thiophene rings are examples of heterocycles with one heteroatom. These chemical moieties have been used safely and effectively in some therapeutic agents, but there are examples of drugs containing a thiophene ring have been withdrawn from the market due to ADRs, and examples of furan containing compounds that can cause toxicity in humans and laboratory animals (Kalgutkar and Soglia, 2005). Structure-toxicity relationship investigations revealed that these moieties can be sites of bioactivation and ultimately result in the toxicity of the compounds. Furosemide (FS), a furan containing diuretic drug, has been shown to produce massive hepatic centrilobular necrosis in mice by a mechanism independent of its diuretic action (Mitchell *et al.*, 1974). Toxicity has been shown to be caused through bioactivation of the furan ring to a reactive epoxide intermediate (Mitchell *et al.*, 1974, Mitchell *et al.*, 1976, Wirth *et al.*, 1976, Williams *et al.*, 2007).

Although furosemide is safe in man, its tendency to cause severe liver necrosis in mice along with other hazard signals, including covalent binding to microsomal protein and adduct formation with trapping reagents, would mean that the drug may not have survived the development process today. However, furosemide provides a useful tool for the investigation of the mechanisms of drug-induced hepatotoxicity in mice. The research conducted in this thesis aims to assess whether replacing the toxicophore (furan ring) in furosemide with a thiophene ring would alter the toxicity profile while maintaining its pharmacological activity, and to investigate the structure-activity relationships of the two moieties in the same chemical environment.

Currently, there are few systems to investigate a drugs propensity to be bioactivated, and even fewer systems to examine the biological effects of drug bioactivation. Urinary mercapturates (breakdown products of GSH-adducts) have been used as

markers of bioactivation to reactive metabolites in *in vitro* and *in vivo* systems (Seutter Berlage *et al.*, 1977). More recently, in the light of improved bioanalytical techniques, drug mercapturates have been used in the quantitative assessment of bioactivation in humans (Staack and Hopfgartner, 2007, Ma *et al.*, 2008). Assessment of the degree of covalent binding to protein is also frequently used in *in vitro* and animal studies, as an indicator of a drugs potential to cause toxicity. Animal models of idiosyncratic ADRs are highly desired, however, only very few are established (Roth *et al.*, 2003, Shenton *et al.*, 2003; Shenton *et al.*, 2004) and the relevance of these models to the human reaction remains unclear. An animal model of an idiosyncratic ADR which displays similar characteristics of the human reaction with a measurable, biological or chemical, endpoint would be highly beneficial, as extrapolations could easily be made to the clinic. With better animal models, a greater understanding of the mechanisms of ADRs would be elucidated and would improve drug survival during development and help implement safe and effective drug use in the clinic.

Nevirapine (NVP) is a non-nucleoside reverse transcriptase inhibitor (NNRTI) used in developing countries for the treatment of HIV-1 infection. NVP is associated with clinically restrictive side effects; NVP-induced skin reactions and hepatotoxicity are thought to be mediated through reactive metabolite formation and subsequent induction of the immune system. Uetrecht and colleagues have characterised extensively a dose-dependent model of NVP-induced skin rash in female Brown Norway rats that resembles the idiosyncratic cutaneous reaction seen in humans (Shenton *et al.*, 2003, Shenton *et al.*, 2004) and appears to be immune mediated (Shenton *et al.*, 2005). Chen *et al.* (2008) have proposed that the skin rash produced in female Brown Norway rats by NVP and 12-hydroxy NVP (12-OH NVP) may be due to NVP quinone methide formed through dissociation of 12-OH NVP sulphonate in the skin.

The work presented in this thesis uses furosemide and NVP to investigate the relationship between chemical structure, bioactivation and toxicity, and examine systems currently used to detect reactive metabolite formation and/or toxicity. More specifically, pharmacokinetics, covalent binding and thioether adduct detection are explored, and the information they can provide regarding the potential toxicity of a drug molecule using these two drugs is examined.

1.2 ADVERSE DRUG REACTIONS

ADRs are defined as a response to a drug that is noxious, unintended or undesired occurring at doses normally used for the prevention, diagnosis or treatment of disease (Edwards and Aronson, 2000). ADRs can differ in terms of mechanism, severity, clinical presentation and the target organ(s) affected. Despite intensive investigation in the fields of chemical toxicology and molecular biology, ADRs remain a major complication of drug therapy (Lazarou *et al.*, 1998, Pirmohamed *et al.*, 2004). ADRs account for 6% of hospital admissions in the UK, and of this fraction there is a 2% mortality rate (Pirmohamed *et al.*, 2004). ADRs present a major problem to the pharmaceutical industry; drug attrition rates are at their highest with the overall success rate for approval of a new chemical entity (NCE) at just 11% (Kola and Landis, 2004). Of the NCEs that fail to make regulatory approval, 62% of attrition occurs at phase II clinical trials (Kola and Landis, 2004). During the period of 1975 to 2000 over 10% of newly approved drugs in the US were withdrawn or given black-box warnings (Lasser *et al.*, 2002). NCEs failing so late in development mean the costs, in terms of financial and time investment, are huge (Kola and Landis, 2004). In 1991 poor pharmacokinetic and bioavailability profiles of NCEs contributed to a total of 40% of attrition. In 2000 this had been reduced to 10%, however, lack of efficacy and safety issues became, and remain, the most common reasons for drug failure, each contributing to 30% of drug attrition (Kola and Landis, 2004).

1.2.1 Classification of ADRs

ADRs are described as either on-target or off-target (referred to as idiosyncratic throughout) reactions. On-target reactions can be predicted from the known primary or secondary pharmacology of the drug and often represent an exaggeration of the pharmacological effect of the drug (e.g. hypotension with antihypertensives and hemorrhage with anticoagulants); either the parent drug or an active metabolite is usually the offending species. They show simple and clear dose–response relationships and, therefore, can usually be avoided by dose reduction and are only rarely life-threatening (Testa and Krämer, 2009). In contrast, idiosyncratic ADRs are those that do not exhibit simple dose-response relationships and cannot be predicted

from knowledge of the basic pharmacology of the drug. Host-dependent factors are important in predisposition of these reactions and therefore, they are only observed in very low numbers of patients (Uetrecht, 2008). The exact mechanisms of idiosyncratic ADRs are unclear; however it is believed that many idiosyncratic reactions are initiated by reactive metabolites (Uetrecht, 2008, Smith and Obach, 2006)), which bind covalently to cellular macromolecules and either cause direct cell damage or trigger an immune response leading to cell death (Uetrecht, 2006, Williams and Park, 2003, Guengerich, 2006).

1.3 PHARMACOKINETICS AND BIOTRANSFORMATION IN ADRS

1.3.1 Absorption, distribution, metabolism and excretion (ADME)

The concentration and length of time (duration) that a drug is in the circulation can be a major determinant on whether a therapeutic effect, or indeed a toxic effect, will be achieved. Pharmacokinetics (PK) is the study of the time course of a drug in the body, where parameters of absorption, distribution, metabolism and excretion (ADME) can be described quantitatively. The PK of a drug will depend on its physicochemical characteristics, the route of administration (ROA) and the individual. PK studies in pre-clinical models and in clinical trials inform dose selection, to achieve safe and effective drug therapy. If exposure to a drug is increased to a level that exceeds the therapeutic window (a range of doses at which an effective balance of efficacy and minimal adverse events is achieved) then the subject could experience an ADR. Increased exposure to a drug may be the result of poor dose selection, increased absorption, DDIs or impaired excretion of the drug from the body.

The dose of a drug and how frequently it is administered will have a major impact on the therapeutic and/or toxicological outcome of therapy. An active surveillance of outpatient adverse drug events has shown that unintentional overdoses accounted for 39% of total reported adverse events and 73% of those that required hospitalization (Budnitz *et al.*, 2005). Another retrospective study reported that poor dose selection contributed to 68% of preventable adverse drug events (Winterstein *et al.*, 2002). The latter study also highlighted that these adverse events are often on-target ADRs;

bleeding with warfarin or heparin overdose accounted for 32.2% of adverse events and hypoglycemic events with insulin overdose accounted for 14.2% of adverse events (Winterstein *et al.*, 2002). Dose is also a critical factor in idiosyncratic ADRs; among US prescription medicines, a statistically significant relationship was observed between daily dose of oral medicines and reports of liver failure, liver transplantation and death caused by DILI (Lammert *et al.*, 2008). Examination of serious DILI cases reported to the Swedish Adverse Drug Reactions Advisory Committee (1970-2004) found that of 598 eligible Swedish DILI cases, 77% caused by drugs administered at $\geq$ 50 mg/day (Lammert *et al.*, 2008). However, genetics, disease state and environmental factors all play a role in idiosyncratic ADRs (Uetrecht, 2007) and are therefore much more complex and less well understood. In order for a drug compound to be a successful therapeutic agent, it has to reach the site of action (e.g. an enzyme or receptor) at an effective concentration; equally a toxic effect will only be achieved if the drug or drug metabolites reaches a certain concentration at the site of either a cellular macromolecule (can either be critical or non-critical).

Drugs that are administered orally have a number of barriers to contend with in order to enter the circulation, and how efficient they are at crossing these barriers, is related to the physicochemical properties of the drug molecule. Drugs need to be soluble in the gut prior to absorption; they also need to be in an un-ionized state in order to diffuse through cellular biological membranes of the gastro-intestinal tract. Some drugs undergo metabolism at the gut wall; those drugs that are successfully absorbed by the gut may be subject to first-pass metabolism in the liver before entering the circulation. Therefore, after oral administration, the plasma levels of a drug may be a fraction of the initial dose. This is illustrated when different ROA result in differences in incidence and severity of ADRs with the same drug. A study set up to identify ADRs in relation to prescribing errors identified that incorrect ROA instructions accounted for 37.6% of total serious or severe errors (Lesar, 2006). Amodiaquine is an anti-malarial drug that has been associated with immune-mediated ADRs in the rat. A positive immune response was observed regardless of the ROA, but the magnitude of the response was in the order intraperitoneal administration (*i.p.*) > intramuscular administration (*i.m.*) > oral administration (*p.o.*) (Clarke *et al.*, 1990). The anti-malarial artemisinin compounds display contradicting

toxicity profiles between humans and laboratory animals. High doses of artemisinin compounds have been shown to cause specific neurotoxic effects on the brain stem in laboratory animals with prominent lesions primarily restricted to the pons and medulla yet have a good safety record in humans (Gordi and Lepist, 2004, Li *et al.*, 1998). A review highlighted that the differences in ROA are likely to account for the discrepancy; treatment with artemisin compounds in man is via an *i.v.* route, where the compounds have a short half life and are rapidly cleared from the system; in rats, the ROA is often *i.m.* and plasma concentration profiles revealed a prolonged apparent elimination half life due to pooling at the site of administration (Gordi and Lepist, 2004).

Drugs and their metabolites can be eliminated through a number of mechanisms but the primary routes of elimination are urinary clearance and hepatic clearance, which includes biliary excretion and metabolism. The degree and rate of drug clearance from the body will directly influence drug plasma concentration; rapid elimination will reduce the risk of toxicity but may also reduce the effectiveness of therapy. Most drugs have the physicochemical properties that allow for absorption through biological membranes into the circulation and to the site of action and are also, therefore, substrates for urinary elimination through glomular filtration and passive diffusion in the kidney. Drug-protein binding and urinary pH can affect these types of clearance mechanisms. Some drug molecules are eliminated via active transport in the kidney and can be subject to competitive inhibition.

Biliary excretion is one of the primary routes of drug elimination; polar drugs and metabolites, such as glucuronides and glutathione conjugates, can be excreted via the bile in an active process by efflux transport proteins (Lai, 2009). The size of compounds that can be excreted in this way, varies with species; humans have a higher molecular weight cut off (~ 500 Da) at the hepato-biliary plasma membrane than rodents or dog (300 – 400 Da). Inhibition of biliary excretion can lead to drug accumulation in the liver; work conducted by Spitznagle, *et al* (1977) indicated that saturation of biliary excretion of furosemide, following a large dose of furosemide or pre-treatment with sulfobromophthalein, is closely associated with the appearance of liver necrosis in the mouse and of furosemide metabolites bound covalently to liver proteins. The anti-depressant nefazodone was withdrawn from the US market in

2004, following withdrawal in Canada and Europe, due to incidences of hepatotoxicity. Nefazodone is predominantly excreted in the bile and there have been investigations into the inhibition of the Bile Salt Export Pump (BSEP), as a cause of nefazodone hepatotoxicity (Kostrubsky *et al.*, 2006). In sandwich cultured human hepatocytes, nefazodone caused a concentration dependent inhibition of taurocholic acid in canaliculi with an IC_{50}=14 μM (Kostrubsky *et al.*, 2006).

1.3.2 Importance of drug biotransformation in ADRs

Drug metabolism generally renders drug molecules less reactive and increases their hydrophilicity, assisting the drug, and its metabolites, elimination from the body. Drug metabolism can also uncover more pharmacologically reactive groups (pro-drug). In some cases the enzymes that catalyze these reactions can render the drug more chemically reactive in a process known as bioactivation. These reactive metabolites are more often than not bioinactivated by mechanisms such as conjugation with glutathione (GSH); however if detoxication mechanisms are impaired (e.g. cellular GSH is depleted) these reactive metabolites are free to bind covalently to cellular macromolecules and elicit toxicity through a number of mechanisms (Figure 1.1).

Drugs can be metabolised in a number of organs in the body, such as the lung, liver, blood and skin. In each organ, the subset of enzymes differs and therefore the drug will be differentially metabolised throughout the body. The liver is the main organ of drug metabolism as the majority of enzymes are found here. Also, all orally administered drugs pass through the liver via the portal vein before reaching the systemic circulation and, as a result, the liver is a frequent target of drug-induced toxicity. In fact, 52% of all cases of acute liver failure in the US are attributed to drug-induced liver injury (DILI; Pelkonen and Raunio, 1997). DILI is the most frequent reason for the withdrawal of an approved drug from the market (Temple and Himmel, 2002).

Drug metabolism and bioactivation are catalysed by a range of enzymes that occur naturally in the body and have endogenous substrates. Examples of the type of reactions involved in drug metabolism include oxidation, reduction, hydrolysis,

hydration, conjugation and condensation. Metabolism is divided into three phases. Phase I involves the addition of functional groups; if the resulting metabolites are sufficiently polar they can be readily excreted. If not, the metabolite can undergo a second reaction with an endogenous substrate to form a more polar conjugate. Phase II metabolism is usually thought of as a detoxication reaction and often involves conjugation reactions of the phase I metabolites rendering them less reactive and more easily eliminated. However, phase II metabolism can occur without phase I and can sometimes generate reactive species. Phase III metabolism can be thought of as the final step of elimination from the body.

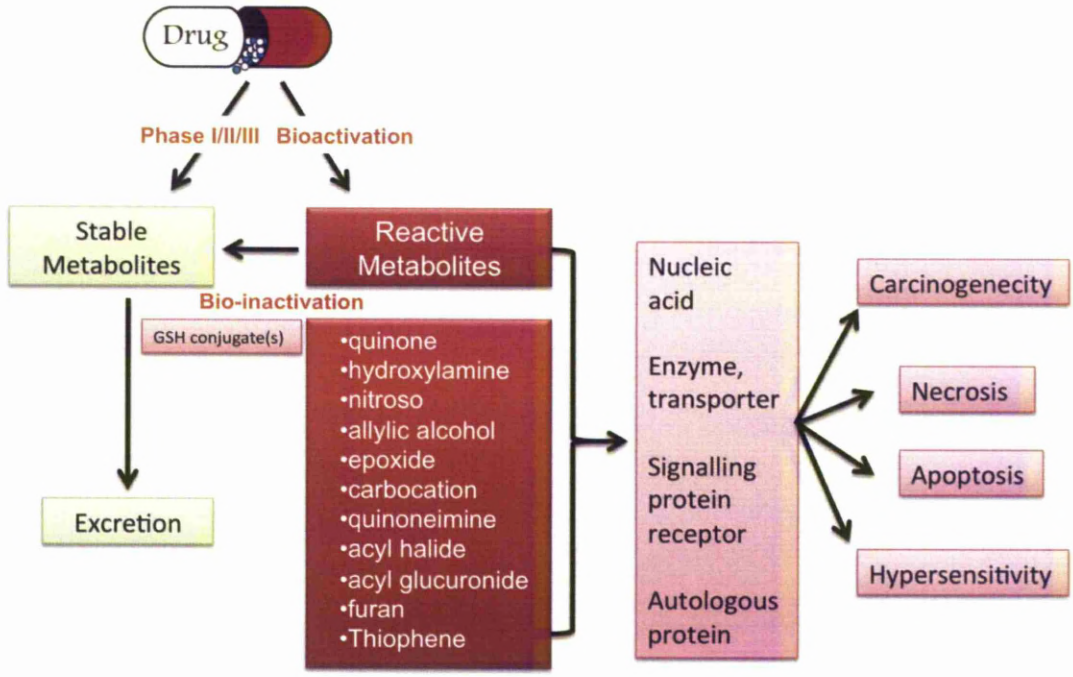

Figure 1.1: Schematic of drug bioactivation and possible targets and consequences. Toxicity may occur through accumulation of parent drug or, via metabolic activation, through formation of a reactive metabolite, which, if not detoxified, can effect covalent modification of biological macromolecules. The identity of the target macromolecule and the functional consequence of its modification will dictate the resulting toxicological response (Park *et al.*, 2005).

1.3.2.1 Phase I drug metabolism

The cytochrome P450 mixed function oxidase system is the primary route for phase I reactions and is found, primarily, in the microsomal fraction of cells, i.e. the endoplasmic reticulum. They are responsible for 95% of phase I metabolism. This is a large superfamily of enzymes that are highly specific for endogenous substrates but are less specific for exogenous drugs and xenobiotics. There are around 40 cytochrome P450 (CYPs) isomers in humans; those that are responsible for xenobiotic metabolism include CYP1, CYP2 and CYP3. CYPs will only accept drugs as substrates if they resemble the enzymes natural substrate; however, there is an overlap in substrate specificity between different isomers. All reactions mediated by CYPs require molecular oxygen, NADPH, NADPH-cytochrome P450 reductase and lipid. Reactions involve the initial insertion of a single oxygen atom which could then be followed by rearrangement or decomposition to the final metabolite. Other enzymes responsible for phase I drug metabolism include alcohol dehydrogenase, aldehyde dehydrogenase, xanthine oxidase, amine oxidases, aromatases and alkylhydrazine oxidase (Gibson and Skett, 2001). Table 1.1 summarizes the different reactions carried out by CYPs, their targets and their products

Reaction	Transformation	Targets
Aromatic hydroxylation	Phenyl to phenol	Carbon atoms of aromatic rings
Aliphatic hydroxylation	Methyl to carbinol	Linear carbon chains
Epoxidation	Cyclic groups to epoxide	Polycyclic compounds
Dealkylation (N, O, and S)	Removal of alkyl groups (intermediate hydroxyl)	Secondary and tertiary amines, alkoxy groups and alky substituted thiols.
Oxidative Deamination	Removal of amine groups, releasing ammonium ions and leaving a corresponding ketone.	Secondary amines in a $CH_3(CH_3)$-NH_2 structure.
N-oxidation	Formation of N-oxides (sometimes forms hydroxylamines)	Amines, amides, imines, hydrazines and heterocyclic compounds.
S-oxidation	Formation of *S*-oxides	Thiol groups
Dehalogenation	Dechlorination or debromination	Halogen atoms
Alcohol oxidation	Alcohol to aldehyde	Alcohol groups

Table 1.1: Summary of phase I reactions listing the functional groups that are targets and the products of each reaction type.

1.3.2.2 Phase II drug metabolism

Phase II reactions are sometimes referred to as the true detoxification pathway. A number of different enzymes catalyse these reactions and often require high energy co-factors (Table 1.2; Gibson and Skett, 2001). Glucuronide formation, GSH and sulphate conjugation are major routes of phase II conjugation reactions; however, GSH conjugation is arguable the most directly protective phase II reaction in terms of detoxification of reactive metabolites.

Reaction	Enzyme	Functional Group
Glucuronidation	UDP-Glucuronoslytransferase	-OH -COOH $-NH_2$ -SH
Glycosidation	UDP-Glycosyltransferase	-OH -COOH -SH
Sulfation	Sulfotransferase	$-NH_2$ $-SO_2NH_2$ -OH
Methylation	Methyltransferase (SAM)	-OH $-NH_2$
Acetylation	Acetyltransferase	$-NH_2$ $-SO_2NH_2$ -OH
Amino acid conjugation		-COOH
Glutathione conjugation	Glutathione-S-transferase	Epoxide Organic halide
Fatty acid conjugation		-OH
Condensation		Various

Table 1.2: Summary of phase II reactions listing the functional groups that are targets and the enzymes required for each reaction type.

1.3.2.3 Importance of GSH in cell protection

GSH is a major hepatocellular antioxidant due to its free thiol group and its relatively high abundance (approximately 10 mM in hepatocytes). It is a tripeptide, comprising of the amino acids cysteine, glutamate, and glycine. GSH is crucial for cell function and survival, and maintains the redox potential of the cell. GSH exists in either a reduced (GSH) or oxidised (GSSG) form and the change in the ratio between the two forms is directly reflective of intracellular redox alterations (Meister and Anderson, 1983). GSH can undergo conjugation reactions with reactive metabolites, either

through enzymatic catalysis by GSTs or spontaneously and thereby prevent the covalent binding of these products to cellular macromolecules and avoid cell injury. Reactive metabolites also introduce the threat of cellular oxidative stress; the formation of reactive metabolites through bioactivation of drugs can push the redox balance towards a more oxidative environment in the cell by stimulating overproduction of reactive oxygen species (ROS), introduction of electrophilic species and disruption of thiol status. ROS can cause cell damage through a number of mechanisms including lipid peroxidation, protein oxidation, DNA oxidation and mitochondrial damage (Boelsterli, 2003). The antioxidant role of GSH is to quench ROS and maintain the redox potential of the cell. GSH is also a hydrogen donor for glutathione peroxidise, the enzyme responsible for the conversion of H_2O_2 to water in parallel with catalase and is also involved in the repair of lipid peroxidation.

GSH synthesis is highly inducible upon conditions of oxidative stress and GSH depletion. Transcription factors controlling the expression of enzymes involved in GSH synthesis can be directly activated by electrophilic species that conjugate to GSH (Copple *et al.*, 2008). Synthesis of GSH occurs in the cytosol through a two-step ATP consuming reaction (Figure 1.2). Initially, γ-glutamylcysteine is synthesised through the condensation of cysteine and glutamate, a reaction catalysed by γ-glutamylcysteinyl ligase. GSH synthetase then further catalyses the formation of GSH from γ-glutamylcysteine and glycine (Meister, 1983, Yuan and Kaplowitz, 2009). It is then utilised either as an enzyme co-substrate, or as a scavenger molecule in the presence of an oxidised substrate, resulting in the formation of GSSG. Under normal physiological conditions GSSG can then be recycled back to GSH by the enzyme GSH reductase (Figure 1.2; Yuan and Kaplowitz, 2009).

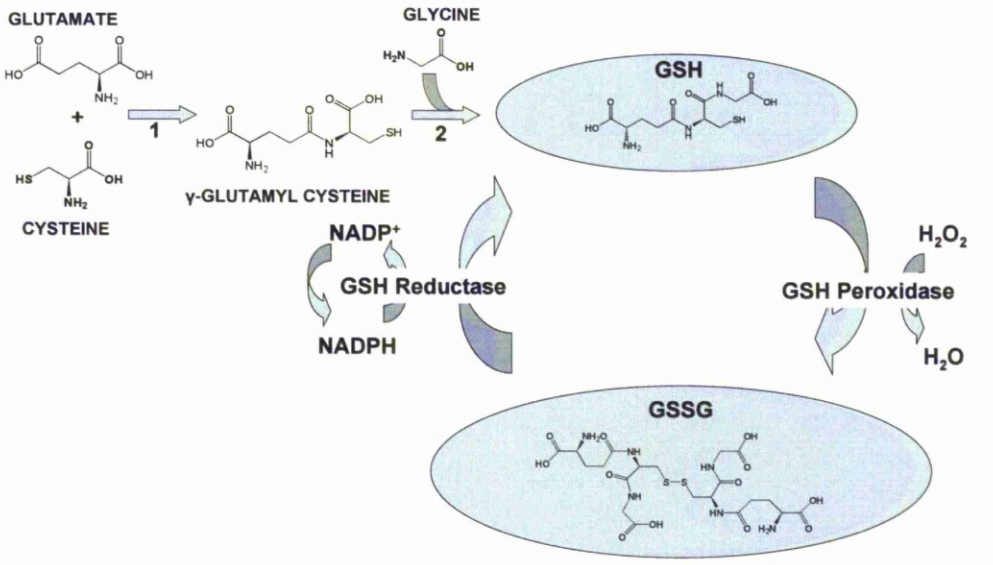

Figure 1.2: Synthesis of GSH. (Adapted from DeLeve *et al.*, 1991) GSH is synthesised by a two-step ATP-dependent pathway. γ-glutamylcysteine is formed from L-glutamate and cysteine, which is catalysed by γ-GCL (1). Glycine is then added at the C-terminal of γ-glutamylcysteine through the catalysis of GSH synthetase (2). Redox cycling between GSH and GSSG is mediated by GSH reductase and GSH peroxidise (DeLeve and Kaplowitz, 1991).

1.3.3 Relationship between structural alerts, bioactivation and ADRs

A number of chemical moieties frequently associated with bioactivation and subsequent toxicity have been identified (Kalgutkar *et al.*, 2005). However, the relationship between the presence of these so called 'structural alerts', their potential to be bioactivated and the downstream effects leading to ADRs, are poorly understood. *In vitro* and *in vivo* research using, clinically relevant, withdrawn or investigational compounds have aimed to provide an understanding of these connections.

Five-membered aromatic heterocyclic rings are widely distributed in nature and they are often incorporated into new chemical entities during drug design to increase pharmacological selectivity and potency (Dalvie *et al.*, 2002). They are, therefore, an attractive replacement to structurally similar moieties during lead compound optimisation. Furan and thiophene rings are examples of heterocycles with one heteroatom. There are many examples where these moieties are used in effective therapeutic agents. However, therapeutic agents containing a thiophene ring have

been withdrawn from the market due to ADRs, and examples of furan containing compounds that can cause toxicity in humans and laboratory animals (Kalgutkar and Soglia, 2005). Structure-toxicity relationship investigations revealed that these moieties can be sites of bioactivation and ultimately result in the toxicity of the compounds.

1.3.3.1 Thiophene containing drugs

Like many drugs, thiophene containing compounds are metabolised by the cytochrome P450 mixed function oxidase system (Kalgutkar *et al.*, 2005). The metabolic and bioactivation pathways of many of these drugs have been investigated and a picture is emerging of possible routes of metabolism a drug containing a thiophene moiety can take. Many examples of thiophene-containing compounds that have been associated with ADRs (Figure 1.3 A), have therapeutic dose ranges that are greater than or equal to 50 mg/day; of the examples of 'safe' thiophene-containing compounds (Figure 1.3 B), three are dosed at less than 50 mg/day, cefoxitin is dosed at many grams per day, however this antibiotic is not taken chronically.

Thiophenes can undergo P450 mediated hydroxylation to 2- and 5-hydroxythiophene, and oxidation to a reactive thiophene *S*-oxide (Mansuy *et al.*, 1991, Dansette *et al.*, 1992), proved by the identification of thiophene *S*-oxide dimers in *in vitro* and *in vivo* studies of thiophene (Treiber *et al.*, 1997). Also, a mercapturic acid conjugate of dihydrothiophene *S*-oxide, resulting from a 1, 4-Michael-type addition of thiol on thiophene *S*-oxide, was identified in the urine of rats treated with radiolabelled thiophene (Dansette *et al.*, 1992).

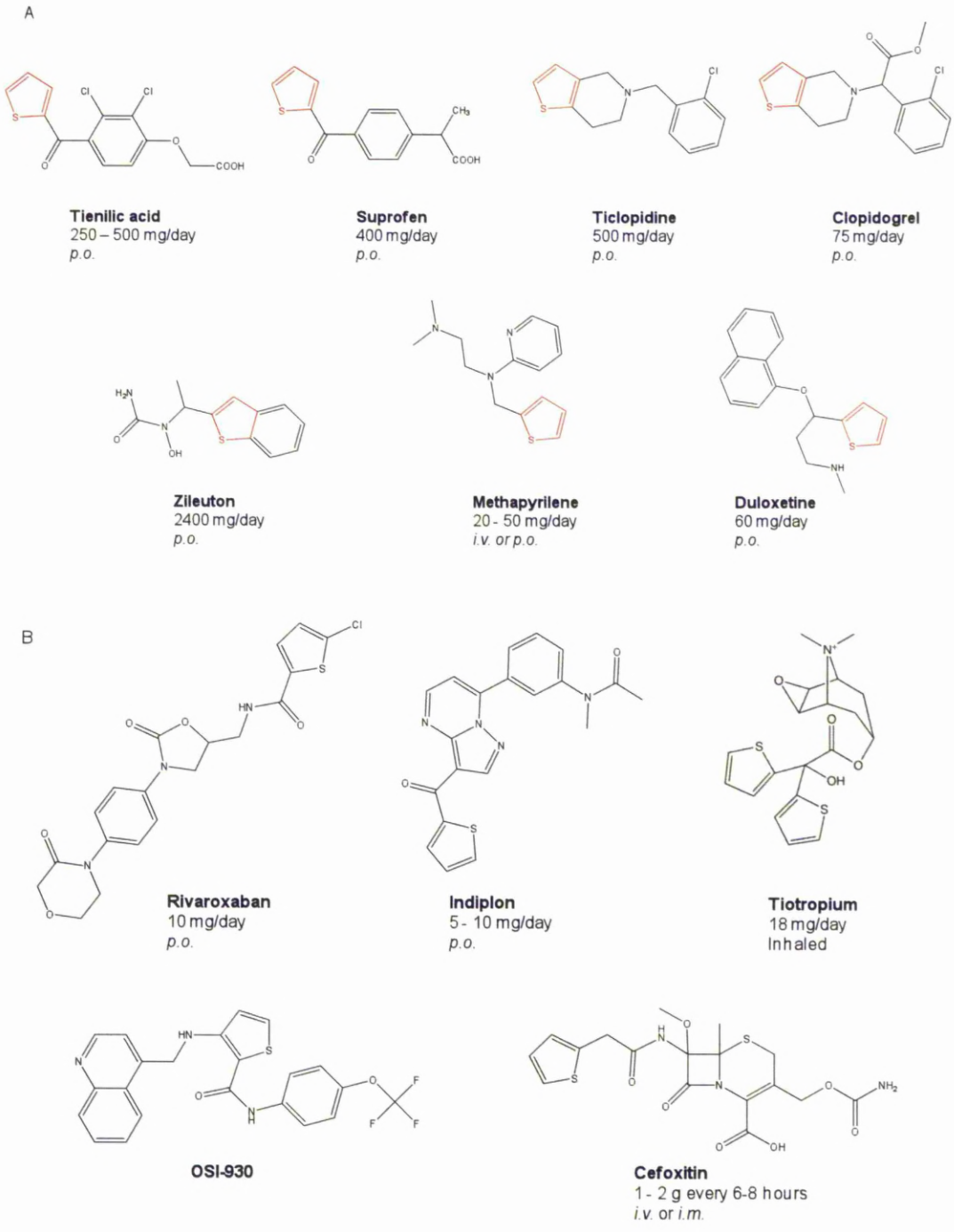

Figure 1.3: Structures of thiophene-based drugs that are associated with ADRs (A) and those that are not (B). Typical dose and ROA given where possible.

Tienilic acid (TA) is a diuretic drug, which was released in the US in 1979 as an antihypertensive. In 1980, TA was withdrawn from the US market due to severe hepatotoxic secondary effects and renal toxicity (Zimmerman *et al.*, 1984). 1 in 10,000 patients taking TA suffered from auto-immune hepatitis (Dansette *et al.*, 1991), an immune-mediated idiosyncratic ADR that was not predicted by animal model studies. Studies with TA have shown that it produces a TA *S*-oxide *in vivo* (Treiber *et al.*, 1997). This metabolite forms an adduct with CYP2C (the enzyme responsible for its formation) via an alkylation reaction (Lecoeur *et al.*, 1994). The major product of TA metabolism is 5-hydroxy TA, formed from the hydroxylation of the C-5 position on the thiophene ring; however oxidised intermediates of this pathway have been shown to covalently bind to microsomal proteins (Dansette *et al.*, 1991b). 5-hydroxy-TA is thought to be formed from TA *S*-oxide in the presence of NADPH and molecular oxygen (Belghazi *et al.*, 2001). Studies using electrospray ionization mass spectrometric analysis have deduced that the reactive intermediate could be an epoxide or a TA *S*-oxide (Koenigs *et al.*, 1999), although the formation of a TA *S*-oxide is more widely supported (Mansuy *et al.*, 1991a, Dansette *et al.*, 1992, López-Garcia *et al.*, 1994).

Suprofen is a thiophene containing NSAID, which, within a short time after its release, displayed severe adverse effects associated with renal toxicity. Within 40 minutes to 8 hours of administration, patients suffered from flank pain and renal failure normally associated with chronic dosing of NSAIDs (Hart *et al.*, 1987). Although some studies suggested that a glucuronic acid conjugate mediated the nephrotoxicity observed with suprofen (Mori *et al.*, 1985, Smith and Liu, 1993), the fact that both TA and suprofen mediate the same renal toxicity symptoms and the confirmation of the CYP 2C isoform family is present in the kidney, suggests they might share the same bioactivation pathway (Kalgutkar *et al.*, 2005). Like TA, suprofen has been shown to be a CYP 2C9 inhibitor (O'Donnell *et al.*, 2003) and one of its major metabolites is 5-hydroxy suprofen (Mori *et al.*, 1984). Similar to reports by Koenigs *et al*, (1999), O'Donnell (2003) observed evidence for the formation of a reactive epoxide intermediate, by the addition of semicarbazide, affording a γ-thioketo α,β-unsturated aldehyde open ring structure. It could be deduced that either the epoxide or the γ-thioketo α,β-unsturated aldehyde is responsible for the covalent binding and subsequent inactivation of CYP 2C9. Incubations of suprofen with

NADPH and semicarbazide, trapped a pyridazine derivative (O'Donnell *et al.*, 2003). This provided more direct evidence of an epoxide intermediate, as a pathway could then be suggested involving the initial epoxidation of the thiophene ring followed by spontaneous ring opening affording a reactive γ-thioketo-α,β-unsaturated aldehyde (O'Donnell *et al.*, 2003). Subsequent condensation of the aldehyde with semicarbazide would lead to the pyridazine adduct.

Although tienilic acid and suprofen have been shown to undergo similar bioactivation, the target organs of the primary toxicities they induce differ. It is clear that bioactivation plays a crucial role in the development of toxicity of these drugs. However, other major factors, that determine individual susceptibility of toxicity and the target organ, are unknown.

There are a number of other thiophene-containing drugs that are believed to cause ADRs through bioactivation to a reactive metabolite. Ticlopidine, an antiplatelet drug, is a thienopyridine derivative containing a fused thiophene ring (Saltiel and Ward, 1987). Its clinical use is associated with a number of serious ADRs including neutropenia, aplastic anaemia, agranulocytosis and cholestatic jaundice (Yim *et al.*, 1997, Ochoa *et al.*, 1998, Symeonidis *et al.*, 2002). However, a structurally similar drug, clopidogrel (antiplatelet and antithrombotic drug) has only minimal adverse events associated with its use. Ticlopidine has been shown to undergo bioactivation to a reactive *S*-oxide in the liver, which acts as a mechanism based inhibitor of CYP enzymes (Liu and Uetrecht, 2000, Evans and Baillie, 2005). Additionally, a GSH adduct of the thiophene moiety has been identified in activated neutrophils *in vitro*, via formation of a reactive S-chloride intermediate (Figure 1.4; Evans and Baillie, 2005). There is no evidence to suggest that clopidogrel undergoes bioactivation to reactive metabolites.

The clinical use of the 5-lipoxygenase inhibitor, zileuton, is limited due to liver toxicity which is believed to be caused by the formation of a reactive *S*-oxide intermediate following degradation to 2 acetylbenzothiophene (Joshi *et al.*, 2004). Another example is methapyrilene; this H_1 receptor anti-histamine was used as a sedative before it was withdrawn following evidence that it caused liver cancer in rats. Methapyrilene has been shown to cause liver toxicity in rats associated with

bioactivation of the thiophene ring to either a reactive *S*-oxide or epoxide (Figure 1.5; Graham *et al.*, 2008). Duloxetine is a serotonin-norepinephrine re-uptake inhibitor associated with liver toxicity. Recently duloxetine adducts have been identified *in vitro*, indicative of bioactivation (Gan *et al.*, 2009, Wu *et al.*, 2010).

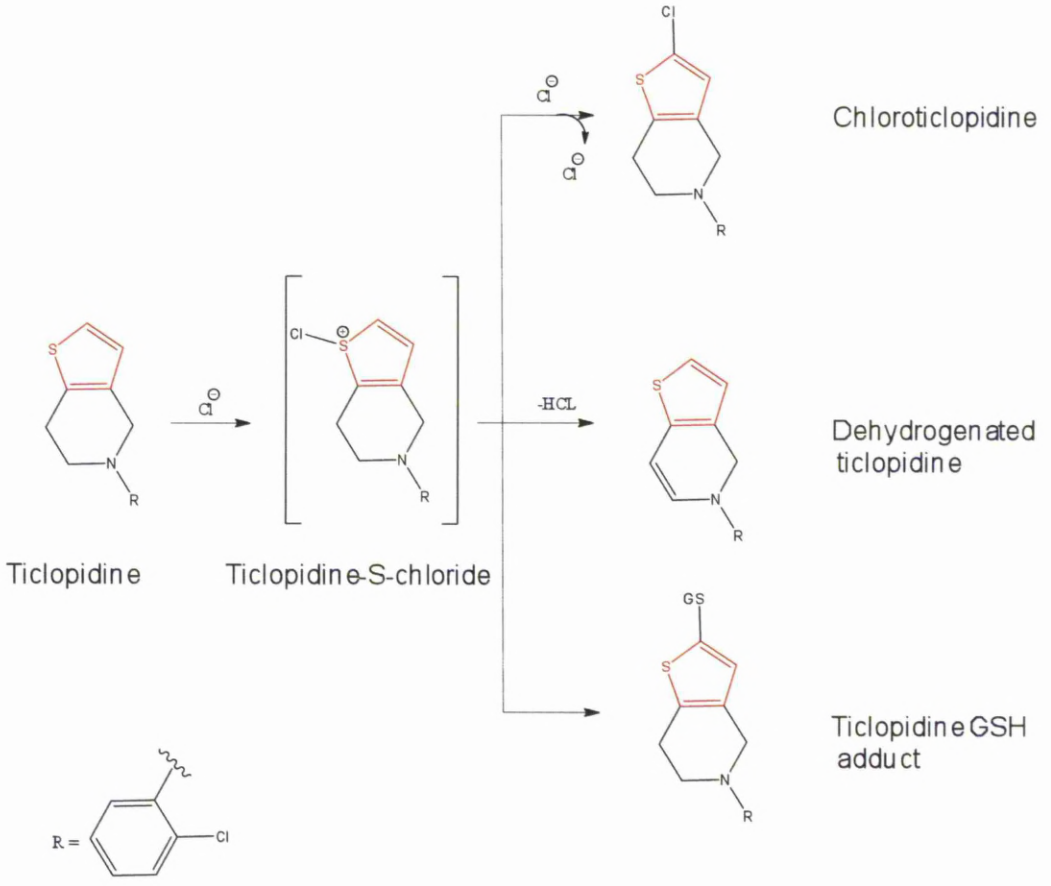

Figure 1.4: Peroxidase-catalysed metabolism of ticlopidine in neutropils. Taken from Dalvie *et al.* (2002).

Despite the extensive list of thiophene containing drugs that are associated with ADRs, there are a number of examples that are not. OS1-930 is an investigational anticancer agent that undergoes bioactivation to an *S*-oxide; however, studies have shown that it is relatively safe in pre-clinical models and in human volunteers (Medower *et al.*, 2008). Tiotropium, a bronchodilator used in the treatment of chronic obstructive pulmonary disease, contains two thiophene rings which contribute to the compounds remarkable affinity to muscarinic receptors (Disse *et al.*, 1993, Disse *et al.*, 1999). The metabolism of tiotropium was described by *in vitro*

studies; metabolites include a variety of glutathione conjugates after oxidation of the thiophene ring system (Price *et al.*, 2009). Tiotropium is used safely in the clinic and does not inhibit cytochrome P450 enzymes (Price *et al.*, 2009). Similarly, indiplon, a hypnotic sedative that has yet to be released onto the market, and rivaroxaban, a oral anticoagulant, both contain a thiophene ring yet there is no evidence of bioactivation at the thiophene ring and clinical trials have shown the drugs to be well tolerated in humans (Roth *et al.*, 2007, Kubitza *et al.*, 2005a, Kubitza *et al.*, 2005b). The antibiotic cefoxitin is also used safely in humans (Lapointe *et al.*, 1994).

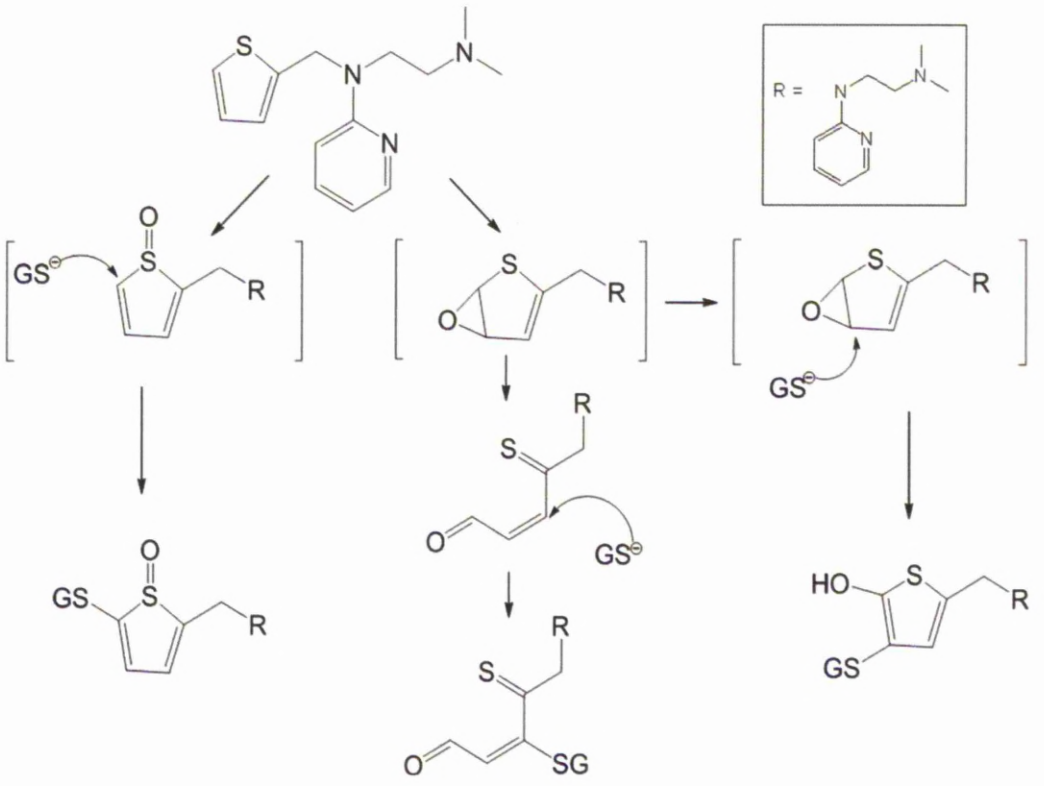

Figure 1.5: Alternative hypothetical pathways of bioactivation of MP to the intermediate trapped as a glutathione conjugate: to MP *S*-oxide, an epoxide that reacts with GSH without opening of the thiophene ring, and an epoxide that undergoes concerted opening of the epoxide and thiophene rings to produce a g-thioketo-α, β-unsaturated aldehyde.

1.3.3.2 Furan containing drugs

Furan is an important heterocycle found in drugs and also occurs in nature. Many naturally occurring furans have been found to be hepatotoxic and hepatocarcinogenic in preclinical species and humans (Dalvie *et al.*, 2002). Furan is a liver toxicant and genotoxic in rats and mice, and studies with radiolabelled furan suggest the primary metabolite involves ring scission followed by oxidation. There are examples of furan containing compounds that have been investigated following reports of human toxicity and there are examples of furan containing drugs used safely in the clinic (Figure 1.6).

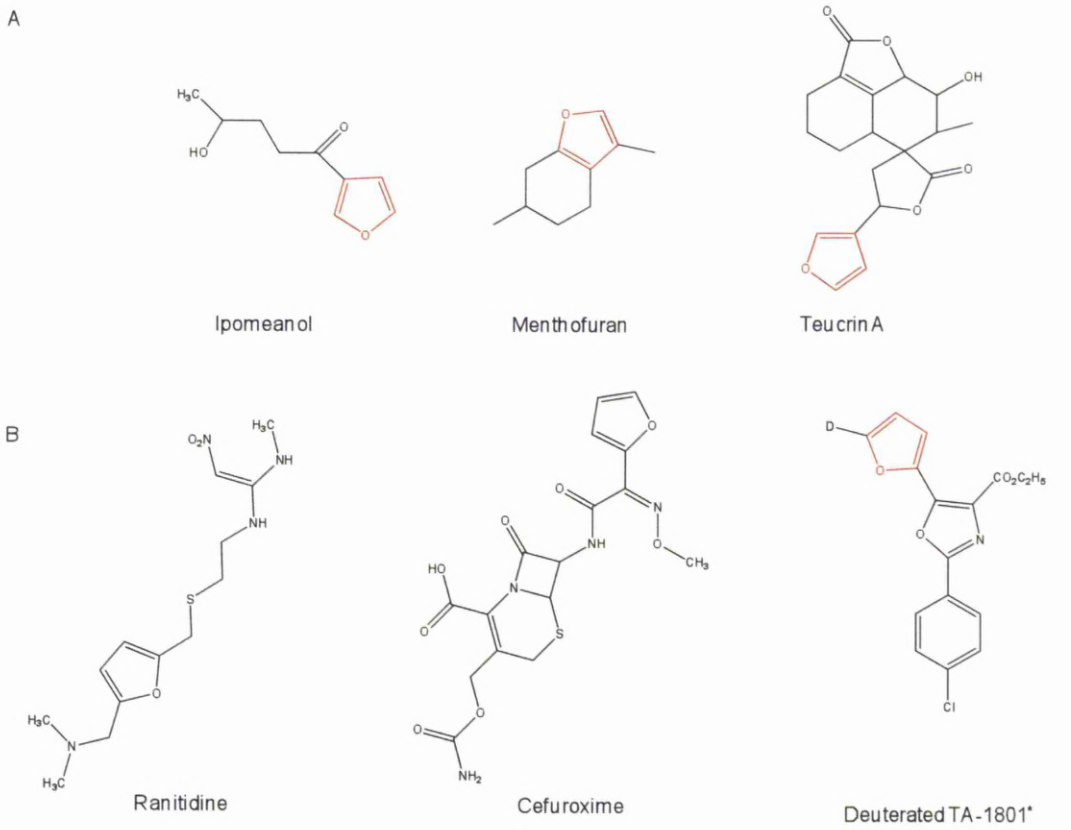

Figure 1.6: Structures of furan-based drugs that are associated with ADRs (A) and those that are used in humans relatively safely (B). * TA-1801 was used as a probe to determine the metabolic fate of a furan ring and isn't associated with ADRs.

Ipomeanol, a naturally occurring product of mould-damaged sweet potatoes (Boyd and Wilson, 1972), causes the development of potentially lethal pulmonary lesions in the rat (Dutcher and Boyd, 1979). Oxidative ring opening of the furan ring and irreversible protein binding of the corresponding substituted γ-ketoenal is thought to be the pathway resulting in toxicity (Figure 1.7; Baer *et al.*, 2005). Menthofuran, the product of P450 catalysed oxidation of pulegone, is the proximate toxic responsible for hepatotoxicity (Moorthy *et al.*, 1989); the furan ring of menthofuran undergoes further oxidation to a γ-ketoenal, which is well established as the ultimate toxin of pulegone (McClanahan *et al.*, 1989). The postulated general mechanism of furan mediated toxicity via oxidative ring opening of the furan ring to a α, β-unsaturated dicarbonyl or a γ-ketoacid proceeds via initial epoxidation to furan-2, 3-epoxide (Le Fur and Labaune, 1985). The 2, 3-epoxide directly rearranges to hydroxyfuran which predominately exists as the lactone tautomer; hydrolysis of the lactone affords the γ-ketocarboxylic acid (Le Fur and Labaune, 1985). Alternately, ring opening of the furanoyl epoxide can also lead to the formation of γ-ketoenal (Khojasteh-Bakht *et al.*, 1999).

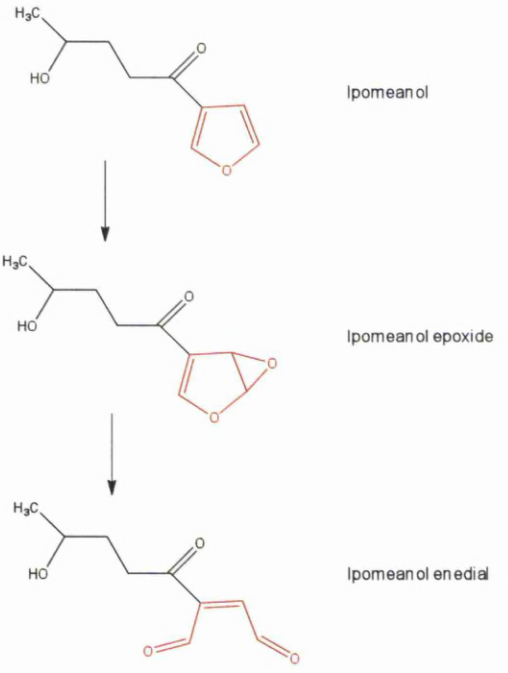

Figure 1.7: Proposed route of bioactivation of ipomeanol. Adapted from Baer *et al.* (2005)

Kobayashi *et al.* (1987) suggested an alternative mechanism for furan ring opening using deuterated TA-1801, a hypolipidemic, as a probe. The C-O bond in the furan ring is directly cleaved following transfer of oxygen from P450 to the substrate. TA-1801 is converted to the corresponding deuterated γ-keto alcohol and nondeuterated γ-keto acid metabolites (Kobayashi *et al.*, 1987). These results have been explained by a pathway in which TA-1801 undergoes an oxidative ring opening to deuterated α, β-unsaturated aldehyde followed by an enzyme assisted reduction to the γ-keto alcohol. Oxidation of this alcohol affords the nondeuterated γ-ketocarboxylic acid. This mechanism argues against the formation of an epoxide intermediate. Evidence for the formation of the epoxide intermediate has been demonstrated by metabolism studies of R-(+)-pulegone and R-(+)-menthofuran by human liver P450s using $^{18}O_2$, $H_2{}^{18}O$ and C-2 deuterium labelled menthofuran (Khojasteh-Bakht *et al.*, 1999).

Ranitidine is metabolised to an *N*-oxide and an *S*-oxide by flavin containing monooxygenase (FMO), neither of which involve the furan ring (Chung *et al.*, 2000). Ranitidine is a histamine H_2-receptor antagonist that inhibits stomach acid production. It is commonly used in treatment of peptic ulcer disease and gastroesophageal reflux disease and it is well tolerated in humans (Brogden *et al.*, 1982). The cephalosporin antibiotic cefuroxime is another example of a furan containing drug that is well tolerated in humans (Bucko *et al.*, 2002).

Thiophene and furan ring substitutions for improved potency and toxicity profiles

Despite the safety concerns thiophenes and furans present, compounds that contain these moieties have been found to show nematocidal (Bakker *et al.*, 1979), insecticidal (Iyengar *et al.*, 1987), antibacterial (Matsuura *et al.*, 1996), antifungal (Chan *et al.*, 1975), antiviral (Hudson *et al.*, 1989) and have antioxidant activity (Malmström *et al.*, 2001). In fact, therapeutic agents containing thiophene and furan rings have motivated researchers in pharmaceutical chemistry so that it now appears that at least one of these heterocyclic compounds has been prepared for every important therapeutic compound containing a benzene nucleus (Meotti *et al.*, 2003). A number of studies have been conducted where a potential structural liability in a lead compound, has been substituted for a structurally similar alternative and

subsequently assessed for potency and safety. Often substitution for a thiophene or furan ring affords a compound that has comparable or improved potency for the target molecule and a comparable safety profile to the original compound (Hagen *et al.*, 2001, Brendle *et al.*, 2002).

1.4 TARGET ORGANS AND MECHANISMS OF ADRS

ADRs can mimic natural disease and nearly every organ in the body could potentially be a target (Park *et al.*, 2000). Furthermore, one or more organs could be adversely affected by a single drug. Although the parent drug can mediate ADRs, there is a large amount of evidence to suggest that drug reactive metabolites are the offending species in many ADRs. Parent drug or reactive metabolites can mediate toxicity through a number of mechanisms and these can be described as either direct or immune-mediated.

1.4.1 Mechanisms of ADRS: direct toxicity

Direct toxicity is damage to cellular macromolecules that can result in cell death or loss or change in cell phenotype (Liebler and Guengerich, 2005). As previously mentioned, parent drug can be responsible for direct toxicity; however, more often than not, it is a reactive metabolite that is the culprit. Drug reactive metabolites are often electron deficient and therefore, electrophilic in nature, for example, epoxides and quinones. Reactive metabolites can bind covalently to cellular proteins, lipids and DNA, causing biochemical changes, changes or loss of protein function, GSH depletion, oxidative stress, redox changes and lipid peroxidation. These events may then directly affect normal functioning of cellular organelles which can ultimately lead to cell death (Liu and Kaplowitz, 2007).

The work of James and Elizabeth Miller provided the first evidence of metabolism to reactive metabolites and subsequent covalent binding during their research into the carcinogenicity of aminoazo dyes (Miller, 1970, Miller, 1994). In 1973, a series of papers from Brodie, Gillete and co-workers elucidated the relationship between acetaminophen (APAP) metabolism, covalent binding and hepatotoxicity (Mitchell *et*

al., 1973a). At therapeutic doses, around 55% and 30% of renally excreted metabolites are as the glucuronide and sulphate conjugates, respectively (Howie *et al.*, 1977). A small proportion of the therapeutic dose (5%) is bioactivated to the electrophilic intermediate *N*-acetyl-*p*-benzoquinonimine (NAPQI; Dahlin *et al.*, 1984). NAPQI is readily detoxified by GSH conjugation and is excreted in the urine as a cysteine or mercapturate product (Mitchell *et al.*, 1973b). In cases of overdose, low capacity sulphation pathways become saturated and a greater fraction of the dose undergoes glucuronidation and oxidation. Under these conditions, NAPQI accumulates and cellular stores of GSH become depleted due to the shift in NAPQI formation and GSH synthesis (Figure 1.8). NAPQI irreversible binding to critical proteins ensues (Mitchell *et al.*, 1973a, Mitchell *et al.*, 1973b, Jollow *et al.*, 1973, Potter *et al.*, 1973, Reid *et al.*, 2005) resulting in necrotic cell death of hepatocytes through mitochondrial destruction (Donnelly *et al.*, 1994). Necrotic cells release damage-associated molecular pattern (DAMP) molecules which are thought to alert the immune system to dying cells (Figure 1.8; Scaffidi *et al.*, 2002, Kono and Rock, 2008).

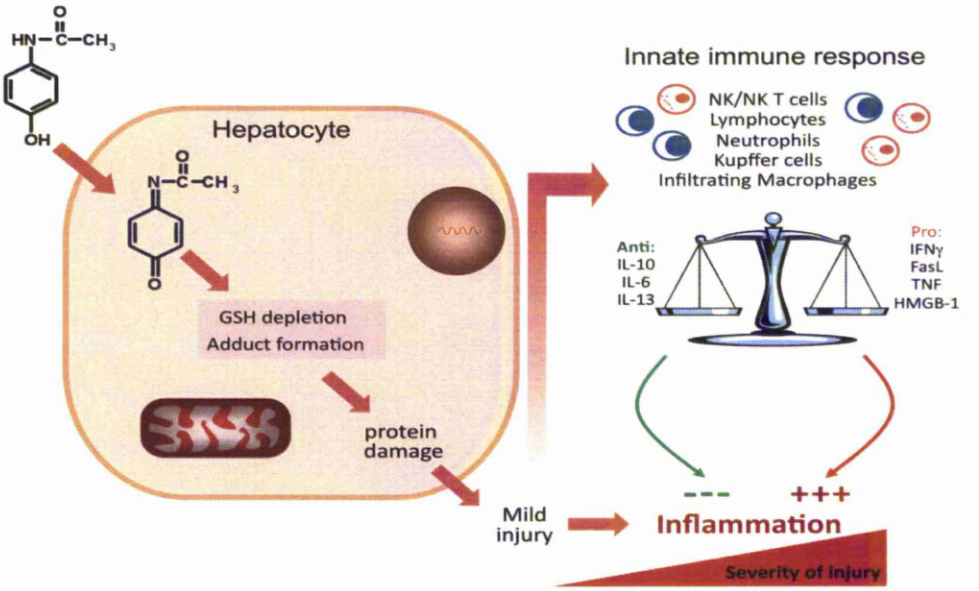

Figure 1.8: Bioactivation and toxicity of APAP. Schematic of the multi-step and multi-cellular processes involved in APAP-induced hepatotoxicity. Adapted from Kaplowitz, *et al* (2005).

1.4.2 Mechanisms of ADRS: immune-mediated toxicity

Some immune-mediated toxicities can be classed as on-target ADRs if they, as described earlier, are an exaggeration of the primary pharmacology of the offending drug. For instance, the immunosuppressant corticosteroids can increase risk of infection (Uetrecht, 2009). The liver is the most frequently affected organ by idiosyncratic ADRs, but skin, kidney and blood are also common targets. Additionally, idiosyncratic ADRs can present as generalised hypersensitivity or anaphylaxis (Park *et al.*, 2011). Although there is a lack of solid evidence, the majority of idiosyncratic ADRs are thought to be immune-mediated, based on clinical characteristics. Some current hypotheses regarding the mechanisms of idiosyncratic immune-mediated ADRs suggest that bioactivation of the parent drug to a reactive metabolite is the first step in the process, followed by binding to a native protein and causing an adaptive immune reaction towards the modified protein (Park and Kitteringham, 1990b). Although bioactivation is highly implicated in idiosyncratic ADRs, the situation is complicated by many other host factors, including genetics, disease state, sex and age, which will influence whether an ADR is experienced or not. Tienilic acid (TA), an antihypertensive, was withdrawn from the US market due to severe hepatotoxic secondary effects and renal toxicity (Zimmerman *et al.*, 1984). TA covalently binds to the enzyme that metabolises it, creating a neo-antigen that is recognized as foreign by the host. In patients suffering from TA-induced hepatitis, auto-antibodies called anti-liver kidney microsomal antibodies where detected in their serum (Homberg *et al.*, 1984).

There are currently three major hypotheses on the mechanism of immune-mediated toxicities that are considered when investigating these reactions (Figure 1.9). The hapten hypothesis proposes that when a reactive metabolite covalently binds to a protein, the protein is altered and so is seen as foreign by the host immune system and leads to an immune response (Park and Kitteringham, 1990b). The danger hypothesis theorizes that foreign proteins alone do not generate an immune response and that a second 'danger signal', possibly from stressed or damaged cells, is required to elicit an immune response (Matzinger, 2002). The pharmacological interaction (PI) hypothesis, unlike the previous two, suggests that bioactivation to a reactive metabolite is not essential to elicit an immune response; instead the drug molecule can bind directly to a receptor on an antigen presenting cell (Pichler, 2002).

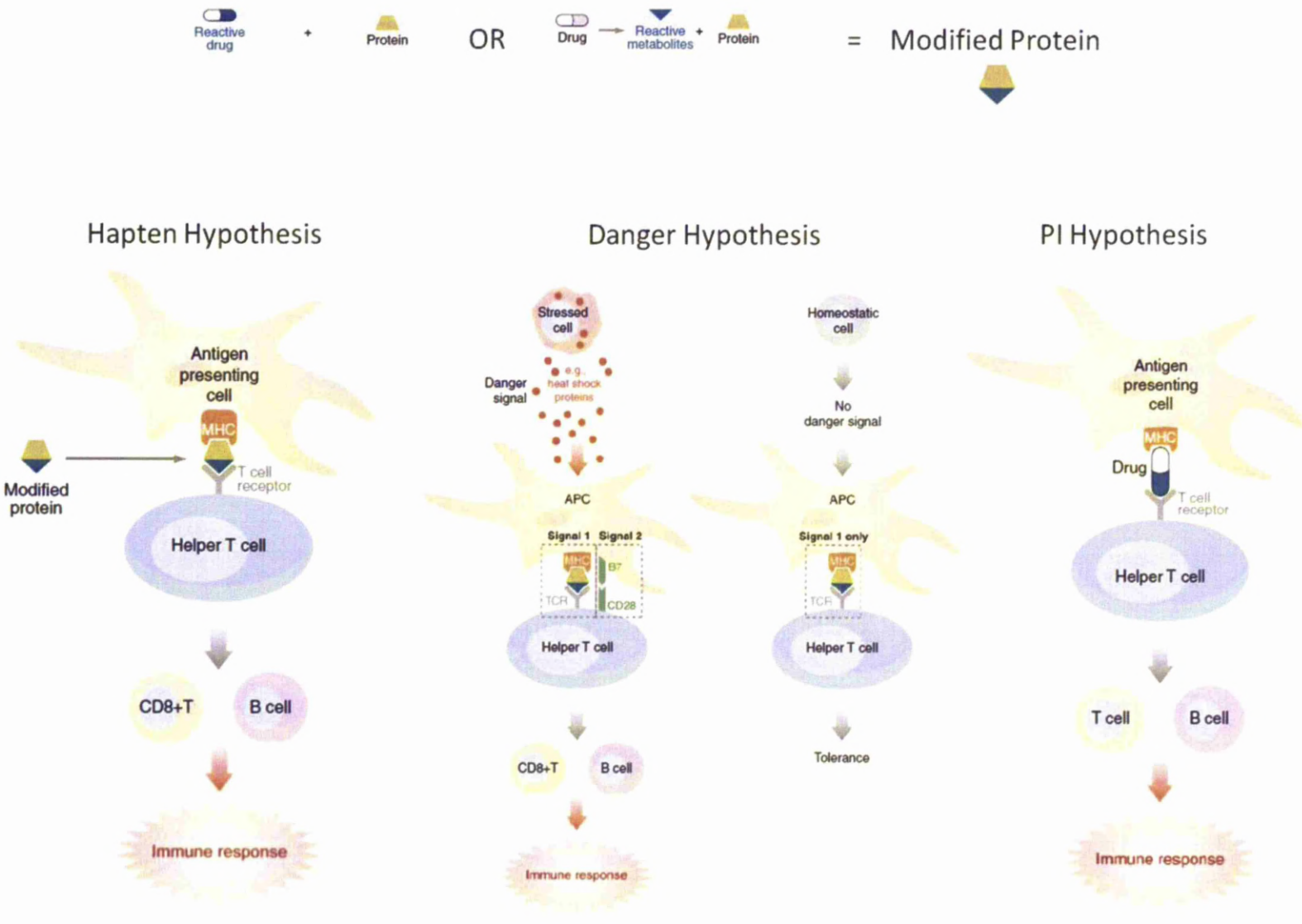

Figure 1.9: Current hypotheses for the mechanisms of drug-induced immune reactions. Adapted from Uetrecht et al. (2007).

1.4.3 Mechanisms of drug-induced liver injury

The liver is a frequent target of drug-induced toxicity; it is the main organ of drug metabolism and all orally administered drugs pass through the liver via the portal vein before reaching the systemic circulation. DILI has been linked to nearly 1000 drugs (Zimmerman, 1999). Approximately, 1 in 100 patients develop DILI during hospitalization when admitted to a department of medicine (Meier *et al.*, 2005). A prospective study, conducted over three years, in a region of France, determined that the incidence of DILI was 13.9 per 100,000 inhabitants (Sgro *et al.*, 2002). Most cases of DILI are idiosyncratic reactions (Kaplowitz, 2005, Björnsson, 2010). In terms of individual drugs, DILI is, overall, fairly rare; it occurs in between 1 in 10,000 to 1 in 100,000 (or less) of those exposed to a single drug (Björnsson, 2010, Larrey, 2002). Clinical trials typically have around 10,000 patients and therefore incidences of idiosyncratic DILI are not likely to emerge until the post-marketing phase (Larrey, 2002).

DILI can simulate almost all forms of acute and chronic liver injuries; it can present as acute or chronic hepatocellular hepatitis, fibrosis or cirrhosis, cholestasis, steatosis, sinusoidal and hepatic artery or vein damage, but DILI usually resembles acute hepatitis, cholestasis or mixed hepatitis/cholestasis (Björnsson, 2010, Kaplowitz, 2004, Holt and Ju, 2006). DILI is difficult to diagnose, clinicians rely on information such as, duration of latency to symptomatic presentation and the pattern of liver test abnormality to help make a diagnosis. Latency of idiosyncratic ADRs can give an indication as to the mechanism of the reaction; latency duration of around 1 to 8 weeks is common of most immune-mediated ADRs and those with a latency duration of up to 1 year are thought to be non-immune-mediated (Abboud and Kaplowitz, 2007, Pirmohamed *et al.*, 2007). Immune-mediated idiosyncratic DILI often presents with fever, rash and eosinophilia (Abboud and Kaplowitz, 2007). Liver tests showing increase levels of serum alanine transaminase (ALT) and aspartate transaminase (AST) are indicative of hepatitis, whereas increases in serum alkaline phosphatise (AP) levels are indicative of cholestasis.

Hepatocellular death, via either apoptosis or necrosis, underlies the clinical manifestations of drug induced hepatitis. Apoptosis is a form of programmed cell death, where the cell undergoes a series of biochemical changes; the cell shrinks and

condenses through disassembly of the cytoskeleton and nuclear envelope, and the nuclear DNA fragments (Alberts *et al.*, 2002). Caspases (cysteine-dependent aspartate specific proteases) are responsible for the disassembly of the cytoskeleton; initiator caspases undergo self-cleavage and initiate a cascade of caspase activation. Necrosis, on the other hand, is regarded as 'uncontrolled' cell death (Alberts *et al.*, 2002); although there is increasing evidence to suggest that necrosis is just another kind of programmed cell death (Festjens *et al.*, 2006). Loss of membrane integrity occurs early in necrosis and cellular contents leak causing an inflammatory response (Kono and Rock, 2008).

Cholestasis is the blockage of bile flow from the liver to the duodenum. Damage to hepatocytes (especially on the canilicular membrane), inhibition of biliary transporters (or genetic defects altering function) or damage to bile ductules and bile ducts can inhibit bile flow and lead to intracellular accumulation of potentially harmful bile constituents and drug or drug metabolites, resulting in the development of cholestatic liver cell damage (Velayudham and Farrell, 2003, Pauli-Magnus and Meier, 2006). Drug-induced cholestasis can be either be 'bland', that is no indication of inflammation or necrosis, or be accompanied by bile duct injury and inflammation (Abboud and Kaplowitz, 2007). The majority of clinically overt cholestatic and mixed hepatitis/cholestatic reactions are associated with bile ductular injury and inflammation (Abboud and Kaplowitz, 2007). Numerous drugs which cause cholestatic DILI in man inhibit BSEP activity *in vitro*, therefore potent BSEP inhibition by marketed drugs is a potential risk factor for idiosyncratic cholestatic DILI in man (Thompson *et al.*, 2011)

1.4.4 Manifestations of drug-induced skin reactions

The skin is the most frequent target of immune-mediated ADRs; they affect 2-3% of hospitalised patients (Bigby *et al.*, 1986), however more severe skin reactions are much less frequent (Figure 1.10). ADRs affecting the skin can range from mild rashes to life-threatening conditions such as toxic epidermal necrolysis (TEN; Nigen *et al.*, 2003, Merk *et al.*, 2007). The most common drugs that cause ADRs associated with the skin include antibiotics, sulphonamides and quinolones, anticonvulsants and non-steroidal anti-inflammatorys (NSAIDS; Lerch and Pichler, 2004). The skin has

the ability to bioactivate drugs; it contains both phase I and phase II drug metabolizing enzymes, including some of those found in the liver and additional isoforms that are not (Du *et al.*, 2006, Bergström *et al.*, 2007). The skin is also immunologically functional, containing antigen presenting cells, Langerhan's cells and dentritic cells (Park *et al.*, 1998, Merk, 2009). Immune-mediated ADRs are therefore possible in the skin, based on the hypothesis that a drug will be bioactivated and bind to cellular proteins creating an antigen that the host will raise an immune response to.

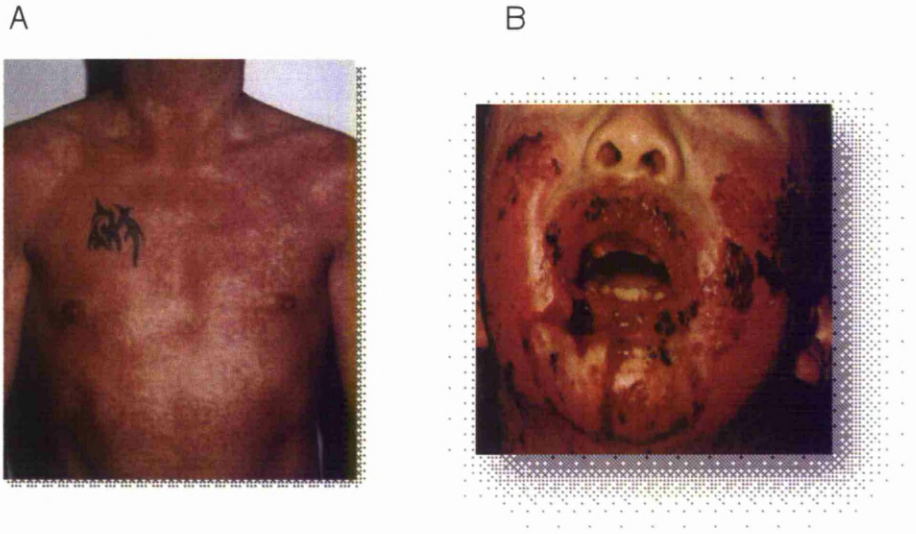

Figure 1.10: Examples of severe drug-induced skin reactions. Skin rashes caused by (A) abacavir and (B) sulphamethoxazole

95% of drug-induced skin reactions are exanthematous or maculopapular drug eruptions and tend to develop within 1 to 2 weeks of drug treatment (Uetrecht, 2009, Merk, 2009). Immunohistological examination of this type of lesion shows mild to moderate mononuclear cell infiltrate with some eosinophils (Lerch and Pichler, 2004). T-cells predominate and most are activated and express human leukocyte antigen DR (major histocompatilibility complex (MHC) class II) (Lerch and Pichler, 2004, Brönnimann and Yawalkar, 2005). Increased numbers of CD4+ and CD8+ T-cells containing the cytotoxic granule proteins, perforin and granzyme B are found in the dermo-epidermal junction or in the epidermis, along with signs of keratinocyte cell damage (Yawalkar *et al.*, 2000). Granule proteins can induce cell death through

pore formation on the target cell membrane. Various cytokines and chemokines are upregulated in these types of maculopapular drug reactions (Yawalkar *et al.*, 2000, Posadas *et al.*, 2000, Posadas *et al.*, 2002, Hari *et al.*, 1999).

More severe ADRs affecting the skin include Stevens-Johnson syndrome (SJS) and toxic epidermal necrolysis (TEN) and have mortality rates of 5% and 30% respectfully (Roujeau and Stern, 1994). Most cases of TEN are drug-induced (Park *et al.*, 1998). In early stages, these more severe ADRs, resemble maculopapular eruptions except patients complain of painful skin (Uetrecht, 2009). As these conditions progress mucus membranes are affected and blisters form followed by skin detachment. Histological examination of the skin of patients with TEN and SJS reveal mainly CD8+ T-cells, suggesting that apoptosis is initiated by cytotoxic T lymphocytes (Nassif *et al.*, 2004, Greenberger, 2006). Keratinocytes in SJS and TEN express the apoptosis inducing Fas receptor and its ligand (Murata *et al.*, 2008).

1.5 TOXICITY HAZARD AND RISK ASSESSMENT AND BIOMARKERS

It stands to reason that research into systems that can detect potential human hazard of NCEs has been of high priority, given the fact that many serious idiosyncratic ADRs are not observed until the drug is used by a much larger population. However, it remains that there are no accepted methods for the detection of idiosyncratic reactions in preclinincal or *in vitro* systems (Park *et al.*, 2005). The two conventional methods for the detection of drug bioactivation in both academic and industrial settings are (1) identification of thioether adducts of drugs and (2) the detection of covalent binding of the drug to protein or DNA. Means of elucidating the downstream effects of bioactivation are currently rare; much hope has been placed on the development of biomarkers and animal models of disease and ADRs to improve the translatability of hazard potential throughout the development process and into the clinic.

1.5.1 Toxicity hazard and risk assessment

In order to drive attrition to an earlier stage in the drug development process, early application of preclinical toxicity assessment has been implemented, making it possible to incorporate an assessment of structure-activity relationships (SARs) and toxicity issue management into drug design (Kramer *et al.*, 2007, Stevens and Baker, 2009). Preclinical safety testing is designed to assess the potential of NCEs to cause toxicity in humans and to determine the dose-limiting toxicity, and whether this toxicity is reversible and if it can be monitored clinically (Stevens and Baker, 2009). If an insight into the mechanisms of these toxicities can be gained from these studies, then rational extrapolations can be made to humans and potential risk can be evaluated (Stevens and Baker, 2009, Stevens, 2006).

In vitro toxicity assessment aims to identify any development-limiting toxicities; that is those with no acceptable margin of safety (Kramer *et al.*, 2007). *In vivo* toxicity assessment identifies dose-limiting toxicities that, taken with other preclinical findings, are used to develop a margin of safety based on the ratio of the no observed adverse effect level by the predicted human efficacious dose (Kramer *et al.*, 2007, Stevens and Baker, 2009). The standard regimen for preclinical toxicity assessment is conducted in at least two species (one rodent and one non-rodent) at doses many multiples of the intended dose in humans, for at least two weeks (Peters, 2005). NCEs are tested for indications of potential genetic toxicity, DDIs, adverse primary or secondary pharmacological effects and metabolite-mediated toxicity (Kramer *et al.*, 2007). A retrospective analysis of concordance of preclinical toxicity data with human toxicity data revealed that 70% of human toxicities were predicted by preclinical animal studies in one or more species (Olson *et al.*, 2000). Of the human toxicities analysed only 4 were considered to be idiosyncratic. The research did not highlight those preclinical studies that show toxicity in animals but may have been safe in human studies. Drugs registered before the introduction of extensive toxicity testing, may have shown hazard signals in preclinical toxicity assessments, but are used safely in humans. Although the predictability of human toxicity through preclinical toxicity assessment is good (70%; Olson *et al.*, 2000), it remains that 30% of on-target toxicities are not predictable and, in addition, idiosyncratic ADRs are not reproducible in animal models.

In light of the increasing evidence to suggest that reactive metabolite formation is an initiating factor in many on-target and idiosyncratic ADRs, the Food and Drug Administration (FDA) have recently released 'Metabolites in Safety Testing (MIST)' guidance in 2008 and 'M3(R2) Nonclinical Safety Studies for the Conduct of Human Clinical Trials and Marketing Authorization for Pharmaceuticals'. These guidelines highlight the importance of the identification and quantification of drug metabolites across human and preclinical species. If a metabolite is identified in man that is produced disproportionately to that in a preclinical species, then the FDA MIST guidelines suggest further investigation into these metabolites is required (FDA, 2008). That may be through toxicity assessment of a species that produces similar levels of the metabolite as the human or synthesising the metabolite and administering it directly. The guidelines also suggest that human metabolites that are formed at, or greater than, 10% of the parent drug systemic exposure at steady state, should be treated with concern (FDA, 2008). Identification of reactive metabolite by the use of chemical trapping reagents, such as GSH or cyanide, in microsomal incubations can provide information on the structure of the reactive metabolite through analysis by tandem mass spectrometry (LC-MS/MS) and/or nuclear magnetic resonance (Evans *et al.*, 2004).

Based on the wealth of evidence to suggest that many direct, and immune-mediated toxicities, are caused through reactive metabolite covalent binding to cellular macromolecules, research at Merck proposed a covalent binding threshold criteria in the safety aspect of drug development (Evans *et al.*, 2004). Using levels of covalent binding of known hepatotoxins to microsomal protein, an upper-level of accepted covalent binding was suggested, 50 pmol drug equivalent per mg of protein (Evans *et al.*, 2004). In order to test this concept, 18 known hepatotoxic and non-hepatotoxic compounds were tested for levels of covalent binding in human liver microsomes (Obach *et al.*, 2008). Of the 18 compounds tested, 14 demonstrated some extent of covalent binding; of the 4 that did not, 2 were hepatotoxins and 2 were non-hepatotoxins (Obach *et al.*, 2008). Recently covalent binding studies conducted in human hepatocytes have provided a means of discriminating between hepatotoxins and non-hepatotoxins by incorporating factors such as daily dose and intrinsic clearance (Bauman *et al.*, 2009; Nakayama *et al.*, 2009). Microsomes have been the system of choice to study covalent binding of drugs, however recent studies suggest

that human hepatocytes might provide a more clinically relevant, metabolically complete system (Bauman *et al.*, 2009; Nakayama *et al.*, 2009). Although the detection of a bioactivation process *in vitro* is relatively straightforward, the downstream consequences *in vivo* are poorly understood; the identities of macromolecular targets, to which bioactivated drugs bind and for which binding results in toxicity, have not been established and remain an area of active research (Obach *et al.*, 2008).

1.5.2 Animal models of ADRs

There are very few animal models of idiosyncratic ADRs; in order for an animal model to be useful, the mechanism of toxicity must resemble the mechanism in humans (Shenton *et al.*, 2004). The mechanisms of most ADRs in humans remain unknown, and therefore, the usefulness of animal models is based upon comparisons of certain characteristics of the reaction seen in humans (Shenton *et al.*, 2004). An animal model also has to have a biological or chemical endpoint that can be measured and that is similar to the clinical appearance of the ADR (Shenton *et al.*, 2004). Most preclinical toxicity assessment is conducted in healthy animals; it may be that performing toxicity assessment in genetically modified animals or animal models of disease would more effectively highlight idiosyncratic ADRs.

1.5.3 Biomarkers

A biomarker is defined as 'a characteristic that can be objectively measured as an indicator of normal biological processes, pathological processes or a pharmacological response to a therapeutic intervention', by the National Institutes of Health (NIH) Biomarkers Definitions Working Group (Atkinson A.J. *et al.*, 2001). Development of biomarkers aims to allow earlier and more robust measures of drug safety and efficacy to get safe and effective drugs to the market (Colburn and Keefe, 2003). In terms of ADRs, biomarkers that are predictive of a toxicological outcome and can be used from *in vitro* toxicity assays to ADR diagnosis and management in the clinic would be highly desirable.

In light of the mechanisms implicated in the development of ADRs, a number of genetic, chemical and molecular markers could potentially be used in the assessment of drug safety. It is likely that a 'biomarker panel' would be used to describe or diagnose an ADR rather than a single biomarker (Colburn and Keefe, 2003). Ideally biomarkers would be: organ specific, reflect the type and degree of injury, predictive (i.e. show elevation compared to normal without irreversible tissue damage), non- or minimally-invasive (found in blood or urine), assayed rapidly, transferable and have a low baseline variability across the population (Antoine *et al.*, 2009a). Novel biomarkers aim to improve drug discovery and development and drug safety through to the clinic, and should be used alongside the gold-standard biomarkers such as serum alanine transaminase (ALT) and aspartate transaminase (AST) for drug-induced hepatitis and serum alkaline phosphatase (AP) for drug-induced cholestasis (Table 1.3; Antoine *et al.*, 2009a).

A common mechanism for the detoxification of reactive metabolite occurs via GSH conjugation (Williams *et al.*, 2002, Williams and Naisbitt, 2002). The identification of drug metabolite-GSH adducts in a preclinical setting is sometimes treated as a hazard signal as it is indicative of reactive metabolite formation, conversely it could be argued that identification of a GSH adduct is an indication of an effective detoxification system. Human urinary mercapturates (breakdown products of GSH-adducts) have been used as biomarkers of human exposure to reactive species (Seutter Berlage *et al.*, 1977). More recently, in the light of improved bioanalytical techniques, drug-mercapturates have been used in the quantitative assessment of *in vivo* bioactivation. Some compounds can be metabolized to several GSH adducts (Amore *et al.*, 1997, Madden *et al.*, 1996, Bu *et al.*, 2007, Rousu *et al.*, 2009, Wang *et al.*, 2009a), suggesting that careful analysis of a drugs metabolites is necessary to identify a thioether derivative suitable for use as a biomarker of metabolic activation. Amongst the human pharmaceuticals the mercapturate conjugates of APAP (Siegers *et al.*, 1984), phenacetin (Veronese *et al.*, 1985), felbamate (Dieckhaus *et al.*, 2002) and valproic acid (Gopaul *et al.*, 2003) have been used for the quantitative assessment of *in vivo* bioactivation.

Proteins released from apoptotic and necrotic cells have been used as biomarkers of drug-induced cell death (Antoine *et al.*, 2009b). Keratins are intermediate filament proteins expressed by epithelial cells responsible for cell structure and integrity.

During necrosis full length keratin-18 (K18) is released passively into the serum (Schutte *et al.*, 2004). In Fas-mediated apoptosis, phophorylation and cleavage of K18 occur during structural rearrangement and a 'caspase-cleaved' K18 accumulates in the blood over time (Schutte *et al.*, 2004). Serum quantification of casapase-cleaved K18 and full length K18 have been used for markers of apoptosis and necrosis, respectively, during pharmacodynamic therapeutic drug monitoring in patients and animal models (Cummings *et al.*, 2006).

High mobility group box protein 1 (HMGB-1) is a nuclear binding protein that has pro-inflammatory activity and targets toll-like receptors (TLR) and the receptor for advanced glycation end-products (RAGE) on target cells (Hori *et al.*, 1995, Park *et al.*, 2004). HMGB-1 is thought to have a role in alerting the innate immune system to dying cells (Scaffidi *et al.*, 2002, Kono and Rock, 2008), which will be a key determinant in the extent of tissue damage. Two forms of HMGB-1 exist; a hyper-acetylated form is released from activated innate immune cells and a hypo-acetylated form is passively released from necrotic cells (Scaffidi *et al.*, 2002). Anti-HMGB-1 antibodies inhibit the inflammatory response associated with APAP hepatotoxicity and endotoxin lethality *in vivo* (Scaffidi *et al.*, 2002, Wang *et al.*, 1999b). An insight to the level of organ damage, the mechanism of cell death and the involvement of the innate immune system might be gained by the quantification of the molecular forms of both K18 and HMGB-1.

Biomarker	Established /novel	Organ specific	Mechanism specific	Compartment	Reference
Alanine amino-transferase 1 (ALT1)	Established	Yes – ALT1	No – Necrosis (leakage)	Blood	(Lindblom *et al.*, 2007)
Glutamate dehydrogenase (GLDH)	Established	No	Yes – mitochondrial damage	Blood	(Carakostas *et al.*, 1986)
Sorbitol dehydrogenase (SDH)	Established	Relatively	No – Necrosis (leakage)	Blood	(Khayrollah *et al.*, 1982)
β-Hydroxy-cortisol	Established	Relatively	Yes - CYP3A4 metabolism	Urine	(Park and Kitteringham, 1990a)
Drug mercapturate	Established / novel	Relatively	Yes – potential reactive metabolite	Urine	(Wagner *et al.*, 2007)
Keratin 18 (K18) – fragmented	Novel	No (epithelial cells only)	Yes – apoptosis	Blood	(Cummings *et al.*, 2006)
Keratin 18 (K18) – full length	Novel	No (epithelial cells only)	Yes – necrosis	Blood	(Cummings *et al.*, 2006)
Ophthalmic acid	Novel	No	Yes – oxidative stress	Blood / urine	(Soga *et al.*, 2006)
High mobility group box protein 1 (HMGB1)	Novel	No	Yes – necrosis and inflammation	Blood	(Scaffidi *et al.*, 2002)
Cytochrome C	Novel	No	Yes – mitochondrial damage	Blood / urine	(Miller *et al.*, 2008)
Serum F protein (HPD)	Novel	Relatively	No – Necrosis (leakage)	Blood	(Foster *et al.*, 1989)
Arginase 1	Novel	Relatively	No – Necrosis (leakage)	Blood	(Ashamiss *et al.*, 2004)
Malate dehydrogenase	Novel	Relatively	Yes – mitochondrial damage	Blood	(Zieve *et al.*, 1985)
Purine nucleoside phosphorylase (PNP)	Novel	Relatively	No – Necrosis (leakage)	Blood	(Ohuchi *et al.*, 1995)
Micro RNAs (miRNA)	Novel	Yes – depending on coded protein	No- potential	Blood	(Wang *et al.*, 2009b)
Paraoxonase 1 (PON-1)	Novel	Relatively	Yes – liver function	Blood	(Meneses-Lorente *et al.*, 2004)

Table 1.3: Summary of established and novel biomarkers to DILI with organ or mechanism specificity for non-invasive assessment not routinely used as part of a standard clinical liver function test. Taken from Antoine *et al.* (2009).

1.6 FUROSEMIDE INDUCED HEPATOTOXICITY

Furosemide (FS; 4-choloro-N-furfuryl-5-sulphanoyl-anthranilic acid) is a potent loop diuretic frequently used in the treatment of edematous states associated with cardiac, renal, and hepatic failure and for the treatment of hypertension (Boles Ponto and Schoenwald, 1990).The pharmacological action of furosemide has been attributed to the inhibition of the active reabsorption of Cl^- ions in the thick ascending limb of the loop of Henle by binding the Cl^- binding site of the $Na^+/2Cl^-/K^+$ co-transport system (Burg *et al.*, 1973, Vree and Van Der Ven, 1999). At therapeutic doses, furosemide is not toxic to humans, although it has been associated with jaundice and hypersensitivity (Noce *et al.*, 2000), and there may be a potential risk of hepatotoxicity when administered in large doses to patients with acute and chronic renal failure (Mitchell *et al.*, 1974). The drug has been marketed in the US since 1966 (Greenblatt *et al.*, 1977). Furosemide has been shown to produce massive hepatic centrilobular necrosis in mice by a mechanism independent of its diuretic action (Mitchell *et al.*, 1974) and therefore represents an important tool as a chemical with a toxicological endpoint to study the relationship between chemical structure and toxicity.

1.6.1 Biotransformation of furosemide

The metabolic fate of furosemide has been investigated a number of times over the years and the identification of metabolites has been the subject of much controversy. It has been demonstrated that furosemide forms an acyl-glucuronide in the plasma and urine of humans (Beermann *et al.*, 1975, Beermann *et al.*, 1977, Benet, 1979, Perez *et al.*, 1979, Smith *et al.*, 1980, Kerremans *et al.*, 1982, Smith and Benet, 1983). More recently the furosemide glucuronide has been identified in the bile of furosemide treated rats and mice (Williams *et al.*, 2007), although the glucuronide has not been identified in the urine of rats (Hammarlund-Udenaes and Benet, 1989, Prandota and Pruitt, 1991). A number of studies have shown that in humans approximately 13 – 17% of an *i.v.* dose of furosemide is excreted as FS-glucuronide in the urine (Smith *et al.*, 1980, Andreasen *et al.*, 1981, Waller *et al.*, 1982, Verbeeck *et al.*, 1982). However variations on this amount have been published; Perez *et al.* (1979) estimated 3-41% of the furosemide dose was excreted in the urine as FS-

glucuronide in patients with acute pulmonary edema. Andreasen *et al.* (1977) found that in healthy volunteers this figure was only 2% and in subjects taking furosemide 6 months prior to the study this figure increased to around 16%. Urinary excretion of furosemide has been demonstrated as the main route of elimination in humans and it appears that furosemide glucuronidation occurs primarily in the kidney (Kerdpin *et al.*, 2008). In the rat, of the total dose excreted in the bile (21.2 ± 2.6%) 12.8 ± 1.8% was excreted as the FS-glucuronide (Williams *et al.*, 2007).

A more controversial metabolite is the N-dealkylated furosemide metabolite (4-chloro-5-sulphamoyl-anthranilic acid; CSA in literature) first identified in 1964 by Haussler *et al.* It has been subsequently been identified in the urine of dogs, monkeys (Yakatan *et al.*, 1976) and in humans (Prandota and Pruitt, 1975, Andreasen *et al.*, 1978). However a number of groups failed to find evidence of this metabolite in humans (Beermann *et al.*, 1975, Smith *et al.*, 1980, Kerremans *et al.*, 1982, Branch *et al.*, 1977). After employing an acidic extraction process Smith *et al.* (1980) and Perez *et al.* (1979) were able to produce the N-dealkylated furosemide metabolites leading them to believe that the metabolite is an analytical artefact. Supporting this argument is the identification of a photodegredation product of furosemide which has a similar retention time to N-dealkylated furosemide under certain analytical conditions (Hammarlund-Udenaes and Benet, 1989). A recent study identified the N-dealkylated furosemide metabolite in the bile of rats and mice without the use of an acid extraction method providing clear evidence that it is a genuine metabolite in these species (Williams *et al.*, 2007). Figure 1.11 shows the metabolism of furosemide *in vivo*.

1.6.2 Bioactivation and toxicity of furosemide

At therapeutic doses, furosemide is not toxic to humans, although it has been associated with jaundice and hypersensitivity (Noce *et al.*, 2000), and there may be a potential risk of hepatotoxicity when administered in large doses to patients with acute and chronic renal failure (Mitchell *et al.*, 1974). Due to the risk of hypotension, the administration of furosemide is carefully controlled and generally only small doses are required due to its high potency. Furosemide is known to cause a decrease in hepatic blood flow by a mechanism dependant on blood volume contraction

(Gaffney *et al.*, 1979), but the hepatotoxic effect is not considered to be an inverse result of diuretic action.

Furosemide has been shown to produce massive hepatic centrilobular necrosis in mice by a mechanism independent of its diuretic action (Mitchell *et al.*, 1974). The hepatocellular damage caused by furosemide is postulated to be the result of CYP450 enzyme-mediated formation of a toxic metabolite that binds covalently with hepatic macromolecules both *in vitro* and *in vivo* (Mitchell *et al.*, 1974, Mitchell *et al.*, 1976). It was found that furosemide binds covalently to microsomal protein, and that the level of binding parallels the severity of necrosis. This binding is decreased by cysteine and GSH, and also by the presence of P450 enzyme inhibitors, suggesting bioactivation of the furosemide molecule (Mitchell *et al.*, 1974, Williams *et al.*, 2007). Early work suggested that an epoxide of furosemide is responsible for the hepatotoxicity observed in the mouse. The level of covalent binding was found to be increased in the presence of an epoxide hydrolase inhibitor (Wirth *et al.*, 1976). More recently, bioactivation of the furan ring was demonstrated by the characterization of three key novel metabolites of furosemide from *in vivo* and *in vitro* studies: FS γ-ketocarboxylic acid, FS-SG conjugate, and a mixed *N*-acetyl lysine and *N*-acetyl cysteine conjugate (Williams *et al.*, 2007). The formation of a FS γ-ketocarboxylic acid *in vivo* is suggestive of formation of an epoxide intermediate (Figure 1.11). These studies provide evidence to conclude that the reactive metabolite of furosemide is an epoxide. Williams *et al*, (2007) also show the reactive metabolite binds covalently to murine hepatic protein; this does not occur in rats, but is excreted in the form of a GSH conjugate, suggesting a possible safety mechanism exists in the rat to protect from furosemide induced hepatotoxicity (Williams *et al.*, 2007). As well as species differences in the balance of bioactivation and bioinactivation, it is possible that furosemide accumulation in the liver due to impaired clearance might also be a factor in development of hepatotoxicity in the mouse. Work conducted by Spitznagle, *et al.* (1977) indicated that saturation of the biliary excretion of furosemide, following a large dose of furosemide or pretreatment with sulfobromophthalein (BSP), is closely associated with the appearance of liver necrosis in the mouse and of furosemide metabolites covalently bound to liver proteins.

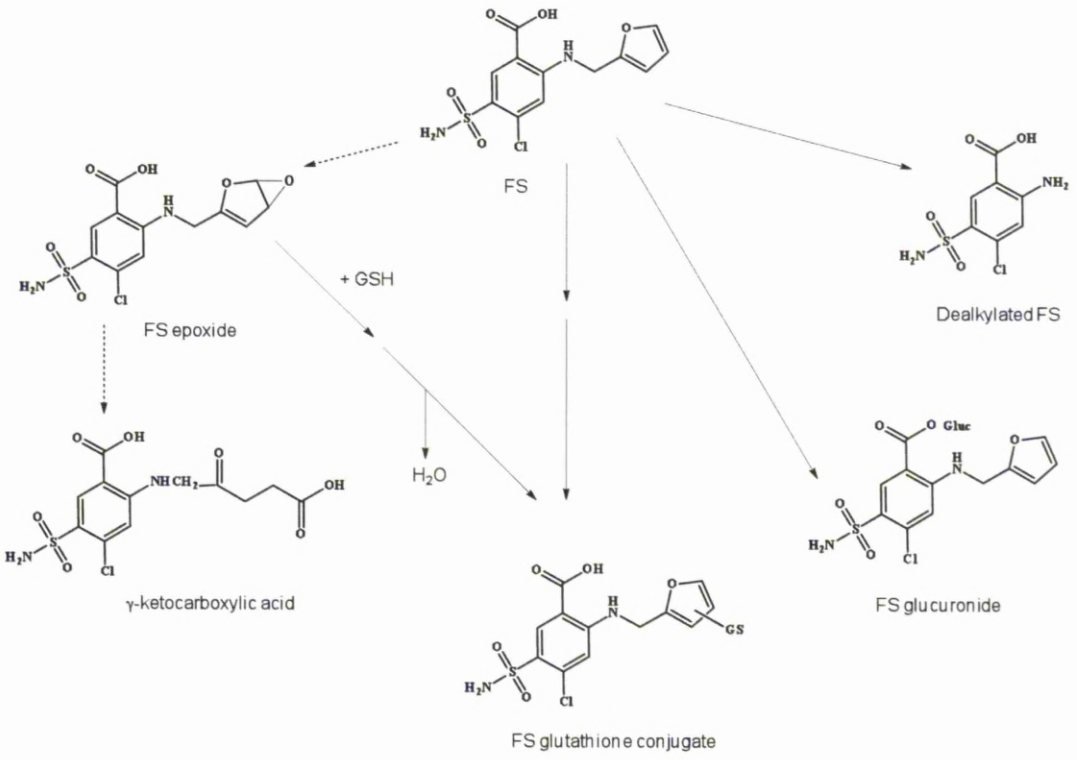

Figure 1.11: Major pathways of metabolism of FS *in vivo*. Broken arrows show postulated pathway for the formation of g-ketocarboxylic acid via a reactive furosemide epoxide intermediate (adapted from Williams *et al.* (2007)).

1.7 NEVIRAPINE

Nevirapine (NVP), used in the treatment of HIV-1 infection, was the first non-nucleoside reverse transcriptase inhibitor (NNRTI) to be approved by the FDA. Both nucleoside and non-nucleoside RTIs inhibit the same target, the reverse transcriptase enzyme. Nucleoside RTIs bind at the enzymes active site whereas NNRTIs bind within a pocket termed the NNRTI pocket and inhibit both the RNA- and the DNA-dependent DNA polymerase activities (De Clercq, 2004). Nevirapine is not effective against HIV-2 as the pocket of the HIV-2 reverse transcriptase enzyme has a different structure. Nevirapine is used widely in developing countries as it is inexpensive and does not require refrigeration. Nevirapine is associated with clinically restrictive adverse effects, namely, skin reactions and hepatotoxicity, which can occur either simultaneously or separately. Although nevirapine is highly

effective, the incidence of severe or life-threatening hepatoxicity has lead to the FDA giving a black-box warning.

1.7.1 Metabolism and bioactivation of nevirapine

Nevirapine is metabolised to a number of stable metabolites in humans by CYP3A4 and CYP2B6 (Erickson *et al.*, 1999). Nevirapine also induces activity of these enzymes and therefore, its own metabolism. Stable metabolites of nevirapine include a number of hydroxylated metabolites; 2-OH NVP, 3-OH NVP, 8-OH NVP and 12-OH NVP (Riska *et al.*, 1999). These hydroxylated metabolites undergo glucuronidation in phase II metabolism and are excreted in the urine. 12-OH NVP is further metabolised to form 4-carboxy NVP (Riska *et al.*, 1999).

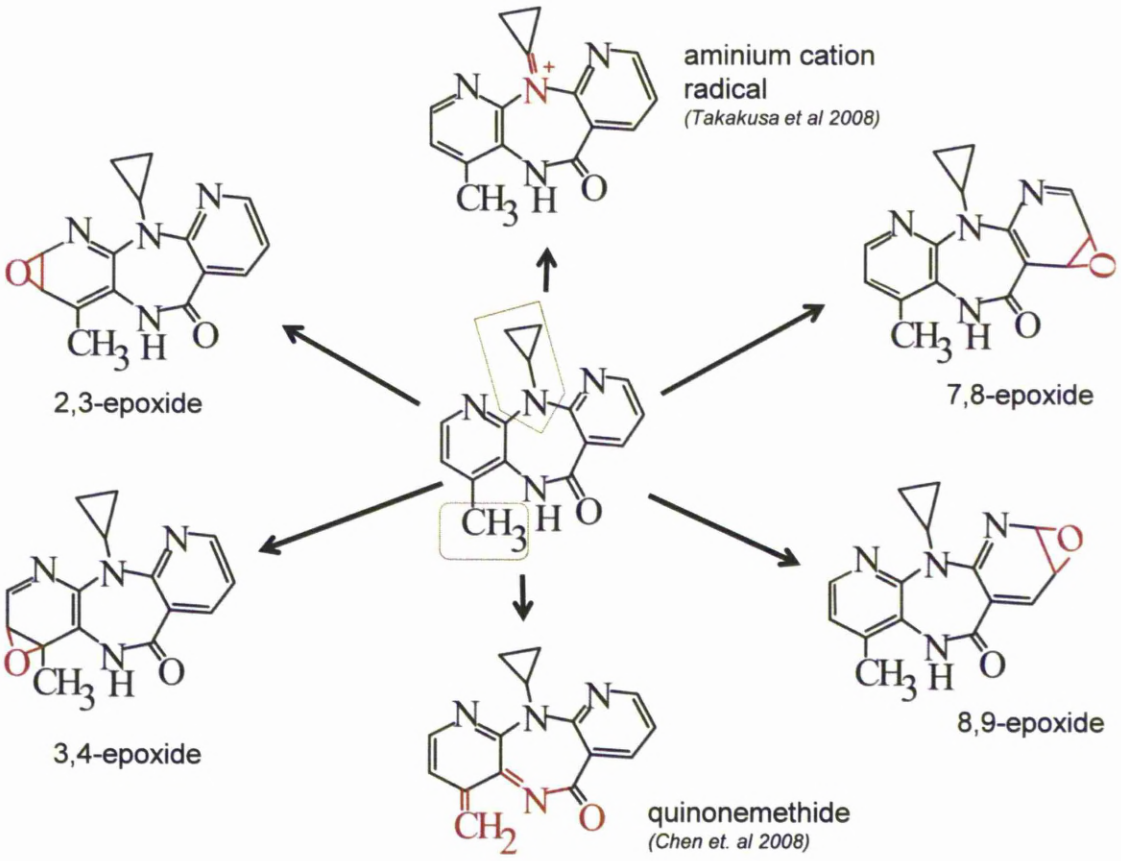

Figure 1.12: Potential reactive metabolites of nevirapine. Potential toxicophores are highlighted by a box.

Nevirapine has the potential to undergo metabolism to various reactive metabolites (Figure 1.12). 12-OH NVP is a substrate for sulphotransferase in rats (Chen *et al.*, 2008), and it has been proposed that the sulphate ester dissociates to form reactive quinone intermediate (Uetrecht, 2006, Chen *et al.*, 2008). Hydroxyheteroaryl metabolites are potential precursors of reactive quinone imines (Wen *et al.*, 2009). The cyclopropylamine group has the potential to be bioactivated to an aminium cation radical via N-dealkylation (Takakusa *et al.*, 2008). Nevirapine could also form one or more heteroarene epoxide metabolites in either of the pyridine rings. A single GSH adduct was identified in HLM and incubations with recombinant CYP 3A4 (Wen *et al.*, 2009) and nevirapine was shown to bind covalently to RLM (Takakusa *et al.*, 2008). Antunes *et al.* (2009) demonstrated the reactivity of 12-sulphoxy nevirapine by formation of multiple DNA adducts in reactions with 12-mesyloxy NVP.

1.7.2 Nevirapine-induced ADRs

Nevirapine treatment is associated with two clinically restrictive adverse effects; skin reactions and hepatotoxicity (Figure 1.13; (Pollard *et al.*, 1998)). These reactions can occur simultaneously or one without the other (Claes *et al.*, 2004, Drummond *et al.*, 2006, Vitezica *et al.*, 2008). The most common adverse event caused by nevirapine is skin rash, which occurs in around 16% of patients usually (65%) within the first 6 weeks of treatment (Pollard *et al.*, 1998, Phanuphak *et al.*, 2007). Severe and life-threatening skin rash, in the form of Steven-Johnson syndrome (SJS) and toxic epidermal necrolysis (TEN), occurs in 0.3–1% of patients taking nevirapine (Pollard *et al.*, 1998, Claes *et al.*, 2004, Fagot *et al.*, 2001). Serum liver enzymes are frequently elevated in patients taking nevirapine; between 5–15% experience asymptomatic increases, however 1-5% of patients experience symptomatic increases as a result of severe hepatotoxicity, including clinical hepatitis and hepatic failure (Pollard *et al.*, 1998, Phanuphak *et al.*, 2007, Chu *et al.*, 2010, Ciccacci *et al.*, 2010, Maniar *et al.*, 2006, Martínez *et al.*, 2001, De Maat *et al.*, 2002). Nevirapine-induced hepatotoxicity has been observed in HIV-infected (Maniar *et al.*, 2006, Buyse *et al.*, 2006) and non-HIV-infected patients (Patel *et al.*, 2004).

The nature of nevirapine-induced liver injury is not clear; cases of hepatotoxicity vary in terms of severity, time to onset and can occur with or without a hypersensitivity reaction (Buyse *et al.*, 2006, De Maat *et al.*, 2003). It is possible that the late-occurring reactions may be non-immune in nature, while those occurring in the first three months may have an immune pathogenesis (Pirmohamed *et al.*, 2007). The time of onset and the nature of the nevirapine-induced skin rash suggest that the reaction is immune-mediated and because of the low incidence it is likely that the reaction may be idiosyncratic (Pirmohamed *et al.*, 2007, Chen *et al.*, 2008). It has been strongly advocated that nevirapine-induced skin rash and hepatotoxicity are immune-mediated reactions (Pirmohamed *et al.*, 2007, Chen *et al.*, 2008); however, it is not clear whether this immune reaction is due to reactive metabolites or nevirapine itself. Nevirapine-reactive T cells have been observed in a patient with early-onset hepatitis in the absence of any cutaneous manifestations. The patients' T cells proliferated *in vitro* on exposure to nevirapine but not its stable metabolites (Drummond *et al.*, 2006). Claes *et al.* (2004) reported the rapid and full clinical recovery of a patient suffering from nevirapine-induced TEN and toxic hepatitis treatment following intravenous treatment with human immunoglobulins and N-acetylcysteine (NAC; 300 mg/kg/day continuous infusion). As NAC is a precursor of GSH, it is possible that replenishment of GSH stores helped to detoxify nevirapine reactive metabolite leading to reduction in toxicity.

Figure 1.13: Adverse effects of nevirapine treatment. Nevirapine treatment is restricted by severe skin reactions including SJS and TEN (A) and hepatotoxicity (B).

Due to the idiosyncratic nature of nevirapine-induced ADRs, it is not possible to predict which patients will suffer from hepatotoxicity or skin rash. Many studies have been conducted to identify patient groups who have increased risk of developing treatment-restricting ADRs. It is advised that, unless the clinical benefits outweigh the risks, nevirapine therapy is not recommended for woman with CD4 cell counts greater than 250 cells/mm^3 or men with CD4 cell counts of 400 cells/mm^3 (Kesselring *et al.*, 2009). The recommended dose of nevirapine, for adults and adolescents older than 16 years, is 200 mg once daily for the first 14 days (lead in dose), followed by 200 mg twice a day (Barreiro *et al.*, 2000). Nevirapine is contraindicated in patients with hypersensitivity to the active substance or to any of the excipients and should not be used in patients with severe hepatic impairment or raised liver enzymes pre-treatment (AST or ALT >5 x ULN). In a large study conducted over seven observation clinics, it was found that undetectable viral load in patients starting nevirapine treatment were less likely to develop hypersensitivity reactions (Kesselring *et al.*, 2009). Patients with Asian ethnicity were also found to have increased risk of developing nevirapine-induced hypersensitivity reactions (Kesselring *et al.*, 2009). Patients with a body-mass index (BMI) of less than 18.5 were found to have an increased risk of developing nevirapine-induced hepatotoxicity (Sanne *et al.*, 2005). Characteristics, of those patients who developed severe hepatotoxicity, vary greatly, and no specific risk factor was common to all (De Maat *et al.*, 2003).

1.7.3 Genetic polymorphisms associated with nevirapine-induced toxicity

A major area of research into nevirapine-induced ADRs has focused on genetic polymorphisms that predispose patients to skin rash and/or hepatotoxicity (Owen *et al.*, 2006). Often genetic polymorphisms in drug metabolising enzymes, drug transporters and the major histocompatibility complex are responsible for variation in toxic response to a drug (Owen *et al.*, 2006).

There are many polymorphisms of the CYP2B6 isoform that can affect the expression and activity of the enzyme (Zanger *et al.*, 2007); the G516T polymorphism is associated with reduced catalytic activity. The G516T polymorphism in CYP2B6 has been shown to significantly increase plasma

nevirapine levels in HIV-infected patients in Uganda (Penzak *et al.*, 2007). A 1.5 fold increase in plasma concentrations is observed in patients with the homozygous, variant allele (546G → T/T) compared to the common allele (516G → G/G; Penzak *et al.*, 2007). A similar study, of a Swiss patient cohort, found a 1.7 fold increase (Rotger *et al.*, 2005). The toxicological result of increased plasma nevirapine concentrations is not clear. Preliminary studies conducted in Spain found that a positive correlation exists between plasma nevirapine levels and the risk of liver toxicity; patients with plasma nevirapine concentrations above 6 μg/ml are thought to have a 92% risk of developing liver toxicity (González De Requena *et al.*, 2002, González De Requena *et al.*, 2005). Other groups have not observed any solid evidence of a relationship, but recognise the need to monitor plasma nevirapine levels when hepatotoxicity is suspected (Almond *et al.*, 2004, Kappelhoff *et al.*, 2005, Vogel *et al.*, 2009).

The 3435C→T polymorphism in MDR1 is significantly associated with reduced risk of nevirapine-induced hepatotoxicity (Haas *et al.*, 2006). P-glycoprotein is a multidrug efflux pump, encoded by MDR1; this membrane-associated protein is responsible for actively removing xenobiotics from the cell (Haas *et al.*, 2006). Changes in p-glycoprotein activity can effect distribution, metabolism and excretion of drugs. Patients who experienced nevirapine-induced hepatotoxicity were less like to have at least one MDR1 T allele at position 3435C→T. The reasons for this association are not well understood however, it is possible that altered P-glycoprotein activity in the intestine associated with the MDR1 variants alters disposition of nevirapine and/or its metabolites that affect intracellular concentrations of nevirapine and toxicity in liver (Saitoh and Spector, 2008).

HLA genes encode for histocompatibility proteins which are responsible for antigen presentation. Polymorphisms in these genes can influence an individuals' or populations' immune response to particular xenobiotics. Genetic screening of patients for *HLA-B*5701* is used routinely before a treatment regimen including abacavir is initiated to reduce the risk of hypersensitivity reactions during treatment (Mallal *et al.*, 2008). Currently no standard genetic screen is in place in the clinic to predict increased risk of nevirapine-induced toxicity; however a number of HLA alleles have been identified that show a correlation to increased risk of nevirapine-

induced hypersensitivity. Studies in Australian (Martin *et al.*, 2005) and French (Vitezica *et al.*, 2008) populations demonstrated that *HLA-DRB1*0101* acts as a predisposing factor for nevirapine hypersensitivity. In a Japanese patient cohort 42% of nevirapine-hypersensitive patients had the *HLA-Cw*08* allele, which is significantly higher than the nevirapine-tolerant group and the general Japanese population (Gatanaga *et al.*, 2007). A study conducted in Thailand reported significantly higher number of patients with the *HLA-Cw*04* allele in those that suffered with nevirapine-induced skin rash (Likanonsakul *et al.*, 2009). In a Sardinian patient cohort 46% of the nevirapine-hypersensitive subjects had the *HLA-Cw*08* and *HLA-B*14* alleles compared with 5% of the nevirapine-tolerant group (Littera *et al.*, 2006).

1.7.4 Animal model of nevirapine-induced skin rash

Animal models of idiosyncratic drug reactions are rare but can be useful tools for investigating the mechanisms of the reactions. Uetrecht and colleagues have extensively characterised a dose-dependent, nevirapine-induced skin rash in female Brown Norway rats that resembles the idiosyncratic cutaneous reaction seen in humans (Shenton *et al.*, 2003, Shenton *et al.*, 2004) and appears to be immune-mediated (Shenton *et al.*, 2005). The nevirapine-induced skin rash in female Brown Norway rats is similar to that in human in terms of; the time of onset, females being more susceptible than males, incidence increases with dose, escalating dose of nevirapine can reduce incidence, rechallenge results in more severe rashes than on initial exposure (Shenton *et al.*, 2003). Chen *et al.* (2008) have proposed that the skin rash produced in female Brown Norway rats by nevirapine and 12-OH NVP may be due to nevirapine quinone methide formed through dissociation of 12-OH NVP sulphonate in the skin. 12-OH NVP caused a rash at a lower dose then required for nevirapine. Histology of nevirapine induced skin rash highlighted various degrees of hyperplasia more prominent adjacent to ulcerated areas. Away from the ulceration there was primarily mononuclear dermal inflammatory infiltrate. There were CD4+, CD8+ and ED1+ (macrophages) cells in both the epidermis and the dermis. Keratinocyte cell death was observed similar to that seen in SJS (Shenton *et al.*, 2003).

1.8 THESIS AIMS

The aims of this thesis are to investigate covalent binding and the formation of thioether metabolites in relation to bioactivation and toxicity of drugs will be examined. The first three experimental chapters describe investigations into the efficacy, toxicity and pharmacokinetics of a thiophene analogue of furosemide (TPA) and comparisions to that of furosemide, in order to directly compare the two heterocycles in the same biological environment. The aims of this section of work are:

- To assess the efficacy and toxicity of TPA and compare to that of furosemide.
- To determine and compare the PK parameters of TPA and furosemide.
- To assess and compare species differences in terms of toxicity, pharmacokinetics and metabolism of furosemide and TPA.
- To analyse the affect of different routes of administration of furosemide and TPA in terms of toxicity and pharmacokinetics.
- To identify any thioether adducts of TPA *in vivo or in vitro*, and investigate whether they are an indication of toxicity or successful detoxification.

The final two experimental chapters describe work conducted to investigate whether mercapturates of nevirapine could be used as markers of exposure to nevirapine reactive metabolites or whether they indicate successful bio*in*activation of reactive metabolites in an animal model. The aims of this section of work are:

- To test *in vitro* and *in vivo* systems for a toxicological end-point of nevirapine.
- Assessing the potential for nevirapine mercapturates to be used as *in vivo* markers of bioactivation.
- Understanding pathways of nevirapine metabolism leading to formation of reactive metabolite(s).

These investigations using furosemide, TPA and nevirapine aim to test the scalability of *in vitro*, pre-clinical and human systems, and to highlight the difficulties in the extrapolation of data to the clinic. The work described here aims to assess the current systems for detecting potential human hazard and draws attention to areas in which

more research and development is required. Some current biomarkers are also used as a tool to measure or detect drug induced toxicity and their use in both preclinical and clinical settings is evaluated.

CHAPTER 2

HETEROCYCLIC RING SUBSTITUTION IN FUROSEMIDE: INVESTIGATING POTENCY AND *IN VITRO* AND *IN VIVO* TOXICITY.

CONTENTS

2.1 INTRODUCTION

Drug induced liver injury (DILI) is the most frequent reason for the withdrawal of newly approved drugs and accounts for 50% of cases of acute liver failure and 75% of idiosyncratic ADRs result in liver transplantation or death (Lee, 2003). Both furan and thiophene groups have been associated with reactive metabolite formation and ADRs, including DILI, in humans and pre-clinical species. There are examples of drugs containing a thiophene group that have been withdrawn from the market due to concerns over ADRs in the clinic (Dalvie *et al.*, 2002). Conversely, there are examples where these heterocyclic moieties have been used successfully in therapeutic compounds and are used safely in the clinic (Michele *et al.*, 2010, Perzborn *et al.*, 2011, Chung *et al.*, 2000, O'Callaghan *et al.*, 1976). *In vitro* and *in vivo* toxicity testing methods are employed during drug development in an effort to identify any potential human hepatotoxins and allow rational structural changes to be made in order to identify a safer lead candidate compound (Uetrecht, 2003, Evans *et al.*, 2004, Peters, 2005).

Furosemide (FS), a potent loop diuretic used safely in humans, has been used as a model compound for the investigation of DILI through a bioactivation-mediated mechanism in mice (Randle *et al.*, 2008, Masubuchi *et al.*, 2007). Furosemide has been shown to produce massive hepatic centrilobular necrosis in mice at 400 mg/kg (*i.p.*) by a mechanism independent of its diuretic action (Mitchell *et al.*, 1974). The hepatocellular damage caused by furosemide is postulated to be the result of CYP450 enzyme-mediated formation of a toxic metabolite that binds covalently with hepatic macromolecules both *in vitro* and *in vivo* (Mitchell *et al.*, 1974, Mitchell *et al.*, 1976, Williams *et al.*, 2007). Bioactivation of the furan ring was demonstrated by the characterization of a FS γ-ketocarboxylic acid in the rat and mouse *in vivo*, indicative of a reactive epoxide intermediate (Williams *et al.*, 2007). Covalent binding of the reactive metabolite to hepatic protein and subsequent hepatotoxicity occurs in the mouse but not in rats. In rats, the FS γ-ketocarboxylic acid is excreted in the form of a GSH conjugate, suggesting a possible safety mechanism exists in the rat to protect from furosemide-induced hepatotoxicity (Williams *et al.*, 2007).

Five-membered aromatic heterocyclic rings are widely distributed in nature and are often incorporated into new chemical entities during drug design to increase pharmacological selectivity and potency (Dalvie *et al.*, 2002). These chemical moieties are used safely and effectively in some therapeutic agents (Kalgutkar and Soglia, 2005). In studies where numerous different chemical substitutions are made to a lead compound in order to improve its pharmacological properties and/or replace a structural liability, authors have noted improved efficacy with a reduction in toxicity where a thiophene ring had replaced the original moiety in the lead compound (Brendle *et al.*, 2002, Hagen *et al.*, 2001). During optimization of a novel 4-hydroxy-5, 6-dihydropyrone, for use against HIV, researchers developed a panel of second generation compounds, where the aniline moiety was replaced by a number of different moieties (Hagen *et al.*, 2001, Turner *et al.*, 1998). Simple heterocycles such as furan and thiophene were prepared with encouraging results; these analogues displayed excellent activity against the HIV-1 protease enzyme, with a *K*i of 1 nM or lower. The thiophene analogue also showed improved antiviral activity (EC_{50} = 0.12 μM) albeit with a slight increase in toxicity (TC_{50} = 91 μM) when compared to the lead compound (Table 2.1). The conclusion was that the thiophene compound proved superior to the lead compound, displaying excellent antiviral efficacy, low toxicity and promising bioavailability across all species tested (Hagen *et al.*, 2001).

Compound	Structure	IC_{50} (nM) HIV Protease	EC_{50} (μM) Infected CEM cell protection	TC_{50} (μM) Uninfected CEM cell cytotoxicity
4-hydroxy-5,6-dihydropyrone	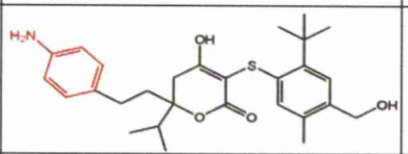	0.11	0.2	210
Thiophene Analogue	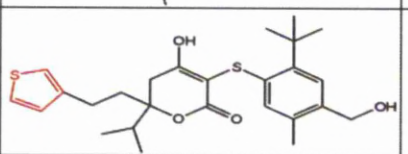	0.13	0.12	91
Furan Analogue	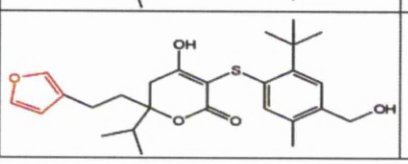	0.78	0.75	190

Table 2.1: Summary of efficacy and toxicity data of 4-hydroxy-5, 6-dihydropyrone analogues. Adapted from Hagen *et al*, 2001.

In another study, furan and thiophene analogues of the anti-leishmanial drug pentamidine were synthesised (Brendle *et al.*, 2002). Although widely used, there are many drawbacks with pentamidine; it requires a parenteral route of administration, making the treatment both more expensive and less practical in developing nations (Sundar *et al.*, 2000). Also, the clinical side effects of the drug include renal and hepatic toxicity among others (Berman, 1997). A thiophene analogue of pentamidine exhibited the greatest potency, possessing 6.2-fold greater antiparasitic activity than pentamidine itself (Table 2.2). This compound was 155-fold more potent against *Leishmania* than against a macrophage cell line (Brendle *et al.*, 2002). The pharmacological action of furosemide has been attributed to the inhibition of the active reabsorption of Cl^- ions in the thick ascending limb of the loop of Henle by binding the Cl^- binding site of the $Na^+/2Cl^-/K^+$ co-transport system (Burg *et al.*, 1973, Vree and Van Der Ven, 1999). The inhibitory effect of compounds towards the $Na^+/2Cl^-/K^+$ co-transport system can be assessed *in vitro*.

Compound	Structure	IC_{50} (μM)	
		L.donovani	Macrophage cell line
Pentamidine	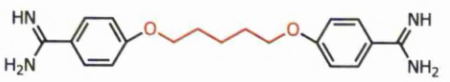	2.59	>100
Furan Analogue	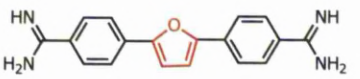	2.76	26.84
Thiophene Analogue	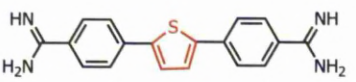	0.42	65.3

Table 2.2: Summary of efficacy and toxicity data of pentamidine analogues. Adapted from Brendle *et al*, 2002.

The standard regimen for preclinical toxicity assessment investigations are conducted in at least two species (one rodent and one non-rodent) at doses many multiples of the intended dose in humans (Peters, 2005). A retrospective analysis of concordance of preclinical toxicity data with human toxicity data revealed that 70% of human

toxicities were predicted by preclinical animal studies in one or more species (Olson *et al.*, 2000). Although furosemide is safe in man its tendency to cause severe liver necrosis in mice would result in a pre-clinical hazard signal and may fail during the development process today. In light of the discovery that the furan ring in furosemide is the bioactivated moiety responsible for development of hepatotoxicty in the mouse (Williams *et al.*, 2007), substitution of the ring for another functional group may eliminate or reduce this toxicity.

Measurement of serum alanine aminotransferse (ALT) activity levels in preclinical models and in the clinic is the gold standard for assessment of liver damage (Amacher, 2002, Ozer *et al.*, 2008). In preclinical models histopathology can be used to visualize tissue damage and hepatic GSH levels can be measured to assess whether depletion has occurred (Owens and Belcher, 1965). In mice, 24 hours following a 400 mg/kg dose of furosemide, hisopathological analysis of liver sections show severe necrosis of hepatocytes in the midzonal and centralobular areas in 92% of animals (Mitchell *et al.*, 1974). Serum ALT levels are also raised significantly compared to control at this dose, however, furosemide does not significantly deplete hepatic GSH levels (Williams *et al.*, 2007). This is unlike the situation with paracetamol (APAP) where, in cases of overdose, the electrophilic intermediate NAPQI accumulates and cellular stores of GSH become depleted allowing NAPQI to bind covalently to critical proteins (Jollow *et al.*, 1973, Mitchell *et al.*, 1973a, Mitchell *et al.*, 1973b, Potter *et al.*, 1973) resulting in cell death of hepatocytes (Antoine *et al.*, 2009, El-Hassan *et al.*, 2003, Jaeschke *et al.*, 2006).

Tienilic acid and suprofen are mechanism based inhibitors of CYP 2C9 and have been withdrawn from the market because of hepatotoxicity (Lecoeur *et al.*, 1996, O'Donnell *et al.*, 2003). Microsomal assays to assess a compounds ability to inhibit P450s are routinely used during the drug development process (Hutzler *et al.*, 2009). Although primary cultured hepatocytes have been used extensively as an *in vitro* system for toxicological studies, their use is limited due to the loss in expression of specific liver functions including cytochrome P450 (Donato *et al.*, 1994). An alternative *ex vivo* model, which enables the investigation of cytotoxicity in parallel with metabolism, is freshly isolated hepatocyte suspensions (Graham *et al.*, 2008, Tettey *et al.*, 2001). The data generated from furosemide incubated with freshly

isolated rat and mouse strongly correlated with the *in vivo* situation, however, it was not predictive of human hazard (Williams *et al.*, 2007). Furosemide has also been shown to undergo NADPH dependant covalent binding to rodent and human microsomal protein, providing evidence of bioactivation (Williams *et al.*, 2007).

The aim of this chapter was to assess the pharmacological and toxicological outcome of substituting the furan ring in furosemide to a thiophene ring (Figure 2.1). It also provided a means of testing the two potential liabilities in the same biological environment. Specifically, the *in vivo* toxicity of the two analogues was to be compared in terms of serum ALT levels and histopathology. The ability of the two compounds to deplete hepatic GSH was also to be assessed. It was also of interest to investigate the *in vitro* efficacy of the two compounds towards the target protein, $Na^+/K^+/Cl^-$ co-transporter, responsible for the diuretic action of the drug. Finally, the chapter aimed to assess the *in vitro* hazard indications for TPA and compare to those of furosemide; bioactivation potential was to be assessed in supplemented microsomes (covalent binding) and hepatocytes (covalent binding and cytotoxicity).

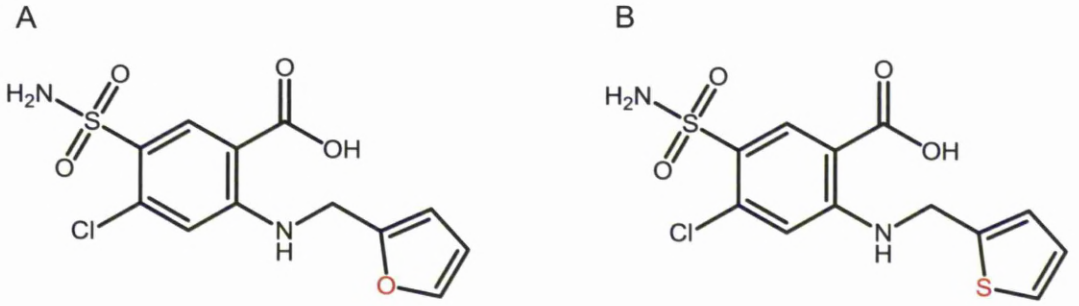

Figure 2.1: Chemical structure of furosemide (A) and its thiophene analogue (TPA; B). The analogue has been synthesized with a sulphur group replacing the oxygen group in the furan ring.

2.2 MATERIALS AND METHODS

2.2.1 Materials

[^{14}C]-Thiophene analogue of furosemide (TPA; Specific activity 592 Mbq/mmol), and unlabelled TPA was provided by Pfizer (Kent, U.K.) and was determined to be >98 % pure by HPLC. The ^{14}C label was incorporated into the carboxyl carbon atom of TPA, and thus expected to be incorporated in all major metabolites. 10x Hanks Balanced salt solution Ca^{2+} was obtained from Gibco (Invitrogen Ltd, Paisley, U.K.). CellTiter 96® AQueous One Solution Cell Proliferation Assay kit was obtained from Promega (Southampton, U.K.). Collagenase A was obtained from Roche Diagnostics (Lewes, U.K.). Unless otherwise stated, reagents were obtained from Sigma-Aldrich Chemical Co. (Poole, U.K.). Ultima Gold scintillation fluid was purchased from PerkinElmer LAS (Seer Green, Beaconsfield, Buckinghamshire, U.K.). All solvents were of HPLC grade and were products of either Fischer Scientific plc (Loughborough, U.K.) or VWR (Lutterworth, U.K.)

2.2.2 Experimental Animals

Protocols described were undertaken in accordance with criteria outlined in a license granted under the Animals (Scientific Procedures) Act 1986 and approved by the University of Liverpool Animal Ethics Committee. Male Wistar rats and male CD-1 mice were obtained from Charles River Laboratories (Margate, U.K) housed in a light-controlled room at a constant temperature, and supplied with a standard chow diet and water *ad libitum*.

2.2.3 Inhibitory effect of furosemide and TPA towards the $Na^+/K^+/Cl^-$ co-transporter

The effects of furosemide and TPA were investigated in an *in vitro* $Na^+/K^+/Cl^-$ cotransporter assay (Chassande *et al.*, 1988). The assay was carried out by Cerep (Le Bois l'Evêque, B.P. 30001, 86 600, Celle l'Evescault, France). The results are expressed as a percent of control specific activity ((measured specific activity/control

specific activity) x100) obtained in the presence of furosemide and TPA. The IC_{50} values (concentration causing a half-maximal inhibition of control specific activity) and Hill coefficients (nH) were determined by non-linear regression analysis of the inhibition curves generated with mean replicate values using Hill equation curve fitting (Y = D + [(A – D)/(1 + (C/C50)nH)], where Y = specific activity, D = minimum specific activity, A = maximum specific activity, C = compound concentration, C_{50} = IC_{50} and nH = slope factor). This analysis was performed using software developed at Cerep (Hill software) and validated by comparison with data generated by the commercial software SigmaPlot® 4.0 for Windows® (© 1997 by SPSS Inc.).

2.2.4 Inhibitory effect of furosemide and TPA towards CYP 2C9 in human liver microsomes

CYP 2C9 in human liver microsomes (HLM) was assayed for residual activity with probe substrate (diclofenac), after a primary incubation with various concentrations of furosemide, TPA and tienilic acid as a positive control (0.5% total organic v/v) in duplicate in a 96-well plate format at 37°C. Incubations consisted of HLM (0.3mg/ml in primary incubation) in 100 mM potassium phosphate buffer (pH 7.4) with a NADPH-regenerating system (3 mM $MgCl_2$, 1 mM, $NADP^+$, 5 mM isocitric acid, and 1 unit/ml isocitrate dehydrogenase). At 0 and 15 minutes aliquots were taken out of the primary incubation mixture and transferred into 200 µl of a secondary incubation mixture containing diclofenac at 25 µM, a concentration 3 times the apparent *K*m for each reaction, to measure residual activity. The 20-fold dilution and saturating concentration of probe substrate in the secondary incubation served to minimize competitive inhibition and any further inactivation. Secondary incubations (6 minutes) were quenched with 400 µl of cold acetonitrile containing an internal standard (200 ng/ml 13C6 4-OH diclofenac). Plates were then centrifuged at 3000*g* for 10 minutes and metabolite formation was analyzed by LC-MS/MS using an AB Sciex API-4000 (AB Sciex, Foster City, CA, U.S.A). Mass spectral analyses were performed using multiple reaction monitoring, with transitions for diclofenac (*m/z*

293.9/249.7), 4-hydroxydiclofenac (*m/z* 309.9 3 265.8), and 13C6 4-OH diclofenac (*m/z* 315.0/272.0).

2.2.5 Preparation of rat and mouse liver microsomes

Rat liver microsomes (RLM) and mouse liver microsomes (MLM) were prepared as described previously (Gill *et al.*, 1995). Adult male Wistar rats or male CD-1 mice were killed by asphyxiation with CO_2. Livers were excised into ice-cold 0.067 M phosphate buffer, pH 7.4, containing 1.15% (w/v) KCL. After rinsing, any extraneous tissue was removed. The livers were roughly chopped with a pair of scissors and homogenised initially with three passes of a motor-driven homogeniser (Kinematica Polytron PT 3000, Phillip Harris, Manchester, UK), and subsequently homogenised with a manual tissue homogeniser. This was followed by centrifugation (Optima L-60 preparative ultra centrifuge and Ti55 rotor; Backman, High Wycombe, Buckinghamshire) at 10,000g for 25 minutes at 4°C to remove cellular debris (nuclei, cell membranes and mitochondria). The resulting supernatant was centrifuged at 105,000g for 65 minutes at 4°C to sediment the microsomes. The microsomal pellet was then resuspended in phosphate buffer containing KCL and centrifuged at 105,000g for 65 minutes at 4°C. The supernatant was discarded and the microsomal pellet resuspended in phosphate buffer minus KCL.

2.2.6 Determination of cytochrome P450 activity of liver microsomes

The protein content of the microsomes was measured by the Lowry assay (Lowry *et al.*, 1951) where bovine serum albumin (BSA) was used as a standard. Cytochrome P450 content was determined by the difference spectroscopy method of Omura and Sato, (1964). Microsomal suspensions were diluted in phosphate buffer (minus KCL) to 1 mg/ml. A few grains of solid sodium dithionate were added to both sample and reference mixtures with gentle mixing. The sample only was bubbled with carbon monoxide (1 bubble/sec) for one minute. Quantitative determination of the haemoprotein was then made using an extinction coefficient for the wavelength couple 450 – 490 of 91 mM/cm.

2.2.7 TPA incubations with RLM and MLM

[^{14}C]-TPA (0.1 μM) was incubated with MLM (1 mg/ml) and RLM (1-2 mg/ml), in the presence or absence of NADPH (1 mM) and in the presence or absence of GSH (0.1 μM), at 37°C for 1 hour. The reaction was terminated by addition of 1 ml ice-cold ACN.

2.2.8 Hepatocyte isolation from male Wistar rats and CD-1 mice

Rat and mouse hepatocytes were isolated using a modified two-step *in situ* collagenase perfusion technique based on the method of Seglen, (1976). Male Wistar rats (150–170 g) and male CD-1 mice (20–30 g) were anesthetized with sodium pentobarbital (60 mg/ml, 1 μl/g *i.p.*). The hepatic portal vein was cannulated, and the liver was perfused for 7 minutes at a constant flow rate of 12 ml/min for mice and 40 ml/min for rats, with a wash buffer containing Hanks' balanced salt solution (from 10X stock: magnesium chloride, magnesium sulfate, sodium bicarbonate; Invitrogen, Paisley, UK). Wash buffer was also supplemented with 5.8 mM HEPES and 4.5 mM $NaHCO_3$. The wash step was followed by a collagenase perfusion using wash buffer supplemented with 5 mM $CaCl_2$, 0.5 mg/ml collagenase A (Roche Applied Science, Indianapolis, IN), and 0.072 mg/ml trypsin inhibitor until the liver constitute had been digested. All wash and digestion solutions were kept at 37°C throughout the perfusion. After *in situ* digestion, the liver was excised, and the liver capsule was removed to release parenchymal and nonparenchymal cells. The cells were suspended in 50 ml of wash buffer supplemented with DNase I (0.1 mg/ml) and filtered through a 125 μm mesh (Lockertex, Cheshire, UK). Cell suspensions were immediately centrifuged at 30*g* for 2 minutes, the resulting supernatant containing nonparenchymal cells was removed, and the cells were resuspended in wash buffer containing DNase I. This centrifuge step was repeated twice at 50*g* with wash buffer alone. The cells were resuspended in an incubation buffer (wash buffer supplemented with 1 mM $MgSO_4.7H_2O$). Hepatocyte viability was assessed by trypan blue exclusion and only used when viability was above 80%. Experimental hepatocyte incubations contained a total volume of 6 ml at a cell concentration of $2x10^6$ viable cells/ml.

2.2.9 Assessment of TPA-induced cytotoxicity in freshly isolated rodent hepatocytes

Hepatocyte incubations were carried out in an orbital shaker set at 190 rpm for 6 hours with TPA [0–1.5 mM in MeOH (0.8% v/v) and 0.1 μCi of [^{14}C]-TPA in ethanol]. Following incubation, cytotoxicity was determined by trypan blue exclusion (100 μl of cell suspension and 20 μl of 0.4% trypan blue solution). Cytotoxicity was also determined by reduction of 3-(4,5-dimethylthiazol-2-yl)-2,5-diphenyl tetrazolium bromide (MTS) solution using the CellTiter 96® AQueous One Solution Cell Proliferation Assay kit (Promega, Southampton, UK), according to the manufacturer's instructions. Cell suspension (100 μl) was combined with MTS solution (20 μl), incubated at 37°C for 1 hour, and centrifuged at 50*g* for 2 minutes, this was performed in triplicate. The absorbance of the resulting supernatant was measured at 490 nm using a microtiterplate reader (Dynex Technologies, Chantilly, VA).

2.2.10 Determination of levels of covalent binding in primary rodent hepatocytes and microsomes by exhaustive solvent extraction

The microsome incubation mixture (1 ml) or remaining portion of the hepatocyte incubation (after cytotoxicity and GSH assessment; 4.6 ml) was placed in an equal volume of ice-cold ACN and centrifuged at 880*g* for 10 minutes. A 100 μl aliquot of supernatant was added to 4 ml scintillation fluid (Ultima Gold) and counted in a Beckman LS1801 Liquid scintillation counter with external standardisation for 1 min. The remaining supernatant was evaporated under a steady stream of N_2 in a 50°C water bath. The residue was reconstituted in 300 μl 50% MeOH for HPLC-radiochromatographic and LC-MS analysis. The protein pellet from the 880*g* spin was used to determine the levels of [^{14}C]-TPA covalently bound to the hepatocyte/microsomal protein. Covalent binding was determined by an exhaustive solvent extraction procedure using 70% methanol as described previously (Pirmohamed *et al.*, 1995). 5 ml or 3 ml of 100% MeOH was added to either the pellet from hepatocytes or microsomes respectively, vortexed and then centrifuged for 10 minutes at 2200 rpm. The above wash step was repeated twice more with 70% (v/v) MeOH. After each extraction step a 100 μl aliquot of the supernatant was added

to 4 ml scintillation fluid (Ultima Gold) and counted in a Beckman LS1801 Liquid scintillation counter with external standardisation for 1 minute, to ensure that all non-covalently bound material had been removed. The remaining supernatant was discarded. Following the final extraction, the protein was dissolved in 1 ml of 1 M NaOH at 60°C. Aliquots of the solubilized protein were taken for quantification of radioactivity by liquid scintillation counting and normalized to protein concentration.

2.2.11 Sample preparation for the determination of GSH levels in primary rodent hepatocytes

From the same incubations used for cytotoxicity assessment, the effect of TPA on total cellular levels of GSH was determined. Cells ($2x10^6$) from the hepatocyte incubation were centrifuged at 50*g* for 2 minutes. The resulting pellet was resuspended in 10 mM HCl. One-fifth of lysed hepatocytes were removed for protein content determination. The remaining hepatocyte lysate was combined with 6.5% (w/v) 5-sulfosalicylic acid (four parts hepatocyte lysate and one part 5-sulfosalicylic acid) and stored on ice for 10 minutes before centrifugation at 18,400*g* for 5 minutes.

2.2.12 Dosing regimen for *in vivo* furosemide and TPA toxicity investigation

Male CD-1 mice (22-24 g) and male Wistar rats (125-149 g) were administered either furosemide or TPA [1.21 mmol/kg in PEG; n=4 per group] either orally or via an *i.p.* dose. After 1, 3, 6 and 24 hours the animals were culled by CO_2 asphyxiation. Blood was taken via cardiac puncture and the livers were removed, snap frozen in liquid N_2 and stored at -80°C until analysis.

2.2.13 Measurement of alanine transaminase (ALT) activity in serum

Serum alanine transaminase (ALT) levels were determined kinetically at 37°C using ThermoTrace Infinity ALT Liquid stable reagent (Alpha Labs, Eastleigh, U.K) according to manufacturer's instructions. ALT levels exceeding 200 U/L that were

significantly different from controls were considered to represent hepatotoxicity (Kitteringham *et al.*, 2000).

2.2.14 Histopathological analysis of liver sections from furosemide and TPA treated male CD-1 mice

At each time point (1, 3, 6 and 24 hours) after administration of either furosemide or TPA [1.21 mmol/kg in PEG; n=4 per group] either orally or via an *i.p.* dose, liver sections were taken from the left lateral lobe left and fixed in formalin (Sigma, UK).

Preparation of histology sections

Histology was performed in collaboration with Prof. Anja Kipar from the Department of Veterinary Pathology, University of Liverpool. Slices (3-4 mm) of the major lobe of the liver were immersed in neutral buffered formalin (10%) for 24 hours until analysis. A transverse section was taken from the formalin fixed samples, which was placed cut side down into a pre-labelled biopsy cassette. Samples were processed using a tissue processor. The tissue processor removes water from the tissues and replaces it with paraffin wax which solidifies tissue and enables it to be cut. Briefly, the samples were dehydrated with a series of increasing concentrations of ethanol to remove free and bound water. The samples were then submersed and washed in xylene which removes the ethanol. The tissues were then removed from their cassette and embedded into a mould of molten paraffin wax with the trimmed side down. The cassette was then placed on top of the mould and topped up with wax and allowed to solidify. After solidification, excess wax was trimmed ready for sectioning.

Hepatic tissue sectioning

Embedded tissues were trimmed to expose all the tissue then cooled on ice. Several thin sections were cut to remove any areas of rough tissue. A fresh blade was used to cut 4 μm sections and floated onto a clean water bath (45°C) to remove creases. The

sections were retrieved with a charged microscope slide and allowed to dry in an oven.

Hematoxylin and eosin staining of hepatic sections

Sections were double stained with the application of the basic dye hematoxylin, which colours basophilic structures with a blue-purple hue and an alcohol-based acidic eosin, which stains eosinophilic structures pink. In brief, sections were initially submerged in xylene (5 minutes) to remove the wax and then transferred to another xylene. The sections were then taken down through descending grades of EtOH (100%, 96%, 85%, 70%) to distilled H_2O. They were then stained with hematoxylin (5 minutes) before being rinsed in running tap water (6 minutes). The sections were then stained with eosin (2 minutes) before being washed three times in 96% EtOH (1 minute). Finally the sections underwent three further washes in 100% EtOH, followed by two washes in xylene. The slides were then cover slipped using DPX.

2.2.15 Determination of hepatic GSH levels in male Wistar rats and CD-1 mice

The glutathione (GSH) assay is based upon the 5, 5-dithiobis (2-nitrobenzoic acid)-GSH disulfate recycling procedure first reported by Owens and Belcher (Owens and Belcher, 1965). The recycling assay for total GSH equivalents is based upon the reactions shown below (Anderson ME., 1985):

$2GSH + DTNB \rightarrow GSSG + TNB$ (1)

$GSSG + NADPH + H^{+} \rightarrow 2GSH + NADP^{+}$ (2)

Reduced GSH is oxidized by DTNB to give glutathione disulphide (GSSG) with stoichiometric formation of 5-thio-2-nitrobenzoic acid (TNB) (1). GSSG is reduced to GSH by the action of the highly specific glutathione reductase enzyme (GSSG reductase) and NADPH (2). The rate of TNB formation is followed at 405 nm (or 412 nm) and is proportional to the sum of GSH and GSSG present.

Total hepatic GSH (GSH + GSSG) levels were determined spectrophotometrically using a microtiter plate assay (Vandeputte *et al.*, 1994). Total hepatic GSH was determined for animals administered furosemide and TPA (1.21 mmol/kg) over 1, 3, 6 and 24 hours. In brief, 30-50 mg of liver tissue from the left lobe was homogenized in 200 µl 5-sulphosalicylic acid (6.5% (w/v)) and 800 µl stock buffer (143 mM NaH_2PO_4, 6.3 mM EDTA, pH 7.4) using ten passes of a glass Teflon homogenizer. The protein was allowed to precipitate on ice for 10 minutes before centrifugation at 14000 rpm for 5 minutes. Supernatants were stored at -80 °C prior to analysis. The pellets were resuspended in 1 ml NaOH (1 M) by warming at 60 °C for 1 hour. Protein levels were determined as described in section 2.2.16. The supernatants were used to determine the total GSH content. 20 µl of sample or GSH standard (0 – 80 nmol/ml) was added to a 96-well plate followed by 20 µl stock buffer to neutralize the pH. 200 µl of assay reagent (1 mM DTNB, 0.34 mM NADPH in 143 mM NaH_2PO_4, 6.3 mM EDTA, pH 7.4) was added to each well. The plate was incubated at room temperature for 5 minutes. The enzymatic reaction was initiated by the addition of 50 µl of GSH reductase (6.96 U/ml). Total GSH was followed kinetically at 412 nm for 2.5 minutes (MRX microplate reader with Max Revelation 3.04 software, Dynotech laboratories, Billinghirst, West Sussex, U.K.). The same assay was used for samples from hepatocyte incubations (section 2.2.11)

2.2.16 Determination of protein concentration

Soluble protein concentration was measured using an assay adapted from Lowry *et al.* (1951). The method combines the reactions of cupric ions with the peptide bonds under alkaline conditions with the oxidation of aromatic protein residues. The Lowry method is based on the reaction of Cu^+, produced by the oxidation of peptide bonds, with Folin-Ciocalteu Phenol reagent (a mixture of phosphotungstic acid and phosphomolybdic acid) in the Folin-Ciocalteu reaction (Lowry *et al.*, 1951). The reaction involves reduction of the Folin reagent by the copper treated protein, resulting in differential colour intensity depending on the amount of protein present.

Concentrations were calculated by reference to a BSA standard curve (0 – 200 µg/ml in 0.5 M NaOH). Samples (from hepatocytes, microsomes and tissue from *in vivo*

experiments) were diluted to fit onto the concentration curve. In a 96-well plate (flat-bottom, clear), 50 µl of Lowry reagent (0.5 ml 1% $CuSO_4.5H_2O$, 0.5 ml 2% NaK Tartarte, 10 ml Na_2CO_3 in 0.5 M NaOH) was added to 50 µl standard or sample and incubated for 15 minutes at room temperature. Subsequently 150 µl of Folin-Ciocalteu Phenol reagent (diluted 1 in 10 with dH_2O) is added to each well and incubated for 30 minutes at room temperature before reading the absorbance at 750 nm (MRX microplate reader with Max Revelation 3.04 software, Dynotech laboratories, Billinghirst, West Sussex, U.K.).

2.2.17 Statistical analysis

All results were expressed as mean + standard deviation. Data sets were analysed for normality using the Shapiro-Wilk test. Where multiple comparisons were made and the data was normally distributed, one-way ANOVA was used with bonferroni correction. Where multiple comparisons were made and the data was not normally distributed, a Kruskal-Wallis test, for all pair-wise comparisons, was used with either Conover-Inman or Dwass-Steel-Chritchlow-Fligner corrections for multiple comparisons. All statistical analysis was performed using the StatsDirect statistical software.

2.3 RESULTS

2.3.1 Inhibitory effect of furosemide and TPA towards the $Na^+/K^+/Cl^-$ co-transporter

Furosemide is a potent loop diuretic which reduces water reabsorption by inhibiting the $Na^+/K^+/Cl^-$ cotransporter in the thick ascending limb of the loop of Henle in the kidney. The inhibitory effect of furosemide and TPA towards the $Na^+/K^+/Cl^-$ cotransporter was assessed with bumetanide included as a positive control. TPA was shown to be three times more potent than furosemide with IC_{50} values at 17 μM and 50 μM respectively (Figure 2.2).

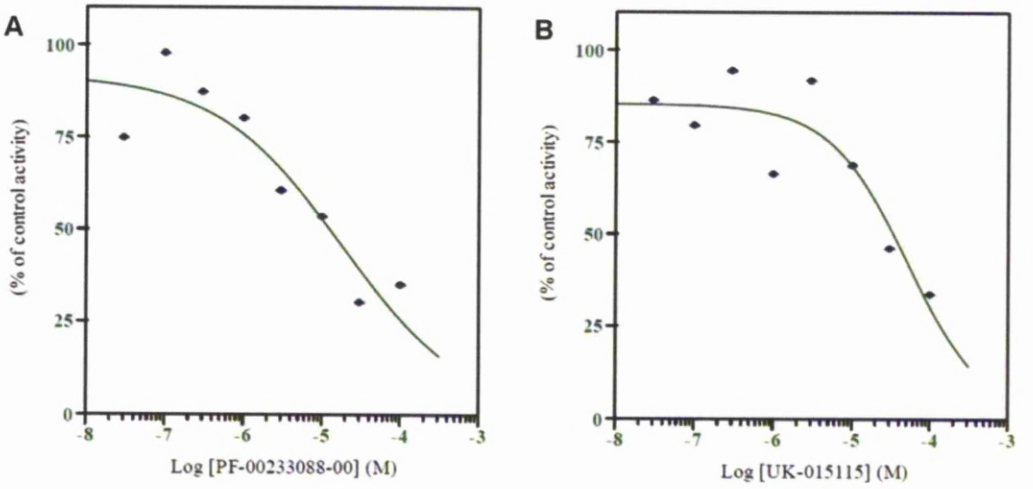

C

$Na^+/K^+/Cl^-$ cotransport Inhibitor	IC_{50} (μM)	n_H
FS	50	0.9
TPA	17	0.5
Bumetanide	1.30	0.8

Figure 2.2: The inhibitory effect of furosemide (UK-015115; A) and TPA (PF-00233088-00; B) towards the $Na^+/K^+/Cl^-$ cotransporter. The results are expressed as a percent of control specific activity ((measured specific activity/control specific activity) x 100) obtained in the presence of furosemide and TPA. Table C shows IC_{50} and Hill coefficients (nH) of furosemide, TPA and positive control, Bumetanide. Adapted from Cerep report

2.3.2 Inhibitory effect of furosemide and TPA towards CYP 2C9 in human liver microsomes

Assays to assess a compounds ability to inhibit P450 enzymess are routinely used during the drug development process. Neither furosemide nor TPA inhibited CYP 2C9 however tienilic acid (TA) displays inactivation of CYP 2C9 through dose-dependent decrease in diclofenac turnover to 4-hydroxydiclofenac (Figure 2.3).

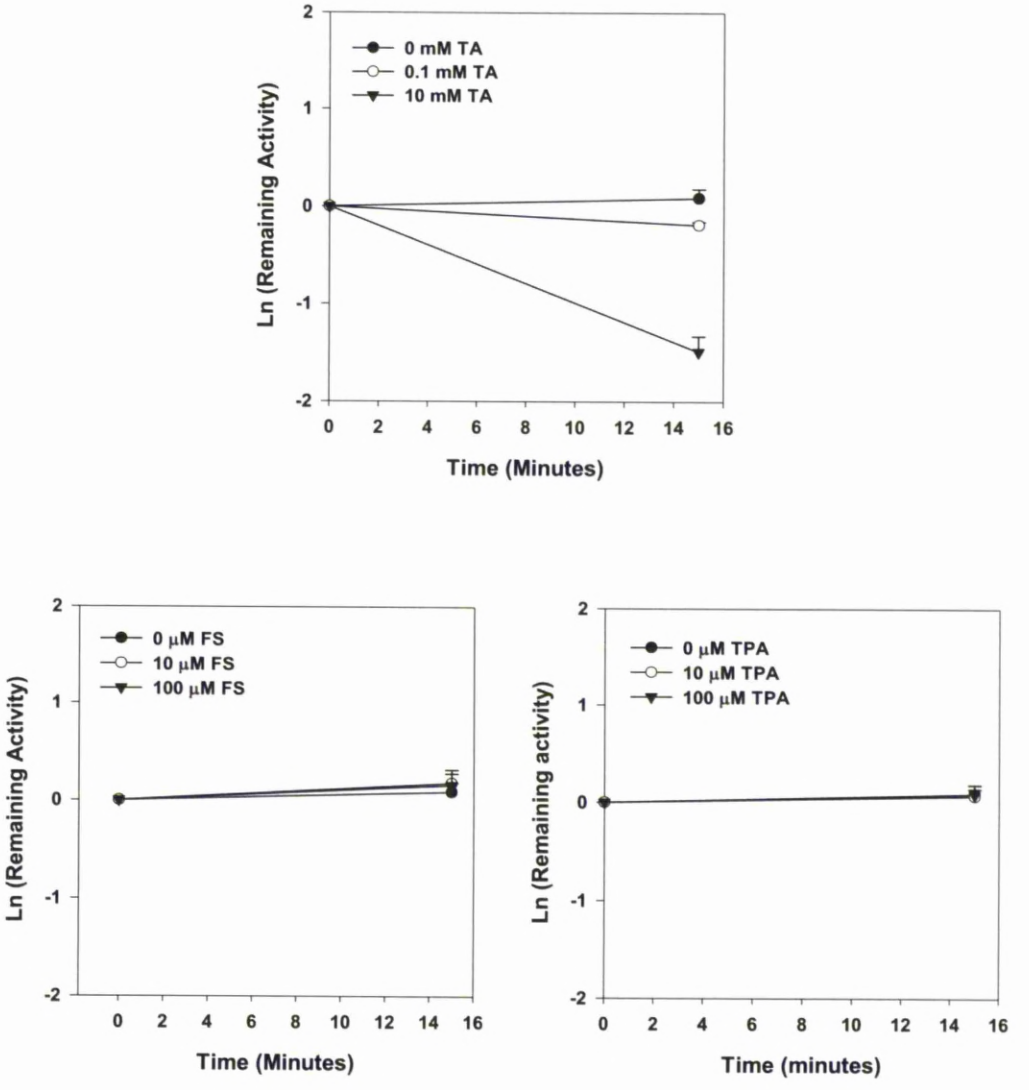

Figure 2.3: Inactivation of CYP 2C9 by furosemide, TPA and TA in HLM. TA displays dose-dependent inactivation of CYP 2C9 (A). furosemide (B) and TPA (C) have no effect on CYP 2C9 enzyme activity. Data expressed at mean + standard deviation.

2.3.3 *In vitro* bioactivation of TPA in CD-1 mouse liver microsomes and Wistar rat liver microsomes

Covalent binding was measured as an indication of bioactivation of TPA. Furosemide has previously been shown to undergo bioactivation in mouse, rat and human microsomes (Williams *et al.*, 2007). Significant covalent binding of radiolabelled TPA to microsomal protein was observed in CD-1 mouse and Wistar rat liver microsomes in the presence of NADPH. Inclusion of GSH in these incubations significantly reduced levels of covalent binding (Figure 2.4).

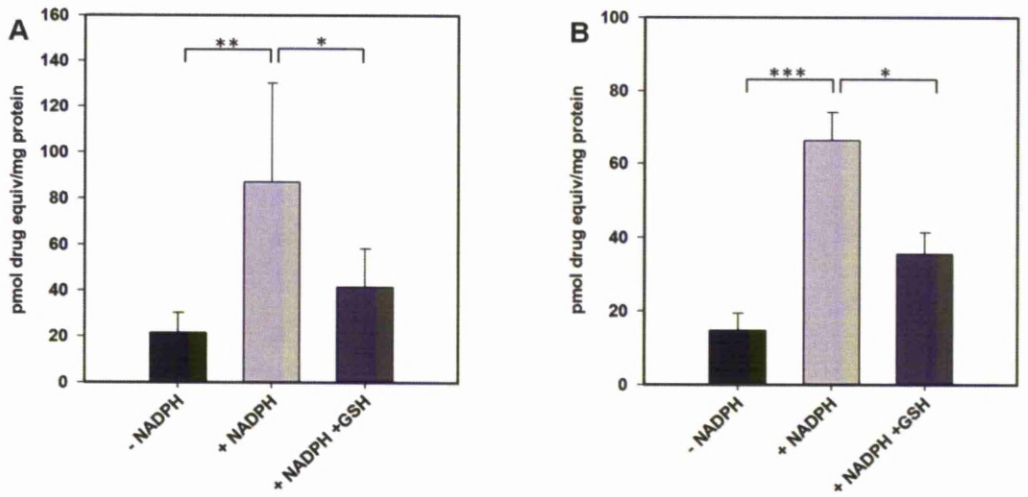

Figure 2.4: Determination of the extent of TPA bioactivation. Covalent binding of [^{14}C]-TPA (0.1 μCi) incubated with (A) RLM (1-2 mg/ml) and (B) MLM (1 mg/ml), in the presence or absence of NADPH (1 mM) and in the presence or absence of GSH (0.1 mM), at 37°C for 1 hour. Data are expressed as mean + standard deviation. RLM n=5; ** $p < 0.005$, * $p < 0.025$ using one-way ANOVA with Bonferroni correction for multiple comparisons (critical $p = 0.025$). MLM n=3: *** $p < 0.001$, * $p < 0.05$ using Kruskal-Wallis all pairwise comparisons (Conover-Inman).

2.3.4 Cytotoxicity of TPA towards primary Wistar rat and CD-1 mouse hepatocytes

A dose-dependent increase in cytotoxicity and GSH depletion was observed in rat hepatocytes incubated with TPA (Figure 2.5 A and B). Dose-dependent GSH depletion occurred at lower doses than cytotoxicity. TPA displayed a dose-dependent increase in cytotoxicity and covalent binding when incubated with mouse hepatocytes which was not associated with a decrease in GSH levels (Figure 2.5 C and D).

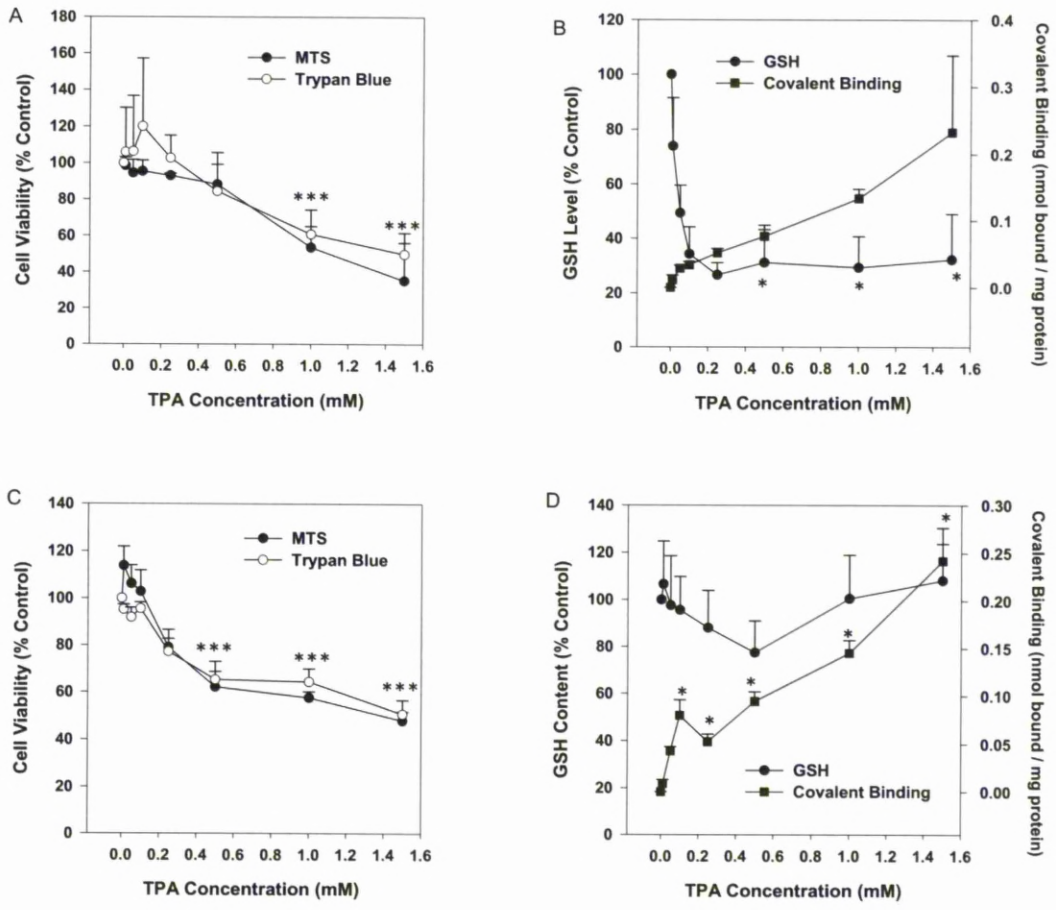

Figure 2.5: Effect of TPA (0 – 1.5 mM + [^{14}C]-TPA (10 μCi); 6 hours) on cytotoxicity, GSH content and covalent binding in Wistar rat (A and B) and CD-1 mouse (C and D) hepatocytes. Data are given as mean + STDEV of 4 to 7 independent isolations. Rat hepatocytes; ***; $p<0.00014$, **; $p<0.0014$, *; $p<0.0071$, comparing to 0 mM TPA incubations (one-way ANOVA with bonferroni correction for multiple comparisons, critical $p<0.0071$). Mouse hepatocytes; ***; $p<0.001$, **; $p<0.01$, *; $p<0.05$, comparing to 0 mM TPA incubations (Kruskal-Wallis test all pair-wise comparisons (Dwass-Steel-Chritchlow-Fligner)).

2.3.5 Investigation of the hepatotoxicity of furosemide and TPA in the mouse and rat, dosed either orally or via an *i.p* injection.

Serum ALT activity levels were measured as an indicator of hepatic damage. Administration of furosemide (1.21mmol/kg in PEG, *i.p.*) to male CD-1 mice caused a significant increase in ALTs of 2742.8 ± 1889.6 U/L, whereas mice administered TPA experienced ALT levels of 202.4 ± 141.9 U/L at the same dose, after 24 hours (Figure 2.6 A).

Neither furosemide nor TPA (1.21mmol/kg in PEG) caused an increase of serum ALT levels over 100 U/L when administered to male CD-1 mice orally (Figure 2.6 B). In the male Wistar rat neither furosemide nor TPA (1.21mmol/kg in PEG) caused an increase in serum ALT levels over 100 U/L when administered by either oral or *i.p* routes (Figure 2.7 A and B).

Histological analysis was performed on liver sections from control, furosemide and TPA treated male CD-1 mice (1.21mmol/kg in PEG; *i.p.*), after 24 hours, in order to confirm the increase in serum ALT levels was in fact due to hepatic injury. The histological findings correlated with the serological evidence; liver sections from the male CD-1 mouse, at 24 hours post *i.p.* administration of furosemide (1.21mmol/kg in PEG), exhibited centrolobular coagulative necrosis of hepatocytes (Figure 2.8 B; arrows). No drug related pathological changes were observed in liver sections from animals from the control and TPA treated groups.

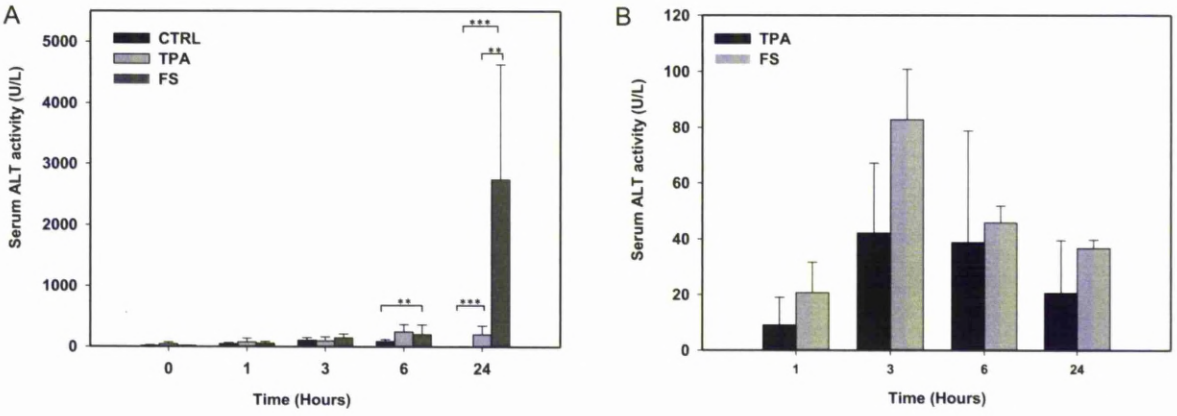

Figure 2.6: The effect of furosemide and TPA on serum ALT levels when administered either orally or by *i.p* injection to mice. Serum ALT levels after 1, 3, 6 and 24 hour administration of furosemide and TPA (1.21mmol/kg in PEG) to male CD-1 mice either by *i.p* injection (A) or orally (B). N=3-7; *** $p<0.001$, ** $p < 0.01$ Kruskal-Wallis test using all pairwise comparisons (Conover-Inman).

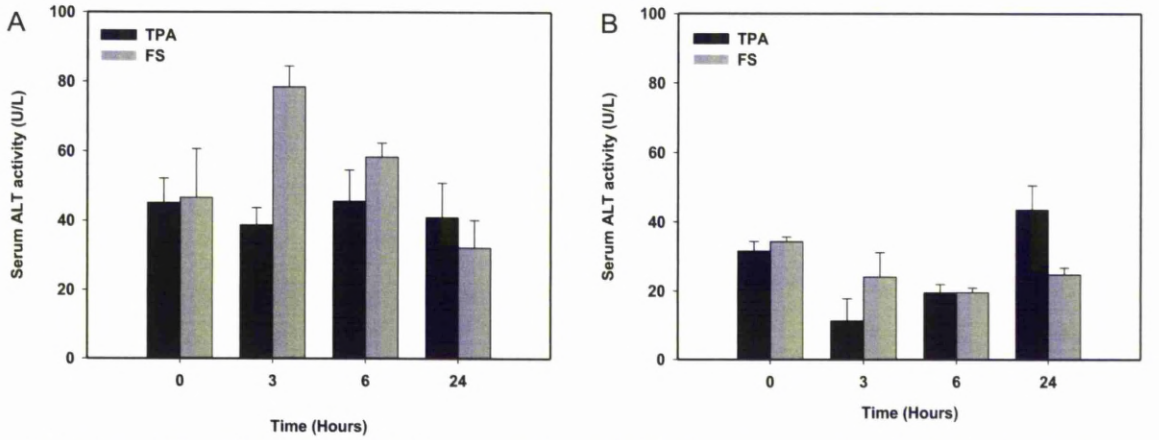

Figure 2.7: The effect of furosemide and TPA on serum ALT levels when administered to male Wistar rat. Serum ALT levels after 1, 3, 6 and 24 hour administration of furosemide and TPA (1.21mmol/kg in PEG) to male Wistar rats *i.p.* (A) and *p.o.* (B).

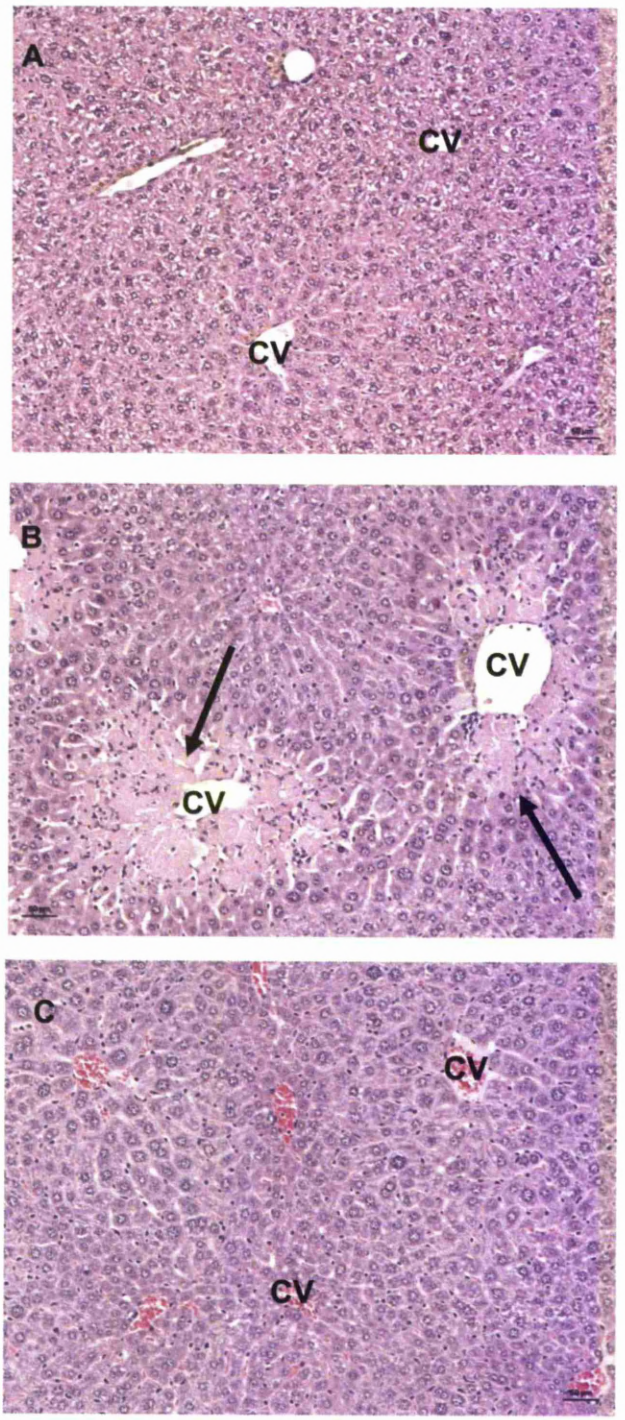

Figure 2.8: Histological analysis of liver sections 24 hours post furosemide and TPA treatment to male CD-1 mice. Haematoxylin-eosin (HE) staining of liver sections from male CD-1 mice treated with (A) Vehicle shows the liver does not exhibit any pathological change, (B) furosemide (1.21mmol/kg in PEG; *i.p.*) shows the liver exhibits centrilobular coagulative necrosis of hepatocytes (arrows) and (C) TPA (1.21mmol/kg in PEG) where the liver does not exhibit any significant drug related pathological changes. CV – central vein.

2.3.6 Effect of furosemide and TPA on hepatic GSH content *in vivo*.

At each time point, after administration of either furosemide or TPA by either ROA, liver sections were taken from the left lateral lobe and reserved to determine hepatic GSH content. GSH was significantly depleted in the mouse after 24 hours following administration of TPA, but not furosemide, (1.21mmol/kg in PEG, *i.p*; Figure 2.9).

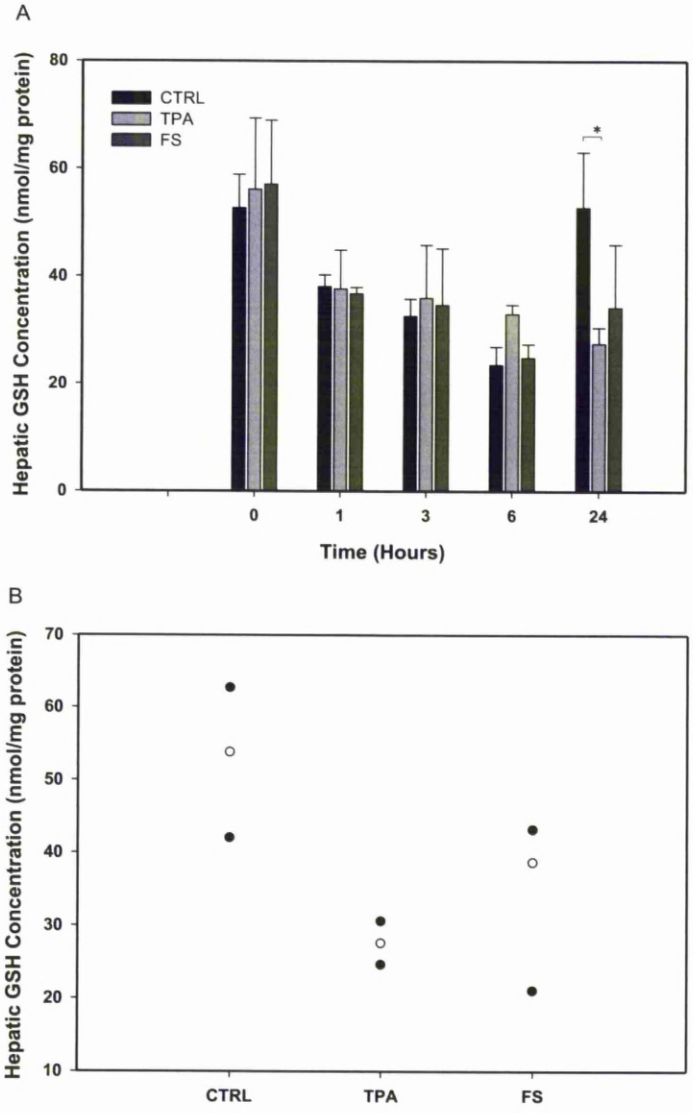

Figure 2.9: The effect of furosemide and TPA on hepatic GSH levels when administered *i.p.* in mice. (A) Hepatic GSH levels after 0, 1, 3, 6 and 24 hour administration of furosemide or TPA (1.21mmol/kg in PEG; *i.p.*) to male CD-1 mice. (B) Spread of data points at 24 hours. Data is expressed as mean + standard deviation. n=3; * $p < 0.05$ using Kruskal-Wallis all pairwise comparisons (Conover-Inman).

2.4 DISCUSSION

The investigations described in this chapter aimed to assess the pharmacological and toxicological outcome of substituting the furan ring in furosemide with a thiophene ring. It also aimed at assessing the two potentially toxic moieties in the same biological environment. In an *in vitro* assay the inhibitory effect of TPA was discovered to be three times more potent towards the $Na^{+}/K^{+}/Cl^{-}$ cotransporter than furosemide. Inclusion of a thiophene ring in a lead compound for improved pharmacological and toxicological properties has been tested previously for the HIV protease inhibitor 4-hydroxy-5, 6-dihydropyone (Hagen *et al.*, 2001, Turner *et al.*, 1998) and the anti-leishmanial drug pentamidine (Brendle *et al.*, 2002). In both cases the thiophene ring substituted compound displayed improved potency while retaining a good safety profile. Despite evidence that the thiophene ring can improve pharmacological and toxicological profile of compounds, there are many examples where the thiophene ring has itself been the structural liability in a compound. The thiophene containing drug, tienilic acid (TA) undergoes bioactivation to an *S*-oxide which forms an adduct with CYP2C9 (the enzyme responsible for its formation) via an alkylation reaction (Lecoeur *et al.*, 1994). 1 in 10,000 patients taking TA suffered from auto-immune hepatitis (Dansette *et al.*, 1991), an immune-mediated idiosyncratic ADR. Another outcome of this bioactivation is that TA is a mechanism based inhibitor of CYP 2C9 and so has the potential to increase the levels of co-administered compounds that are also CYP 2C9 substrates. This can be particularly important if the co-administered drug has a narrow therapeutic window (e.g. S-warfarin). Thus, it would be important when adding a thiophene moiety into a new compound to check that the compound is not a mechanism based inhibitor of CYP 2C9. In the present study TA (positive control) was shown to be an inhibitor of CYP 2C9 that became more potent following a 15 minute pre-incubation period as judged by an increased ability to prevent formation of 4-OH diclofenac. No such mechanism based inhibition of CYP 2C9 was seen with either furosemide or TPA.

Furosemide has previously been shown to undergo covalent binding to microsomal protein in NADPH supplemented mouse, rat and human micrcosomes indicating that furosemide is bioactivated (Williams *et al.*, 2007). Rodent liver microsomes were used to assess the potential of TPA to be bioactivated and covalently bind to

microsomal protein. Significant covalent binding of radiolabelled TPA to microsomal protein was observed in CD-1 mouse and Wistar rat liver microsomes in the presence of NADPH. Inclusion of GSH in these incubations significantly reduced levels of covalent binding. Samples from microsomes were analysed by HPLC and mass spectrometry, but no metabolites could be identified. Thiophenes can be bioactivated to either reactive epoxide intermediates or thiophene *S*-oxides (Kalgutkar *et al.*, 2005). Thiophenes can undergo P450 mediated hydroxylation to 2- and 5- hydroxythiophene and oxidation to a reactive thiophene *S*-oxide (Mansuy *et al.*, 1991a, Mansuy, 1991b, Dansette *et al.*, 1992), proved by the identification of thiophenes *S*-oxide dimers in *in vitro* and *in vivo* studies of thiophene (Treiber *et al.*, 1997). Studies with the 2-aroylthiophene-containing NSAID, suprofen, provides evidence that the thiophene ring could potentially undergo bioactivation to an epoxide. Incubations of suprofen with NADPH and semicarbazide, trapped a pyridazine derivative, suggesting initial epoxidation of the thiophene ring (O'Donnell *et al.*, 2003).

Freshly isolated rodent hepatocytes were used to assess the cytotoxicity and metabolism (Chapter 4) of TPA in the same test system. In mouse hepatocytes, furosemide caused a significant, dose- and time-dependent decrease in cell viability and, similar to the *in vivo* situation, there was no decrease in GSH levels (Williams *et al.*, 2007). TPA caused a dose-dependent decrease in cell viability in freshly isolated mouse hepatocytes, with no decrease in the levels of GSH. *In vivo*, it was shown that TPA only caused a significant decrease in hepatic GSH after 24 hours; in the freshly isolated hepatocyte model, it may be that an incubation time of 6 hours was not enough to deplete GSH to the same degree. Alternatively, the bioactivation product of TPA might preferentially bind to protein in this system, indeed the levels of covalent binding significantly increased in a dose-dependent manner. Although furosemide did not elicit hepatotoxicity or deplete hepatic GSH levels in the rat *in vivo*, in freshly isolated rat hepatocytes furosemide displayed dose- and time-dependent cytotoxicity and GSH depletion (Williams *et al.*, 2007). The same was observed for TPA; although it did not elicit acute toxicity in rats *in vivo*, in freshly isolated rat hepatocytes, a dose-dependent decrease in cell viability and GSH content was observed. *In vivo* TPA may undergo detoxification through conjugation with

GSH and be cleared from the system and not covalently bind to hepatic protein or elicit toxicity. In isolated hepatocytes in suspension, TPA may deplete the finite pool of GSH in hepatocytes which could lead to cell death. Furthermore, unlike a whole animal system, TPA and metabolites cannot be eliminated from the suspension.

In concordance with previous studies, we have demonstrated that furosemide causes hepatic necrosis in mice (Mitchell *et al.*, 1974, Williams *et al.*, 2007, Wong *et al.*, 2000). Liver injury was assessed by the measurement of serum ALT activity levels at time points after furosemide administration and histological examination at 24 hours confirmed the serological evidence. It has been shown previously that the level of furosemide covalent binding to liver proteins coincides with increased ALT levels in the mouse at an *i.p.* dose of 1.21mmol/kg (Williams *et al.*, 2007). However, when furosemide is administered at the same dose via the oral route, no significant increase in serum ALT activity levels are observed. This suggests that, in addition to bioactivation and covalent binding, liver accumulation of furosemide may be required for induction of hepatotoxicity. This observation is supported by a study linking covalent binding and development of liver necrosis in the mouse, with inhibition of biliary excretion of furosemide following a large dose of furosemide or pretreatment with sulfobromophathlein (Spitznagle *et al.*, 1977).

TPA, despite only a one atom difference from furosemide, induced no hepatotoxicity in either rats or mice (*i.p.* or *p.o.*) and the histological analysis of livers from mice treated with TPA (1.21 mmol/kg *i.p.*) after 24 hours confirms this. In previous work there was no evidence of TPA covalently binding to liver proteins to a significant degree *in vivo* (Butler, 2006). In agreement with more recent reports (Williams *et al.*, 2007), furosemide failed to elicit a hepatotoxic response in rats in these investigations. Lagarriga *et al* (1977) demonstrated toxicity of furosemide (1.21 mmol/kg) in rats following a pre-dose of phenobarbital, a CYP P450 inducer. Phenobarbital has been shown to increase acetaminophen (APAP)-mediated hepatotoxicity in cultured human hepatocytes by inhibition of uridine 5'-diphosphate-gluccuronosyltransferases (UGTs) and therefore blocking the detoxifying glucuronidation pathway of APAP (Kostrubsky *et al.*, 2005). The furosemide-induced toxicity observed in rats in the work by Lagarriga *et al* (1977) may be due to induction of CYP 2B and 2C enzymes by leading to relatively higher

degree of oxidative metabolism, bioactivation and covalent binding. An alternative explanation may be that inhibition of UGTs by phenobarbital may inhibit glucuronidation, leading to a higher level of bioactivation to a reactive metabolite.

In concordance with previously published data, it was found that furosemide (1.21 mmol/kg i.p) did not significantly deplete hepatic GSH levels in either rats or mice *in vivo* (Mitchell *et al.*, 1974, Williams *et al.*, 2007, Wong *et al.*, 2000). This suggests that in the mouse, the reactive metabolite furosemide covalently binds preferentially to hepatic proteins rather than binding to hepatic GSH and subsequently induces toxicity. This is in contrast to other hepatotoxins such as APAP where GSH depletion greater that 90% is required before APAP can covalently bind to hepatic proteins and induce hepatotoxicity (Davis *et al.*, 1974). Conversely TPA (1.21 mmol/kg *i.p*) caused a small but statistically significantly depletetion of hepatic GSH levels compared to control at 24 hours. Despite this GSH depletion, there was minimal evidence of ALT elevation and the livers were histologically normal. Possible explanations of the differences in GSH depletion include TPA being a better substrate for glutathione transferases (GSTs) compared to furosemide and so more GSH conjugation is taking place leading to significant GSH depletion. Equally, more than one GSH conjugate could be formed compared to the one FS-GSH conjugate identified in previous studies (Williams *et al.*, 2007).

In light of the fact that furosemide causes liver necrosis in mice *in vivo*, as well as a number of *in vitro* hazard signals, the aims of this chapter were to investigate the effect of substituting the furan ring in furosemide with a thiophene ring, on the pharmacological and toxicological profile of the compound. TPA was shown to be three times more potent towards the $Na^+/K^+/Cl^-$ cotransporter than furosemide, with IC_{50} values of 17 μM and 50 μM respectively. TPA displayed an improved safety profile *in vivo* in terms of serum ALT activity levels compared to furosemide (237.3 and 4441.4 U/L respectively, 1.21 mmol/kg i.p for 24 hours). However, in *in vitro* systems, rodent liver microsomes and freshly isolated hepatocytes, the two analogues were comparable in terms of cytotoxicity, GSH depletion and covalent binding hazard signals. The work in this chapter provided evidence that the novel thiophene analogue of furosemide underwent bioactivation, and that the reactive metabolite(s) produced can covalently bind to hepatic protein *in vitro*. It was shown that the degree

of covalent binding could be reduced with the inclusion of GSH in microsomal incubations. Investigating the pharmacokinetics and metabolism of TPA *in vitro* and *in vivo* may provide a rationale for the differences in the toxicological profile of these two structurally similar compounds.

A particularly interesting finding from the work in this chapter was the observation that *i.p.* administration of furosemide-induced hepatotoxicity in male mice, yet, at the same dose, orally administered furosemide failed to do so. This suggests that the toxicity of furosemide could be partly attributed to high concentrations in the liver, in addition to bioactivation to a reactive metabolite. Conducting pharmacokinetic and toxicokinetic studies using the two compounds, in both rats and mice, via *i.p.* and oral routes of administration may put this finding into context, as exposure time and hepatic furosemide levels can be measured over time.

CHAPTER 3

HETEROCYCLIC RING SUBSTITUTION IN FUROSEMIDE: INVESTIGATING THE EFFECT OF STRUCTURAL CHANGES ON PHARMACOKINETICS.

CONTENTS

3.1 INTRODUCTION

In the previous chapter (Chapter 2) it was shown that the thiophene analogue of furosemide, TPA, was more potent than furosemide against the pharmacological target. In addition, it was shown that the novel thiophene analogue of furosemide undergoes bioactivation and can covalently bind to hepatic protein *in vitro*. TPA was more toxic than furosemide towards freshly isolated hepatocytes, where it caused dose-dependent GSH depletion and covalent binding. However, *in vivo*, no toxicity of the compound was observed. In contrast furosemide causes hepatotoxicity following *i.p.* dosing in mice. There are a number of possible explanations that may help to explain the differing *in vivo* toxicity profiles; (1) the two compounds have very different levels of exposure *in vivo* so that concentrations of TPA and therefore the toxic metabolite are not reached or (2) the two compounds have different metabolic/excretory pathways. In this chapter the pharmacokinetics (PK), toxicokinetics (TK) and liver concentrations of furosemide and TPA are investigated in order to provide further understanding of the species and route dependent differences in toxicity observed in Chapter 2.

Drugs that are administered orally have a number of barriers to contend with in order to enter the systemic circulation. The solubility and intestinal permeability of a compound are the two main determinants of the fraction of a dose of compound absorbed after oral dosing. In addition, some drug molecules undergo metabolism in the gut wall, and those molecules that successfully cross the intestine will then enter the liver, through the portal vein, and may be subject to first-pass metabolism before entering the circulation. Therefore, after oral administration, the plasma levels of drug usually only represent a fraction of the initial dose; this is described quantitatively as bioavailability. In contrast when a compound is dosed intraperitoneally (*i.p.*) the compound will bathe the external surface of the liver as well as being absorbed in to the systemic circulation and it is possible that following *i.p.* dosing the local concentration in the liver and the plasma exposure is significantly higher than after oral dosing (Giuliano *et al.*, 2005, Ytrestøyl and Bjerkeng, 2007).

If liver concentrations are higher after *i.p.* dosing, this may explain why toxicity of furosemide is seen only after this ROA. The possibility that this is a plausible

rationale for the toxicity findings with furosemide come from previous studies with amodiaquine. Amodiaquine is an anti-malarial drug that has been associated with immune-mediated hepatotoxicity in rats. An amodiaquine-induced positive immune response was observed in rats regardless of the ROA, but the magnitude of the response was in the order intraperitoneal administration (*i.p.*) > intramuscular administration (*i.m.*) > oral administration (*p.o.*) (Clarke *et al.*, 1990).

Drugs and their metabolites can be cleared from the body through a number of mechanisms, but the primary routes are through renal and hepatic clearance, which includes biliary excretion and metabolism. The degree and rate of parent drug clearance from the body will directly influence drug plasma concentration; rapid elimination of parent drug will reduce the risk of toxicity but may also reduce the effectiveness of therapy. The AUC (area under plasma concentration-time curve) and C_{max} (maximum plasma concentration) can be used as a measure of drug exposure in toxicology. Biliary excretion is one of the primary routes of drug elimination; polar drugs and metabolites, such as glucuronides and glutathione conjugates, can be excreted via the bile in an active process by efflux transport proteins (Lai, 2009). Inhibition of biliary excretion can lead to drug accumulation in the liver. Work conducted by Spitznagle, *et al* (1977) indicated that saturation of the biliary excretion of furosemide, following a large dose of furosemide or pretreatment with sulfobromophathlein (a compound used to compete with the biliary excretion of various compounds (Cantarow and Wirts, 1948)), is closely associated with the appearance of liver necrosis in the mouse and of furosemide metabolites covalently bound to liver proteins.

Reference	Assay	Subjects	Dose	C_{max}	T_{max} (h)	$T_{1/2}$ (h)	Cl_{r} (ml/min)	F (%)
Beermann *et al*. (1975)	Radiolabelled	7		5 - 12 % dose	1	1.5 ± 0.28		65
Tilstone *et al*. (1978)	Radiolabelled	11						68.9 ± 7.1
Branch *et al*. (1977)	Fluorometric	6	80 mg/kg					50
Hammarlund *et al*. (1984)	HPLC	8	40 mg	0.23-0.77 mg/L	1.9-3.3		97.1 ± 6.2	43.3
Smith *et al*. (1980)	HPLC	9	80 mg				111 ± 17	42.8
Vree *et al*. (1995)	HPLC	7		2.2 ± 0.84 ug/ml	1.98 ± 0.98			53 ± 7

Table 3.1: Pharmacokinetic parameters of furosemide in human subjects administered furosemide orally.

Furosemide is a weak acid and although it is stable in gastric and duodenal fluid for two hours (Beermann *et al.*, 1975) it is incompletely absorbed from the GI tract (Hammarlund *et al.*, 1984, Lee and Chiou, 1983). Estimates of furosemide absorption are 30% in the rat (Lee and Chiou, 1983), 50-60% from an oral solution dosing in the dog (Yakatan *et al.*, 1976) and 43-69% in humans (see Table 3.1 for references). In the rat 40% of the administered furosemide dose remained in the GI tract for 8-9 hours after dosing (Lee and Chiou, 1983), and as furosemide absorption was calculated as 30% in this study, the remaining 30% had undergone metabolism either through hepatic first pass metabolism (~10%) or metabolism in the gut wall (~20%; (Lee and Chiou, 1983, Kim *et al.*, 2000)). Beermann *et al.* (1975), after administering radiolabelled furosemide orally to healthy volunteers, found that total urinary excretion was 55.1 ± 32 % and the total fecal excretion was 34.7 ± 5.2% after 5 days. Following an *i.v.* dose the total urinary excretion, for the two subjects exposed, was 82% and 84%, and total fecal excretion was 6% and 9% (Beermann *et al.*, 1975). Using this data the bioavailability was calculated to be 66% ((% in urine after oral dose / % in urine after *i.v.* dose)*100%). Low biliary excretion of parent compound has also been reported in rats (Lee and Chiou, 1983, Inui *et al.*, 1982). This is in contrast to the excretion in the mouse where furosemide undergoes significant biliary excretion; more than 30% of furosemide is excreted in bile after doses of 50 and 100 mg/kg (Spitznagle *et al.*, 1977).

The aim of this chapter was to determine the PK and TK parameters of furosemide and TPA in rats and mice in order to further understand the exposure and clearance of the two compounds and correlate the information with toxicity data. PK analyses were to be conducted in rats and mice to compare the ADME parameters of furosemide and TPA. With the aim of providing a rationale for the differences observed in toxicity between furosemide and TPA, and also between different ROA, TK analyses were planned, at 400 mg/kg, to allow the plasma and liver exposure of the two compounds to be measured in both rats and mice. *In vitro* plasma and liver protein binding experiments were to be conducted at a range of furosemide and TPA concentrations (based on exposures calculated in the PK and TK studies) in order to contextualize the PK and TK data.

3.2 MATERIALS AND METHODS

3.2.1 Materials

[^{14}C]-Thiophene analogue of furosemide (TPA; Specific activity 592 Mbq/mmol), and unlabelled TPA was provided by Pfizer (Kent, U.K.) and was determined to be >98 % pure. The ^{14}C label was incorporated into the carboxyl carbon atom of TPA, and thus expected to be incorporated in all major metabolites. Unless otherwise stated, reagents were obtained from Sigma-Aldrich Chemical Co. (Poole, U.K.). Ultima Gold scintillation fluid was purchased from PerkinElmer LAS (U.K.), Seer Green, Beaconsfield, Buckinghamshire, U.K. All solvents were of HPLC grade and were products of either Fischer Scientific plc (Loughborough, U.K.) or VWR (Lutterworth, U.K.)

3.2.2 Experimental animals

Protocols described were undertaken in accordance with criteria outlined in a license granted under the Animals (Scientific Procedures) Act 1986 and approved by the University of Liverpool Animal Ethics Committee. Male Wistar rats and male CD-1 mice were obtained from Charles River Laboratories (Margate, U.K), housed in a light-controlled room at a constant temperature, and supplied with a standard chow diet and water *ad libitum.*

3.2.3 Dosing Regimen

The PK studies were conducted at Pfizer, UK.

Male CD-1 mice (35-40 g) were administered furosemide or TPA [5 mg/kg in 10% DMSO 90% water; *i.v.*]. Blood samples (100 µl) were taken and animals were culled at different time points (Table 3.2). The pharmacokinetic study conducted in male Wistar rats (350-400 g) was performed as an *i.v.*/oral (*p.o.*) crossover study over 3 days. On day one animals were administered either furosemide or TPA [1 mg/kg in 10% DMSO and 90% water; *i.v.*] followed by a wash-out period on day two, and on day three they were administered either furosemide or TPA [3 mg/kg in 10% DMSO

90% water; *p.o.*]. Sample collection times for days 1 and 3 are given in Table 3.3 below.

The TK studies were conducted at the University of Liverpool and are described in section 2.2.2.

	Collection Times (hours)								
Mouse	**0**	**0.25**	**0.5**	**1**	**2**	**4**	**6**	**10**	**24**
1	100 µl	100 µl	T						
2			100 µl	100 µl	T				
3					100 µl	100 µl	T		
4							100 µl	100 µl	T

Table 3.2: Blood sampling and culling times for the CD-1 mouse PK study with furosemide or TPA. T = terminal sample.

Sample Type	Collection Times (hours)											
Blood (175µl)	PD	0.1*	0.3	0.5	0.75**	1	2	4	7	10	16	22
Urine	0-22											

Table 3.3: Blood and urine collection times for the Wistar rat PK study with furosemide or TPA. PD = pre-dose, **i.v.* only and ***p.o.* only

3.2.4 Plasma protein binding of furosemide and TPA to rat and mouse plasma

The extent of plasma protein binding *in vitro* was determined by equilibrium dialysis using a Rapid Equilibrium Dialysis (RED) Device (Thermo Scientific Pierce Protein Research Products, Rockford, IL, U.S.A.). Samples of rat and mouse plasma (200 µl, n = 6) containing compound at various concentrations (based on C_{max} values at different doses and ROA) were dialyzed against Dulbecco's phosphate buffered saline (dPBS; 350 µl) for 4 hours at 37°C and 450 rpm. After dialysis, the plasma and

buffer were transferred into a clean 96-well block for analysis. Compounds were extracted and the concentrations of drug in plasma and buffer were determined by LC-MS analysis, as described below. For the plasma TK data, log(drug concentration) was plotting against the fraction unbound values (MasterPlexQT (version 5; MiraiBio Group, Hitachi Solutions America LTD.)); the curve was then used to predict the fraction unbound at each time point. Plasma protein binding values were determined using the following equation:

$$\text{Plasma protein binding (\%)} = 100 - \left(\frac{buffer\ concentration}{plasma\ concentration}\right) \times 100$$

3.2.5 Blood-plasma partitioning of furosemide and TPA in human and rat whole blood

The extent of drug partitioning into the cellular fraction of blood was determined by incubation of the compounds (1 μg/ml) in whole blood (human, rat) for 0, 60 and 90 minutes at 37°C and 450 rpm. After the time point was reached a whole blood sample was taken and the plasma was collected by centrifugation for 1 minute at 10,000 rpm. The whole blood and plasma samples were transferred to a clean 96-well block for analysis. Compounds were extracted and the concentrations of drug in plasma and buffer were determined by LC-MS/MS analysis, as described below.

3.2.6 Liver sample preparation for LC-MS/MS analysis

Liver concentrations of furosemide and TPA were determined in liver from animals administered furosemide or TPA (1.21 mmol/kg) over 1, 3, 6 and 24 hours. In brief, 500 mg of liver tissue was homogenized in 2.5 ml dPBS (pH 7.5)) using a glass Teflon homogenizer. 100 μl of liver homogenate was added to 200 μl ice-cold ACN. The protein was allowed to precipitate on ice for 10 minutes before centrifugation at 14000 rpm for 5 minutes. The supernatant was used for quantification of compounds by LC-MS/MS.

3.2.7 Liver protein binding of furosemide and TPA to rat and mouse liver

The extent of liver protein binding was determined by equilibrium dialysis using Rapid Equilibrium Dialysis (RED) Device. Samples of rat or mouse liver homogenate (200 µl, n = 6) containing compound at various concentrations (based on C_{max} values at different doses and ROA) were dialyzed against Dulbecco's phosphate buffered saline (dPBS; 350 µl) for 4 hours at 37°C and 450 rpm. After dialysis, the liver homogenate and buffer were transferred into a clean 96-well block for analysis. Compounds were extracted and the concentrations of drug in liver homogenate and buffer were determined by LC-MS analysis, as described below. Liver protein binding values were determined using the following equation:

$$\text{Liver protein binding (\%)} = 100 - \left(\frac{buffer\ concentration}{liver\ concentration}\right) \times 100$$

3.2.8 Furosemide and TPA quantification in plasma and liver by LC-MS/MS

Plasma or liver homogenate (50 µl) were extracted by liquid-liquid extraction using ethyl acetate in a 96-well format and the organic layer was dried down by a stream of N_2 and then reconstituted in methanol (75 µl). All samples were quantified using an AB Sciex API-4000 (Turbo V Ionspray source) triple quadruple mass spectrometer (AB Sciex, Foster City, CA, U.S.A.) and an Agilent 1100 binary pump LC system (Agilent Tech. Inc., Palo Alto, CA, U.S.A.). Chromatographic separation was achieved using a Zorbax XDB C18 analytical column (4.6 x 50 mm, 5 µm particle size); column temperature was 45°C. The aqueous mobile phase (H_2O/MeOH, 90/10 v/v; pH 7) contained 10 mM Ammonium Acetate and the organic mobile phase was MeOH. The flow rate was 0.6 ml/min. Detection was by negative-ion electrospray ionisation. MRM transitions for furosemide and TPA and MS working parameters are given in Table 3.4. PK and TK parameters were calculated using WinNonLin software (Pharsight, St. Louis, MO, U.S.A.).

Parameters	FS MRM	TPA MRM
Source temperature (°C)	500.0	500.0
Nebulizing gas (gas-1) (arbitrary units)	10.00	10.00
Ion spray voltage (V)	4500	4500
Collision energy (eV)	-30.00	-24.00
Declustering potential (V)	-26.00	-26.00
Focusing potential (V)	-220.0	-170.0
Entrance potential (V)	-10.00	-10.00
Mode of analysis	Negative	Negative
Ion transition products (*m/z*)	328.9/204.9	344.9/300.8

Table 3.4: Main working parameters for LC-MS/MS MRM quantification of furosemide and TPA

3.2.9 Pharmacokinetic and toxicokinetic parameter definitions and calculations

Area under the plasma concentration-time curve (AUC) describes the amount of drug in the circulation over time, after the dose has been administered. In WinNonLin (Pharsight, St. Louis, MO, U.S.A.), AUC is calculated using linear, linear/log trapezoidal or linear up/log down rules.

C_{max} is the maximum concentration of drug in the circulation after administration, and T_{max} is the time at which this concentration is achieved.

Volume of distribution (V_d) is a theoretical concept that allows the fraction of drug in the circulation and fraction of drug in the tissues to be calculated. Blood volume is roughly 60 - 80 ml/Kg; a drug that does not distribute into tissues and remains in the circulation will have a V_d of about 0.08 L/Kg. Drugs that distribute into extracellular water will have a V_d of about 0.2 L/kg, the volume of total body water is 0.6 l/kg and if a drug has a V_d greater than this it distributes significantly into the tissues. V_d is

calculated either from the initial concentration (C_0), which is extrapolated from the plasma concentration vs. time profile, or by using the AUC.

$V_d = \text{Dose} / C_0$

$V_d = \text{Dose} \times F / \text{AUC} \times K_{el}$

Clearance (Cl) values describe the volume of blood totally cleared of drug per unit time. Clearance values that approach the hepatic blood flow indicate that metabolic clearance is high; hepatic blood flow for man, rat and mouse are approximately 20, 70 and 90 ml/min/Kg respectively.

$Cl = \text{Dose} / \text{AUC}$

Blood arriving at the kidneys and liver will only have a fraction of total drug present in the body at that time as distribution into tissues will have occurred. The duration the drug is in the body will therefore be a function of clearance and fraction of drug in the blood. The amount of drug in the blood is related to the V_d and so the elimination rate constant (K_{el}) is calculated by the following equation.

$K_{el} = Cl / V_d$

The half-life ($t_{1/2}$) is the time taken for the plasma concentration of a drug to decline by 50%. It can be calculated as follows:

$t_{1/2} = \ln 2 / K_{el} = (\ln 2 \times V_d) / Cl$

Drugs can bind, with differing affinities, to plasma and tissue proteins; only drug molecules in the unbound state are free to interact with pharmacological target, off-target proteins and be subject to elimination. It is therefore routine to calculate the fraction of free drug in the circulation and quote the above parameters in terms of unbound fraction of drug. The method for determining plasma protein binding is described in section 3.2.3.

Bioavailability (F) compares the concentration of the drug in systemic circulation following non-intravenous with the concentration of the same drug following intravenous administration.

$F = (AUC_{oral} / AUC_{IV}) \times (Dose_{IV} / Dose_{oral})$

In addition to calculating the plasma AUC, C_{max} and F values, the liver AUC was also determined for the toxicokinetic study. Liver protein binding was determined to contextualize the data (section 3.2.6).

3.2.10 Statistical analysis

All results were expressed as mean + standard deviation. Data sets were analysed for normality using the Shapiro-Wilk test. An unpaired T-test was used for single comparisons of normal data. Where multiple comparisons were made and the data was normally distributed, one-way ANOVA was used with bonferroni correction. All statistical analysis was performed using the StatsDirect statistical software.

3.3 RESULTS

3.3.1 The extent of protein binding of furosemide and TPA to rat and mouse plasma and liver tissue

Plasma protein binding (PPB) values of furosemide and TPA for each species were determined *in vitro* at concentrations similar to those achieved in the plasma *in vivo* at low doses (1 mg/kg; Table 3.5). For the toxicokinetic study, a range of concentrations of furosemide and TPA were used in the *in vitro* binding assay in order to construct a plasma dose-response curve for each species (PPB values for 20 μM are shown in Table 3.6). The curves were then used to calculate the fraction unbound based on the total plasma concentration at a given time point (Figure 3.1). Liver protein binding (LPB) was carried out at the C_{max} concentrations (Table 3.7).

Species	Compound	Concentration (nM)	Fraction Unbound	PPB %
Mouse	FS	3024	0.028	97.2
	TPA	2899	0.018	98.2
Rat	FS	3024	0.013	98.7
	TPA	2899	0.007	99.3

Table 3.5: Plasma protein binding data determined for PK parameter contextualization. Concentrations chosen based on C_{max} values in PK studies.

Species	Compound	Fraction Unbound	PPB %
Mouse	FS	0.0144	98.6
	TPA	0.0103	99.9
Rat	FS	0.0129	98.7
	TPA	0.0264	97.4

Table 3.6: Plasma protein binding data determined for TK parameters contextualization. Values of fraction unbound were determined with 20 μM of either FS or TPA. The complete range of concentrations were used to construct the curves in Figure 3.1

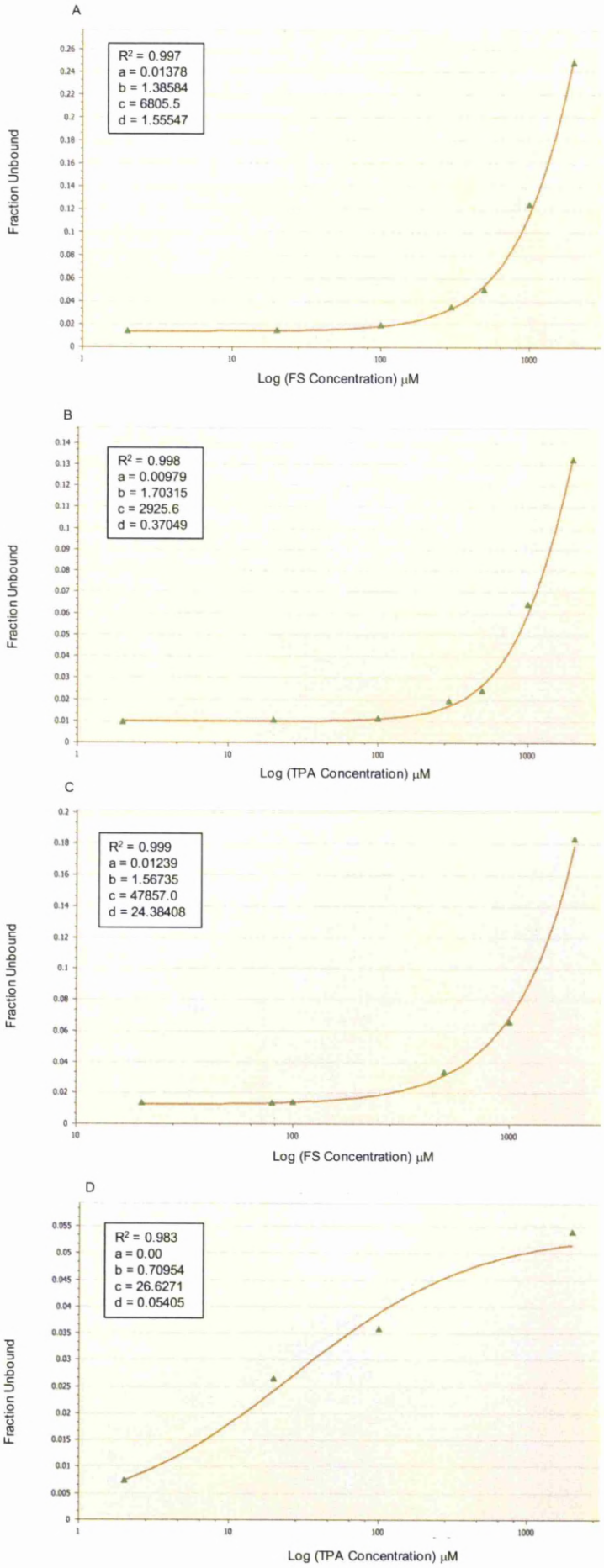

Figure 3.1: Dose-response curves showing drug concentration vs fraction unbound. The degree of binding of FS (A and C) and TPA (B and D) was determined, *in vitro*, in mouse (A and B) and rat (C and D) plasma over a range of concentrations. The equation of the dose-response curves is as follows:

$$y = \frac{A-D}{\left(1+\left(\frac{x}{C}\right)^{B}\right)} + D$$

Species	Compound	Concentration (μM)	Fraction Unbound	LPB %
Mouse	FS	48.4	0.109	89.1
		302	0.079	92.1
	TPA	162	0.056	94.4
Rat	FS	6.05	0.097	90.3
	TPA	23.2	0.042	95.8
		406	0.05	95.0

Table 3.7: Liver protein binding data determined for TK parameters contextualization. Concentrations chosen based on liver C_{max} values in TK studies.

3.3.2 Determination of the pharmacokinetic parameters of furosemide and TPA in male Wistar rats and CD-1 mice

The pharmacokinetic parameters for furosemide and TPA in both male Wistar rats and male CD-1 mice (dosing regimens, Tables 3.2 and 3.3) are described in Tables 3.8 and 3.9 respectively. AUC graphs are shown in Figures 3.2 and 3.3, where data points are missing samples were not collected.

Furosemide and TPA comparison

In the mouse the unbound clearance was calculated to be 107 and 300 ml/min/kg for furosemide and TPA respectively and free systemic exposure reached 3485 and 1370 nM for furosemide and TPA respectively, suggesting that, after *i.v.* dosing, furosemide is retained in the system longer and at higher concentrations compared to TPA, which would reflect the toxicity data gathered in Chapter 2. In the Wistar rat the PK parameters of furosemide and TPA are comparable; clearance, systemic exposure and bioavailability values are all similar.

Species comparison

The species difference between the rat and mouse in terms of furosemide toxicity has previously been explained by a species specific FS-GSH conjugate formed in the rat (Williams *et al.*, 2007). However, the PK data presented here shows that species differences in PK may also contribute to the susceptibility of the mouse to

furosemide-induced liver damage. The free C_{max} and half-life are all greater in the mouse model (3485 nM, 0.7 hours) compared to that of the rat (80.9 nM, 0.18 hours) and the unbound clearance in the rat, at 1147 ml/min/kg, is much faster than in the mouse (at 107 ml/min/kg) suggesting that the mouse has greater exposure to furosemide.

ROA comparison

In the mouse the free AUC and free C_{max} are greater when furosemide is given via an *i.p.* dose (742 ng.h/ml and 3485 nM) compared to an oral dose (*p.o.*) (250 ng.h/ml and 466 nM).

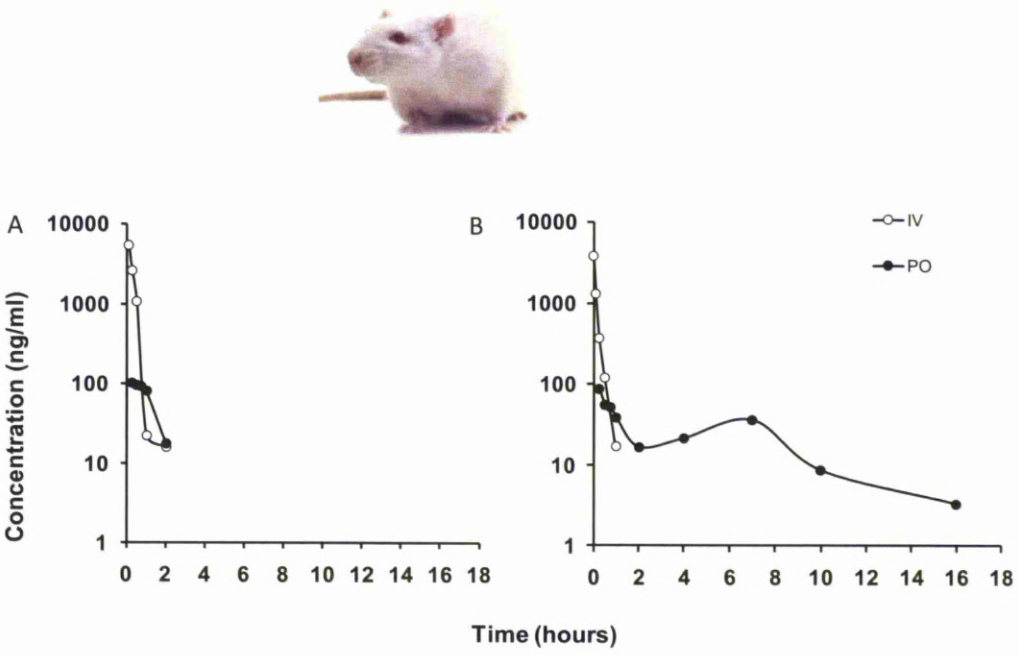

Figure 3.2: Plasma concentration vs. time plots of FS (A) and TPA (B) in the Wistar rat. Graphs plotted using WinNonLin show total compound concentrations in plasma over time following a bolus 1 mg/kg *i.v.* (○) dose or 3 mg/kg *p.o.* (●) dose.

	**FS (*i.v.*; 1mg/kg)**	**FS (*p.o.*; 3mg/kg)**	**TPA (*i.v.*; 1 mg/kg)**	**TPA (*p.o.*; 3 mg/kg)**
$AUC_{0-\infty}$ (ng.h/ml)	**664** ± 438	**330** ± 109	**1336** ± 424	**558** ± 154
Free $AUC_{0-\infty}$ (ng.h/ml)	**8.60** ± 5.7	**4.3** ± 1.4	**9.4** ± 3.0	**3.9** ± 1.1
Total C_{max} (nM)	**6219** ± 2815	**477** ± 99.1	**9544** ± 3517	**541** ± 280
Free C_{max} (nM)	**80.9** ± 36.6	**5.63** ± 2.2	**73.8** ± 27.2	**4.2** ± 2.17
T_{max} (h)	-	**0.47** ± 0.2	-	**0.5** ± 0.38
$T_{1/2}$ (h)	**0.18** ± 0.03	-	**0.3** ± 0.31	-
Cl (ml/min/kg)	**25.0** ± 13.2	-	**12.4** ± 5.36	-
Cl_u (ml/min/kg)	**1147** ± 588	-	**1174** ± 370	-
Vd_{ss} (L/Kg)	**0.38** ± 0.24	-	**0.3** ± 0.11	-
Vd_{uss} (L/Kg)	**17.3** ± 11.1	-	**23.9** ± 17.1	-
F (%)	-	**14.0** ± 14.2	-	**14.9** ± 4.93

Table 3.8: Plasma PK parameters of furosemide and TPA administered either orally or via an *i.v.* dose to male Wistar rats. N=3 for each group. Parameters were calculated using WinNonLin software and are expressed as mean ± standard deviation.

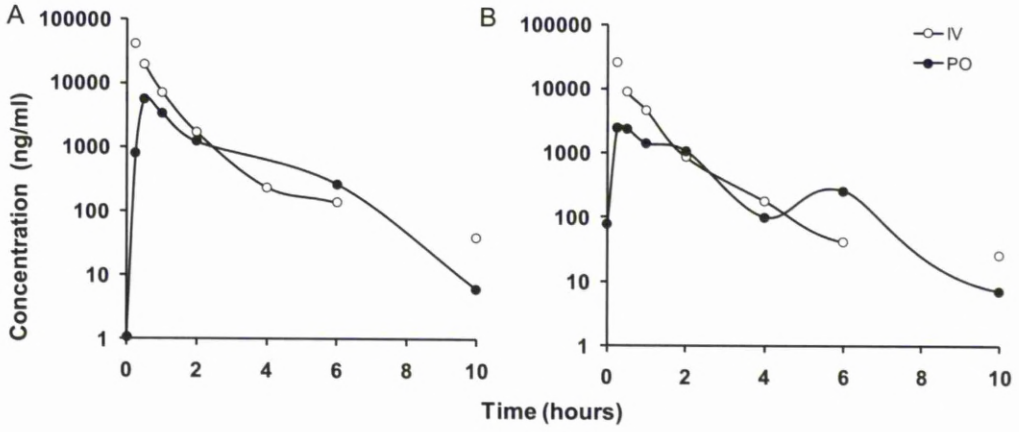

Figure 3.3: Plasma concentration vs. time plots of FS (A) and TPA (B) in the CD-1 mouse. Graphs plotted using WinNonLin show total compound concentrations in plasma over time following a bolus 1 mg/kg *i.v.* (○) dose or 5 mg/kg *p.o.* (●) dose.

	FS (*i.v*; 1mg/kg)	FS (*p.o.*; 5mg/kg)	TPA (*i.v.*; 1mg/kg)	TPA (*p.o.*; 5 mg/kg)
$AUC_{0-\infty}$ (ng.h/ml)	26,485	8912	15,254	5194
Free $AUC_{0-\infty}$ (ng.h/ml)	742	250	275	93.5
Total C_{max} (nM)	124,471	16,640	79,758	7347
Free C_{max} (nM)	3485	466	1370	126
T_{max} (h)	-	0.5	-	0.25
$T_{1/2}$ (h)	0.7	-	0.6	-
Cl (ml/min/kg)	3	-	5.4	-
Cl_u (ml/min/kg)	107.1	-	300	-
Vd_{ss} (L/Kg)	0.2	-	0.3	-
Vd_{uss} (L/Kg)	6.1	-	14.4	-
F (%)	-	34	-	34

Table 3.9: Plasma PK parameters of FS and TPA administered either orally or via an *i.v.* dose to male CD-1 mice. Parameters were calculated from a composite profile of 4 mice over 24 hours using WinNonLin.

3.3.3 Determination of the toxicokinetic parameters of furosemide and TPA in male Wistar rats and CD-1 mice

TK studies were undertaken to determine the kinetics of furosemide and TPA at a higher dose where toxicity is observed for furosemide in the mouse. The concentrations of the compounds were also measured in the liver to identify possible accumulation that might contribute to hepatotoxicity.

Liver and plasma exposure levels of furosemide and TPA were determined over 24 hours in male CD-1 mice and male Wistar rats administered either furosemide or TPA (1.21 mmol/kg in PEG) either orally or via an *i.p.* dose (Tables 3.10, 3.11, 3.12 and 3.13). The furosemide and TPA plasma AUC increased supraproportionally (from 240-fold to 4300-fold) as the dose was increased from 3 or 5 mg/kg to 400 mg/kg orally in the mouse and rat suggesting that, in both species, clearance for both compounds becomes saturated at high oral doses (Figure 3.8 B).

The plasma and liver exposure of both TPA and furosemide were comparable in the mouse (*i.p.* ROA; Figure 3.8 A) suggesting that the two compounds undergo similar disposition and clearance at high doses (~400 mg/kg). When comparing the rat and mouse in terms of furosemide exposure (*i.p.* ROA), plasma levels, in terms of free AUC, were comparable; however total liver exposure in the mouse was more than twice that in the rat with AUC values at 3032 and 1280 μg.h/ml respectively (Figure 3.8 C). Oral administration of furosemide in the mouse resulted in significantly reduced plasma and liver exposure compared to *i.p.* administration (Figure 3.8 D). The free plasma AUC when furosemide is delivered via an *i.p.* injection to a mouse is 3 times that of an oral delivery (495 μg.h/ml *i.p.* and 153 μg.h/ml *p.o.*). Likewise, the free liver AUC when furosemide is delivered via an *i.p.* injection is more than 4 times that of an oral delivery (3032 μg.h/ml *i.p.* and 646 μg.h/ml *p.o.*).

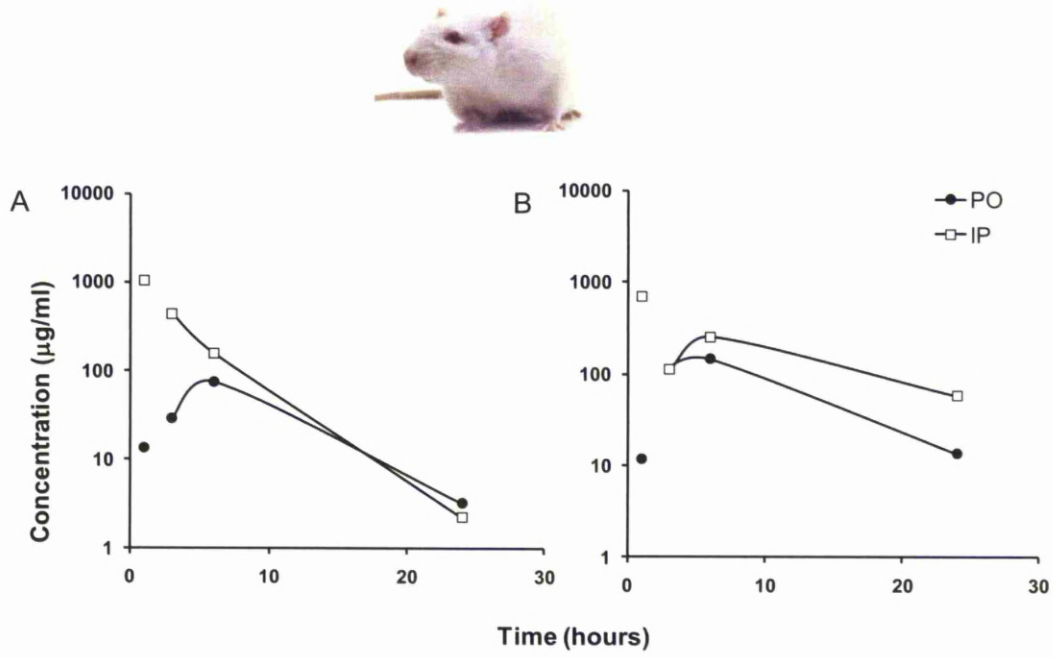

Figure 3.4: Plasma concentration vs. time plots of FS (A) and TPA (B) in the Wistar rat. Graphs plotted using WinNonLin show total compound concentrations in plasma over time following a bolus 1.21 mmol/kg *i.p.* (□) or *p.o.* (●) dose.

	FS (*IP*)	FS (*PO*)	TPA (*IP*)	TPA (*PO*)
Total $AUC_{0-\infty}$ (µg.h/ml)	**4932** ± 2298	**1123** ± 372	**8213** ± 3324	**2586** ± 950
Free $AUC_{0-\infty}$ (µg.h/ml)	**1057** ± 1008	**21.4** ± 12.0	**405** ± 162	**118** ± 53.1
T_{max} (h)	**1.00** ± 0.00	**5.25** ± 1.50	**1.50** ± 1.00	**4.50** ± 1.73
Total C_{max} (µg/ml)	**1103** ± 484	**86.4** ± 32.8	**479** ± 292	**193** ± 98.7
Free C_{max} (µg/ml)	**542** ± 543	**1.81** ± 1.15	**38.8** ± 15.6	**9.35** ± 5.15
Total C_{24} (µg/ml)	**2.30** ± 0.56	**7.51** ± 8.91	**80.2** ± 70.2	**16.9** ± 13.2
Free C_{24} (µg/ml)	**0.03** ± 0.01	**0.10** ± 0.12	**3.63** ± 3.52	**0.58** ± 0.57
Cl (ml/kg/hr)	**94.4** ± 40.0	**389** ± 136	**54.9** ± 23.4	**167** ± 45.4
Cl_u (ml/kg/hr)	**707** ± 539	**23112** ± 10982	**1114** ± 482	**3801** ± 1211

Table 3.10: Plasma toxicokinetic parameters of FS and TPA (1.21mmol/kg in PEG; *p.o.* or *i.p.*) in male Wistar rats. Parameters were calculated using WinNonlin software. Mean ± standard deviation; n=4.

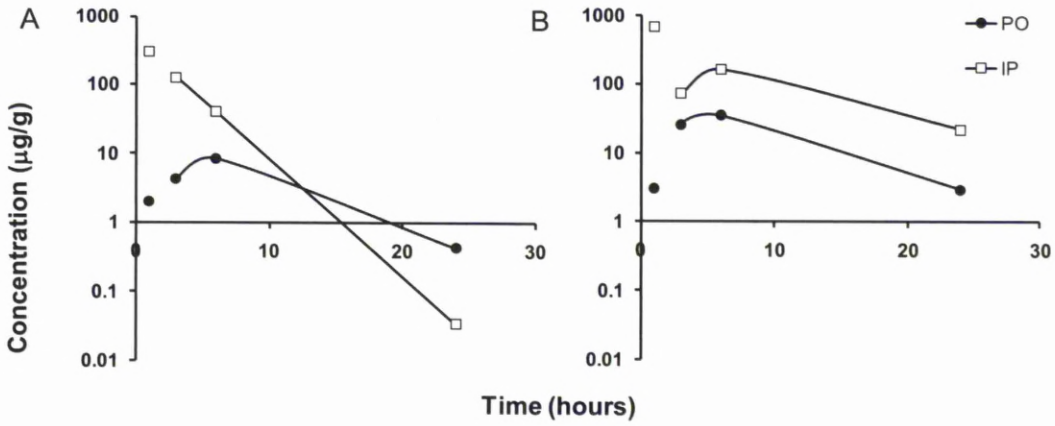

Figure 3.5: Liver concentration vs. time plots of FS (A) and TPA (B) in the Wistar rat. Graphs plotted using WinNonLin show compound concentrations in liver over time following a bolus 1.21 mmol/kg *i.p.* (□) or *p.o.* (●) dose.

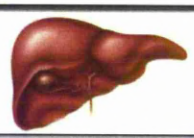	FS (*IP*)	FS (*PO*)	TPA (*IP*)	TPA (*PO*)
Total $AUC_{0-\infty}$ (µg.h/ml)	**1280** ± 228	**141** ± 51.2	**4459** ± 1157	**578** ± 222
Free $AUC_{0-\infty}$ (µg.h/ml)	**128** ± 22.8	**14.1** ± 5.1	**223** ± 57.9	**28.9** ± 11.1
Total C_{max} (µg/g)	**308** ± 39.0	**10.2** ± 5.77	**696** ± 164	**42.7** ± 23.7
Free C_{max} (µg/g)	**30.8** ± 3.89	**1.02** ± 0.58	**34.8** ± 8.2	**2.13** ± 1.18
Total C_{24} (µg/g)	**0.08** ± 0.08	**1.03** ± 1.11	**26.3** ± 20.0	**3.75** ± 2.88
Free C_{24} (µg/g)	**0.01** ± 0.01	**0.10** ± 0.11	**1.31** ± 1.0	**0.19** ± 0.14

Table 3.11: Liver toxicokinetic parameters of FS and TPA (1.21mmol/kg in PEG; *p.o.* or *i.p.*) in male Wistar rats Parameters were calculated using WinNonlin software. Mean ± standard deviation; n=4.

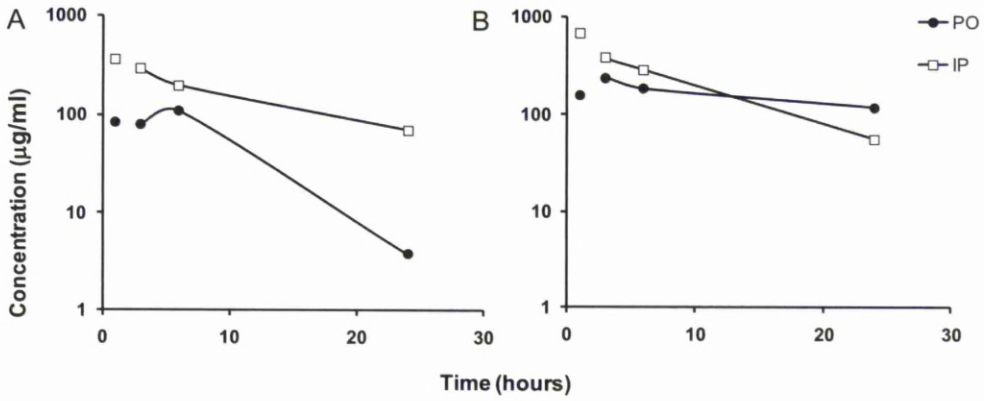

Figure 3.6: Plasma concentration vs. time plots of FS (A) and TPA (B) in CD-1 mice. Graphs plotted using WinNonLin show compound concentrations in plasma over time following a bolus 1.21 mmol/kg *i.p.* (□) or *p.o.* (●) dose.

	FS (*IP*)	FS (*PO*)	TPA (*IP*)	TPA (*PO*)
Total $AUC_{0-\infty}$ (µg.h/ml)	**5505** ± 1520	**2125** ± 1467	**6587** ± 1399	**4329** ± 1486
Free $AUC_{0-\infty}$ (µg.h/ml)	**495** ± 485	**153** ± 156	**1350** ± 850	**441** ± 101
T_{max} (h)	**3.25** ± 2.06	**3.50** ± 3.00	**1.50** ± 1.00	**2.75** ± 2.36
Total C_{max} (µg/ml)	**433** ± 340	**209** ± 171	**778** ± 345	**499** ± 265
Free C_{max} (µg/ml)	**103** ± 156	**23.4** ± 31.0	**373** ± 270	**164** ± 160
Total C_{24} (µg/ml)	**74.2** ± 30.3	**5.36** ± 4.18	**58.0** ± 16.6	**88.4** ± 97.4
Free C_{24} (µg/ml)	**2.22** ± 1.40	**0.08** ± 0.06	**2.15** ± 0.78	**7.00** ± 10.4
Cl (ml/kg/hr)	**78.9** ± 30.0	**314** ± 262	**63.1** ± 15.0	**99.8** ± 33.0
Cl_u (ml/kg/hr)	**1526** ± 1210	**12211** ± 14752	**443** ± 350	**940** ± 222

Table 3.12: Plasma toxicokinetic parameters of FS and TPA (1.21mmol/kg in PEG; *p.o.* or *i.p.*) in male CD-1 mice. Parameters were calculated using WinNonlin software. Mean ± standard deviation; n=4

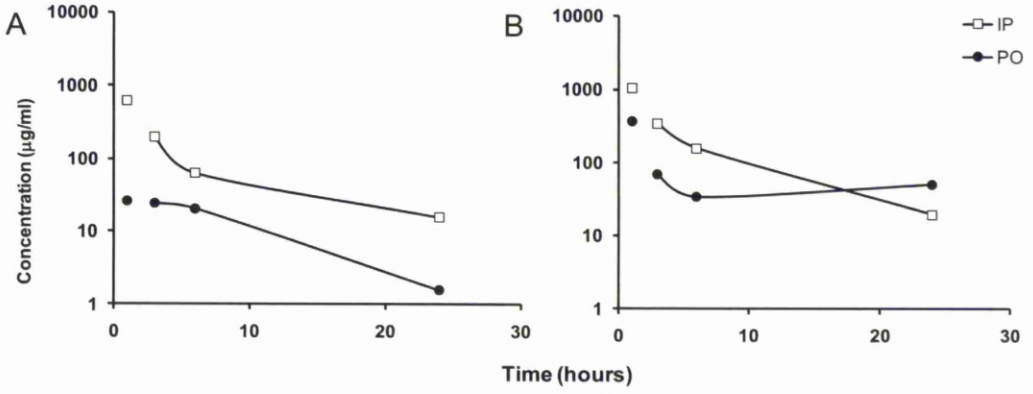

Figure 3.7: Liver concentration vs. time plots of FS (A) and TPA (B) in CD-1 mice. Graphs plotted using WinNonLin show compound concentrations in liver over time following a bolus 1.21 mmol/kg *i.p.* (□) or *p.o.* (●) dose.

	FS (*IP*)	FS (*PO*)	TPA (*IP*)	TPA (*PO*)
Total $AUC_{0-\infty}$ (µg.h/ml)	**3032** ± 1162	**646** ± 448	**5092** ± 1850	**1362** ± 742
Free $AUC_{0-\infty}$ (µg.h/ml)	**243** ± 93.0	**51.7** ± 35.8	**306** ± 111	**81.7** ± 44.5
Total C_{max} (µg/g)	**634** ± 159	**81.1** ± 97.6	**1191** ± 613	**281** ± 187
Free C_{max} (µg/g)	**50.7** ± 12.8	**6.49** ± 7.8	**71.4** ± 36.8	**16.9** ± 11.2
Total C_{24} (µg/g)	**17.1** ± 8.5	**1.75** ± 0.77	**23.1** ± 13.3	**38.0** ± 58.9
Free C_{24} (µg/g)	**1.37** ± 0.68	**0.14** ± 0.06	**1.39** ± 0.08	**2.28** ± 3.53

Table 3.13: Liver toxicokinetic parameters of FS and TPA (1.21mmol/kg in PEG; *p.o.* or *i.p.*) in male CD-1 mice. Parameters were calculated using WinNonlin software. Mean ± standard deviation; n=4

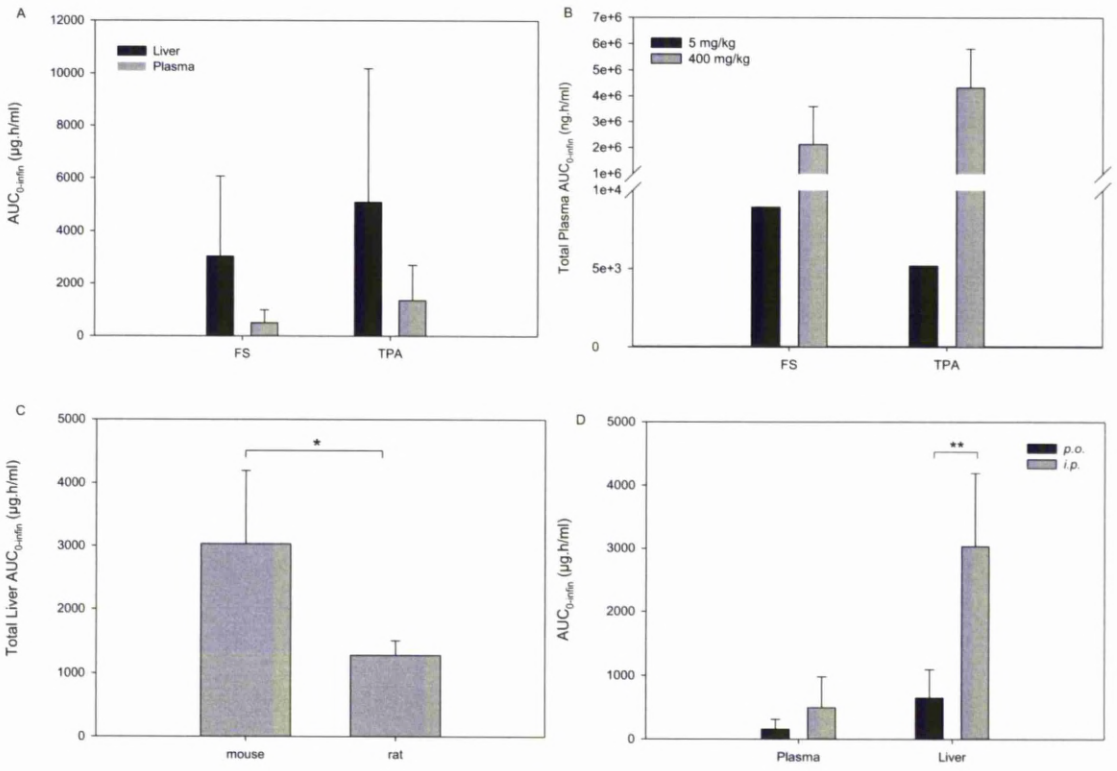

Figure 3.8: Summary graphs of TK comparisons between (A) furosemide and TPA, in male CD-1 mice (1.21 mmol/kg *i.p.*), (B) dose of furosemide, in male CD-1 mice (*p.o.*), (C) species, in male CD-1 mice and Wistar rats (furosemide 1.21 mmol/kg *i.p.*) (D) ROA, in male CD-1 mice (furosemide 1.21 mmol/kg). Data are expressed as mean + standard deviation (except B for 5 mg/kg where the data was composite). * p=0.05, ** p=0.01 unpaired T test.

3.4 DISCUSSION

The aims of this chapter were to investigate whether the differences in hepatotoxicity observed between furosemide and TPA could be explained by differences in pharmacokinetics. TPA did not induce severe hepatotoxicity in mice when administered via an *i.p.* or oral route. It has been observed that in mice, following a large dose of furosemide or pretreatment with sulfobromophathlein (BSP; BSP has been used previously to compete with the biliary excretion of a number of compounds including bilirubin (Cantarow and Wirts, 1948, Spitznagle *et al.*, 1977)), saturation of biliary excretion of furosemide occurred and that it was is closely associated with the appearance of liver necrosis (Spitznagle *et al.*, 1977). Here, it was hypothesised that the differences in the toxicity of furosemide and TPA in the mouse may be due to the saturable, dose-dependent nature of furosemide excretion and not that of TPA. In Chapter 2 it was found that *i.p.* administration of furosemide-induced hepatotoxicity in male mice. However, at the same dose, orally administered furosemide failed to do so, suggesting that the toxicity of furosemide could be partly attributed to accumulation in the liver, as well as bioactivation.

The bioavailability of furosemide and TPA were similar in both rats (~14%) and mice (~35%) suggesting that the two compounds are absorbed and undergo pre-systemic metabolism to a similar extent. The bioavailability of furosemide in rats in the literature ranges from around 30 to 60% (Lee and Chiou, 1983, Kim *et al.*, 2000, Kim *et al.*, 1993, Park *et al.*, 1998).

Plasma protein binding (PPB) of TPA was 99.3% and 98.2 % in rat and mouse, respectively at 1 μg/ml. PPB of furosemide in the mouse was 97.2 % at 1 μg/ml. In the rat PPB of furosemide was 98.7% (at 1 μg/ml); in the literature PPB ranged from 87.2 ± 5.3% to 96.81% (Table 3.14). The extent of furosemide binding to plasma protein is in the range of 96-98% in humans (Table 3.16). The substantial amount of binding is reflected in the low volume of distribution, which is in the range of 0.07-0.21 L/kg in humans (Table 3.16) and 0.12-0.25 L/kg in rats (Table 3.14). The calculated half-life of furosemide from the literature data ranges from 0.43 to 1.53 hours in humans (Table 3.16) and 0.68 - 1.25 hours in rats (Table 3.14) after an *i.v.* dose. The volume of distribution and half-life of furosemide in rats determined in this study were 0.38 ± 0.24 L/Kg and 0.18 ± 0.03 hours respectively. Hammarlund *et*

al. (1982) observed that increasing the dose of furosemide given to rats increased the half-life. This change could be detected as a change in the apparent volume of distribution caused by decreased protein binding at increasing plasma concentrations of furosemide. The data collected from the literature support this conclusion: increasing the dose from 10 mg/kg to 20 mg/kg decreased plasma protein binding from 96.81 ± 0.3% to 87.2 ± 5.3% (Table 3.14).

In the mouse the unbound clearance was calculated to be 107 and 300 ml/min/kg for furosemide and TPA respectively and free systemic exposure reached 3485 and 1370 nM of furosemide and TPA respectively, suggesting that furosemide is retained in the system longer and at higher concentrations which would reflect the toxicity data gathered in Chapter 2. In the Wistar rat the PK parameters of furosemide and TPA are comparable; clearance, systemic exposure and bioavailability values are all similar. The species difference between the rat and mouse in terms of furosemide toxicity has previously been explained by a species specific FS-GSH conjugate formed in the rat (Williams *et al.*, 2007). However, the PK data presented here shows that species differences in PK may also contribute to the susceptibility of the mouse to furosemide-induced liver damage. The free C_{max}, half-life and bioavailability are all greater in the mouse model (3485 nM, 0.7 hours, 34%) compared to that of the rat (80.9 nM, 0.18 hours, 14%) and the clearance in the rat, at 1147 ml/min/kg, is faster than in the mouse (at 107 ml/min/kg). If the clearance values represent elimination of parent drug from the system (and not metabolic clearance to a reactive metabolite) than the data would suggest that the mouse has greater exposure to furosemide.

Toxicity is observed in the mouse at a dose many times greater than that used in the PK study. In order to understand the disposition of the compounds at a 'toxic' dose a toxicokinetic study was carried out. In addition, the drug levels in the liver were also measured over time. The plasma and liver exposure of both TPA and furosemide were comparable in the mouse (*i.p.* ROA) suggesting that the two compounds undergo similar disposition and clearance at 400 mg/kg. The furosemide and TPA plasma AUC increased supraproportionally (≈240-fold to 4300-fold) as the dose was increased from 3/5 to 400 mg/kg orally in the mouse and rat suggesting that, in both species, clearance for both compounds becomes saturated at high oral doses. This has

been observed previously; the metabolic clearance of furosemide decreased with increasing dose in the rat (Hammarlund and Paalzow, 1982).

As well as comparing the two analogues, the investigation also allowed comparisons to be made between species and ROA, in terms of plasma and liver drug concentrations relative to toxicity observed. Species differences in furosemide-induced hepatotoxicity between rats and mice have been investigated. Identification of a FS γ-ketocarboxylic acid in mice and rats *in vivo* suggested the existence of a reactive epoxide intermediate (Williams *et al.*, 2007). It was proposed that this reactive metabolite covalently bound to hepatic protein, and toxicity was observed in mice; however in rats this does not occur. A species specific GSH conjugate was identified in the bile of furosemide dosed rats, suggesting a possible safety mechanism exists in the rat to protect from furosemide-induced hepatotoxicity (Williams *et al.*, 2007). The investigations presented in this chapter highlight that increased furosemide liver exposure (or reduced clearance of reactive metabolite) in mice may also contribute to the species differences in furosemide-induced hepatotoxicity. The free plasma AUCs of furosemide in the rat and mouse were comparable (*i.p.* ROA), however liver exposure in the mouse was twice that in the rat, with free liver AUC values at 243 and 128 μg.h/ml respectively.

Oral administration of furosemide in the mouse resulted in significantly reduced plasma and liver exposure compared to *i.p.* administration. The free plasma AUC when furosemide is delivered via an *i.p.* injection is 3 times that of an oral delivery (495 μg.h/ml *i.p.* and 153 μg.h/ml *p.o.*). Likewise, the free liver AUC when furosemide is delivered via an *i.p.* injection is 5 times that of an oral delivery (243 μg.h/ml *i.p.* and 51.7 μg.h/ml *p.o.*). The massive difference observed may be a result of poor bioavailability after an oral dose and essentially a direct liver load after administration into the peritoneal cavity.

The aims of this chapter were to use pharmacokinetic and toxicokinetic studies to help explain the differences observed in furosemide-induced hepatotoxicity between furosemide and its thiophene analogue (TPA). Despite differences observed in the PK parameters, a high-dose toxicokinetic study revealed that the two compounds undergo very similar disposition, suggesting that toxicity of furosemide in mice may be attributed to different metabolic fate of furosemide. Comparisons were also made

between species and ROA, in terms of plasma and liver drug concentrations relative to toxicity observed. These comparisons provided evidence that liver accumulation may also be a contributing factor to furosemide-induced hepatotoxicity in the mouse.

Reference	Assay	Animals	Dose	ROA	% PPB	Free C_{max} (nM)	$T_{1/2}$ (h)	Cl (ml/min/kg)	Cl_r (ml/min/kg)	Cl_{nr} (ml/min/kg)	Vd_{ss} (L/Kg)
Kim *et al.* (1993)	HPLC	10	10 mg/kg	IV	96.81 ± 0.27		0.68 ± 0.28	8.41 ± 1.96	3.26 ± 0.97	5.05 ± 1.39	0.25 ± 0.06
Lee *et al.* (1983)	HPLC	4	2 mg	IV			0.74 ± 0.15	5.91 ± 1.04	4.16 ± 1.04	1.64 ± 0.49	
Kim *et al. (2000)*	HPLC	4	20 mg/kg	IV			1.24 ± 0.09	5.7 ± 1.06	3.34 ± 0.76	2.33 ± 0.39	0.127 ± 0.04
Park *et al.* (1998)	HPLC	10	6 mg	IV	89.6		0.75 ± 0.11	7.05 ± 0.87	4.33 ± 1.16	2.2 ± 0.52	0.119 ± 0.03
Yang *et al.* (2009)	HPLC	7	20 mg/kg	IV	87.2 ± 5.31	293 ± 111	1.25 ± 0.28	5.32 ± 0.43	1.95 ± 0.413		

Table 3.14: Pharmacokinetic parameters of FS in rats administered FS via an *i.v* route. Cl_r = renal clearance, Cl_{nr} = non-renal clearance. All other abbreviations are stated in the material and methods section.

Reference	Assay	Animals	Dose	ROA	$T_{1/2}$ (h)	Cl_r (ml/min/kg)	F (%)
Kim *et al.* (1993)	HPLC	6	20 mg/kg	PO	2.6 ± 3.0	4.95 ± 6.15	27.6
Lee *et al.* (1983)	HPLC	4	6 mg	PO	2.07 ± 0.78	6.4 ± 1.57	30.2 ± 12.8
Kim *et al.* (2000)	HPLC	5	20 mg/kg	PO		5.7 ± 0.49	28.9
Park *et al.* (1998)	HPLC	9	6 mg	PO		4.57 ± 2.2	60

Table 3.15: Pharmacokinetic parameters of FS in rats administered FS via an oral route. Cl_r = renal clearance, Cl_{nr} = non-renal clearance. All other abbreviations are stated in the material and methods section.

Reference	Assay	Subjects	Dose	% PPB	$T_{1/2}$ (h)	Cl (ml/min)	Cl_r (ml/min)	Cl_{nr} (ml/min)	Vd_{ss} (L/Kg)
Rupp and Hajdu (1970)	Fluorometric	7	40 mg		0.95 ± 0.1	114			
Cutler *et al.* (1974)	Fluorometric	4	0.5, 1 and 1.5 mg/kg	95	0.5 ± 0.1	162	149 ± 37	12 ± 17	
Kelly *et al.* (1974)	Fluorometric	4	80 mg		0.43 ± 0.17	142 ± 39			
Beermann *et al.* (1975)	Radiolabelled	2			0.78 - 0.88				
Beermann *et al.* (1977)	HPLC	5			0.87 ± 0.25	194 ± 35	95 ± 24	99 ± 48	0.21 ± 0.06
Branch *et al.* (1977)	Fluorometric	6	80 mg		1.13	125	75	50	
Andreasen *et al.* (1977)	Fluorometric + TLC	8	40 mg		1.2 ± 0.48	166 ± 42	116 ± 67	50	0.181 ± 0.1
Honari *et al.* (1977)	HPLC	4	1 mg/kg		0.6 ± 0.08	155 ± 24	134 ± 23	21 ± 3	0.176 ± 0.02
Homeida *et al.* (1977)	Fluorometric	6	40 mg		0.63 ± 0.05	268 ± 19	90 ± 10	178 ± 20	
Andreasen *et al.* (1978)	Fluorometric + TLC	7	40 mg	98.3	1.1 ± 0.48	219 ± 49			0.174 ± 0.03
Tilstone *et al.* (1978)	Radiolabelled	11			0.8 ± 0.06	112			0.07
Smith *et al.* (1978)	HPLC	4	40 mg		1.17 ± 0.27	159 ± 15	166 ± 16	42 ± 12	0.13
Rane *et al.* (1978)	HPLC	6		95.9 ± 0.1	0.85 ± 0.07	158	80	77	0.11 ± 0.01
Smith *et al.* (1980)	HPLC	9	40 mg	98.5-99.1	1.53 ± 0.12	164 ± 26	110 ± 24	54.4 ± 9.6	0.11 ± 0.02
Verbeek *et al.* (1982)	HPLC	10	80 mg	94	1.0 ± 0.1	156 ± 7	87 ±8	69 ± 8	0.12
Hammarlund *et al.* (1984)	HPLC	8	40 mg		0.6	162 ± 10.8	117 ± 11.3	45	0.129 ± .008
Vree *et al.* (1995)	HPLC	7		98 ± 2	1.25 ± 0.75	131 ± 26.5	90.2 ± 169.9	41 ± 16.5	

Table 3.16: Pharmacokinetic parameters of FS in human subjects administered FS via an *i.v* route. Cl_r = renal clearance, Cl_{nr} = non-renal clearance. All other abbreviations are stated in the material and methods section.

CHAPTER 4

HETEROCYCLIC RING SUBSTITUTION IN FUROSEMIDE: INVESTIGATING THE EFFECT OF STRUCTURAL CHANGES ON *IN VITRO* AND *IN VIVO* BIOTRANSFORMATION.

CONTENTS

4.1 INTRODUCTION

The findings reported in Chapter 3 revealed that furosemide (FS) and its thiophene analogue (TPA) have a similar disposition in mice *in vivo,* and therefore failed to explain the differences between the hepatotoxicity of the two compounds described in Chapter 2. Species differences in furosemide-induced hepatotoxicity have been observed previously and explained by alternative detoxication mechanisms (Williams *et al.*, 2007). It was shown that the TPA undergoes bioactivation and can covalently bind to hepatic protein *in vitro.* In light of this observation it was hypothesized that TPA may undergo a different, and more effective, mechanism of detoxification compared to furosemide.

It has been demonstrated that furosemide forms an acyl glucuronide, which is found in the plasma and urine of humans (Beermann *et al.*, 1975, Beermann *et al.*, 1977, Benet, 1979, Perez *et al.*, 1979, Smith *et al.*, 1980, Smith and Benet, 1983, Kerremans *et al.*, 1982). More recently the furosemide glucuronide has been identified in the bile of furosemide-treated rats and mice (Williams *et al.*, 2007). In humans, approximately 13 – 17% of an *i.v.* dose of furosemide is excreted as furosemide glucuronide in the urine (Smith *et al.*, 1980, Andreasen *et al.*, 1981, Waller *et al.*, 1982, Verbeeck *et al.*, 1982). In the rat, of the total dose excreted in the bile (21.2 ± 2.6%), 12.8 ± 1.8% was excreted as the furosemide glucuronide (Williams *et al.*, 2007). The furosemide glucuronide has been shown to be unreactive in terms of covalent binding to human serum albumin *in vitro* (Bolze *et al.*, 2002). A more controversial metabolite is the N-dealkylated furosemide metabolite (4-chloro-5-sulphamoyl-anthranilic acid; CSA in literature) first identified in 1964 by Haussler *et al.* It has subsequently been identified in the urine of dogs and monkeys (Yakatan *et al.*, 1976) and in humans (Prandota and Pruitt, 1991, Andreasen *et al.*, 1978). However a number of groups failed to find evidence of this metabolite in humans (Beermann *et al.*, 1975, Smith *et al.*, 1980, Kerremans *et al.*, 1982, Branch *et al.*, 1977). A recent study identified the N-dealkylated furosemide metabolite in the bile of rats and mice without the use of an acid extraction method (Williams *et al.*, 2007); providing clear evidence that it is a genuine metabolite in these species.

The hepatocellular damage caused by furosemide is postulated to be the result of P450 enzyme-mediated formation of a toxic metabolite that binds covalently with

hepatic macromolecules both *in vitro* and *in vivo* (Mitchell *et al.*, 1974, Mitchell *et al.*, 1976). It was found that furosemide binds covalently to microsomal protein, and that the level of binding parallels the severity of necrosis. Furosemide covalent binding is decreased by cysteine and GSH, and also by the presence of P450 enzyme inhibitors, suggesting bioactivation of the furosemide molecule (Williams *et al.*, 2007, Mitchell *et al.*, 1974). Early work suggested that an epoxide of furosemide is responsible for the hepatotoxicity observed in the mouse (Wirth *et al.*, 1976).

More recently, bioactivation of the furan ring was demonstrated by the characterization of three key novel metabolites of furosemide from *in vivo* and *in vitro* studies: FS γ-ketocarboxylic acid, FS-SG conjugate, and a mixed *N*-acetyl lysine and *N*-acetyl cysteine conjugate (Williams *et al.*, 2007). The formation of a FS γ-ketocarboxylic acid *in vivo* is suggestive of formation of an epoxide intermediate. The reactive metabolite binds covalently to murine hepatic protein; this does not occur in rats; the reactive metabolite is excreted in the form of a GSH conjugate, suggesting a possible safety mechanism exists in the rat to protect them from furosemide-induced hepatotoxicity (Williams *et al.*, 2007). As well as species differences between the balance of bioactivation and bioinactivation, it is possible that furosemide accumulation in the liver due to impaired clearance might also be a factor in development of hepatotoxicity in the mouse, as demonstrated in Chapter 3.

Although prior to these studies little was known about the metabolism of TPA, some metabolic pathways can be speculated upon for this compound based on previous studies using other thiophene containing drugs. Tienilic acid (TA) is a diuretic drug, which was released in the US in 1979 as an antihypertensive. In 1980, TA was withdrawn from the US market due to severe secondary hepatotoxic effects and renal toxicity (Zimmerman *et al.*, 1984). The major product of TA metabolism is 5-hydroxy TA, formed from the hydroxylation of the C-5 position on the thiophene ring; however oxidised intermediates of this pathway have been shown to bind covalently to microsomal proteins (Dansette *et al.*, 1991). Studies using electrospray ionization mass spectrometric analysis have deduced that the reactive intermediate could be an epoxide or the TA *S*-oxide (Koenigs *et al.*, 1999), although the formation of the TA *S*-oxide is more widely supported (Mansuy *et al.*, 1991, Dansette *et al.*, 1992, López-Garcia *et al.*, 1994). OSI-930 is an investigational, thiophene anticancer

agent that also undergoes microsomal bioactivation to an *S*-oxide; however studies have shown that it is well tolerated in pre-clinical models and in human volunteers (Medower *et al.*, 2008). Suprofen is a thiophene NSAID, which, within a short time after its release, displayed severe adverse effects associated with renal toxicity. Within 40 minutes to 8 hours of administration, patients suffered from flank pain and renal failure normally associated with chronic dosing of NSAIDs (Hart *et al.*, 1987).

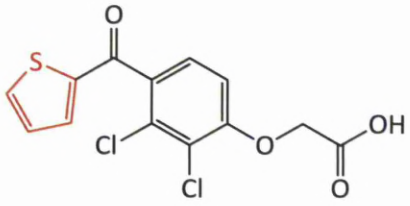

Tienilic Acid (TA)

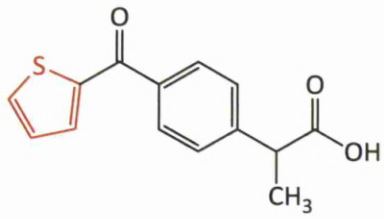

Suprofen

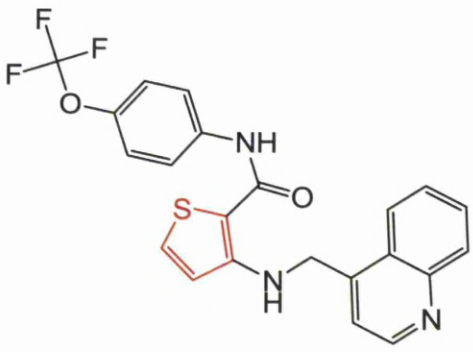

OSI-930

Figure 4.1: Examples of thiophene-containing compounds believed to undergo metabolism to either an *S*-oxide or an epoxide intermediate.

Although previous studies suggested hypothetically a reactive acyl glucuronic acid conjugate might mediate the nephrotoxicity observed with suprofen (Mori *et al.*, 1985, Smith and Liu, 1993), the fact that TA and suprofen produce the same renal toxicity symptoms and the confirmation that the CYP2C subfamily is present in the kidney, suggests they might share the same bioactivation pathway (Kalgutkar *et al.*, 2005). Like TA, suprofen has been shown to be a mechanism-based CYP2C9

inhibitor *in vitro* (O'Donnell *et al.*, 2003, Hutzler *et al.*, 2009) and one of its major metabolites is 5-hydroxy suprofen (Mori *et al.*, 1984, Mori *et al.*, 1985). Mechanism-based P450 inhibition signifies localised generation of a reactive drug metabolite, and a trend towards clinical hepatotoxicity has been associated with marked Mechanism-based P450 inhibition (Reese *et al.*, 2010). Similar to reports by Koenigs *et al.* (1999), O'Donnell *et al.* (2003) obtained evidence for the formation of a reactive epoxide intermediate, by the addition to recombinant CYP2C9 incubations of semicarbazide affording a pyridizine adduct of γ-thioketo α,β-unsaturated aldehyde open-ring structure. It could be deduced that either the epoxide or the γ-thioketo α,β-unsaturated aldehyde is responsible for the covalent binding and subsequent inactivation of CYP2C9.

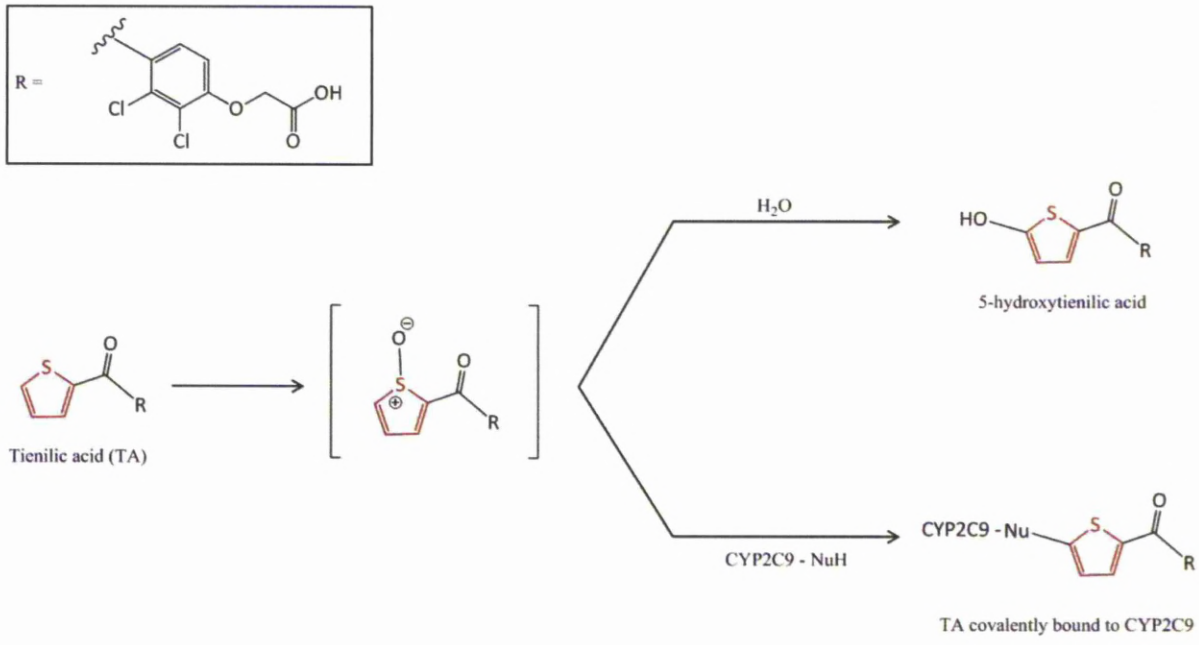

Figure 4.2: Postulated bioactivation pathway of tienilic acid. Formation of 5-hydroxy TA and covalent binding of the reactive TA *S*-oxide to CYP2C9. Adapted from Dalvie *et al.* (2002).

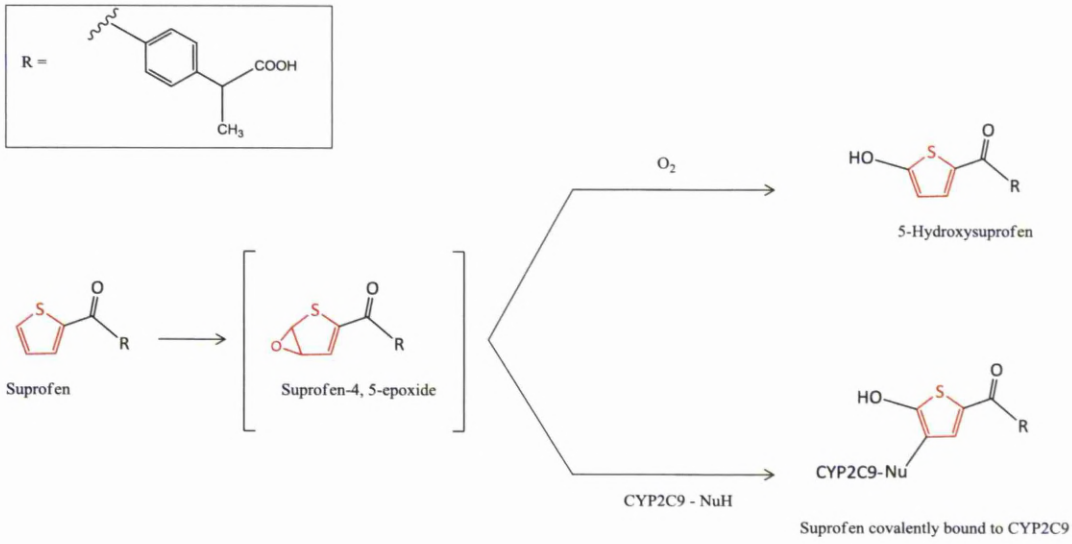

Figure 4.3: Postulated bioactivation pathway of suprofen. Formation of 5-hydroxysuprofen and covalent binding of the reactive suprofen epoxide to CYP2C9. Adapted from O'Donnell *et al.* (2003).

The investigations presented in this chapter aimed to elucidate the metabolism of TPA *in vivo* and *in vitro*. In particular it was intended to explore the detoxification products of TPA's reactive metabolite(s) in mice and rats and compare them with those of furosemide. To assess the degree of glucuronidation of furosemide or TPA in multiple species, glucuronidation assays in hepatic microsomes were employed. The biliary metabolites of TPA in the rat were investigated using radiometric HPLC and LC-MS/MS techniques. TPA metabolism was investigated, *in vitro*, in rat and mouse hepatocytes as a surrogate for an appropriate *in vivo* system (Gebhardt *et al.*, 2003).

4.2 MATERIALS AND METHODS

4.2.1 Materials

[^{14}C]-Thiophene analogue of furosemide (TPA; specific activity 592 Mbq/mmol) and unlabelled TPA were provided by Pfizer (Kent, U.K.) and was determined to be >98 % pure by HPLC. The ^{14}C label was incorporated into the carboxyl carbon atom of TPA, and thus was expected to be retained in all major metabolites. Unless otherwise stated, reagents were obtained from Sigma-Aldrich Chemical Co. (Poole, U.K.). Ultima Gold scintillation fluid was purchased from PerkinElmer LAS (U.K.), Seer Green, Beaconsfield, Buckinghamshire, U.K. All solvents were of HPLC grade and were products of either Fischer Scientific plc (Loughborough, U.K.) or VWR (Lutterworth, U.K.)

4.2.2 Experimental animals

Protocols described were undertaken in accordance with criteria outlined in a license granted under the Animals (Scientific Procedures) Act 1986 and approved by the University of Liverpool Animal Ethics Committee. Male Wistar rats and male CD-1 mice were obtained from Charles River Laboratories (Margate, U.K), housed in a light-controlled room at a constant temperature, and supplied with a standard chow diet and water *ad libitum*.

4.2.3 *In vitro* assessment of glucuronidation rate of furosemide and TPA in UDPGA-supplemented hepatic microsomes

Incubations contained: 0.76 mg/ml microsomal protein of either rat liver microsomes (RLM), mouse liver microsomes (MLM) or human liver microsomes (HLM), 50 μg/ml of alamethicin (a peptide that forms membrane pores, and thereby enhances microsomal glucuronidation; without affecting P450 activity (Fisher *et al.*, 2000)), 5 mM $MgCl_2$, 100 mM Tris-HCl (pH 7.4), 2% BSA (used to increase the microsomal glucuronidation of many substrates (Kilford *et al.*, 2009)) and 5 mM UDPGA (not added to control incubations) to give a total volume of 600 μl. Alamethicin solution was prepared by dissolution in methanol. The substrates, furosemide and TPA, were

at 5 μM and the positive control, naloxone (a highly selective substrate of the UGT2B7 isoform (Di Marco *et al.*, 2005)), was at 1 μM. Before the addition of UDPGA, the mixture was preincubated on ice for 15 minutes and then transferred to a shaking incubator for 5 minutes at 37°C. To initiate the reaction, UDPGA was added to a final concentration of 5 mM, and 50 μl aliquots were removed at 0, 5, 10, 20, 30, 60, 120, 180, and 240 minutes. A Pfizer global internal standard (100 μl of 1000 ng/ml) in acetonitrile containing 2% phosphoric acid was used to terminate the reaction at each time point. Levels of parent compound were measured for each time-point using an LC-MS/MS method described below.

4.2.4 LC-MS/MS method for substrate-depletion assay of incubation with UDPGA-supplemented hepatic microsomes

LC-MS/MS analyses were performed using an AB Sciex API 4000 Q-trap mass spectrometer with TurboIonSpray source (AB Sciex, Foster City, CA, USA) and an Agilent 1100 binary pump LC system (Agilent Tech. Inc., Palo Alto, CA, U.S.A.). Analytes were resolved on an Onyx monolithic C18 column (100 × 3.0; Phenomenex, Macclesfield, Cheshire, U.K.) using a gradient of ACN containing 0.1% formic acid (0% for 0.30 minutes, 0-100% over 0.95 minutes) in water containing 5% ACN and 0.1% formic acid at a flow rate of 1.2 ml/min. Data were acquired and processed with the Analyst software (ver. 1.4; AB Sciex). Mass spectral analyses were performed using multiple reaction monitoring, with transitions for furosemide (*m/z* 331/81), TPA (*m/z* 345/190), and Naloxone (*m/z* 328/212).

4.2.5 Investigation of biliary TPA metabolites in the Wistar rat

Male Wistar rats (200-400 g) were terminally anaesthetised with urethane (1.4 g/ml in isotonic saline; 1.0 ml/kg *i.p.*) and cannulated via the trachea, femoral vein and the common bile duct. Drug-free bile was collected over 30 minutes before administration of TPA. [^{14}C]-TPA (10 μCi) and 151 μmol/kg unlabelled TPA dissolved in DMSO was administered *i.v.* via the femoral vein over 5 minutes. Bile was then collected hourly for 3 hours into microcentrifuge tubes. Protein within the bile was precipitated by addition of an equal volume of ice-cold acetonitrile. The

samples were centrifuged at 2200 rpm for 10 minutes. The resultant supernatant was collected, and stored at -20°C until analysis by radiometric HPLC and LC-MS/MS.

4.2.6 Investigation of TPA metabolites in Wistar rat and CD-1 mouse freshly isolated hepatocytes

Details of the hepatocyte isolation procedure and incubation details are given in sections 2.2.8 and 2.2.9, respectively.

4.2.7 Detection and identification of biliary [^{14}C]-TPA metabolites in the Wistar rat by radiometric HPLC and LC-MS/MS using an API 2000 instrument

The metabolites of [^{14}C]-TPA were resolved with an UltraCarb C8 column (25 × 0.46 cm, 5-μm particle size; Thermo Fisher Scientific, Runcorn, Cheshire, U.K.). The mobile phase consisted of a combination of acetonitrile and 10 mM ammonium formate buffer (adjusted to pH 3.5 with formic acid). A sample aliquot of 50 μl was injected onto the column, and eluted at 0.9 ml/min with a gradient of 10 to 60% ACN over 30 minutes, maintaining 60% ACN for 10 minutes, and finally reverting to 10% acetonitrile over 5 minutes. The eluent gradient was delivered with a Dionex Summit HPLC system (Dionex Corporation, Sunnyvale, CA, U.S.A.). The analytes were detected by a UVD170S UV detector (Dionex) at 240 nm and a radioactivity detector (Radiomatic Flo-Oneβeta A250, PerkinElmer LAS (U.K.), Seer Green, Beaconsfield, Buckinghamshire, U.K.).

LC-MS/MS analyses were performed using an AB Sciex API 2000 mass spectrometer with TurboIonSpray source (AB Sciex, Foster City, CA, USA) interfaced to a Perkin Elmer Series 200 pump and Perkin Elmer Series 200 autosampler (Perkin Elmer, Seer Green, Beaconsfield, Buckinghamshire, U.K.). Analytes were resolved on an UltraCarb C8 column according to the method described above. Eluate split-flow to the LC-MS interface was approximately 200 μl/min and nitrogen was used as collision gas. TPA and metabolites were detected in the multiple-reaction monitoring (MRM) mode with the transitions given in Table

4.1. Data were acquired and processed with the Analyst software (ver. 1.4; AB Sciex). The main working parameters are given in Table 4.1.

Parameters	Selected Reaction Monitoring
Source temperature (°C)	400
Nebulizing gas (gas-1) (arbitrary units)	50
Heater gas (gas-2) (psi)	80
Curtain gas (arbitrary units)	20
Ion spray voltage (V)	-4200
Collision energy (eV)	-18
Declustering potential (V)	-91
Focusing potential (V)	-270
Entrance potential (V)	-9.5
Dwell time (ms)	150
Mode of analysis	Negative
Ion transition products (*m/z*)	**M1** 668/620, 668/306; **M2** 670/306, 670/363, 670/249; **M3** 249/205, 249/79; **M4** 521/345, 521/301, 521/176.

Table 4.1: Main working parameters of API 2000 for tandem mass spectrometric analyses of TPA and TPA metabolites

4.2.8 Detection and identification of [^{14}C]-TPA metabolites, generated by freshly isolated rodent hepatocytes, by radiometric HPLC and LC-MS/MS using API 4000-Qtrap and LTQ Orbitrap instruments

LC-MS/MS analyses were performed using an AB Sciex API 4000-Qtrap mass spectrometer with TurboIonSpray source (AB Sciex, Foster City, CA, U.S.A.) interfaced to an Agilent 1100 binary pump LC system (Agilent Technologies. Inc., Palo Alto, CA, U.S.A.). Analytes were resolved on an UltraCarb C8 column according to the method described above. Eluate split-flow to the LC-MS interface was approximately 200 µl/min and nitrogen was used as collision gas. TPA and metabolites were detected in the negative ion MRM mode with the transitions given in Table 4.1. Data were acquired and processed with the Analyst Software (ver. 1.4; AB Sciex).

Product ion analyses were performed using an LTQ Orbitrap mass spectrometer (Thermo Scientific, Hemel Hempstead, UK) interfaced to an Agilent 1100 binary pump LC system (Agilent Technologies. Inc., Palo Alto, CA, U.S.A.). Analytes were resolved on a Phenomenex Kinetex C18 column (150 × 2.1 mm; 2.6 µm). Eluate flow was 250 µl/min and the mobile phases used were 2 mM ammonium formate and 10:90 water:ACN.

4.3 RESULTS

4.3.1 *In vitro* assessment of glucuronidation of furosemide and TPA

Glucuronidation of furosemide and TPA were assessed using UDPGA-supplemented RLM, MLM and HLM incubations. Naloxone was used as a positive control (Kilford *et al.*, 2009, Di Marco *et al.*, 2005). In incubations including naloxone and UDPGA cofactor, the levels of parent compound decreased rapidly compared to incubations omitting UDPGA, where parent compound levels remained constant throughout the experiment. However, in incubations containing UDPGA and either furosemide or TPA, parent compound levels did not decrease; suggesting little furosemide- or TPA-glucuronide was formed. It is known that naloxone undergoes much more rapid glucuronidation than furosemide by HLM and, especially, RLM (Di Marco *et al.*, 2005)

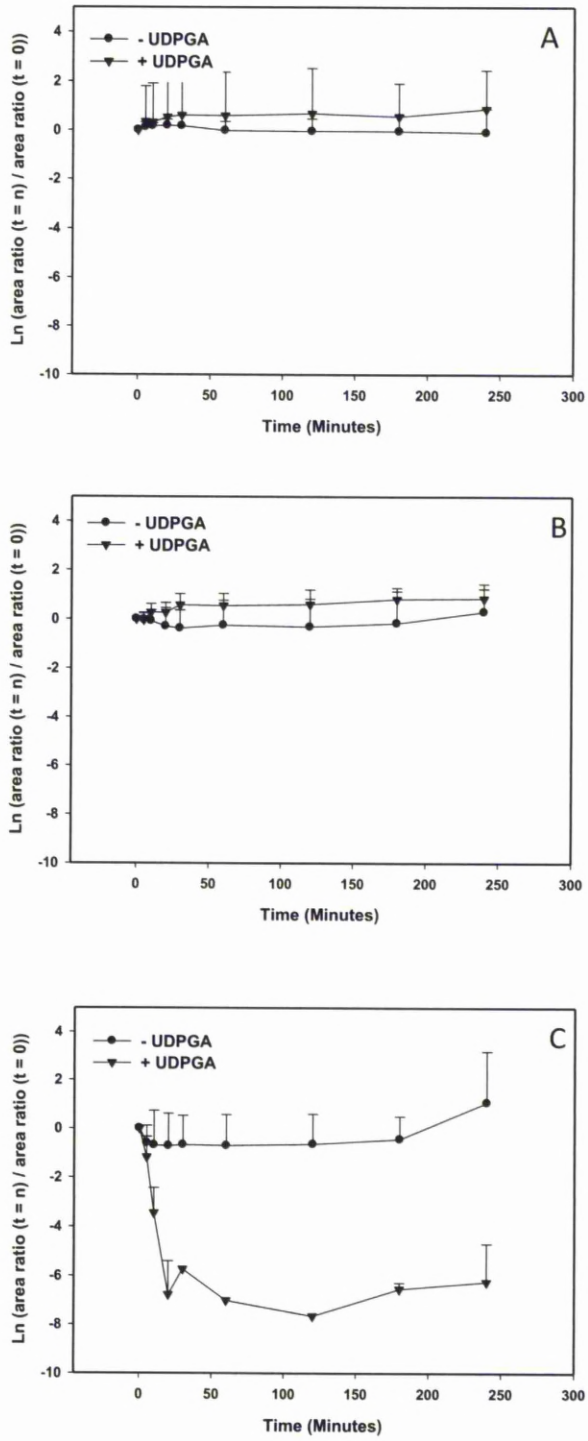

Figure 4.4: Assessment of glucuronidation of furosemide, TPA and naloxone in RLM. Graphs show levels of parent compound, (A) furosemide, (B) TPA and (C) naloxone, over time, with (▼) and without (●) UDPGA. Data presented as mean + standard deviation for n = 3.

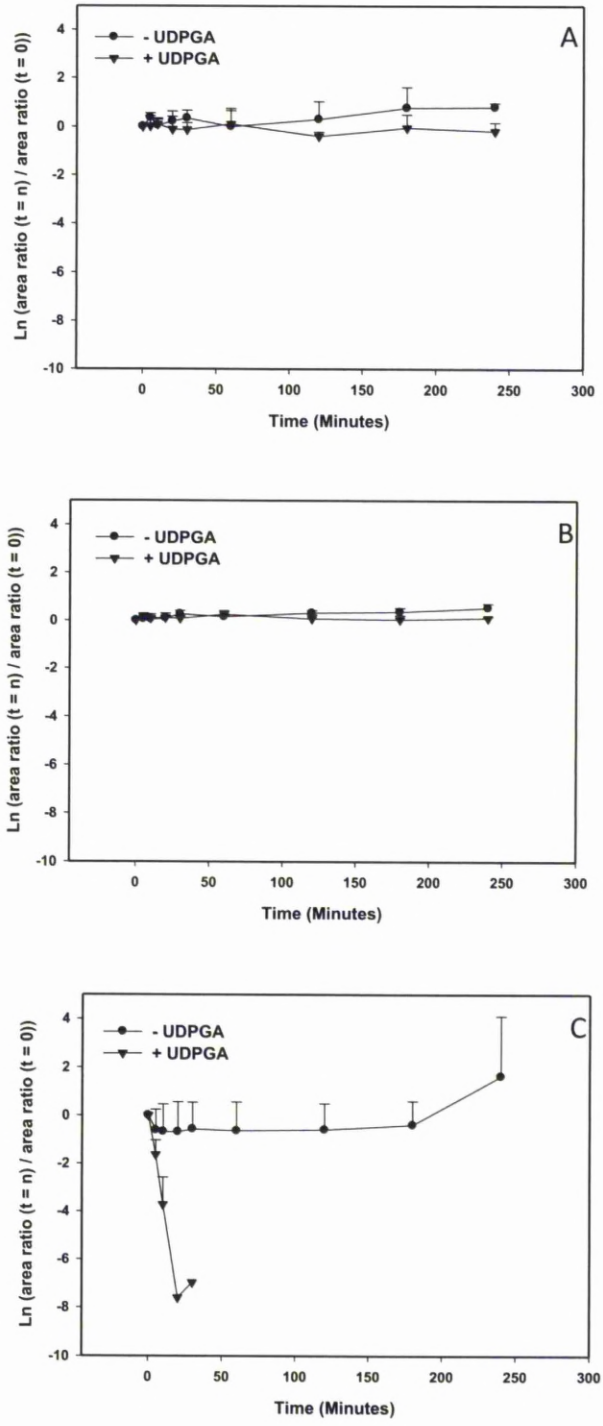

Figure 4.5: Assessment of glucuronidation of furosemide, TPA and naloxone in MLM. Graphs show levels of parent compound, (A) furosemide, (B) TPA and (C) naloxone, over time, with (▼) and without (●) UDPGA. Data presented as mean + standard deviation for n = 3.

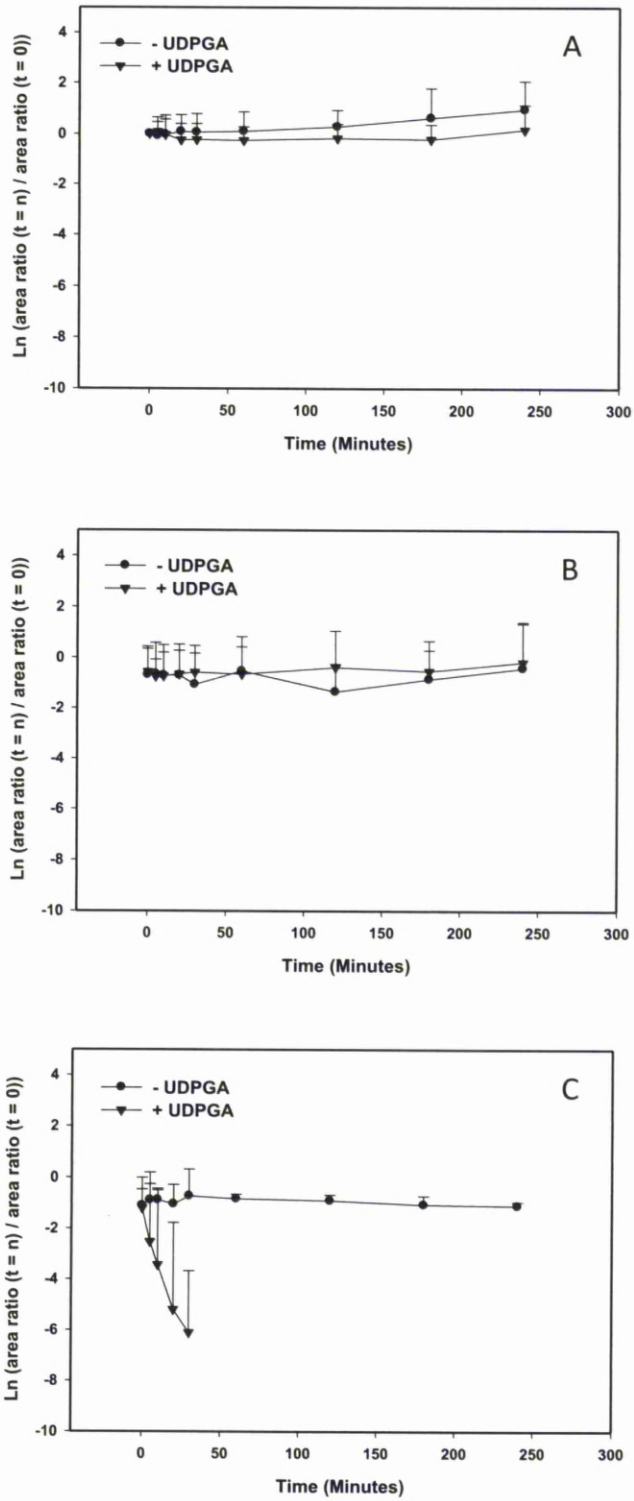

Figure 4.6: Assessment of glucuronidation of furosemide, TPA and naloxone in HLM. Graphs show levels of parent compound, (A) furosemide, (B) TPA and (C) naloxone, over time, with (▼) and without (●) UDPGA. Data presented as mean + standard deviation for n = 3.

4.3.2 Identification of biliary [^{14}C]-TPA metabolites in the Wistar rat by radiometric HPLC and LC-MS/MS

Analysis of the biliary metabolites of TPA in the rat and mouse has been performed previously (Butler, 2006). Figure 4.7 shows the radiochromatogram and LC-MS/MS profile of metabolites of TPA in rat bile. The parent compound (TPA) eluted at 28.9 minutes on the radiochromatogram and constituted 31.4 ± 0.81% (mean ± SEM) of the excreted dose. A corresponding peak on the LC-MS total-ion chromatogram (*m/z* 345, $[M-1]^-$) eluted at 29.2 minutes, and in-source fragmentation gave confirmation that this was the parent compound by fragments at *m/z* 301 (loss of CO_2 from the carboxylic acid function) and *m/z* 78 (NSO_2). At 5.0 minutes a small peak (M1) was seen on the radiochromatogram. A peak of *m/z* 668 eluting at a similar time was seen by LC-MS analysis. Fragments at *m/z* 345 (TPA anion), *m/z* 306 (GS^-) and *m/z* 249 (loss of the thiophene-2-ylmethyl moiety from TPA anion) suggest that M1 (1.36 ± 0.65% excreted dose) could correspond to a GSH conjugate of a monooxygenated species, i.e., schematically, M+GSH+O. Apparent formation of *m/z* 345 from *m/z* 668 implies neutral loss of GSH-2H (305 amu) and dehydration of the [O]TPA moiety. Neutral loss of 305 amu from GSH conjugates is somewhat unusual but has been observed previously (Wen *et al.*, 2008). A wide radioactive peak with a retention time of 14.6 minutes could potentially be overlapping peaks of two separate metabolites (amounting to 47.58 ± 3.75% of excreted dose). LC-MS analysis identified two putative metabolites, *m/z* 670 (M2) and *m/z* 249 (M3) eluting at 15.4 minutes and 15.7 minutes respectively. Fragmentation patterns, from Butler, 2006, (PhD thesis, University of Liverpool), of these compounds suggest M2 may be another TPA-GSH conjugate, with hypothetically an 18 amu increment on the thiophene ring and M3 may be the TPA N-dealkylated metabolite; in which case, M3 will be identical to the N-dealkylated metabolite of furosemide described by Williams *et al.* (2007). The radioactive peak eluting at 21.2 minutes (M4) corresponds to a peak of *m/z* 521 on the LC-MS chromatogram. Fragments at *m/z* 345 (TPA) and *m/z* 175 (dehydroglucuronic acid anion; (Bosken *et al.*, 2000)) suggest that M4 (19.62 ± 3.64% of excreted dose) is a TPA-glucuronide metabolite.

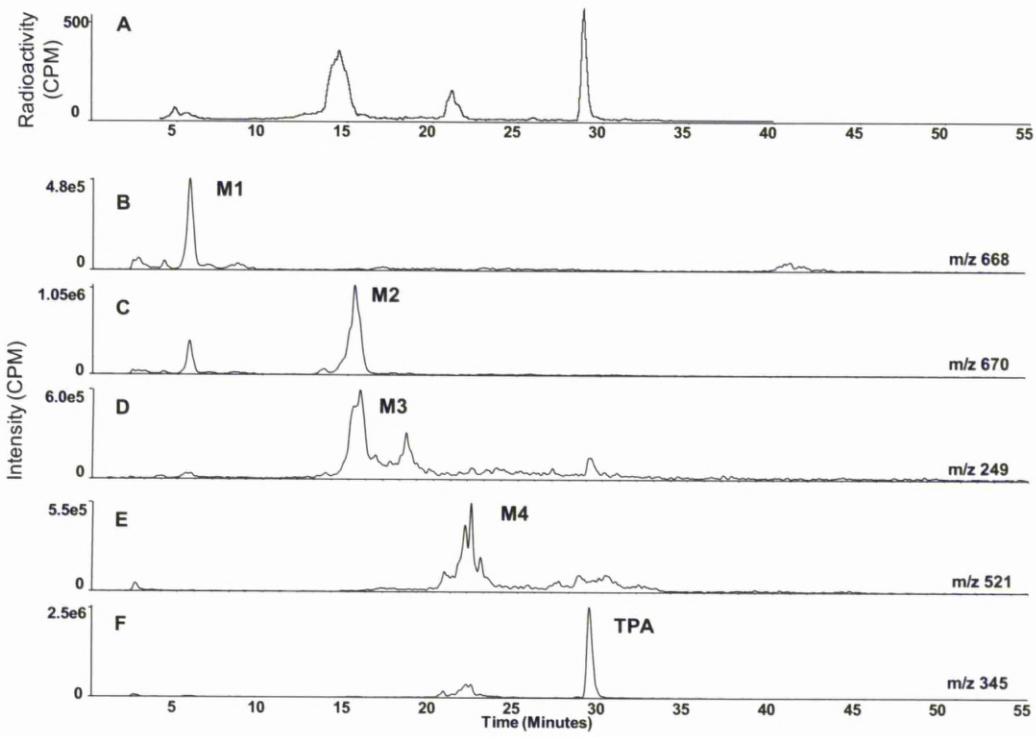

Figure 4.7: Radiometric HPLC and API 2000 LC-MS/MS analysis of TPA and metabolites in rat bile. (A) Radiochromatogram and (B –F) extracted ion-current (XIC) chromatograms (negative-ion analysis) of (B) M1 at *m/z* 668, (C) M2 at *m/z* 670, (D) M3 at *m/z* 249, (E) M4 at *m/z* 521 and (F) parent compound (TPA) at *m/z* 345. 0 to 1 hour biliary metabolites of [^{14}C]-TPA administered to anaesthetised rats (144 µmol/kg TPA + 10µCi [^{14}C]-TPA in DMSO administered *i.v*).

4.3.3 Identification of [^{14}C]-TPA metabolites in freshly isolated Wistar rat hepatocytes.

The radiochromatogram of TPA metabolites in rat hepatocytes (Figure 4.8) shows drug-related compounds with retention times similar to those of metabolites found in rat bile, suggesting that they could be N-dealkylated TPA, TPA glucuronide and two TPA-GSH conjugates (Figure 4.7). The MRM data, generated using the 4000-Qtrap mass spectrometer, indicated the presence of an N-dealkylated TPA metabolite and the glucuronide metabolite (Figure 4.9).

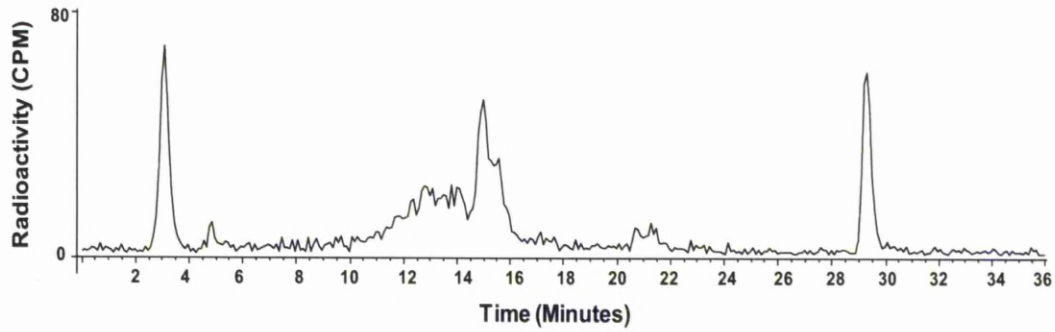

Figure 4.8: Radiochromatogram of metabolites of [^{14}C]-TPA from rat hepatocytes. Incubations contained 0.6 μCi [^{14}C]-TPA (50 μM) in 6 ml incubation for 6 hours. Retention times of metabolites are consistent with those seen in rat bile (Figure 4.7).

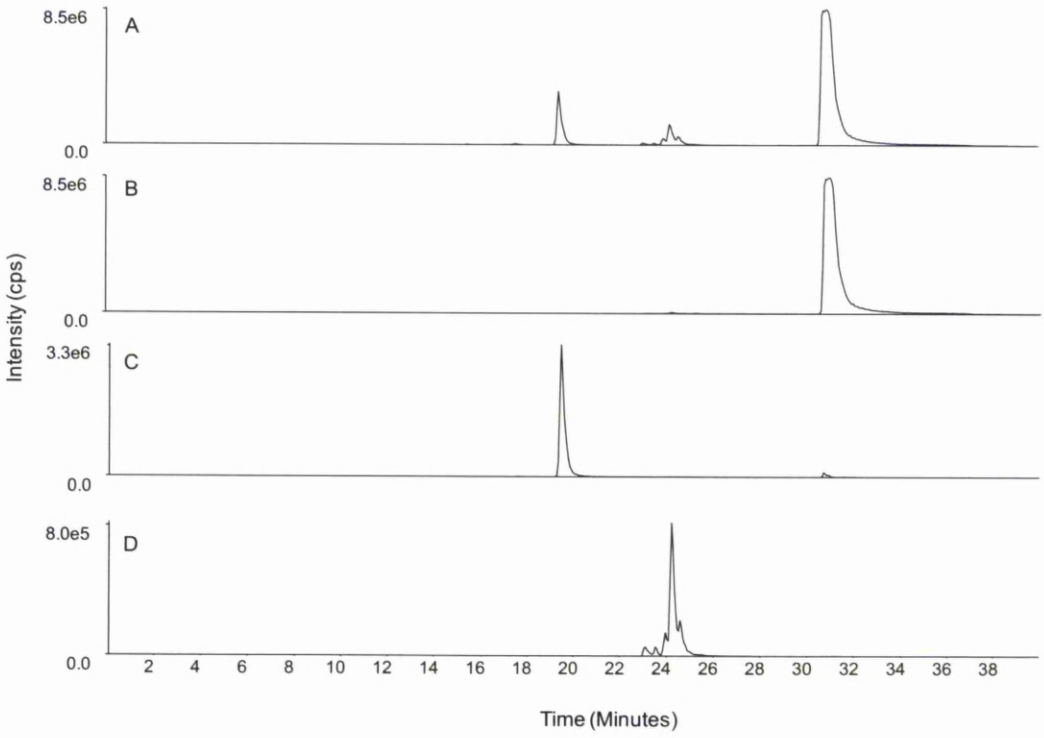

Figure 4.9: LC-MS/MS MRM analysis of TPA and metabolites in rat hepatocytes, using the API 4000-Qtrap instrument. (A) Total ion-current (TIC) chromatogram of TPA metabolites from hepatocytes and XIC chromatograms for MRM transitions (B) *m/z* 345 → *m/z* 301 (TPA), (C) *m/z* 249 → *m/z* 205 (N-dealkylated TPA) and (D) *m/z* 521 → *m/z* 345 (TPA glucuronide).

Data generated using the LTQ-Orbitrap mass spectrometer, operating in negative-ion mode, detected the presence of multiple putative metabolites ($[M-H]^-$) at *m/z* 650, 668 and 670; masses consistent with substitution of GSH (GSH-2H), addition of GSH + O and addition of GSH + 2H + O, respectively (Figure 4.10). Detection of a ^{37}Cl isotope peak for each of the species provided confirmation that they were drug-related compounds. For both the *m/z* 668 (TPA + GSH + O) and *m/z* 670 (TPA + GSH + 2H + O) metabolites, MS/MS (product-ion) data were generated (Figure 4.13 and 4.15). The signals from the two peaks at *m/z* 650 were weak and therefore no MS/MS data were generated.

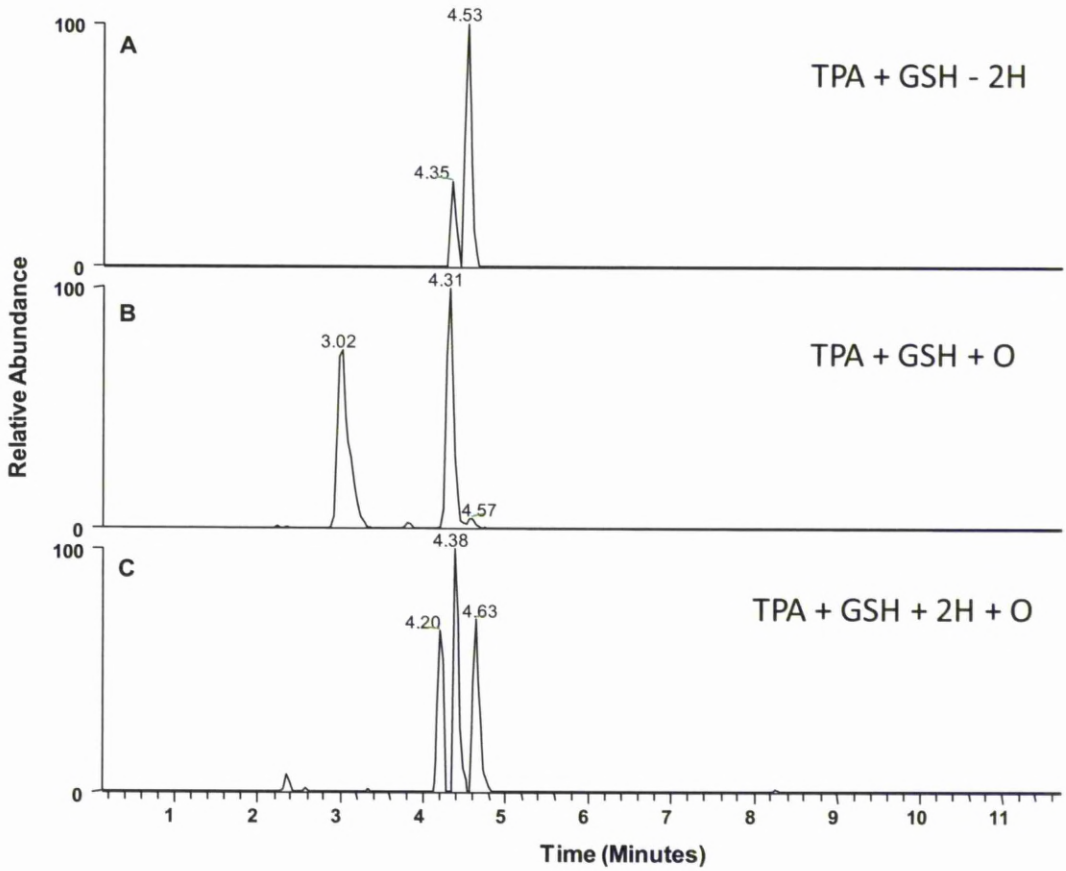

Figure 4.10: LC-MS analysis for putative GSH adducts of TPA (1000 μM) formed in rat hepatocytes, using the LTQ Orbitrap mass spectrometer. XIC chromatograms of (A) *m/z* 650, corresponding to the substitution of glutathione for hydrogen; (B) *m/z* 668, corresponding to the addition of GSH to monoxygenated TPA; and (C) *m/z* 670, corresponding to the addition of GSH to monoxygenated and reduced TPA. (NB, for 'A' and 'B', the sequence of additions is representative and does not imply knowledge of the metabolic pathway).

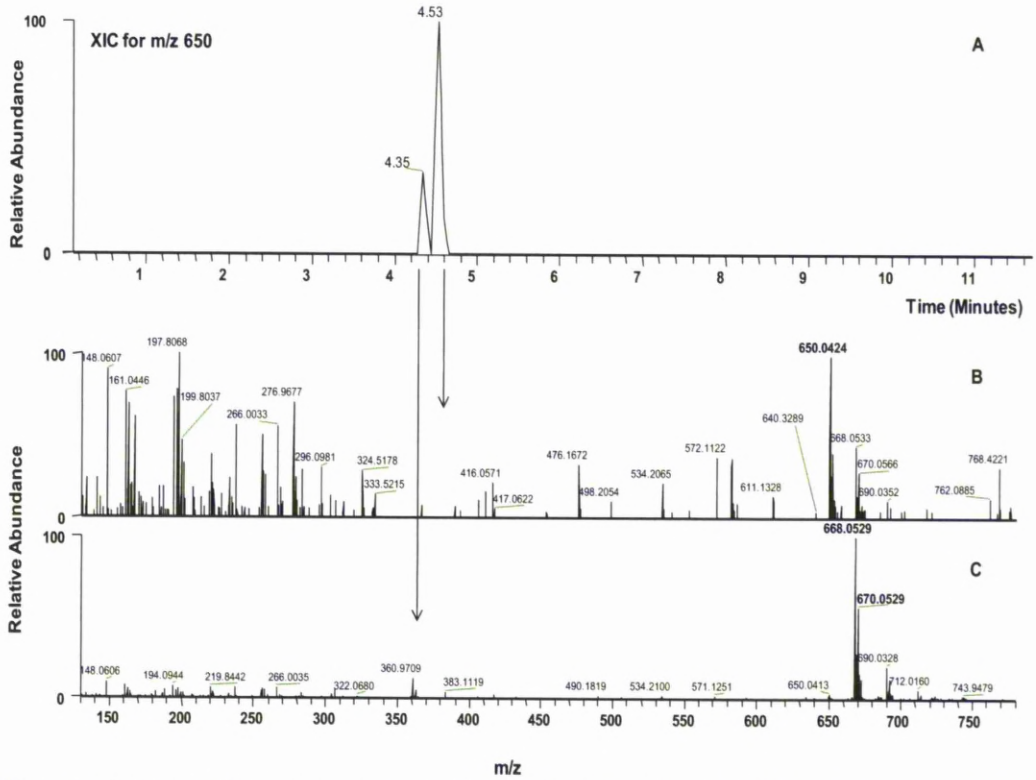

Figure 4.11: XIC chromatogram for *m/z* 650 (A) and full ion scans for peaks detected in the XIC chromatogram for *m/z* 650 (B, C). Analysis carried out using a LTQ Orbitrap mass spectrometer.

The full ion scans from the peaks detected in the XIC chromatogram for *m/z* 650 (Figure 4.11 A) indicated that the first eluting peak (RT 4.35 minutes) may be a dehydration ($[M\text{-}1\text{-}H_2O]^-$) fragment of an *m/z* 668 metabolite; *m/z* 668 (and its ^{37}Cl isotopologue at *m/z* 670) were the most abundant ions present (Figure 4.11 C) and the retention time (4.35 minutes) was essentially the same as that of the second eluting peak in the XIC chromatogram for *m/z* 668 (4.31 minutes; Figure 4.10 B). Dehydration is a common mass spectral fragmentation of GSH adducts of oxygenated drugs and metabolites (Madden *et al.*, 1996, Chen *et al.*, 2002, Subramanian *et al.*, 2002) but can also occur in the case of non-oxygenated GSH adducts (Maggs *et al.*, 1995, Wen *et al.*, 2009); implying that the GSH residue can undergo dehydration. An *m/z* 650 ion and its ^{37}Cl isotopologue were the most abundant ions in the full ion scan from the later eluting peak (RT 4.53 minutes; Figure 4.11 B), indicating a possible TPA metabolite with a GSH substituent, however the signals were too low to generate any MS/MS data. Unfortunately, the later eluting peak of *m/z* 650 may also represent a dehydration fragment of an *m/z*

668 species (Figure 4.10 B; RT 4.57 minutes); a somewhat abundant *m/z* 668 ion was present in the full scan of this peak (Figure 4.11 B).

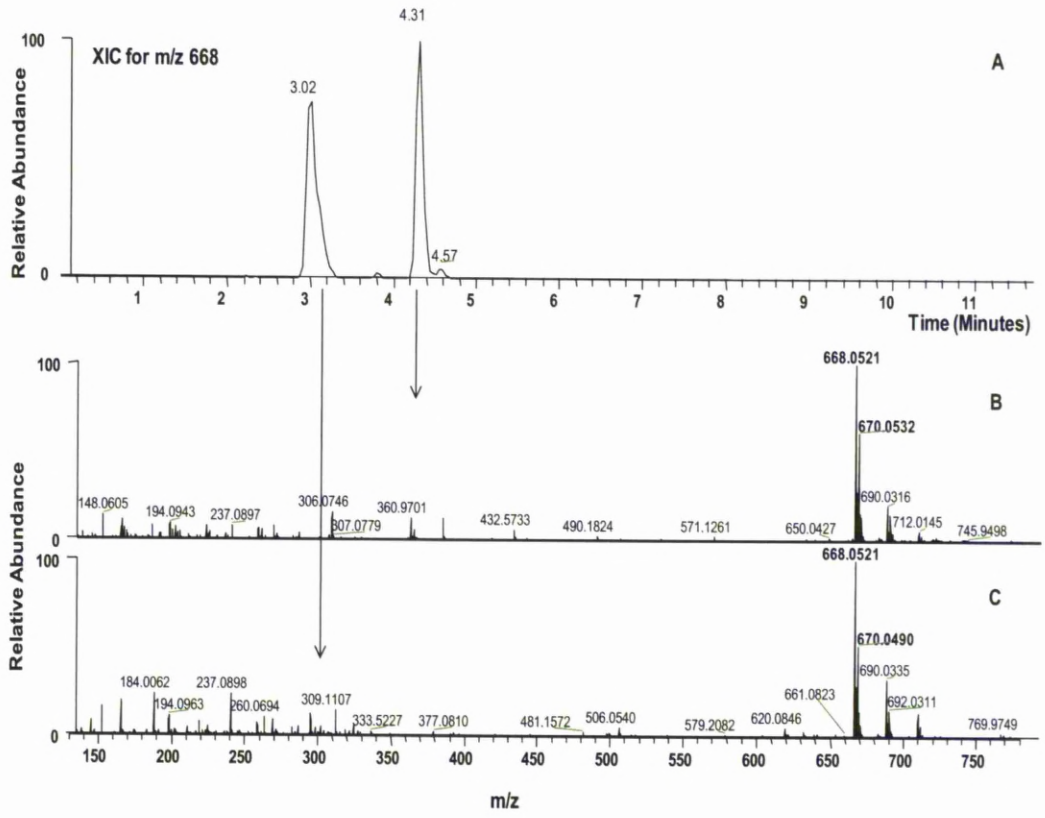

Figure 4.12: XIC chromatogram for *m/z* 668 (A) and full ion scans for peaks detected in the XIC chromatogram for *m/z* 668 (B, C). Analysis carried out using a LTQ Orbitrap mass spectrometer.

The *m/z* 668 ion was the most abundant in the full ion scans (Figure 4.12 B and C) for both major peaks detected in the XIC chromatogram for *m/z* 668 (Figure 4.12 A). An MS/MS product ion spectrum (Figure 4.13 A) of the first eluting peak (RT 3.02) showed fragments at *m/z* 620 (loss of SO (48 amu) from a thiophene S-oxide moiety (Dansette *et al.*, 2005, Shimizu *et al.*, 2009), *m/z* 344.9 (loss of 305 amu ([GSH-2H]) and 18 amu (H_2O)) and *m/z* 300.9 (loss of 44 amu (CO_2) from *m/z* 345). There was also a fragment at *m/z* 272, found generically in the negative-ion spectra of GSH adducts (Subramanian *et al.*, 2002, Dieckhaus *et al.*, 2005), representing GS^- minus

H_2S (Figure 4.12 A). An MS/MS product ion spectrum (Figure 4.13 B) of the second eluting peak of *m/z* 668 (RT 4.31) showed fragments at *m/z* 361 ([M-1-GSH]$^-$) and *m/z* 306 (GS$^-$). There was also a fragment at *m/z* 249 representing the N-dealkylated TPA (Figure 4.13 B). How these two GSH adducts relate structurally to the radiolabelled peak of *m/z* 668 found in rat bile is not entirely clear: the biliary metabolite yielded fragments at *m/z* 345 (seen in mass spectrum of hepatocyte metabolite '*m/z* 668 I'), 306 ('*m/z* 668 II') and 249 ('*m/z* 668 II'). Neutral loss of GSH, i.e. retro-Michael elimination of GSH, is often seen in positive-ion spectra of GSH adducts (Wen *et al.*, 2008, Leblanc and Sleno, 2011, Yan and Caldwell, 2005), including those of certain oxygenated thiophenes (Dansette *et al.*, 2005, Shimizu *et al.*, 2009). The same loss might be expected in negative-ion spectra of GSH adducts but these spectra are often dominated by GS$^-$, i.e. the glutathione anion, and its fragments (Subramanian *et al.*, 2002, Dieckhaus *et al.*, 2005). The present case, with a dominant [M-1-GSH]$^-$, is clearly an exception to this observation. The complete absence of losses of 48 amu and H_2O from the parent ion of the second M+O+GSH metabolite implies the structures of these metabolites are fundamentally different. Divergent bioactivation pathways of a thiophene, yielding, ultimately, isomeric GSH adducts, are known (Dansette *et al.*, 2005, Shimizu *et al.*, 2009) but the diagnostic fragmentations of the TPA '*m/z* 668' adducts differ more markedly than those of published isomeric structures. Thus MS/MS data from both peaks suggest two GSH adducts of a molecular weight of 669 may be formed from TPA.

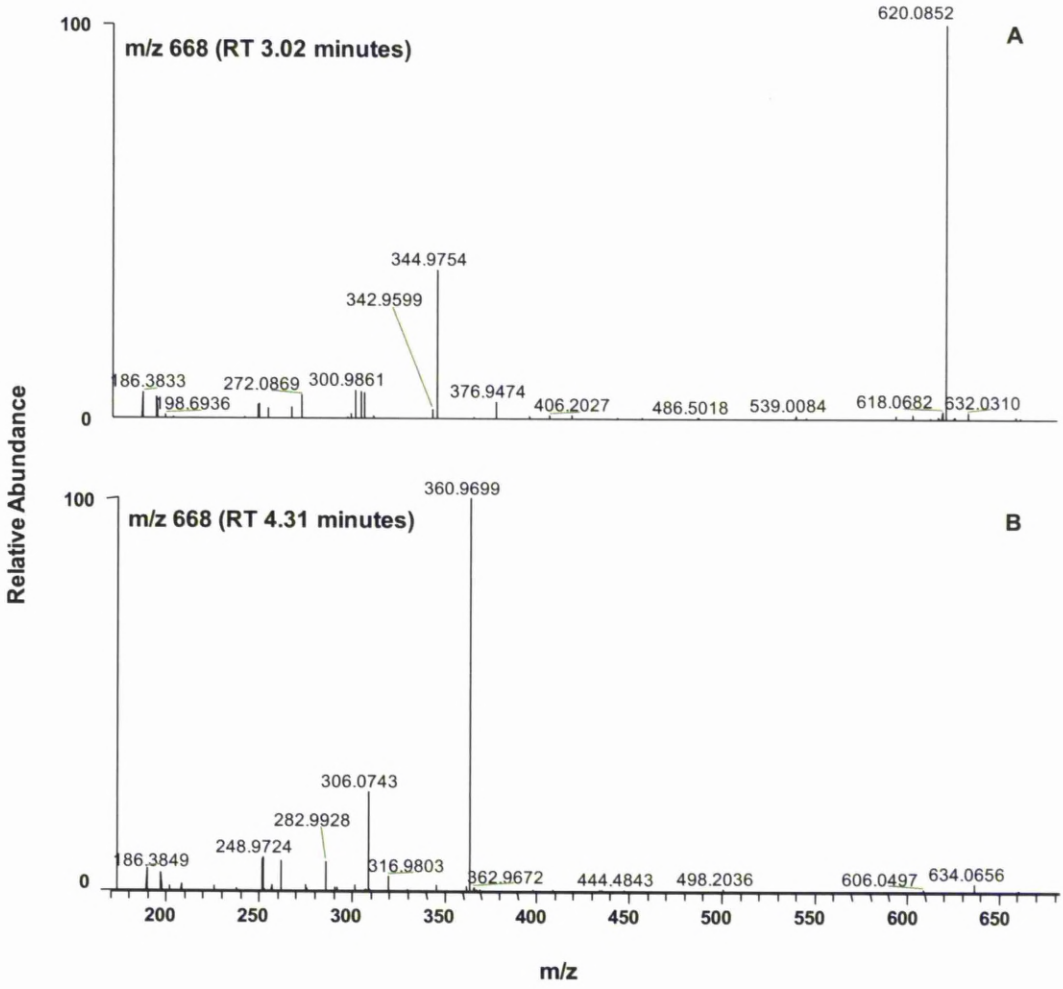

Figure 4.13: MS/MS analysis of TPA metabolites, from rat hepatocytes, detected at *m/z* 668. Analysis carried out using a LTQ Orbitrap mass spectrometer.

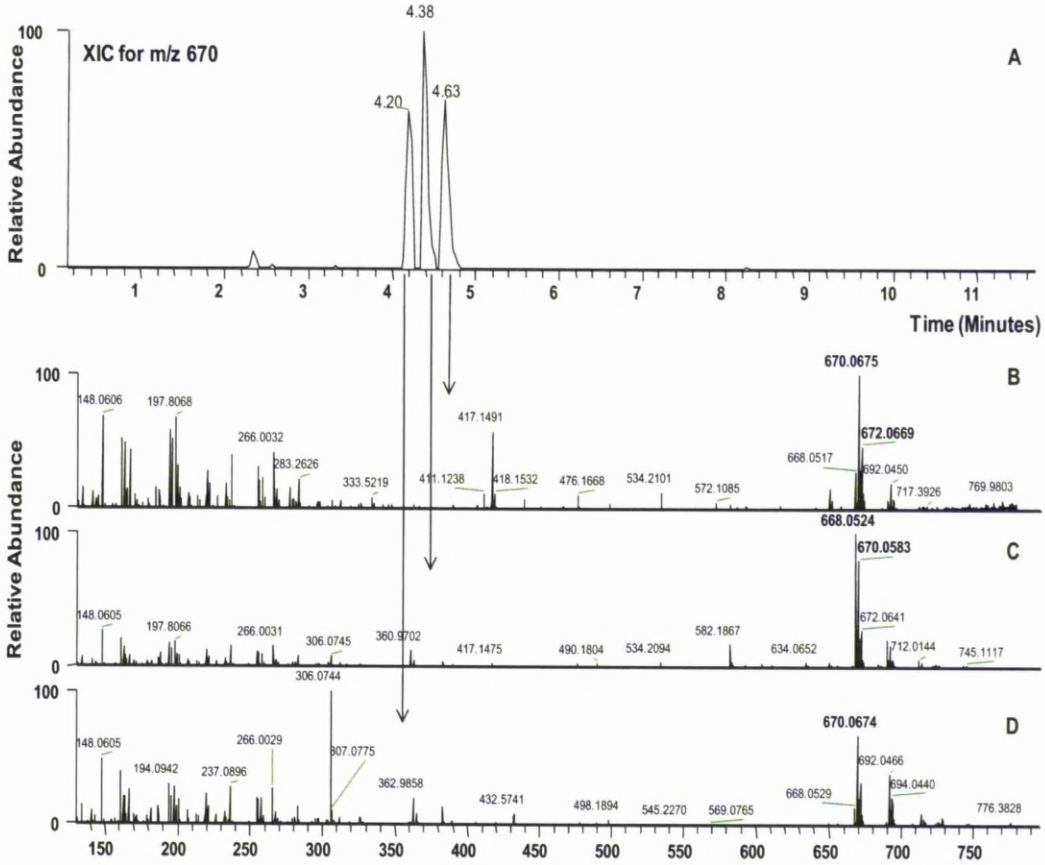

Figure 4.14: XIC chromatogram for *m/z* 670 (A) and full ion scans for peaks detected in the XIC chromatogram for *m/z* 670 (B, C). Analysis carried out using a LTQ Orbitrap mass spectrometer.

The full ion scans from the peaks detected in the XIC chromatogram (Figure 4.14 B-D) for *m/z* 670 suggest that the peak at RT 4.38 minutes may be interference from the coterminal *m/z* 668 metabolite; *m/z* 668 and the putative ^{37}Cl isotope peak at *m/z* 670 were the most abundant ions present (Figure 4.1.4 C) and the retention time (4.38 minutes) was essentially the same as that of the second eluting peak in the XIC chromatogram for *m/z* 668 (4.31 minutes; Figure 4.12 A). Full ion scans of both the first (4.2 minutes) and last (4.63) eluting peaks show that the most abundant ion is *m/z* 670 (and the ^{37}Cl isotope peak at *m/z* 672), suggesting that these peaks are TPA-related and may be formed by addition of GSH, O and 2H. MS/MS data were only generated for the last eluting peak as the signals of the others were too weak. An MS/MS product ion spectrum of the last eluting peak of *m/z* 670 (RT 4.63; Figure

4.15) showed GSH fragments at *m/z* 272 (GS^- minus H_2S) and *m/z* 254 ($[272-H_2O)]^-$) another known negative-ion fragment of GSH adducts (Subramanian *et al.*, 2002, Dieckhaus *et al.*, 2005) as well as *m/z* 306 (GS^-). Fragments at *m/z* 345 (TPA anion) and *m/z* 249 (loss of the thiophene-2-ylmethyl moiety from the TPA anion) were also detected. The abundant ion at *m/z* 608 ($[M-62]^-$) cannot be assigned to fragmentations characteristic of either GSH adducts or thiophene S-oxides. Hypothetically, it can be attributed to independent loss of H_2O and CO_2 (from a carboxylic acid function?). Loss of GSH from *m/z* 670 would yield the ion at *m/z* 363. Dehydration of *m/z* 363, in turn, would yield *m/z* 345. These fragmentations do not allow a derivation of the metabolites' structure and metabolic origin but do imply the adduct is not an S-oxide. The retro-Michael elimination of GSH and formation of GS^- suggest a structural similarity with '*m/z* 668 II' (Figure 4.13), while the unusual formation of the ion at *m/z* 608 indicates an additional, major, biotransformation. Nevertheless, the TPA+O+GSH-2H adduct might as easily be a product of a discrete metabolic pathway as a derivative of '*m/z* 668 II'.

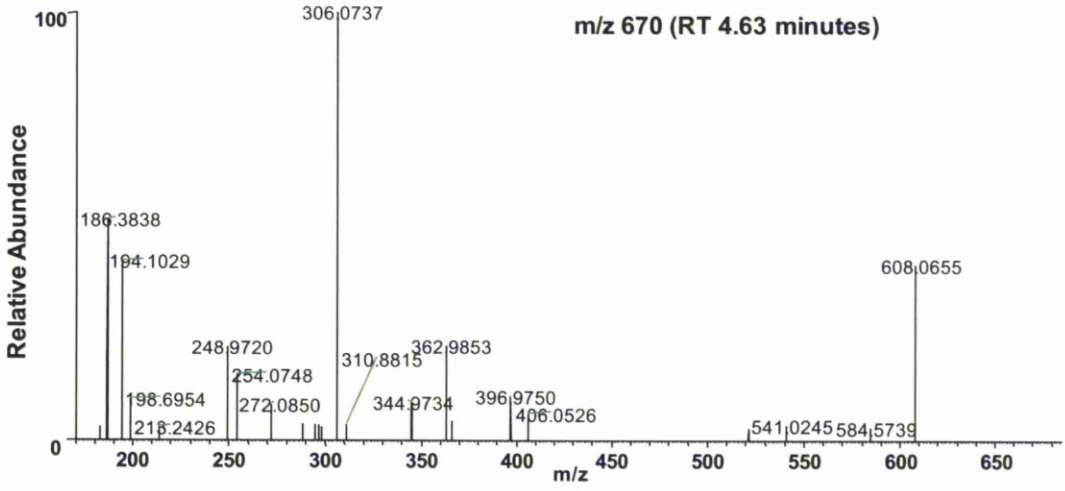

Figure 4.15: MS/MS analysis of a TPA metabolite, from rat hepatocytes, detected at *m/z* 670. Analysis carried out using a LTQ Orbitrap mass spectrometer.

4.3.4 Identification of [^{14}C]-TPA metabolites in freshly isolated CD-1 mouse hepatocytes.

The radiochromatogram of TPA metabolites in mouse hepatocytes shows drug-related compounds with retention times similar to those of metabolites found in rat bile (Figure 4.16). Based on co-elution with metabolites seen in rat bile it is suggested that TPA was metabolised to N-dealkylated TPA, TPA glucuronide and one/two TPA-GSH conjugates in mouse hepatocytes. The MRM data generated using the 4000-Qtrap mass spectrometer indicated the presence of the N-dealkylated TPA metabolite and the glucuronide metabolite (Figure 4.17)

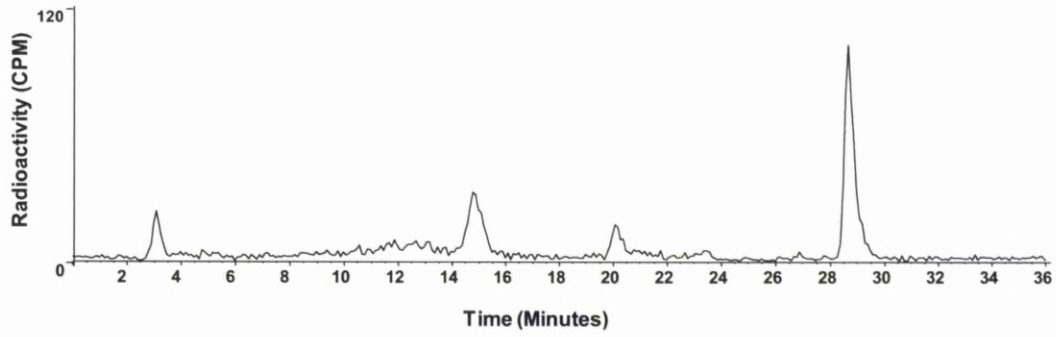

Figure 4.16: Radiochromatogram of metabolites of [^{14}C]-TPA from mouse hepatocytes. Incubations contained 0.6 μCi [^{14}C]-TPA (50 μM) in 6 ml incubation for 6 hours. Retention times of metabolites are consistent with those seen in rat bile.

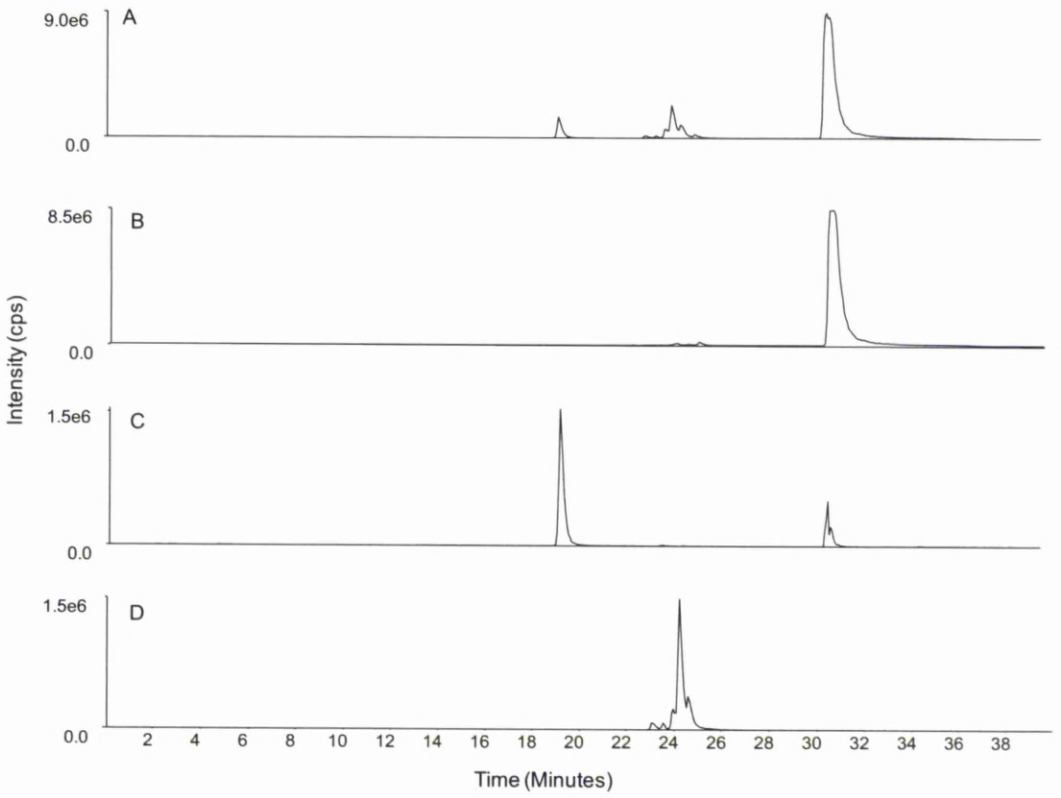

Figure 4.17: LC-MS/MS MRM analysis of TPA and metabolites in mouse hepatocytes, using the API 4000-Qtrap instrument. (A) Total ion-current (TIC) chromatogram of TPA metabolites from hepatocytes and XIC chromatograms for MRM transitions (B) *m/z* 345 → *m/z* 301 (TPA), (C) *m/z* 249 → *m/z* 205 (N-dealkylated TPA) and (D) *m/z* 521 → *m/z* 345 (TPA glucuronide).

Data generated using the LTQ-Orbitrap mass spectrometer operating in negative-ion mode, detected the presence of TPA metabolites at *m/z* 668 and 670, masses consistent with addition of GSH + O and GSH + O + 2H, respectively, but not, as in the case of rat hepatocytes (Figure 4.10), at *m/z* 650 (Figure 4.18 A). Detection of a ^{37}Cl isotope peak for each of the metabolites provided confirmation that they were drug-related. MS/MS data were not generated for any of the putative GSH adducts detected in mouse hepatocyte samples as the signals were too weak.

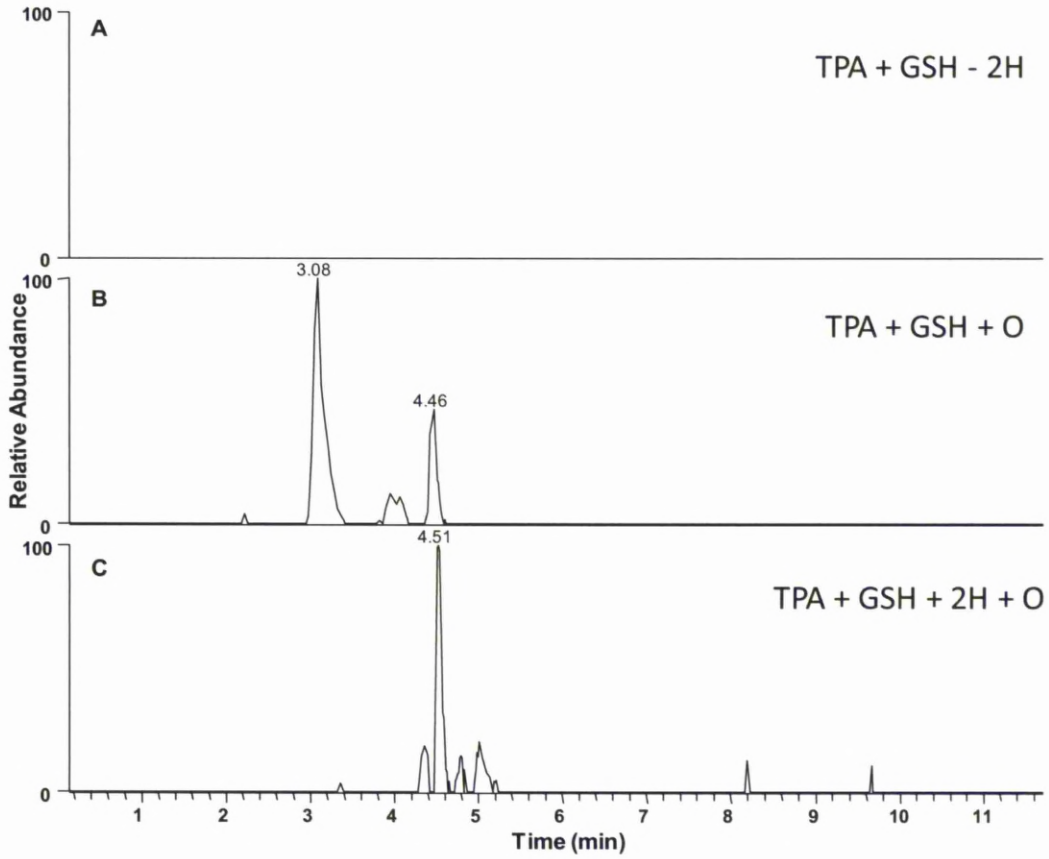

Figure 4.18: LC-MS analysis for putative GSH adducts of TPA (1000 μM) formed in mouse hepatocytes, using the LTQ Orbitrap mass spectrometer. XIC chromatograms of (A) *m/z* 650, corresponding to the substitution of glutathione for hydrogen; (B) *m/z* 668, corresponding to the addition of GSH to monoxygenated TPA; and (C) *m/z* 670, corresponding to the addition of GSH to monoxygenated and reduced TPA. (NB, for 'A' and 'B', the sequence of additions is representative and does not imply knowledge of the metabolic pathway).

The full ion scans from the peaks detected in the XIC chromatogram for *m/z* 668 (Figure 4.19 A) indicated that the later eluting peak (RT 4.46 minutes) may overlap the *m/z* 670 metabolite as the retention time (4.46 minutes) was similar to that of a peak in the XIC chromatogram for *m/z* 670 (4.51 minutes; Figure 4.18 C) and the *m/z* 670 ion was more abundant. An *m/z* 668 ion and its ^{37}Cl isotopologue were the most abundant ions in the full ion scan from the first eluting peak (RT 3.08 minutes; Figure 4.19 C), indicating a possible TPA metabolite with addition of GSH + O. However, MS/MS data could not be generated to confirm this deduction.

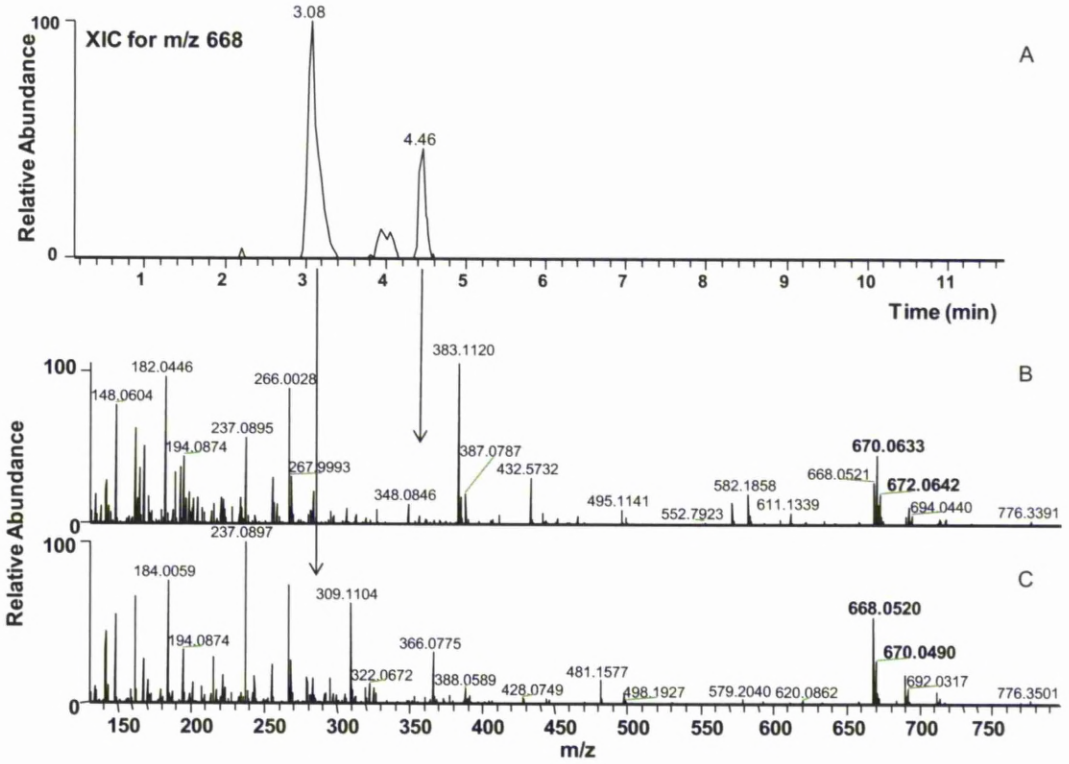

Figure 4.19: XIC chromatogram for *m/z* 668 (A) and full ion scans for peaks detected in the XIC chromatogram for *m/z* 668 (B, C). Analysis carried out using a LTQ Orbitrap mass spectrometer.

An *m/z* 670 ion and its ^{37}Cl isotopologue were amongst the most abundant ions in the full ion scan (Figure 4.20 B) from the peak detected in the XIC chromatogram for *m/z* 670 (RT 4.51 minutes; Figure 4.20 A), indicating a possible TPA metabolite with addition of GSH + O + 2H. However, MS/MS data could not be generated to confirm this deduction.

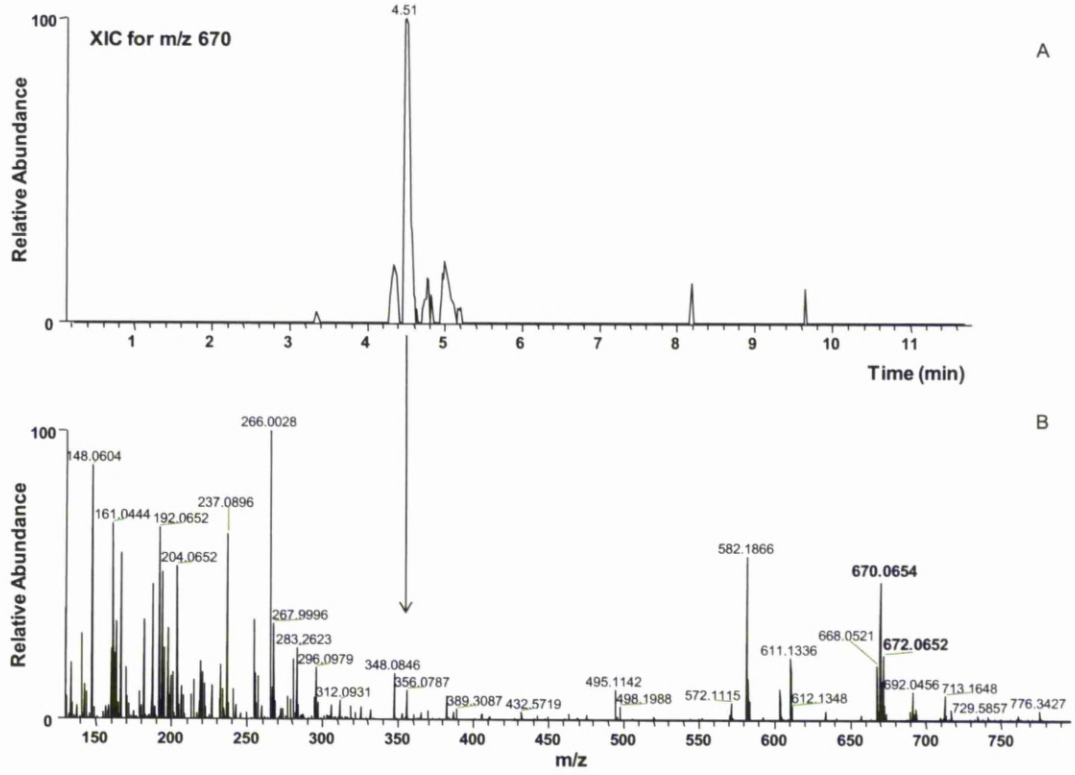

Figure 4.20: XIC chromatogram for *m/z* 670 (A) and full ion scan for the peak detected in the XIC chromatogram for *m/z* 670 (B). Analysis carried out using a LTQ Orbitrap mass spectrometer.

4.4 DISCUSSION

The principal aims of the work described in this chapter were to investigate whether the differences between the hepatotoxicity of furosemide and TPA in mice could be explained by differences between bioactivation and detoxification of the compounds' reactive metabolites. TPA did not induce severe hepatotoxicity in mice when administered via an *i.p* or oral route. TPA did however significantly deplete hepatic GSH at 24 hours compared to vehicle control and was shown to undergo bioactivation and bind covalently to hepatic protein *in vitro*. The reactive metabolite of furosemide binds covalently to murine hepatic protein *in vivo* and elicits hepatotoxicity. This does not occur in rats, in which the metabolite is excreted in the form of a GSH conjugate; suggesting a possible safety mechanism exists in rats to protect them from furosemide-induced hepatotoxicity (Williams *et al.*, 2007). It was suggested that TPA's reactive metabolite may be a better substrate for GSTs in the mouse liver and therefore undergoes detoxification via GSH conjugation. Elucidating the putative detoxification pathways of TPA and comparing them with those of furosemide may provide a rational for the differences between the hepatotoxicity of the two compounds.

The work described in Chapter 2 provided evidence that TPA undergoes bioactivation, and that the reactive metabolite(s) produced can bind covalently to hepatic protein *in vitro*. It was also shown that the degree of covalent binding could be reduced by the inclusion of GSH in microsomal incubations. The thiophene ring is often bioactivated in drugs and other xenobiotics to either a thiophene S-oxide or an epoxide (Medower *et al.*, 2008, Kalgutkar *et al.*, 2005, Dansette *et al.*, 2005, Machinist *et al.*, 1995, Dalvie *et al.*, 2002, Chen *et al.*, 2011) and has been associated with toxicity in certain cases (O'Donnell *et al.*, 2003, Lecoeur *et al.*, 1996, Graham *et al.*, 2008). A common mechanism for the detoxification of reactive drug metabolites occurs via GSH conjugation (Williams *et al.*, 2007). GSH conjugation can occur either spontaneously or through an enzyme (GST) mediated reaction (DeLeve *et al.*, 1991); GSH conjugation of NAPQI, the reactive metabolite of APAP, is spontaneous and GSH depletion is required before covalent binding to proteins and toxicity ensues (Mitchell *et al.*, 1973b). The reactive metabolite of furosemide does not undergo conjugation with GSH in the mouse *in vivo*, however it was shown in Chapter 2 that TPA caused GSH depletion at 24 hours. The identification of drug

metabolite-GSH adducts in a preclinical setting is sometimes treated as a hazard signal as it is indicative of reactive metabolite formation (Reese *et al.*, 2010, Gan *et al.*, 2009), conversely it could be argued that a GSH adduct is an indication of an effective detoxification system. In the latter case, it follows that individuals will become vulnerable to drug toxicity if their tissue GSH is depleted substantially (Nishiya *et al.*, 2008, Shimizu *et al.*, 2011). The FS-GSH conjugate is only seen in the rat, where there is no evidence of covalent binding to hepatic protein or hepatotoxicity (Williams *et al.*, 2007).

In an investigation into the biliary metabolites of TPA in the rat, two TPA-GSH adducts were detected. The metabolic pathways of TPA are similar to those of furosemide. Fragments at *m/z* 345 (TPA anion), *m/z* 306 (GS^-) and *m/z* 249 (dealkylated TPA) suggest that M1 (1.36 ± 0.65% excreted dose) could correspond to a GSH conjugate with an additional oxygen. LC-MS/MS analysis identified, tentatively in the case of M2, the two co-eluting metabolites M2 (*m/z* 670) and M3 (*m/z* 249), which represented 47.58 ± 3.75% of the excreted dose. Fragmentation patterns of these compounds (Butler, 2006) suggest M2 may be another TPA-GSH conjugate, with a 18 amu (nominally, O + 2H) addition to the thiophene ring, and M3 may be the TPA N-dealkylated metabolite. Fragments at *m/z* 345 (TPA) and *m/z* 175 (dehydroglucuronic acid anion) suggest that M4 is a TPA-glucuronide metabolite (19.62 ± 3.64% of excreted dose); presumably, by analogy with the corresponding metabolites of furosemide (Williams *et al.*, 2007, Mizuma *et al.*, 1998), the acyl glucuronide. As observed previously for furosemide (Di Marco *et al.*, 2005), the rate of furosemide and TPA glucuronidation in hepatic microsomal incubations was relatively slow compared to naloxone. Because of their chemical reactivity, unstable acyl glucuronides have been associated almost generically, if somewhat inconclusively, with a potential for causing clinical drug toxicity (Regan *et al.*, 2010). furosemide's acyl glucuronide is relatively stable under standard in vitro conditions (Stachulski *et al.*, 2006), and it seems unlikely that substitution of its furan ring with a thiophene ring will affect chemical reactivity greatly. However, LC-MS/MS analysis of TPA's metabolites in rat bile and rat hepatocytes, revealed multiple closely eluting peaks in the mass chromatograms corresponding to the TPA glucuronide. This pattern is characteristic of an (unstable) acyl glucuronide that has

undergone positional isomerisation through acyl migration at pH ≥ 7.0 (Stachulski *et al.*, 2006, Kenny *et al.*, 2004).

Biliary metabolites of furosemide are well represented by furosemide metabolism in hepatocytes (Williams *et al.*, 2007). Freshly isolated rat and mouse hepatocytes were used to investigate TPA cytotoxicity (Chapter 2) and metabolism. Although TPA did not induce hepatotoxicity *in vivo*, it was cytotoxic in freshly isolated rat and mouse hepatocytes, caused GSH depletion and underwent covalent binding, all in a dose-dependent manner. The radiochromatogram of TPA metabolites in rat hepatocytes shows drug-related compounds with retention times similar to those found in rat bile. This study identified the presence of an N-dealkylated TPA metabolite and the glucuronide metabolite from rat and mouse hepatocytes. Analysis using the LTQ-Orbitrap mass spectrometer detected the presence of metabolites at *m/z* 668 and 670 in mouse hepatocytes, masses consistent with addition of GSH; however the identities of these metabolites could not be confirmed with MS/MS analysis as the signals were too weak. Analysis of metabolites from rat hepatocytes using the LTQ-Orbitrap mass spectrometer detected the presence of metabolites at *m/z* 650, 668 and 670, masses consistent with substitution or additions of GSH; the identities of the GSH adducts were confirmed with MS/MS analysis.

GSH adducts formed by metabolic pathways that result in net substitution of hydrogen or by addition of GSH to an oxygenated intermediate, such as an S-oxide or an epoxide (Dansette *et al.*, 2005, Shimizu *et al.*, 2009), with retention of the oxygen, are well documented (Zheng *et al.*, 2007, Wen and Fitch, 2009a). The structure of the *m/z* 650 $[M-H]^-$ ion given in Figure 4.21 (A) is certainly the conventional representation of a thiophene-ring substituted GSH adduct (O'Donnell *et al.*, 2003). However, the data described here suggests, quite strongly, and certainly in one case that the *m/z* 650 analyte ions are dehydration *fragments* of the *m/z* 668 $[M-H]^-$ *metabolite* ions (schematically, equivalent to M+O+GSH; figure 4.21 B) based on the fact that they are chromatographically coincidental. Thiophene-ring substitution adducts (M+GSH-2H), as observed metabolites, are in most cases thought to be formed, *in vitro* or *in vivo*, by spontaneous dehydration of the primary GSH addition product (M+O+GSH); derived from an epoxide or *S*-oxide intermediate (O'Donnell *et al.*, 2003). The interesting exceptions are GSH adducts of

2,5-diaminothiophene derivatives, apparently derived from 2,5-diimine thiophene reactive intermediates (Hu *et al.*, 2010). Although it is probable that adducts of the M+O+GSH type (i.e. *m/z* 668 for $[M-H]^-$) will in practice be seen only rarely because of dehydration, or possibly thiolysis (Valadon *et al.*, 1996), *in situ* or during sample work up, two such metabolites were isolated in the case of 2-phenylthiophene (Dansette *et al.*, 2005); one derived from an epoxide, the other from the *S*-oxide intermediate. The two M+O+GSH adducts of TPA formed by rat hepatocytes, based upon their mass spectral fragmentations, also had markedly different structures, and thereby are likely to be end products of divergent pathways of metabolic activation.

One of the metabolites ('*m/z* 668 I') gave a fragmentation ($[M-SO]^-$) highly diagnostic of an *S*-oxide (Dansette *et al.*, 2005, Shimizu *et al.*, 2009). The structure, and possible metabolic origins, of the other adduct ('*m/z* 668 II') could not be deduced from the mass spectral data. Retro-Michael elimination of GSH was obtained from the GSH adduct of 2-phenylthiophene *S*-oxide but not from the ex-epoxide adduct (Dansette *et al.*, 2005). Both of the 2-phenylthiophene adducts but neither of the TPA adducts underwent parent-ion dehydration. Exceptionally, neither of the TPA metabolites, unlike the 2-phenylthiophene adducts, eliminated pyroglutamate (129 amu); the essentially generic neutral fragment of GSH thioether conjugates (Wen *et al.*, 2008, Subramanian *et al.*, 2002).

The M2 adduct (*m/z* 670), represented schematically by the addition of GSH, an oxygen atom and two hydrogens to TPA, has no counterpart amongst the many GSH (and GSH ethyl ester) adducts of various structural types reported by Zheng *et al.* (2007), Wen and Fitch (2009a) and Wen *et al.* (2009). Therefore the precise structure and mechanism of formation of M2 remain ambiguous. Valadon *et al.* (1996) observed some open-ring intermediate structures from their study of the NADPH-dependent microsomal metabolism of a tienilic isomer in the presence of mercaptoethanol. They proposed an addition of thiol to an *S*-oxide, with subsequent thiol additions caused thiophene ring opening (note, however, their stable *end products* were closed-ring structures). *Conceivably* a similar pathway in the metabolism of TPA could yield the structure shown in Figure 4.21 (E). The proposed metabolic activation pathways of TPA are shown in Figure 4.22.

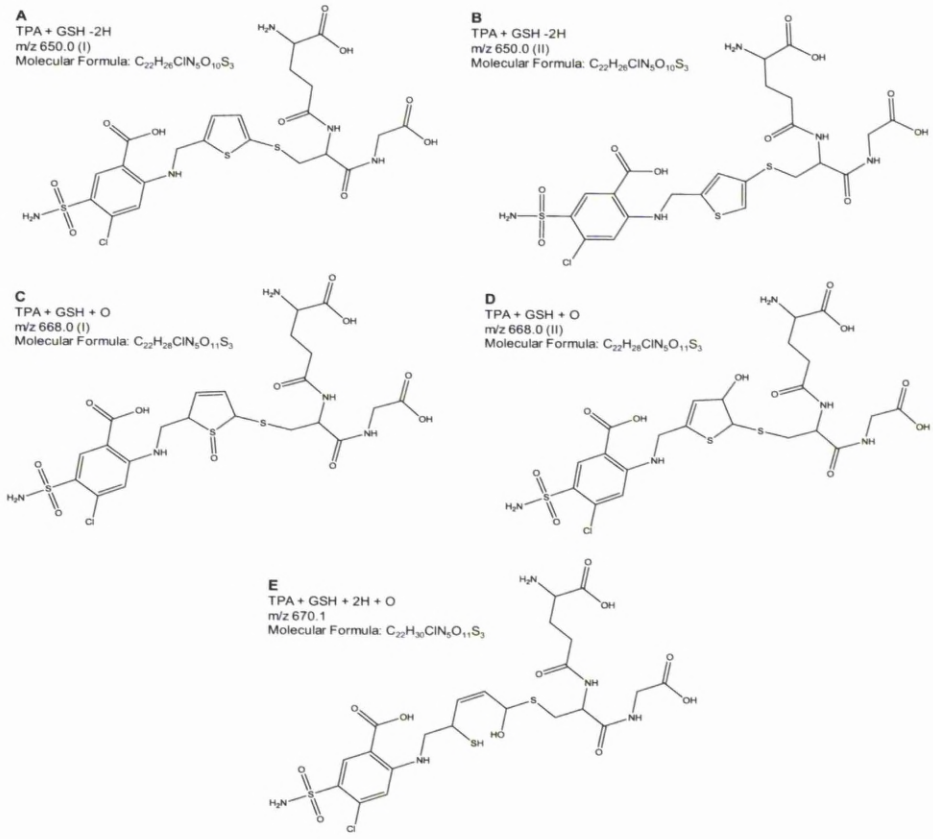

Figure 4.21: Proposed structures of TPA GSH adducts. No MS/MS data was generated for the compounds at *m/z* 650 I (A), 650 II (B), therefore their structures have been tentatively assigned; they may be in-source dehydration products of an *m/z* 668 analyte ion. A neutral loss of 48 amu signifies that 668 I (C) is an *S*-oxide; *m/z* 668 II (D) peaks can be assigned to a GSH adduct by virtue of the neutral loss of GSH but it does not yield fragments that allow characterization, the structure presented here is tentative. Assumed structure of *m/z* 670 (E), based on the masses determined during analysis using the LTQ-Orbitrap mass spectrometer.

The aim of this chapter was to describe the metabolism of TPA *in vivo* and *in vitro*, and compare it to that of furosemide. It was hypothesized that the differences between the hepatotoxicity of furosemide and TPA reported in Chapter 2 could be explained through identification of differential detoxification mechanisms. A TPA-GSH adduct was identified in rat bile and another metabolite was tentatively assigned to a TPA-GSH adduct. Additionally, rat and mouse hepatocyte incubations with TPA also produced TPA-GSH adducts; suggesting that a successful detoxification mechanism exists in both species, potentially contributing to a lack of hepatotoxicity of TPA.

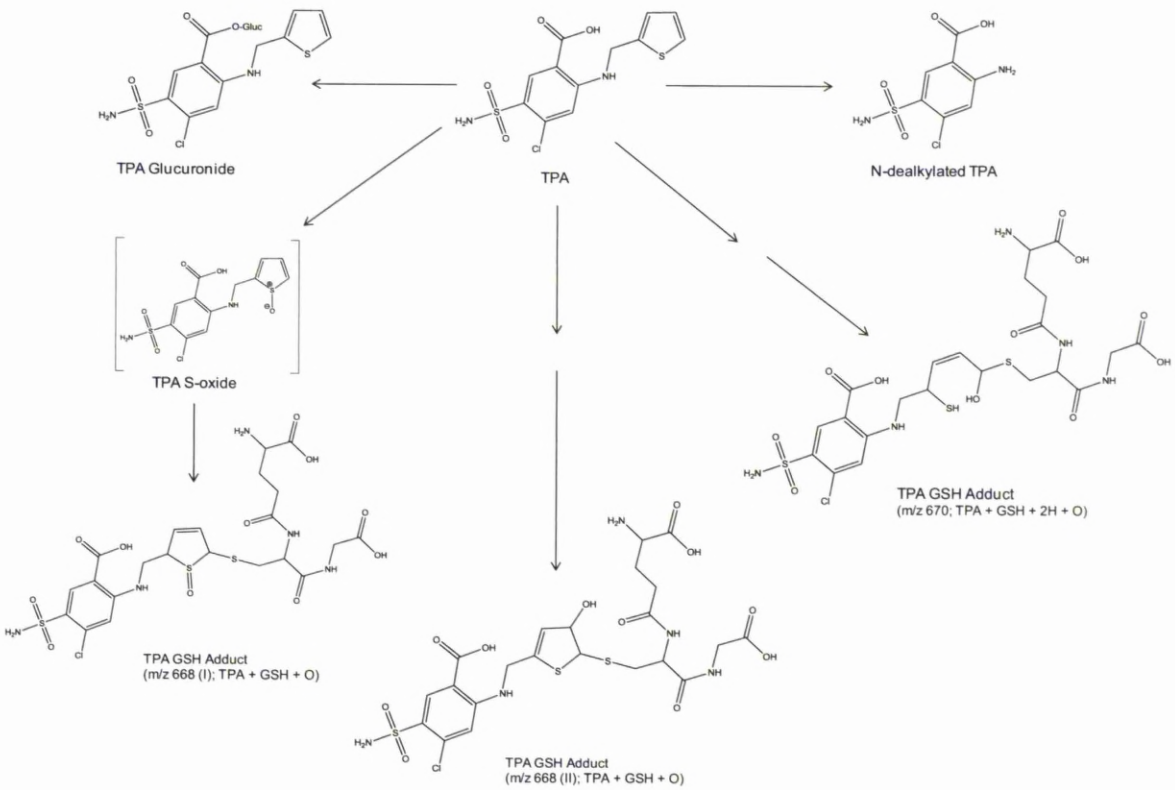

Figure 4.22: Proposed metabolic pathways of TPA. The metaboplic pathways represented by double arrows signify uncharacterised metabolic pathways producing GSH adducts of uncertain structure; the two adduct structures (*m/z* 668 II and *m/z* 670) in are representative of potential structures.

CHAPTER 5

NEVIRAPINE MERCAPTURATES AS MARKERS OF *IN VITRO* AND *IN VIVO* BIOACTIVATION AND TOXICITY

CONTENTS

5.1 INTRODUCTION

Nevirapine (NVP) is a non-nucleoside reverse transcriptase inhibitor (NNRTI) used in the treatment of HIV-1 infection. Adverse effects of nevirapine include skin rash and hepatotoxictiy. The incidence of nevirapine-induced skin rash in man has been reported in 3.4 – 48% of adults (Carr and Cooper, 2000, Pollard *et al.*, 1998, Phanuphak *et al.*, 2007, Barreiro *et al.*, 2000, Bersoff-Matcha *et al.*, 2001, Bonnet *et al.*, 2002, Pujari *et al.*, 2004, Barner and Myers, 1998, Havlir *et al.*, 1995). Severe or life-threatening skin reactions, including Stevens - Johnson syndrome (SJS), toxic epidermal necrolysis (TEN) and hypersensitivity, have been observed in 1.5% of patients (Carr and Cooper, 2000, Pollard *et al.*, 1998, Phanuphak *et al.*, 2007, Fagot *et al.*, 2001, Claes *et al.*, 2004). Nevirapine has been associated with varying degrees of hepatotoxicity (De Maat *et al.*, 2002, Chu *et al.*, 2010, Brück *et al.*, 2008), and can cause severe or life-threatening hepatotoxicty in around 1.0 - 3.2% of HIV patients (Pollard *et al.*, 1998, Pujari *et al.*, 2004, Martínez *et al.*, 2001, Sanne *et al.*, 2005). There is evidence to suggest that nevirapine undergoes bioactivation to a reactive metabolite (Takakusa *et al.*, 2008, Wen *et al.*, 2009, Antunes *et al.*, 2010); a common mechanism for the detoxification of reactive metabolite occurs via GSH conjugation (Williams and Naisbitt, 2002). Human urinary mercapturates (breakdown products of GSH-adducts) have been used as biomarkers of human exposure to reactive species (Seutter Berlage *et al.*, 1977). The investigations in this chapter aimed to assess whether nevirapine mercapturates are indicative of bioactivation and toxicity in the rat, *in vivo* and *in vitro*.

Freshly isolated hepatocyte suspensions have been shown to be an important tool in investigations into the bioactivation-dependant mechanisms of idiosyncratic hepatotoxins (Higaki *et al.*, 1989, Masubuchi *et al.*, 1998, Graham *et al.*, 2008). They provide a physiological relevant system to assess the toxicological outcomes of phase I and phase II metabolism of drugs, as they contain all sub-cellular organelles and all metabolically relevant enzymes and co-factors, at levels that reflect the *in vivo* situation (Elaut *et al.*, 2006). Rat hepatocytes were found in be a good system to study bioactivation-dependant toxicity of amodiaquine and methapyrilene, both human idiosyncratic hepatotoxins (Graham *et al.*, 2008, Tafazoli and O'Brien, 2009). However, there are limitations with this system; not all human idiosyncratic hepatotoxins induce toxicity in rat hepatocytes. Isoniazid, is thought to induce

idiosyncratic hepatotoxicity through metabolism of the parent compound, however fails to induce cytotoxicity in rat hepatocytes.

Animal models of idiosyncratic drug reactions can provide a means of investigating mechanisms of toxicity. However, these models are rare as is it difficult to reproduce an infrequent clinical ADR, reproducibly, in a laboratory species. Uetrecht and colleagues have extensively characterised a dose-dependent, nevirapine-induced skin rash in female Brown Norway rats (Shenton *et al.*, 2003, Shenton *et al.*, 2005, Popovic *et al.*, 2006, Chen *et al.*, 2008, Uetrecht *et al.*, 2010). The rash appears to be immune-mediated (Shenton *et al.*, 2005), resembling the idiosyncratic cutaneous reaction seen in humans (Shenton *et al.*, 2003, Shenton *et al.*, 2004), and keratinocyte cell death was observed similar to that seen in SJS (Shenton *et al.*, 2003). The nevirapine-induced skin rash in Brown Norway rats holds other similarities to that seen in humans in terms of; the time of onset, females being more susceptible than males, incidence increases with dose, escalating dose of nevirapine can reduce incidence, rechallenge results in more severe rashes than on initial exposure (Shenton *et al.*, 2003, Uetrecht *et al.*, 2010).

Nevirapine has the potential to be bioactivated to various reactive intermediates (Figure 5.1) and evidence for the bioactivation of nevirapine has been shown in various *in vitro* studies. Nevirapine has been shown to bind covalently to RLM (Takakusa *et al.*, 2008). A single GSH adduct was identified in HLM and incubations with recombinant CYP 3A4 (Wen *et al.*, 2009). The pathway of metabolism through 12-hydroxy nevirapine has been implicated in formation of the nevirapine reactive metabolite. Antunes *et al.* (2009) demonstrated the reactivity of 12-sulphoxy nevirapine by formation of multiple DNA adducts in reactions with 12-mesyloxy nevirapine. 12-OH NVP was found to be a substrate for sulphotransferase in rats (Chen *et al.*, 2008), and it has been proposed that the sulphate ester dissociates to form reactive quinone methide intermediate (Chen *et al.*, 2008, Uetrecht, 2006). The quinone methide could also be generated by enzymic oxidation (Wen *et al.*, 2009). Hydroxyheteroaryl metabolites (Riska *et al.*, 1999) are potential precursors of reactive quinine imines (Wen *et al.*, 2009). The cyclopropylamine group has the potential to be bioactivated to an aminium cation radical via N-dealkylation

(Takakusa *et al.*, 2008). Nevirapine could also form one or more heteroarene epoxide metabolites in either of the pyridine rings.

GSH conjugation of drug reactive metabolites is a common mechanism detoxification (Williams *et al.*, 2002). The identification of drug metabolite-GSH adducts in a preclinical setting is sometimes treated as a hazard signal as it is indicative of reactive metabolite formation (Gan *et al.*, 2009, Reese *et al.*, 2010), conversely it could be argued that a GSH adduct is an indication of an effective detoxification system. In light of improved bioanalytical techniques, urinary mercapturates (breakdown products of GSH-adducts) have been used as biomarkers of human exposure to reactive species and in the quantitative assessment of *in vivo* bioactivation (Seutter Berlage *et al.*, 1977).

With the aim to assess the plausibility of using nevirapine mercapturates as a translational marker of nevirapine bioactivation and toxicity, the work presented in this chapter intended to test the current model of nevirapine-induced skin toxicity and correlate with formation of nevirapine mercapturates. Freshly isolated rat hepatocytes were used initially, as a well defined *in vitro* system, to investigate the bioactivation and toxicity of nevirapine. Uetrecht's model of nevirapine-induced skin rash in Brown Norway rats was employed to test the hypothesis *in vivo*. A dosing schedule over three weeks was designed to measure nevirapine mercapturate levels over time and to assess the degree of toxicity induced. Nevirapine and nevirapine metabolites were to be quantified by a LC-MS/MS MRM method against chemically synthesized and biologically produced standards. Nevirapine-induced toxicity is measured primarily by histopathological analysis of the skin and other tissues. Observational information regarding the condition of the nevirapine-treated animals was also recorded by a pathologist. Clinical chemistry markers of liver toxicity were also to be measured in light of nevirapine-induced hepatotoxicity in man; these included hepatic GSH concentration and serum ALT activity measurements.

Cell death is the ultimate cause of tissue injury in DILI and drug-induced skin reactions. Proteins released from apoptotic and necrotic cells have been used as biomarkers of drug-induced cell death (Antoine *et al.*, 2009). Serum quantification HMGB1 was to be measured by ELISA throughout the time course of nevirapine treatment. High mobility group box protein 1 (HMGB1) is released passively from

necrotic cells and is and thought to have a role in alerting the innate immune system to dying cells (Scaffidi *et al.*, 2002, Kono and Rock, 2008), which will be a key determinant in the extent of tissue damage.

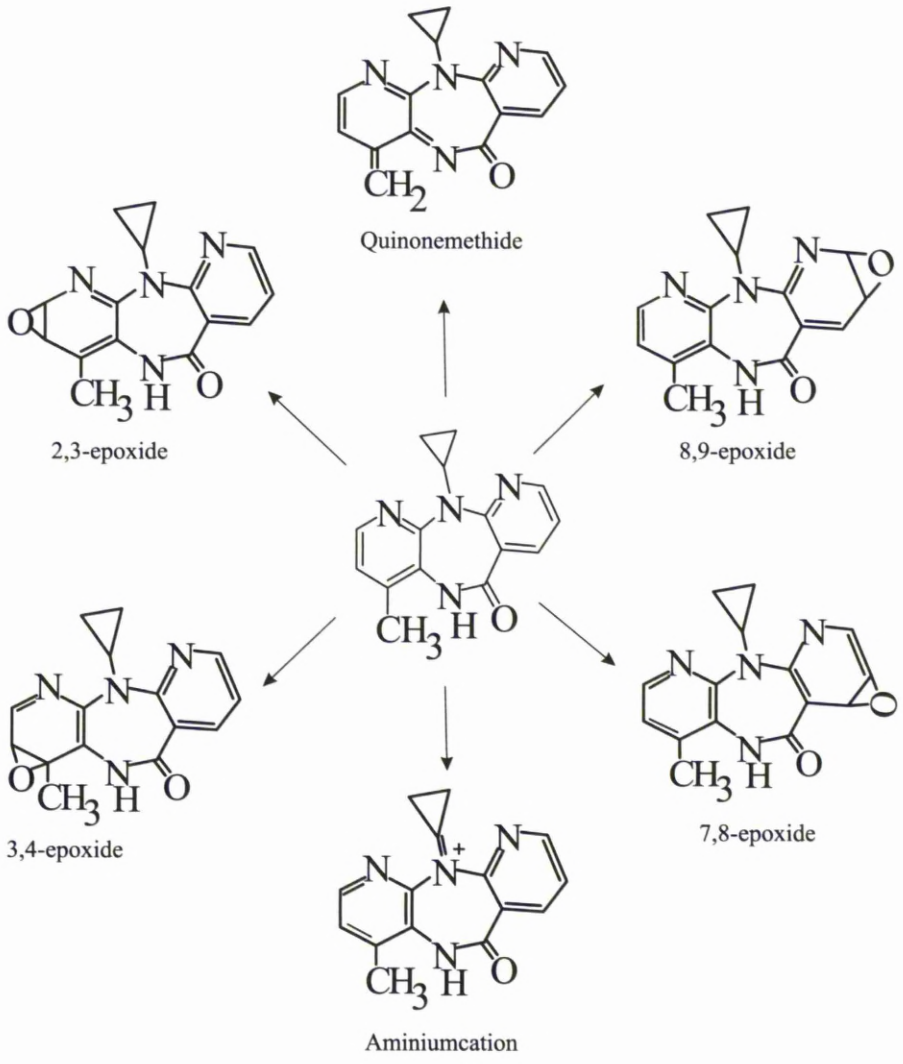

Figure 5.1: Potential bioactivation pathways of nevirapine.

5.2 MATERIALS AND METHODS

5.2.1 Materials

Nevirapine and standards of two known metabolites of nevirapine (3-OH NVP and 12-OH NVP), were gifts from Pfizer Global Research and Development (Sandwich, Kent, U.K.). They were 99% pure as determined by HPLC and NMR. Nevirapine was also purchased from Bosche Scientific (New Brunswick, NJ, U.S.A.). 10x Hanks Balanced salt solution Ca^{2+} was obtained from Gibco (Invitrogen Ltd, Paisley, U.K.). CellTiter 96® AQueous One Solution Cell Proliferation Assay kit was obtained from Promega (Southampton, U.K.). Collagenase A was obtained from Roche Diagnostics (Lewes, U.K.). Unless otherwise stated, reagents were obtained from Sigma-Aldrich Chemical Co. (Poole, U.K.). Ultima Gold scintillation fluid was purchased from PerkinElmer LAS (Seer Green, Beaconsfield, Buckinghamshire, U.K.). All solvents were of HPLC grade and were products of either Fischer Scientific plc (Loughborough, U.K.) or VWR (Lutterworth, U.K.)

5.2.2 Experimental animals

Protocols described were undertaken in accordance with criteria outlined in a license granted under the Animals (Scientific Procedures) Act 1986 and approved by the University of Liverpool Animal Ethics Committee. Male wistar rats were obtained from Charles River Laboratories (Margate, U.K.) and female Brown Norway rats were obtained from Harlan Laboratories (Bicester, Oxfordshire, U.K.). Animals were housed in a light controlled room at a constant temperature and, unless otherwise stated, supplied with a standard chow diet and water *ad libitum*.

5.2.3 Dosing regimen for 21 day nevirapine administration in food to female Brown Norway rats

Female Brown Norway rats (150 – 200 g) were singly housed after a 7 day acclimatization period and given nevirapine in food (60 – 80 mg/kg/day; 1.12 g nevirapine / kg food; Sequoia Research Products, Pangbourne, U.K.). Animals were weighed daily and food (and therefore dose) was adjusted accordingly. Food was

weighed on a daily basis and dose received was calculated (Figure 5.2). On days 6, 13 and 20, 3 nevirapine dosed animals and 3 control animals were placed in metabolism cages for 24 hours; urine and feces was collected over this time and stored at -80°C until analysis. Animals receiving nevirapine were culled by CO_2 asphyxiation on days 7, 14 and 21 and control animals (receiving normal chow) were culled on day 21 (n=3 for each group). Animals were sheared and pictures were taken of affected areas (non-affected corresponding areas in control animals). Blood was taken via cardiac puncture and selected parts of the liver were removed, snap frozen in liquid N_2 and stored at -80°C until analysis. Selected organs (liver, kidney, heart, lungs, spleen, adrenal glands, small intestine, large intestine, popliteal and mesenteric lymph nodes and brain) and skin sections (from footpad, ear, tail, interscapular, ventral neck and lumbo-sacral region) were taken and fixed in 4% paraformaldehyde (PFA) until histopathological analysis. The remaining skin was removed as a whole and fixed in 10% formalin. After routine paraffin wax embedding, sections (3-5 μM) of [list organs] were prepared, stained with hematoxylin and eosin and examined by light microscopy.

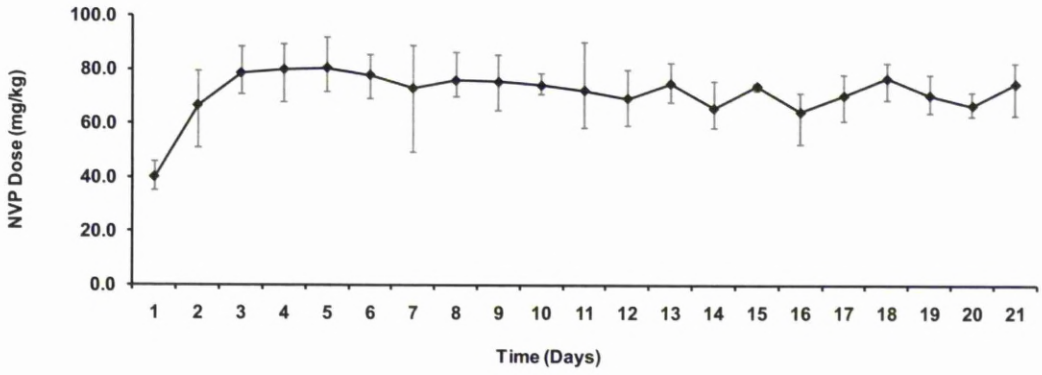

Figure 5.2: Daily average dose of nevirapine received over 21 days. Female Brown Norway rats were singly housed and given nevirapine in food (1.12 g nevirapine / kg food). Animals were weighed daily and given enough food to give a dose of 150 mg/kg/day nevirapine; the graph shown the actual dose of nevirapine received (60 – 80 mg/kg/day).

5.2.4 Determination of hepatic glutathione levels in female Brown Norway rats following nevirapine treatment

The glutathione (GSH) assay is based upon the 5, 5-dithiobis (2-nitrobenzoic acid)-GSH disulfate recycling procedure first reported by Owens and Belcher (1965) and is described fully in section 2.2.10.

5.2.5 Determination of protein concentration

Soluble protein concentration was measured using the Lowry assay adapted from Lowry *et al*, 1951 and is described in section 2.2.12.

5.2.6 Histological analysis of skin and liver sections from nevirapine treated female Brown Norway rats

Histological analysis (section 2.2.15) was carried out on PFA fixed skin sections described earlier.

5.2.7 Measurement of alanine transaminase (ALT) activity in female Brown Norway rat serum following nevirapine treatment

Serum alanine transaminase (ALT) levels were determined kinetically at 37°C using ThermoTrace Infinity ALT Liquid stable reagent (Alpha Labs, Eastleigh, U.K) according to manufacturer's instructions. ALT levels exceeding 200U/L that were significantly different from controls were considered to represent Hepatotoxicity (Kitteringham *et al.*, 2000).

5.2.8 Measurement of HMGB1 levels in female Brown Norway rat serum following nevirapine treatment

Serum HMGB1 levels were determined by ELISA (Shino-test Corporation, Tokyo, Japan) according to manufacturer's instructions using a chicken anti-HMGB1 antibody as a catcher antibody (1 μg/well) compared to known standards using 3,3',5,5'-tetramethyl-benzidine turnover by a peroxidise-linked anti-HMGB1 antibody. The detection limit was 0.1 ng/ml.

5.2.9 Hepatocyte isolation from male Wistar rats and female Brown Norway rats

Rat hepatocytes were isolated using a modified two-step *in situ* collagenase profusion based on Seglen (1976) as described in section 2.2.7.

5.2.10 Assessment of nevirapine-induced cytotoxicity in freshly isolated rat hepatocytes

Hepatocyte incubations were carried out in an orbital shaker set at 190 rpm for 6 hours with nevirapine [0 – 500 μM in MeOH (1% v/v). Following incubation, cytotoxicity was determined by trypan blue exclusion (100 μl of cell suspension and 20 μl of 0.4% trypan blue solution). Cytotoxicity was also determined by reduction of 3-(4,5-dimethylthiazol-2-yl)-2,5- diphenyl tetrazolium bromide (MTS) solution using the CellTiter 96® AQueous One Solution Cell Proliferation Assay kit (Promega, Southampton, UK), according to the manufacturer's instructions. Cell suspension (100 μl) was combined with MTS solution (20 μl), incubated at 37°C for 1 hour, and centrifuged at 50*g* for 2 minutes, this was performed in triplicate. The absorbance of the resulting supernatant was measured at 490 nm using a microtiterplate reader (Dynex Technologies, Chantilly, VA).

5.2.11 Sample preparation for the determination of GSH levels in primary rat hepatocytes

From the same incubations used for cytotoxicity assessment, the effect of nevirapine on total cellular levels of GSH was determined. Cells ($1x10^6$) from the hepatocyte incubation were centrifuged at 50*g* for 2 minutes. The resulting pellet was resuspended in 10 mM HCl. One-fifth of lysed hepatocytes were removed for protein content determination. The remaining hepatocyte lysate was combined with 6.5% (w/v) 5-sulfosalicylic acid (four parts hepatocyte lysate and one part 5-sulfosalicylic acid) and stored on ice for 10 minutes before centrifugation at 18,400*g* for 5 minutes. The GSH levels were determined as described section 2.2.10.

5.2.12 Quantification of nevirapine and nevirapine metabolites in rat urine using LC-MS/MS

Mass spectrometric analysis was carried out at the University of Liverpool (U.K.) and Pfizer, U.K using synthetic and biologically produced standards (Srivastava *et al.*, 2010).

Liverpool - LC-MS/MS analyses were performed using an AB Sciex API 2000 mass spectrometer with TurboIonSpray source (AB Sciex, Foster City, CA, U.S.A.) interfaced to a Perkin Elmer Series 200 pump and Perkin Elmer Series 200 autosampler (Perkin Elmer, Seer Green, Beaconsfield, Buckinghamshire, U.K.). Analytes were resolved on a Hypersil BDS C18 column (25 x .046 cm, 5 µm particle size; Thermo Fisher Scientific, Runcorn, Cheshire, U.K.). The mobile phase consisted of 15 mM ammonium formate (adjusted to pH 4 with formic acid; aqueous) and ACN containing 0.05% formic acid (organic). A sample aliquot of 5 µl was injected onto the column, and eluted at 1 ml/min with a gradient profile as described in Table 5.2 (LC-MS/MS 1). Eluate split-flow to the LC-MS interface was approximately 200 µl/min. Nitrogen was used as the curtain and collision gas. The interface temperature was 200 °C. Nevirapine and metabolites were detected in the

multiple-reaction monitoring (MRM) mode with the transitions described in Table 5.3. Data were processed with Analyst 1.4. software (AB Sciex).

Method	Column	Mobile Phase	Gradient	
LC-MS/MS 1	Hypersil BDS C18 (25 cm)	**A:** Ammonium formate (pH 4) **B:** ACN (0.05% FA)	0 min	5% B
			5 min	17% B
			15 min	25% B
			19 min	50% B
			19 min	50% B
			26 min	5% B
LC-MS/MS 2	Onyx C18 (10 cm)	**A:** Water (5% ACN, 0.07% FA) **B:** ACN (0.1% FA)	0 min	0% B
			1 min	0% B
			6 min	30% B
			8 min	95% B
			9 min	95% B
			9 min	0% B
			13 min	0% B

Table 5.2: LC methods used for the quantification of nevirapine and nevirapine metabolites by LC-MS/MS

Pfizer - LC-MS/MS analyses were performed using an AB Sciex API 4000 mass spectrometer with TurboIonSpray source (AB Sciex, Foster City, CA, U.S.A.). The LC system used was an Agilent 1100 binary pump LC system (Agilent Tech. Inc., Palo Alto, CA, U.S.A.). Analytes were resolved on an Onyx C18 column (100 x 10 mm; Phenomenex, Macclesfield, Cheshire, U.K.). The mobile phase consisted of dH_2O containing 5% ACN and 0.1% formic acid (aqueous) and ACN containing 0.1% formic acid (organic). A sample aliquot of 20 µl was injected onto the column, and eluted at 1 ml/min with a gradient described on Table 5.2 (LC-MS/MS 2). Nitrogen was used as the curtain and collision gas. The interface temperature was 750 °C. Nevirapine and metabolites were detected in the multiple-reaction monitoring (MRM) mode with the transitions described in Table 5.4. Data were processed with Analyst 1.4.1 software (AB Sciex).

Parameters	Selected Reaction Monitoring
Source temperature (°C)	200.0
Nebulizing gas (gas-1) (arbitrary units)	30.00
Heater gas (gas-2) (arbitrary units)	30.00
Curtain gas (arbitrary units)	35.00
Ion spray voltage (V)	5000
Collision energy (eV)	30.00
Declustering potential (V)	20.00
Focusing potential (V)	200.0
Entrance potential (V)	10.00
Dwell time (ms)	150.0
Mode of analysis	Positive
Ion transition products (*m/z*)	**NVP:** 266.8/226.1 **12-OH NVP:** 282.9/265.0 **3-OH NVP:** 282.9/213.9 **M1:** 428.0/265.0 **M2:** 428.0/299.0

Table 5.3: Main working parameters for tandem mass spectrometric analyses of nevirapine and nevirapine metabolites (University of Liverpool).

Parameters	Selected Reaction Monitoring
Source temperature (°C)	750.0
Nebulizing gas (gas-1) (arbitrary units)	40.00
Heater gas (gas-2) (arbitrary units)	40.00
Curtain gas (arbitrary units)	35.00
Ion spray voltage (V)	4500
Collision energy (eV)	27.00 – 54.00
Declustering potential (V)	59.00 – 104.0
Entrance potential (V)	10.00
Dwell time (ms)	50.0
Mode of analysis	Positive
Ion transition products (*m/z*)	**NVP:** 266.8/226.1 **12-OH NVP:** 282.9/265.0 **3-OH NVP:** 282.9/213.9 **M1:** 428.0/265.0 **M2:** 428.0/299.0

Table 5.4: Main working parameters for tandem mass spectrometric analyses of nevirapine and nevirapine metabolites (Pfizer, U.K.).

5.2.13 Statistical analysis

All results were expressed as mean + standard deviation. Data sets were analysed for normality using the Shapiro-Wilk test. For single comparisons of normal data an unpaired T-test was used. Where multiple comparisons were made and the data was normally distributed, one-way ANOVA was used with bonferroni correction. Where multiple comparisons were made and the data was not normally distributed, a Kruskal-Wallis test, for all pair-wise comparisons, was used with either Conover-Inman or Dwass-Steel-Chritchlow-Fligner corrections for multiple comparisons. All statistical analysis were performed using the StatsDirect statistical software.

5.3 RESULTS

5.3.1 Investigating the effect of nevirapine on the viability and GSH levels of freshly isolated hepatocytes in suspension

The effect of nevirapine on the viability and GSH levels on hepatocytes freshly isolated from male Wistar and female Brown Norway rats was investigated in order to identify bioactivation-dependent toxicity. Male Wistar rats are used as this is the strain in which most experience has been had in terms of hepatocytes isolations; female Brown Norway rats were chosen as this strain has been found to be sensitive to a nevirapine-induced toxicity. Nevirapine failed to induce statistically significant cytotoxicity in freshly isolated hepatocytes in either strain (Figure 5.3 A and B). GSH levels were significantly depleted at 500 μM nevirapine in male Wistar rat hepatocytes (Figure 5.3 A). In female Brown Norway rat hepatocytes GSH levels were significantly depleted at 200 and 500 μM nevirapine (Figure 5.3 B).

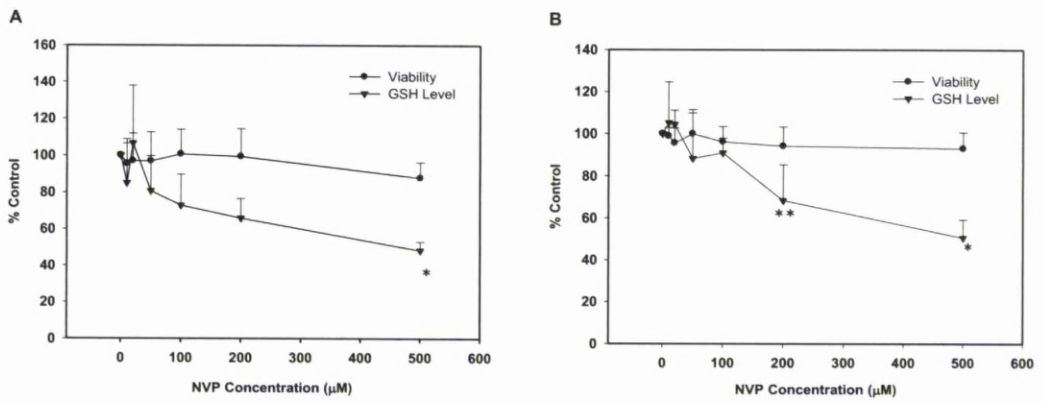

Figure 5.3: Assessment of the dose-dependent effect of nevirapine on the viability and GSH levels on hepatocytes freshly isolated from male Wistar rats and female Brown Norway rats. Effect of nevirapine (0 – 500 μM; 6 hours) on cytotoxicity and GSH content in male Wistar (A) and female Brown Norway (B) rat hepatocytes. Data are given as mean + standard deviation of 3-4 independent isolations. **; $p<0.0017$, *; $p<0.0083$, comparing to 0 μM nevirapine incubations (one-way ANOVA with bonferroni correction for multiple comparisons, critical $p<0.0083$).

5.3.2 21 day time-course of nevirapine-induced skin rash development in female Brown Norway rats

On day 7, 14 and 21 after each animal was sheared, lesions on the body were analysed by eye and counted (Table 5.4). Photographs of the lesions were taken (Figure 5.4) and histopathology was performed on affected areas (Figure 5.5).

Nevirapine-induced skin rash increased in severity in a time-dependent fashion. On day 7 no abnormalities of the skin or ears were observed in any animal. On day 14, in all animals, both ears displayed multifocal linear dark red areas (approximately 0.2 cm), predominately towards the rim of the ear. The skin on the lumbo-sacral region exhibited several (5-10), approximately 1 mm, raised dark red crusts. Similar findings were observed 2 – 3 cm caudal of the shoulder area along the mid-line and on the left hand or right and left hand side. On day 21 the skin between the shoulders of all animals exhibited several (7 - 10), partly confluent (2 – 5 cm), raised (1 – 7 mm) dark red crusts. The lesions were more severe on the left shoulder and were distributed over the entire body surface from the ears to the pelvic area.

Day	Animal	Skin Lesions
7	1	None
	2	None
	3	None
14	4	Mild
	5	Moderate
	6	Mild
21	7	Moderate
	8	Moderate
	9	Severe
21 (control)	10	None
	11	Mild
	12	Mild

Table 5.4: Severity of skin lesions of nevirapine treated female Brown Norway rats over 21 days. Female Brown Norways rats were administered nevirapine (70 – 90 mg/kg/day) in the diet for either, 7, 14 or 21 days. Skin was examined and grading in terms of number of lesions was performed; mild = 1 - 5, moderate = 6 - 20 and severe = >21 (Shenton *et al.*, 2003).

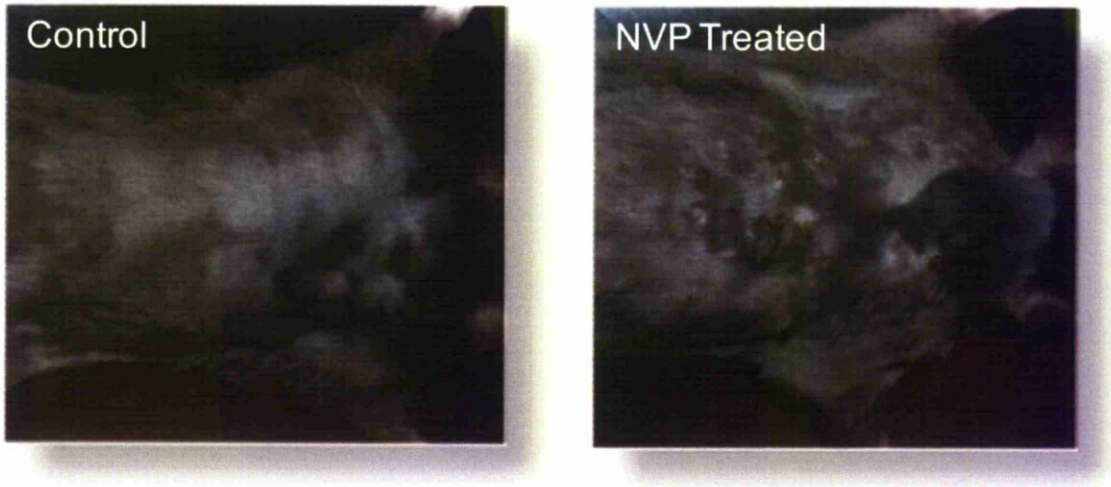

Figure 5.4: Appearance of the skin on the shoulders and cranial back of nevirapine treated female Brown Norway rats. Photographs show a control rat on day 21 of a normal chow diet and nevirapine treated rat on day 21 of a diet containing nevirapine. Dose received was approximately 70 – 90 mg/kg/day.

Mild sporadic microscopic findings occurred in the skin of control animals and consisted of a mixed (lymphocytes, plasma cells, macrophages and neutrophils) inflammatory infiltrate in the dermis of two rats (interscapular region), accompanied by focal serocellular crust and epidermal hyperplasia in one. These findings were focally extensive, mild in severity and are consistent with minor everyday trauma occurring naturally in laboratory animals. Similar findings occurred with comparable incidence and severity in the 3 nevirapine-treated rats culled on day 7 and were not deemed test article-related. On day 14 skin from the lumbo-sacral region of all 3 nevirapine treated animals displayed ulceration extending to the deeper dermis associated with the presence of degenerate neutrophils, serocellular crust formation, moderate epidermal hyperplasia, multifocal epidermal spongiosisand/or moderate mixed cellular perivascular infiltrate in the dermis. Similar lesions were detected in 2 animals, in the skin from the throat and from the ear, respectively. On day 21 lumbo-sacral skin of all 3 nevirapine treated animals, and skin from the shoulder in two animals, displayed severe ulceration accompanied by epidermal and dermal mixed cell infiltration, multifocal serocellular crust formation, intracorneal pustules and/or moderate epidermal hyperplasia and spongiosis.

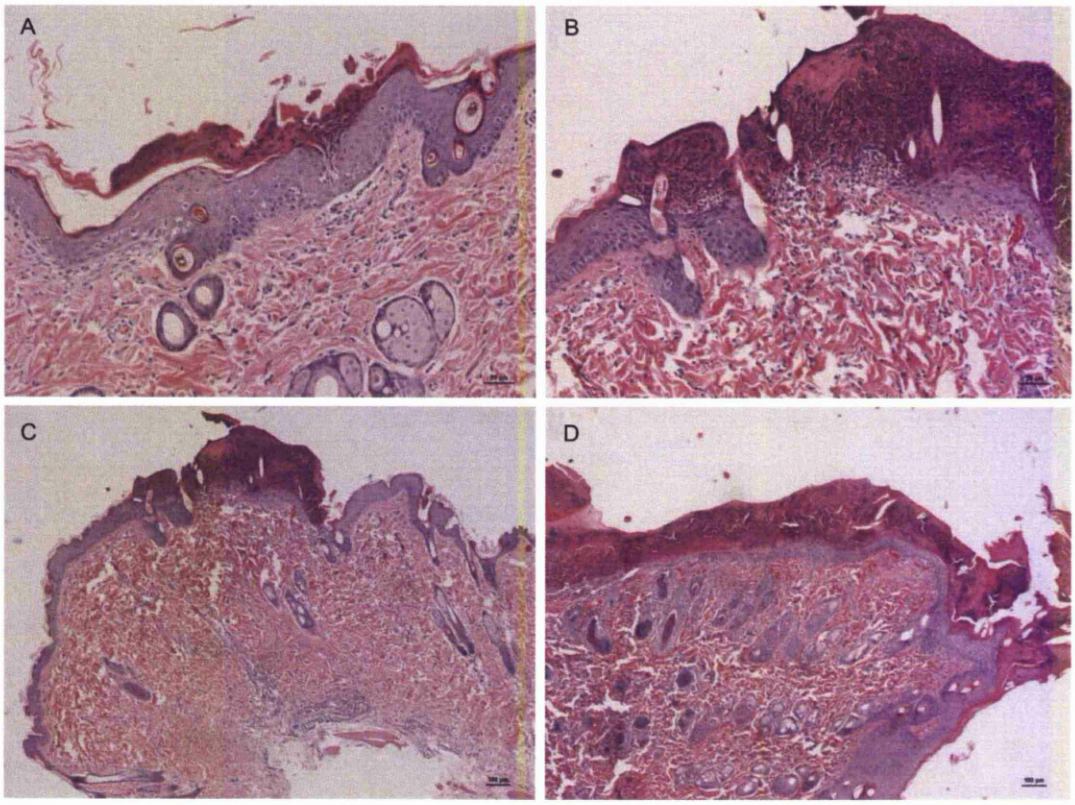

Figure 5.5: Histological analysis of skin sections from female Brown Norway rats following nevirapine treatment. Skin from the interscapular area of a rat from the control group (A) shows a focal serocellular crust associated with mild epidermal hyperplasia and mild mononuclear cell inflammatory infiltrate in the superficial dermis and the epidermis. Skin from the lumbo-sacral region of a rat administered nevirapine for 21 days (B) displayed locally extensive serocellular crusts with an underlying superficial ulceration, accompanied by marked neutrophilic infiltration and epidermal hyperplasia. Multiple, differently sized ulcers with serocellular crust occurring on the skin from the lumbo-sacral region (C and D) in a rat administered nevirapine for 21 days. H&E, 10 x magnification.

5.3.3 Hepatic and serum biochemical analysis from 21 day time-course of nevirapine treatment in female Brown Norway rats

No significant difference was observed in hepatic GSH levels or serum ALT levels between control and nevirapine treated animals (Figure 5.6 A and B). Although no significant increase in serum HMGB-1 concentration was observed, there does appear to be a trend of increasing levels over time of nevirapine treatment (Figure 5.6 C).

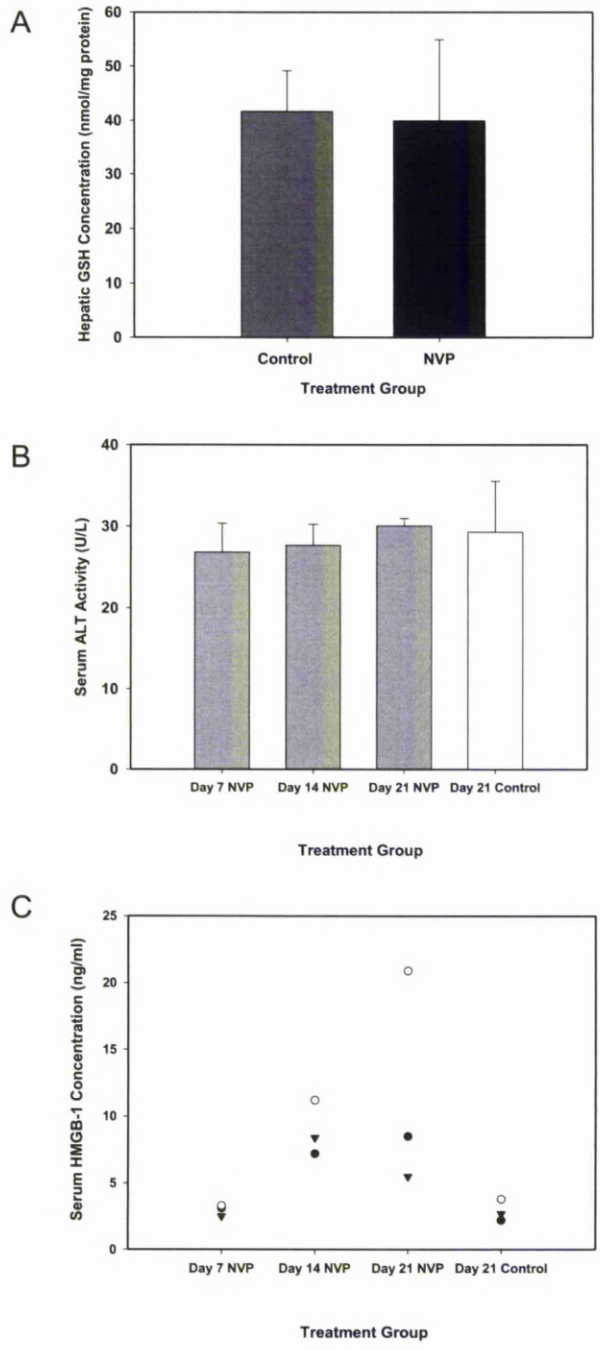

Figure 5.6: The effect of nevirapine treatment on hepatic GSH, serum ALT activity and HMGB-1 concentration in female Brown Norway rats. Female Brown Norway rats were given nevirapine in food (60 – 80 mg/kg/day). Hepatic GSH concentration (A), serum ALT activity (B) and serum HMGB1 levels (C) were measured 7, 14 and 21 for dosed animals and on day 21 only for control animals. Data presented as mean + standard deviation of n=3.

5.3.4 Quantification of nevirapine and nevirapine metabolites in the urine from female Brown Norway rats treated with nevirapine

Nevirapine and nevirapine metabolites were quantified used mass spectrometry (Figure 5.7); no significant trends were identified with any of the metabolites over time.

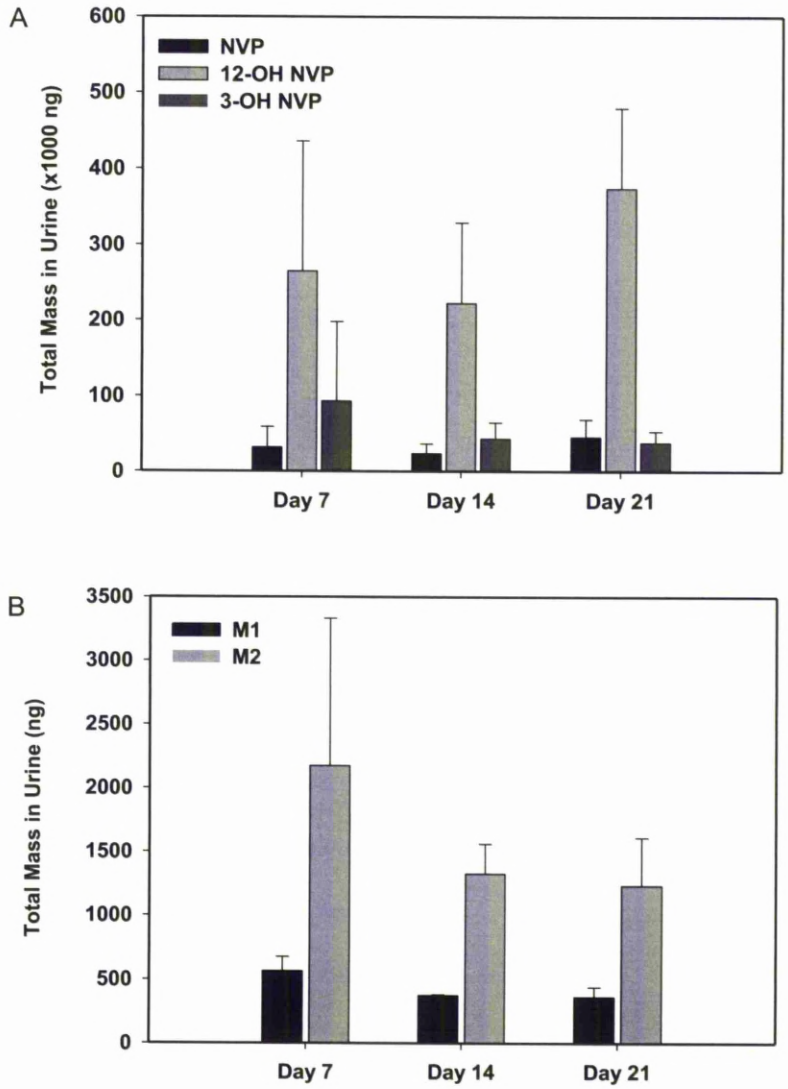

Figure 5.7: Quantification of nevirapine and metabolites in rat urine. Female Brown Norway rats were given nevirapine in food (60 – 80 mg/kg/day) for 21 days; on days 6, 13 and 20, urine was collected. Nevirapine and hydroxylated metabolites (A) and nevirapine mercapturates (B) were quantified. Data is presented as mean + standard deviation of n=3.

5.4 DISCUSSION

The investigations in this chapter aimed to assess the potential of nevirapine mercapturates to be used as quantitative markers of nevirapine bioactivation and toxicity. Freshly isolated rat hepatocyte suspensions have been used successfully for the investigation of bioactivation and toxicity of human idiosyncratic hepatotoxins (Higaki *et al.*, 1989, Masubuchi *et al.*, 1998, Graham *et al.*, 2008), however limitations in this system have also been identified. Nevirapine has been shown to cause severe or life-threatening liver toxicity in 1.0 - 3.2% of HIV patients (Pollard *et al.*, 1998, Pujari *et al.*, 2004, Martínez *et al.*, 2001, Sanne *et al.*, 2005). Nevirapine failed to induce cytotoxicity in hepatocytes isolated from both male Wistar rats and female Brown Norway rats in the current study. Significant GSH depletion was observed in isolated hepatocytes from both male Wistar and female Brown Norways rats.

The animal model of nevirapine-induced skin rash, established by Uetrecht's group, was successfully replicated in these investigations. The time course of skin rash development was consistent with previous reports (Shenton *et al.*, 2003). Various degrees of hyperplasia more prominent adjacent to ulcerated areas and mononuclear dermal inflammatory infiltrate have been described previously and histopathological findings in skin samples taken from rump and between shoulder blades are consistent with the studies presented here, however only one animal on day 14 group displayed moderate mixed cellular infiltration (Shenton *et al.*, 2003). In rats administered nevirapine for 21 days, multiple skin lesions are present at different sites on the body and show increased severity when compared to control animals, However, histopathological analysis of skin samples from control and treated rats indentified that lesions are consistent with self induced trauma.

No evidence of liver injury was seen in the female Brown Norway rats following chronic nevirapine administration, as previously described (Shenton *et al.*, 2003); histological analysis of liver tissue found no evidence of drug-induced insult, ALT levels were not significantly raised and hepatic GSH levels remained normal throughout. Skin rash was observed in animals from day 14 onwards, both visibly and by histopathological analysis. HMGB-1 is a non-organ-specific biomarker of necrosis and inflammation and data must be considered with other biomarkers and

histopathological data. Serum HMGB-1 levels were not significantly elevated at any time point in the 21 day experiment; however, there does appear to be a non-significant increase which would have to be further explored with repeat studies with more animals per group. The most common drug-induced skin reaction is an exanthemous drug eruption, which accounts for about 95% of all drug rashes. In this relatively mild rash, apoptosis is seen in a small number of basal keratinocytes (Uetrecht, 2009). TEN and SJS appear to be mediated by CD8+ T cells that induced massive necrosis of epidermal cells ultimately resulting in blister formation and skin detachment (Lerch and Pichler, 2004).

Investigations using integrated mass spectrometry and NMR (nuclear magnetic resonance) techniques have identified nevirapine mercapturates in human and rat urine following administration of nevirapine (Srivastava *et al.*, 2010). Amongst the human pharmaceuticals the mercapturate conjugates of APAP (Siegers *et al.*, 1984), phenacetin (Veronese *et al.*, 1985), felbamate (Dieckhaus *et al.*, 2002) and valproic acid (Gopaul *et al.*, 2003) have been used for the quantitative assessment of *in vivo* bioactivation. Nevirapine and its urinary metabolites were quantified by mass spectrometry on day 7, 14 and 21 of the study; no time-dependant trend in any nevirapine metabolite was observed. It would be premature to conclude that quantification of nevirapine mercapturates would not be able to provide the same type of marker in animals or in the clinic; the data discussed here is based on a small study of just three animals per group. To further assess the hypothesis further quatification of other GSH breakdown products could be utilized; for example measuring cysteine conjugates.

Although no correlation between skin rash and mercapturate levels were identified, the work presented here may provide a platform for future studies. All animals in this study developed a rash and there was no negative control; we might expect to see a difference in mercapturate levels between a nevirapine-sensitive strain compared to a non-sensitive strain, or in a strain where less than 100% incidence of skin rash is observed. In light of evidence to suggest that metabolism of nevirapine through the 12-OH NVP pathway is responsible for bioactivation, using enzyme inhibitors to block this pathway and chemically inhibit bioactivation and toxicity, would provide a means to establish a quantitative relationship between the two processes.

CHAPTER 6

CHEMICAL INHIBITION OF THE NEVIRAPINE BIOACTIVATION PATHWAY

CONTENTS

6.1 INTRODUCTION

In Chapter 5, the model of nevirapine-induced skin rash in female Brown Norway rat, was successfully replicated. However, no correlation between nevirapine mercapturate level and the onset of skin rash was observed. The results from the previous chapter also highlighted a need for a negative control or chemical inhibition of bioactivation in the chronic nevirapine experiments, and so various enzyme inhibitors were investigated. These experiments would also provide further mechanistic data on the bioactivation pathway of nevirapine. There is evidence to suggest that bioactivation of nevirapine through the 12-hydroxynevirapine (12-OH NVP) pathway is responsible for nevirapine-induced skin rash (Chen *et al.*, 2008). This chapter aimed to characterize the thioether end-products of the 12-OH NVP pathway.

Metabolism of nevirapine through the 12-OH NVP metabolic pathway has been implicated in development of nevirapine-induced skin rash in rats (Chen *et al.*, 2008, Chen *et al.*, 2009). It was discovered that 12-OH NVP causes skin rash in female Brown Norway rats at a lower dose than nevirapine itself (Chen *et al.*, 2008). In experiments where the 12-methyl hydrogens were replaced by deuterium (which decreases 12 hydroxylation and rash but does not affect other properties of the drug), urinary levels of 12-OH NVP were decreased and skin rash in female Brown Norway rats was reduced by 80% (Chen *et al.*, 2008). It has previously been shown that 12-OH NVP is a substrate for sulphotransferase in rats (Chen *et al.*, 2008), and it has been proposed that the sulphate ester dissociates to form a reactive quinone methide intermediate (Chen *et al.*, 2008, Uetrecht, 2006). Antunes *et al.* (2009) demonstrated the reactivity of 12-sulphoxy nevirapine by formation of multiple DNA adducts in reactions with 12-mesyloxy nevirapine.

In an effort to relate these findings with the immunological aspects of the ADR, Uetrecht and colleagues removed lymph nodes from Brown Norway rats treated with nevirapine or 12-OH NVP, and measured the response of lymphocytes to nevirapine and 12-OH NVP by cytokine production and proliferation (Chen *et al.*, 2009). Lymphocytes from animals re-challenged with nevirapine or 12-OH NVP proliferated on treatment with nevirapine, but not with 12-OH NVP (Chen *et al.*, 2009). Similarly, nevirapine-reactive T cells have been observed in a patient with

early-onset hepatitis in the absence of any cutaneous manifestations. The patient's T cells proliferated *in vitro* on exposure to nevirapine but not its stable metabolites (Drummond *et al.*, 2006).

Evidence to suggest that metabolism to 12-OH NVP is not a required step for the formation of nevirapine-induced toxicity has been described. No relationship between serum 12-OH NVP concentrations and skin rash has been identified in patients (Hall and MacGregor, 2007) and high serum nevirapine concentrations correlated with incidence of skin rash in rats (Chen *et al.*, 2008). Furthermore, alternative bioactivation pathways of nevirapine have been hypothesized that do not require 12-OH NVP formation. The quinone methide could also be generated by enzymic oxidation (Wen *et al.*, 2009). Nevirapine could also form one or more heteroarene epoxide metabolites in either of the pyridine rings (Figure 6.1).

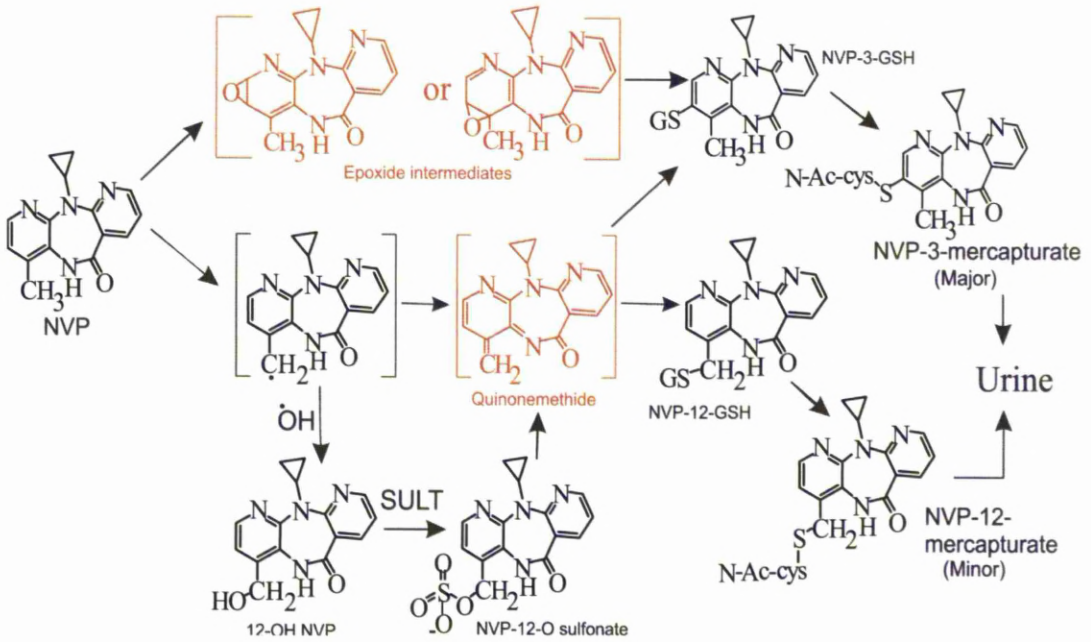

Figure 6.1: Possible routes of bioactivation of nevirapine.

The work presented in this chapter aimed to test the hypothesis that 12-OH NVP is a precursor of a nevirapine mercapturate by administering 12-OH NVP directly to rats and identifying its thioether metabolites, if any. In light of the data presented in Chapter 5, it was also of interest to assess possible chemical inhibitors of nevirapine bioactivation (aminobenzotriazole and 2, 6-dichloro-4-nitrophenol), in order to further elucidate the mechanism underlying the ADR.

6.2 MATERIALS AND METHODS

6.2.1 Materials

Nevirapine and standards of two known metabolites of nevirapine (3-OH NVP and 12-OH NVP), were gifts from Pfizer Global Research and Development (Sandwich, Kent, U.K.). They were 99% pure as determined by HPLC and NMR. Nevirapine was also purchased from Bosche Scientific (New Brunswick, NJ, U.S.A.). Unless otherwise stated, reagents were obtained from Sigma-Aldrich Chemical Co. (Poole, U.K.). Ultima Gold scintillation fluid was purchased from PerkinElmer LAS (Seer Green, Beaconsfield, Buckinghamshire, U.K.). All solvents were of HPLC grade and were products of either Fischer Scientific plc (Loughborough, U.K.) or VWR (Lutterworth, U.K.)

6.2.2 Experimental animals

Protocols described were undertaken in accordance with criteria outlined in a license granted under the Animals (Scientific Procedures) Act 1986 and approved by the University of Liverpool Animal Ethics Committee. Male wistar rats were obtained from Charles River Laboratories (Margate, U.K). Animals were housed in a light controlled room at a constant temperature and, unless otherwise stated, supplied with a standard chow diet and water *ad libitum*.

6.2.3 Investigation of the effects of various, low molecular weight inhibitors on the biliary thioether metabolites of nevirapine and 12-OH NVP in the Wistar rat

Male Wistar rats (200-400 g) were terminally anaesthetised with urethane (1.4 g/ml in isotonic saline; 1.0 ml/kg *i.p.*) and cannulated via the trachea, femoral vein and the common bile duct. Bile was collected over 30 minutes before administration of nevirapine or 12-OH NVP. Nevirapine or 12-OH NVP (50 mg/kg in DMSO) was administered *i.v.* via the femoral vein over 5 minutes. Bile was then collected hourly for into microcentrifuge tubes. In inhibitor studies 1-aminobenzotriazole (50 mg/kg *i.p.*; ABT) and 2, 6-dichloro-4-nitrophenol (6.76 mg/kg *i.p.*; DCNP) were

administered 3 hours and 45 minutes prior to nevirapine/12-OH NVP dose, respectively. Bile was stored at -80°C until extraction and analysis.

6.2.4 Bile preparation by solid phase extraction for LC-MS/MS

Solid phase extraction was used to clean samples for LC-MS/MS analysis. An Oasis® HLB plate (30mg/30µm; Waters, Hertforshire, U.K.) was conditioned with 200 µl MeOH and 200 µl 4% phosphoric acid. Samples and standards were then loaded with internal standards and pulled through by a vacuum. Wells were then washed with 1 ml dH_2O. Samples were eluted into a clean 96-well block with 500 µl 100% ACN. Samples were dried under a steam of nitrogen and reconstituted in 200 µl 10% ACN. The 96-well block was then centrifuged for 5 minutes to pellet any particulate.

6.2.5 Identification of nevirapine mercapturates in rat bile by LC-MS/MS

LC-MS/MS analyses were performed using a TSQ Quantum Access tandem quadrupole mass spectrometer (Thermo Fisher Scientific, San Jose, CA, U.S.A.; main working parameter described in table 6.1). Analytes were resolved on a Thermo Hypersil BDS C18 column (10 x 2.1 cm; Thermo Fisher Scientific, Runcorn, Cheshire, U.K.) at 0.3 ml/min with a gradient profile as described in Table 6.2. The mobile phase consisted of water + 0.05% formic acid (FA) and ACN. Nevirapine and metabolites were detected in the multiple-reaction monitoring (MRM) mode with the transitions described in Table 6.3.

Parameters	Selected Reaction Monitoring
Spray Voltage (kV)	4000
Vaporizer Temperature (°C)	200
Sheath Gas Pressure*	40
Ion Sweep Gas Pressure*	0
Aux Gas Pressure*	55
Capillary Temperature (°C)	277
Skimmer Offset (V)	0
Collision Pressure (Torr)	1.5

Table 6.1: The main working parameters for the TSQ Quantum Access tandem quadrupole mass spectrometer. * Arbitrary units

Time (min)	% ACN	%Water +0.05% FA
0.0	10	90
1	20	80
3	20	80
6	45	55
7	70	30
8	80	20
8.1	7	93
10	10	90

Table 6.2: Step-wise gradient program used for the separation of analytes.

NVP / NVP Metabolite	Parent Mass	Product Mass	Collision energy	T Lens offset
NVP	267.00	227.00	17	83
12-OH NVP	283.00	144.500	30	83
M1	428.20	265.100	25	119
M2	428.210	299.500	17	119
NVP-GSH	572.0	265.00	25	119

Table 6.3: MRM transitions for nevirapine and nevirapine metabolites.

6.2.6 Quantification of nevirapine and nevirapine metabolites in rat bile using LC-MS/MS

Mass spectrometric analysis was carried out at the University of Liverpool (U.K.) and Pfizer, U.K. as described in section 5.2.15.

6.2.7 Statistical analysis

All results were expressed as mean + standard deviation. Data sets were analysed for normality using the Shapiro-Wilk test. For single comparisons of normal data an unpaired T-test was used. Where multiple comparisons were made and the data was normally distributed, one-way ANOVA was used with Bonferroni correction. Where multiple comparisons were made and the data was not normally distributed, a Kruskal-Wallis test, for all pair-wise comparisons, was used with either Conover-Inman or Dwass-Steel-Chritchlow-Fligner corrections for multiple comparisons. All statistical analysis was performed using the StatsDirect statistical software.

6.3 RESULTS

6.3.1 Identification of mercapturate conjugates of 12-OH NVP

In order to assess whether 12-OH NVP is a precursor of a nevirapine mercapturate and therefore undergoes bioactivation, 12-OH NVP was directly administered to anaesthetised male Wistar rats. Bile from rats administered nevirapine or 12-OH NVP (50 mg/kg *i.v.* in DMSO) was analysed by LC-MS/MS to identify the minor (M1) and/or major (M2) nevirapine mercapturates.

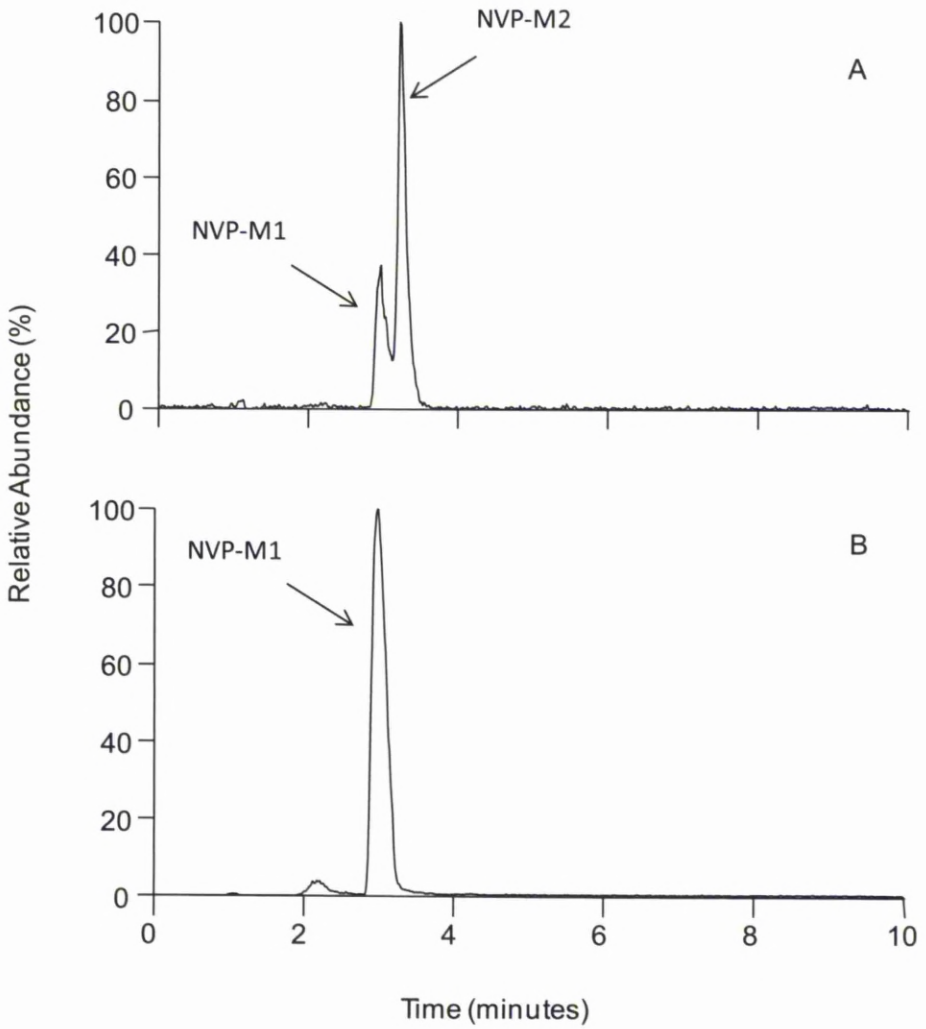

Figure 6.2: Total MRM chromatograms of biliary nevirapine mercapturates following administration of nevirapine or 12-OH NVP to anaesthetised rats. Bile was collected following administration of 50 mg/kg (*i.v.* in DMSO) of either nevirapine (A) or 12-OH NVP (B) to anaesthetised male Wistar rats. Bile was analysed by LC-MS/MS using the TSQ Quantum Access tandem quadrupole mass spectrometer (Thermo Fisher Scientific, San Jose, CA, U.S.A.)

Both M1 and M2 were identified in the bile from male Wistar rats following administration of nevirapine (Figure 6.2 A). However, after 12-OH NVP treatment only a single mercapturate could be seen at a retention time identical to M1 (Figure 6.2 B). To confirm the identity of the mercapturate, bile from the 12-OH NVP dosed rat (93%) was mixed with that from the nevirapine dosed rat (7%). The mercapturate from the 12-OH NVP dosed rat co-eluted with M1 from the nevirapine dosed rat suggesting that they are identical (Figure 6.3 B).

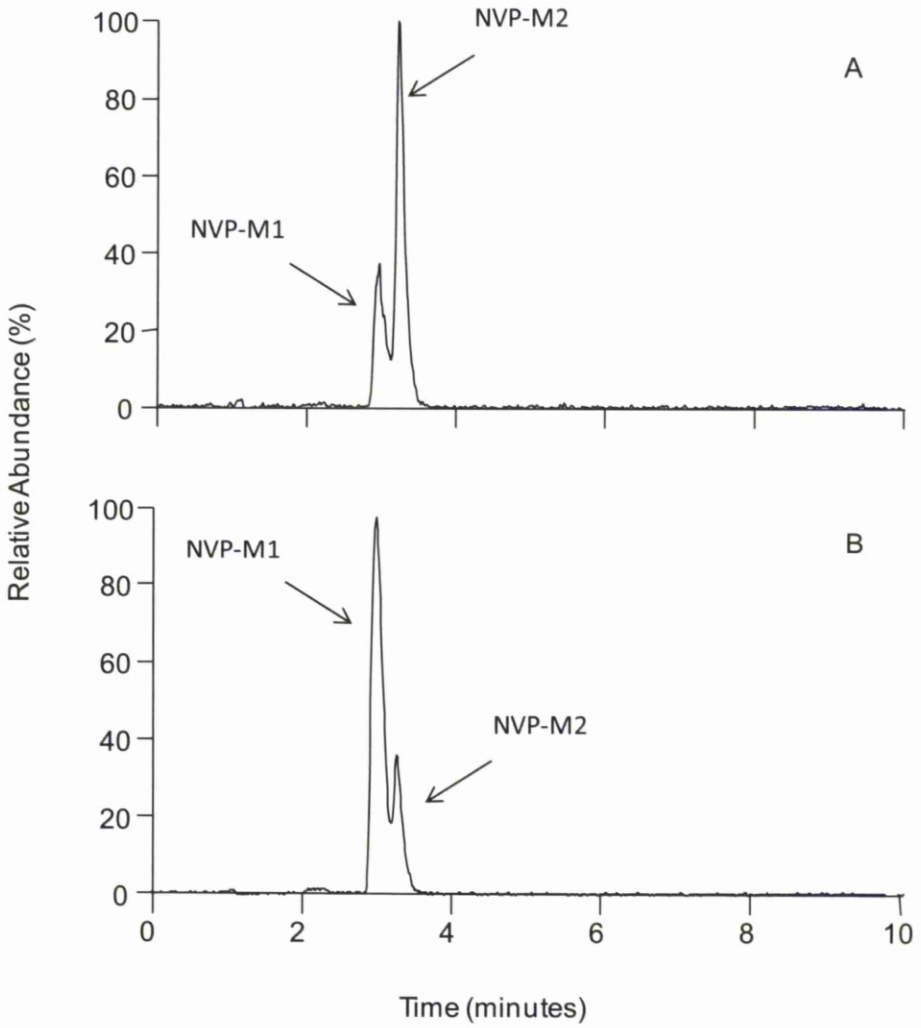

Figure 6.3: Total MRM chromatograms of mixed bile samples from nevirapine mercapturates following administration of nevirapine or 12-OH NVP to anaesthetised rats. Bile from anaesthetised male Wistar rats administered nevirapine (A; 50 mg/kg *i.v.* in DMSO) was mixed with bile from rats treated with 12-OH NVP (B; 50 mg/kg *i.v.* in DMSO) in a 7:93 ratio. Bile was analysed by LC-MS/MS using the TSQ Quantum Access tandem quadrupole mass spectrometer (Thermo Fisher Scientific, San Jose, CA, U.S.A.)

6.3.2 Investigation of inhibitors of nevirapine and 12-OH NVP bioactivation: 1-Aminobenzotriazole

A non-specific cytochrome P450 inhibitor, ABT, was used in an attempt to block the oxidative metabolism of nevirapine and 12-OH NVP in anaesthetised male Wistar rats. Reduction in M1 production suggests that bioactivation through the 12-OH NVP pathway has been inhibited. Pre-treatment with ABT resulted in a decrease in nevirapine (50 mg/kg *i.v.* in saline) metabolism to 12-OH NVP, M1 and M2 (Figure 6.4) in rats. In the same experiment using 12-OH NVP, M1 levels were also reduced with the pre-treatment of ABT; however this reduction was not significant (Figure 6.5 B).

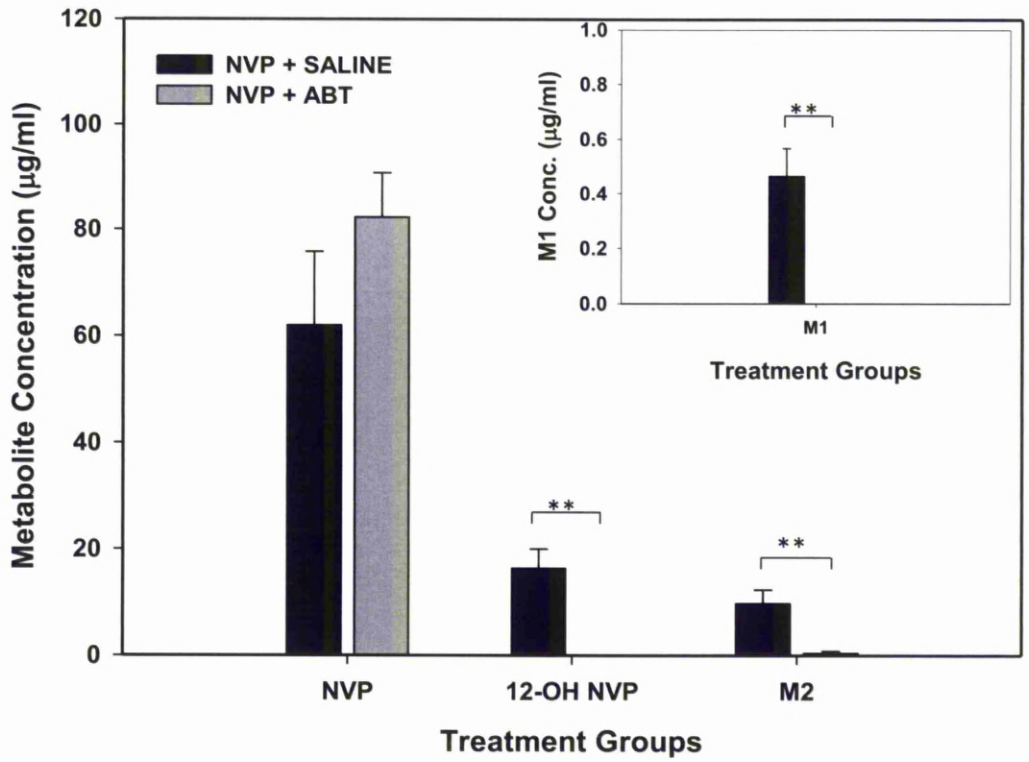

Figure 6.4: Effect of ABT pre-treatment on nevirapine metabolism in rats. Bile was collected from anaesthetized male Wistar rats which were pre-treated with ABT (50 mg/kg *i.p.*) 3 hours prior to administration of nevirapine (50 mg/kg *i.v* in DMSO). 1 hour biliary metabolites (nevirapine, 12-OH NVP and M2 are shown in the primary graph, M1 is shown in the insert) were quantified by LC-MS/MS. Data are presented as mean + standard deviation; n=3.

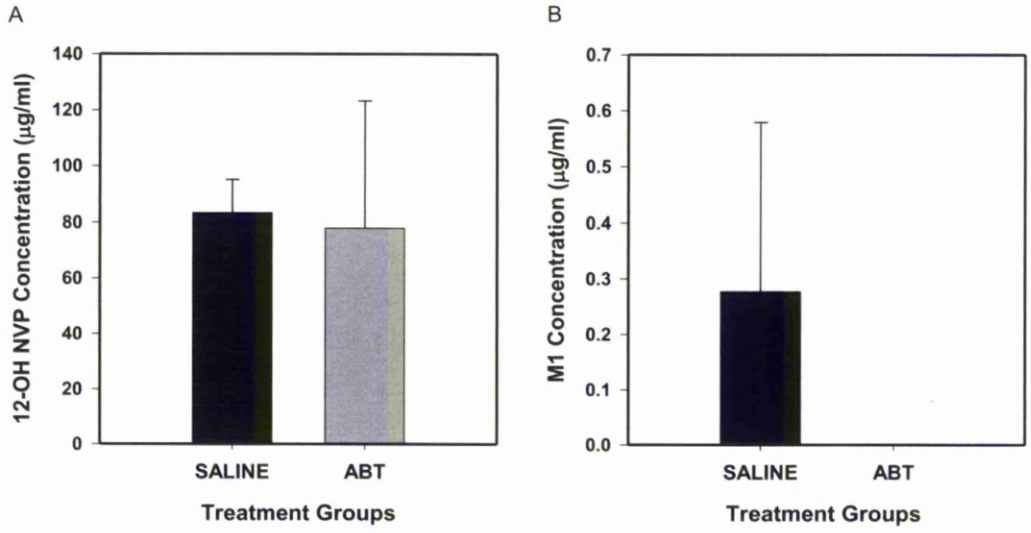

Figure 6.5: Effect of ABT pre-treatment on 12-OH NVP metabolism in rats. Bile was collected from anaesthetized male Wistar rats which were pre-treated with ABT (50 mg/kg *i.p.*) 3 hours prior to administration of 12-OH NVP (50 mg/kg *i.v* in DMSO). 1 hour biliary was analysed and 12-OH NVP (A) and M1 (B) were quantified by LC-MS/MS. Data are presented as mean + standard deviation; n=3.

6.3.3 Investigation of low molecular weight inhibitors of nevirapine and 12-OH NVP bioactivation: 2, 6-dichloro-4-nitrophenol

2, 6-dichloro-4-nitrophenol (DCNP) was used as a sulphotransferase inhibitor (Mulder and Scholtens, 1977) in anaesthetized male Wistar rats to investigate the role of sulphation in nevirapine bioactivation. Reduction in M1 production would suggest that bioactivation through the 12-OH NVP pathway was inhibited. Pre-treatment with DCNP (6.76 mg/kg *i.p*) did not significantly inhibit M1 formation when administered prior to nevirapine (50 mg/kg *i.v.* in saline) in rats (Figure 6.6). M1 levels were also unaffected when DCNP was administered prior to 12-OH NVP treatment (Figure 6.7 B).

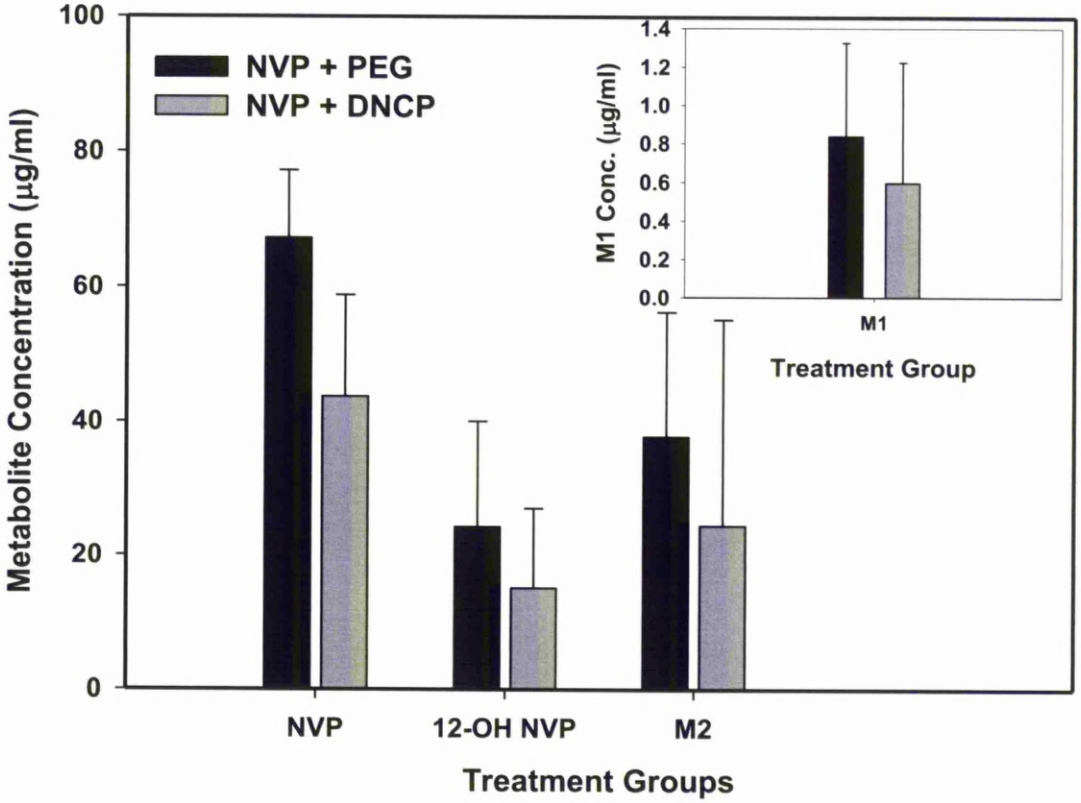

Figure 6.6: Effect of DCNP pre-treatment on nevirapine metabolism in rats. Bile was collected from anaesthetized male Wistar rats which were pre-treated with DCNP (6.76 mg/kg *i.p.*) 45 minutes prior to administration of nevirapine (50 mg/kg *i.v* in DMSO). 1 hour biliary metabolites (nevirapine, 12-OH NVP and M2 are shown in the primary graph, M1 is shown in the insert) were quantified by LC-MS/MS. Data are presented as mean + standard deviation; n=3.

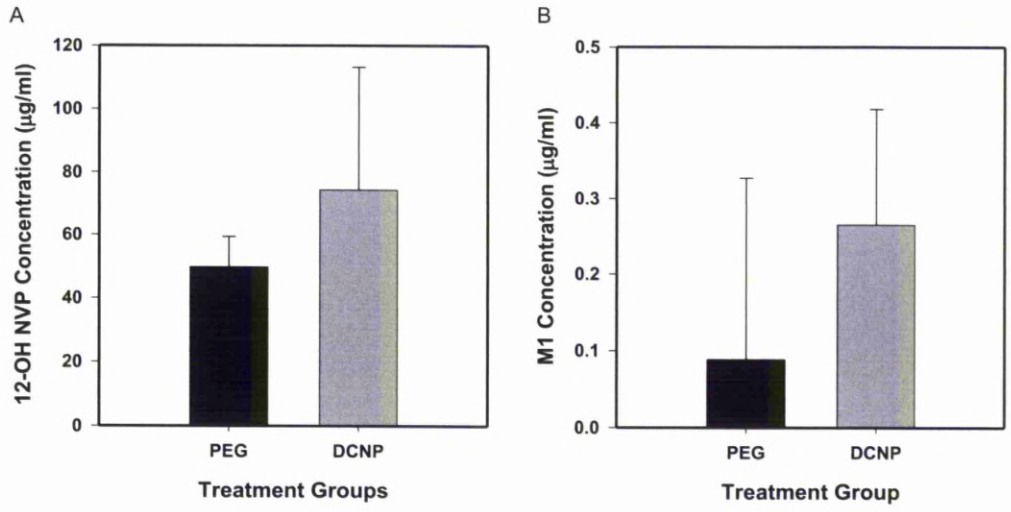

Figure 6.7: Effect of DCNP pre-treatment on 12-OH NVP metabolism in rats. Bile was collected from anaesthetized male Wistar rats which were pre-treated with DCNP (6.76 mg/kg *i.p.*) 45 minutes prior to administration of 12-OH NVP (50 mg/kg *i.v* in DMSO). 1 hour biliary was analysed and 12-OH NVP (A) and M1 (B) were quantified by LC-MS/MS. Data are presented as mean + standard deviation; n=3.

6.4 DISCUSSION

Metabolism of nevirapine through the 12-OH NVP metabolic pathway has been implicated in development of nevirapine-induced skin rash in rats (Chen *et al.*, 2008, Chen *et al.*, 2009). It has previously been shown that 12-OH NVP is a substrate for sulphotransferase in rats (Chen *et al.*, 2008), and it has been proposed that the sulphate ester dissociates to form a reactive quinone methide intermediate in the skin (Chen *et al.*, 2008, Uetrecht, 2006). However, some studies have provided evidence to contest this hypothesis. The investigations conducted in this chapter intended to characterise thioether metabolites of 12-OH NVP thereby providing evidence that it is a substrate for bioactivation.

Investigations conducted in our labs, have identified nevirapine mercapturates in human and rat urine following administration of nevirapine, using integrated mass spectrometry and NMR (nuclear magnetic resonance) techniques (Srivastava *et al.*, 2010). Male Wistar rats were used to conduct these metabolism studies initially as they are the strain with which we have the most experience, and given more time these studies would have been repeated in female Brown Norway rats. This work provided evidence of nevirapine bioactivation in humans and rats. Following administration of nevirapine to male Wistar rats, both mercapturates (M1 and M2) were identified in the bile. However, after 12-OH NVP treatment only a single peak could be seen at a retention time identical to M1. The identity of the mercapturate was confirmed by co-elution of the peak with M1 from the bile from the nevirapine dosed rat.

In the previous chapter, investigations were conducted to find a correlation between the onset of skin rash and mercapturate levels in the female Brown Norway rat. No such relationship was observed but the work may have provided a platform to develop future studies. In light of evidence to suggest that metabolism of nevirapine through the 12-OH NVP pathway is responsible for bioactivation, the use of enzyme inhibitors to block this pathway and inhibit bioactivation and toxicity was investigated.

ABT has been used previously to inhibit oxidative metabolism of nevirapine in rats (Chen *et al.*, 2008); authors found that urinary concentrations of all metabolites

decreased, except 12-OH NVP. They also correlated this finding with an increase in incidence of skin rash from 0% to 100%. More relevant was the fact that following a 50 mg/kg/day dosing regimen plus ABT, serum nevirapine concentrations increased to levels similar to those seen at a dose that was three times that (150 mg/kg/day), without ABT pre-treatment (Chen *et al.*, 2008). The work described here provides evidence that pre-treatment with ABT decreases 12-OH NVP and M1 formation and therefore does not support the finding described above; the discrepancy may be due to the use of β-glucuronidase treatment of samples prior to metabolite measurement in the work conducted by Chen, *et al* (2008). Using ABT pre-treatment in a chronic dosing experiment, similar to that described in Chapter 5, would likely provide evidence for the role of oxidative metabolism in development of nevirapine-induced skin rash in female Brown Norway rats.

A role of sulphation in bioactivation of nevirapine has been suggested; Antunes *et al.* (2009) demonstrated the reactivity of 12-sulphoxy nevirapine by formation of multiple DNA adducts in reactions with 12-mesyloxy nevirapine. 12-OH NVP was found to be a substrate for sulphotransferase in rats (Chen *et al.*, 2008), and it has been proposed that the sulphate ester dissociates to form a reactive quinone methide intermediate (Chen *et al.*, 2008, Uetrecht, 2006). However, preliminary studies indicate that the sulphate is not very reactive (Chen *et al.*, 2008). In the present study 2, 6-dichloro-4-nitrophenol (DCNP) was used to inhibit sulphation and observe the effect on bioactivation by measuring mercapturate levels in rats. Pre-treatment with DCNP (6.76 mg/kg *i.p*) did not significantly inhibit M1 formation when administered prior to nevirapine or 12-OH NVP (50 mg/kg *i.v.* in saline) in rats. This suggests sulphation is not a crucial step in nevirapine bioactivation. The quinone methide could also be generated by enzymic oxidation (Wen *et al.*, 2009) and nevirapine could also form one or more heteroarene epoxide metabolites in either of the pyridine rings

In summary, the evidence surrounding the role of 12-OH NVP in development of nevirapine-induced toxicity is controversial. Evidence has been provided in the work presented here that 12-OH NVP is a substrate for bioactivation. Although it is clear metabolism through this pathway is related to development of skin rash in female Brown Norway rats, the relationship to nevirapine toxicities in the clinic is not so

clearly understood. In order to rigorously test the plausibility of using nevirapine mercapturates as urinary markers of nevirapine bioactivation and susceptibility to nevirapine-induced toxicities, a large clinical study would have to be conducted in for the test to be validated. A number of risk factors associated with nevirapine-induced toxicities have been identified (Kesselring *et al.*, 2009, Sanne *et al.*, 2005, Stern *et al.*, 2003) and a major area of research has been into genetic polymorphisms that predispose patients to nevirapine-induced skin rash and/or hepatotoxicity (Zanger *et al.*, 2007, Penzak *et al.*, 2007, Rotger *et al.*, 2005, Haas *et al.*, 2006, Martin *et al.*, 2005b).

The G516T polymorphism in CYP2B6 has been shown to significantly increase plasma nevirapine levels in HIV-infected patients in Uganda (Penzak *et al.*, 2007). The toxicological result of increased plasma nevirapine concentrations is not clear. Preliminary studies conducted in Spain found that a positive correlation exists between plasma nevirapine levels and the risk of liver toxicity; patients with plasma nevirapine concentrations above 6 μg/ml are thought to have a 92% risk of developing liver toxicity (González De Requena *et al.*, 2002, González De Requena *et al.*, 2005). The 3435C→T polymorphism in MDR1 was significantly associated with reduced risk of nevirapine-induced hepatotoxicity (Haas *et al.*, 2006). P-glycoprotein is a multidrug efflux pump, encoded by MDR1; this membrane-associated protein is responsible for actively removing xenobiotics from the cell (Haas *et al.*, 2006). It is believed it is possible that altered P-glycoprotein activity in the intestine associated with the MDR1 variants alters disposition of nevirapine and/or its metabolites that affect intracellular concentrations of nevirapine and toxicity in liver (Saitoh and Spector, 2008).

CHAPTER 7

CONCLUDING DISCUSSION

CONTENTS

7.1 INTRODUCTION

The work presented here has shown that the development of an assessment framework that encompasses all aspects of drug disposition and metabolism, and their relationship with bioactivation and toxicity, would be a valuable tool in drug development. The construction of a decision tree that can be populated with quantitative data could be used in the assessment of NCEs and highlight properties that require optimisation. Outcomes of changes or interventions to a new therapy could then be measured quantitatively and mechanisms defined. A caveat to this framework would stipulate that the model systems employed would have to be carefully selected to best represent the clinical situation. This work has highlighted that a better understanding of current systems for detecting potential human hazard is required. Development of translational biomarker panels that can monitor hazard posed by a drug, from the pre-clinical stage and into the clinic, would improve safety and also be used to reduce attrition in clinical studies.

Idiosyncratic ADRs are rare but can be fatal. Dose, drug accumulation and/or the formation of reactive metabolites have been implicated in many idiosyncratic ADRs (Park *et al.*, 2011). The dose of a drug will have a major impact on the toxicological outcome of therapy; there are no examples of drugs that are dosed below 10 mg/day that cause idiosyncratic ADRs (Uetrecht, 2003). The work of James and Elizabeth Miller provided the first evidence of drug metabolism leading to the formation of reactive metabolites, subsequent covalent binding to protein and ultimately resulting in toxicity (Miller, 1994, Miller, 1970). This concept is now well established, and there is a wealth of evidence to suggest that bioactivation to a reactive metabolite is the initiating step in a number of direct and immune mediated toxicities (Park *et al.*, 2005, Kalgutkar and Soglia, 2005). However, it is widely accepted that presentation of idiosyncratic ADRs largely depends on the individual, in terms of genetics, disease state and environmental factors etc.

Drug-induced liver injury accounts for more than half the cases of acute liver failure in the US (Ostapowicz *et al.*, 2002). The liver is the most frequently affected organ by idiosyncratic ADRs, but skin, kidney and blood are also common targets. Additionally, idiosyncratic ADRs can present as generalised hypersensitivity or anaphylaxis (Park *et al.*, 2011). It stands to reason that research into systems that can

detect potential human hazard of NCEs has been of high priority, however, it remains that there are no accepted methods for the detection of hypersensitivity reactions in preclinincal or *in vitro* systems (Park *et al.*, 2005).

Identification of thioether adducts of drugs is one of two conventional methods for the detection of drug bioactivation. These investigations can be carried out in a range of systems including hepatic microsomes, fresh hepatocyte suspensions, preclinical animal models and in the clinic (Park *et al.*, 2011, Ma *et al.*, 2008). In *in vitro* systems trapping agents can be included in incubations to detect and provide structural information about the drug reactive metabolite(s). The identification of drug metabolite-GSH adducts in a preclinical setting is often treated as a hazard signal (Gan *et al.*, 2009, Reese *et al.*, 2010), however, it could be argued that detection of a GSH adduct is an indication of an effective detoxification system. Drug bioactivation can be detected through identification and/or quantification of thioether metabolites or some stable metabolites of drugs in human plasma and urine (Staack and Hopfgartner, 2007, Wen and Fitch, 2009, Srivastava *et al.*, 2010, Orhan and Vermeulen, 2011). Dihydrodiols are indicative of arene oxide intermediates (Forgue and Allen, 1982, Madden *et al.*, 1996, Maggs *et al.*, 2000) and urinary mercapturates of several drugs have been used as markers of reactive metabolite exposure (Siegers *et al.*, 1984, Veronese *et al.*, 1985, Dieckhaus *et al.*, 2002, Gopaul *et al.*, 2003). Still, it remains that detection of a thioether conjugate or stable metabolite represents successfully bio*in*activated reactive metabolite.

The work presented in this thesis investigates the relationship between chemical structure, bioactivation and toxicity, and examines the concept of thioether adduct detection and the information it can provide regarding the potential toxicity of a drug molecule. This was investigated in two ways;

(1) Using the model hepatotoxin, furosemide (FS), the pharmacological and toxicological consequence of substituting the toxicophore of FS (furan ring) and replacing it with a thiophene ring was investigated. Not only did this allow for the direct comparison of the two heterocycles, it also provided an opportunity to test the current systems used to identify a compounds propensity to be bioactivated and investigate the downstream toxicity effects *in vitro* and *in vivo*.

(2) Investigating whether mercapturates of NVP, a popular treatment for HIV in developing countries, could be used as markers of exposure to NVP reactive metabolites or whether they indicate successful bio*in*activation of reactive metabolites in an animal model. Idiosyncratic ADRs, associated with NVP treatment, have limited its clinical use.

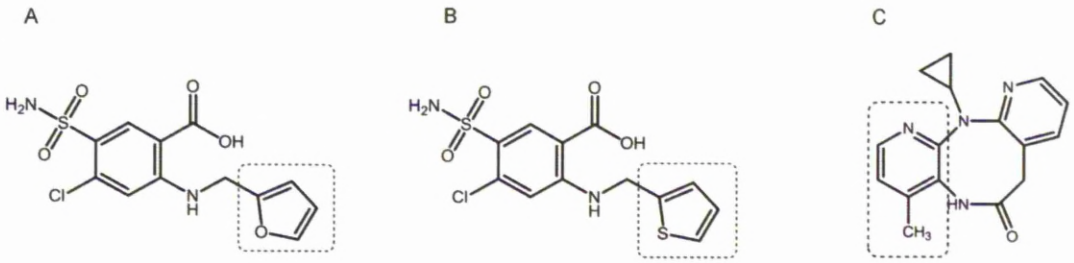

Figure 7.1: Structures of FS (A), TPA (B) and NVP (C). Toxicophores are shown by a box.

7.2 SPECIES DIFFERENCES CAUSE A DISCONNECT IN DRUG SAFETY EVALUATION

Genetic differences between species can influence how a drug is tolerated, as they can manifest as differences in drug metabolising enzymes and drug transporters. This is important when using various animal models to predict the potential hazard of a drug to cause toxicity in humans. The importance of ADME properties and their effects on drug toxicity have been discussed throughout this thesis; it is obvious, therefore, that changes in these properties caused by genetic differences between species will ultimately effect the toxic outcome of drug administration. Species differences in glutathione S transferases (GST) provide a good example of this.

There are seven classes of mammalian cytosolic GST subunits, alpha, mu, pi, sigma, theta, omega and zeta; these exist as largely as homodimers and the alpha and mu subunits can form heterodimers. Different species will have different compositions of GST isoenzymes, as well as different levels of expression and activity (Hayes and Pulford 1995). Species differences in susceptibility to drug induced toxicity, mediated by reactive electrophilic intermediates or indeed by activation by GSH

conjugation, can, for some drugs, be explained by differences in GSTs. Species differences in the toxicity of alfltoxin B1 exemplifies this.

Hepatotoxic effects of aflatoxin B1 (AFB1) have been observed in various experimental and farm animals. AFB1 has been shown to be metabolised to two isomers of AFB1-epoxide; the exo-8,9-epoxide is a highly reactive intermediate and the principle mediator of cellular injury. Both isomers of AFB1-epoxide can be conjugated with GSH by GST. It is thought that the formation of the exo-8,9-epoxide and its subsequent GSH conjugation are major determinants of the variation in species susceptibilities to AFB1. The rate of AFB1-GSH formation in the male Fischer rat was less then half of that of the ICR (imprinting control region) mouse and accordingly the rat was more susceptible to AFB1 induced toxicity compared to the mouse (Tulayakul *et al.*, 2005).

In the work presented here, FS was shown to induce hepatotoxicity in mice but not in rats. The reactive metabolite of FS covalently binds to murine hepatic protein; this does not occur in rats, instead the CRM is excreted in the form of a GSH conjugate, suggesting a possible safety mechanism exists in the rat to protect from FS-induced hepatotoxicity (Williams *et al.*, 2007). In order to identify whether this was as a result of species differences in GSTs, an experiment, using mouse microsomes incubated with rat S9 and FS, was set up to see if a FS-GSH metabolite could be identified. Unfortunately, no metabolites could be observed from any microsomal incubation with FS and therefore no results where generated. As well as the species differences in the balance of bioactivation and detoxification, the toxicokinetic studies conducted here also highlighted differences in the concentrations of FS in the liver of rats and mice. The liver exposure in the mouse was twice that in the rat, with free liver AUC values at 243 and 128 μg.h/ml respectively.

If the technology were available, pre-clinical safety evaluation packages would solely use human/humanised systems and models, and eliminate the need for translational research. One of the overall limitations of the work presented in this thesis is the lack of human safety and metabolic data generated with each of the compounds. This has resulted in an inability to relate the data generated in rodent models with a human system, and has limited the conclusions we can make in terms of the suitability of these models to predict human hazard. If human FS and TPA

metabolites would have been identified, the conclusions drawn, regarding GSH conjugation and safety, might have been strengthened (or further exemplified species differences). Similarly with NVP, using patient samples to investigate NVP mercapturates as markers of exposure to a NVP reactive metabolite and toxicity, would have been more useful than using an animal model. The animal model was limited in that it only displayed a skin reaction (not hepatotoxicity) and the rash appeared to be caused by scratching. However, to generate such data for humans, and make it statistically powerful, a huge patient population would have been required.

As well as selecting the most appropriate species to conduct preclinical safety investigations, the *system* should also be carefully considered. Microsomes have been the system of choice to study covalent binding of drugs, however recent studies suggest that human hepatocytes might provide a more clinically relevant, metabolically complete system (Bauman *et al.*, 2009; Nakayama *et al.*, 2009). 18 known hepatotoxic and non-hepatotoxic compounds were tested for levels of covalent binding in human liver microsomes (Obach *et al.*, 2008). Of the 18 compounds tested, 14 demonstrated some extent of covalent binding; of the 4 that did not, 2 were hepatotoxins and 2 were non-hepatotoxins (Obach *et al.*, 2008). Recently covalent binding studies conducted in human hepatocytes have provided a means of discriminating between hepatotoxins and non-hepatotoxins by incorporating factors such as daily dose and intrinsic clearance (Bauman *et al.*, 2009; Nakayama *et al.*, 2009).

7.3 BIOACTIVATION IN DRUG SAFETY EVALUATION

Bioactivation of drugs to reactive metabolites is highly implicated as a causal factor in the development of drug-induced toxicities. Although bioactivation is not solely responsible for all drug toxicities, often, metabolism data is considered alone rather than in context with other aspects of ADME. Additionally, there are few methods of assessing the toxic consequences of drug administration, and therefore minimising the potential of bioactivation is the current approach for hazard reduction in drug discovery and development.

In drug development, structural liabilities are often identified in NCEs and, depending on the involvement of the moiety in the pharmacology; these liabilities

can be modified or substituted in order to obtain a compound with reduced potential to be bioactivated, while retaining potency. The work conducted using FS and TPA aimed to assess the result of substituting a toxicophore (furan ring) for another structurally similar moiety, in terms of potency and hepatotoxicity in model systems. It was found that TPA was three times more potent towards the $Na^{+}/K^{+}/Cl^{-}$ cotransporter than FS, and TPA had an improved safety profile in mice. The data generated during this study and previous data, suggested that both FS and TPA are bioactivated to reactive metabolites, however the reactive metabolite(s) of TPA (possibly the *S*-oxide) could be bio*in*activated through GSH conjugation and therefore did not induce toxicity.

The data, generated from the studies with FS and TPA, show a link between GSH conjugate formation and an apparent lack of toxicity, and therefore question the paradigm of using GSH conjugates as markers of exposure to a reactive metabolite and ultimately risk of an ADR. Using mercapturates (breakdown products of GSH conjugates) as markers of reactive metabolite exposure has been demonstrated with several compounds, but as the data here suggests, each compound must be investigated on a case-by-case basis to assess whether a thioether metabolite implies risk or safety.

One of the limitations with the work presented here is that metabolite quantification was not completed. Having numerical values for each metabolite across all the systems tested might have strengthened the conclusions drawn with regards to the deferential metabolism between species, compounds and systems and the degree of toxicity observed. This applies not only to the thioether metabolites that were focused on in this study, but also to other metabolites that represent a non-toxic endpoint of metabolism (e.g. glucuronides).

In the case of NVP, the assumed toxicophore is incorporated into the structural scaffold of the molecule (Figure 7.1) and therefore would have been difficult to design out during the development process (toxicophore = pharmacophore). Additionally, human hazard was not observed in pre-clinical studies (Table 7.1). NVP mercapturates had been identified prior to the initiation of the work conducted in this thesis; one of the hypotheses laid out was that NVP mercapturates could act as

markers of exposure to NVP reactive metabolites in rats, and that exposure could be correlated to the development and severity of NVP-induced skin rash.

The animal model of NVP-induced skin rash, established by Uetrecht's group, was selected as the system to address the hypothesis. This model was successfully replicated in Chapter 5; the time course of skin rash development was consistent with previous reports (Shenton *et al.*, 2003). After 3 weeks NVP treatment (~80 mg/kg/day in food), NVP and its urinary metabolites were quantified by mass spectrometry on day 7, 14 and 21 of the study however, no time-dependent trend in any NVP metabolite was observed. It became clear that in order to use NVP mercapturates as markers of exposure to a reactive metabolite, more information regarding the bioactivation pathways of NVP was required. In Chapter 6 investigations were designed to elucidate a metabolic pathway of NVP that resulted in the formation of mercapturates, and, by implication, reactive metabolites.

12-OH NVP has been implicated as an important metabolite in the metabolic pathway responsible of NVP-induced skin rash (Chen *et al.*, 2008, Uetrecht, 2006). The work conducted in Chapter 6 has shown that 12-OH NVP is a substrate for bioactivation; 12-OH NVP was administered directly to male Wistar rats and the minor mercapturate (M1) only was identified in the bile. Following administration of NVP to male Wistar rats, both mercapturates (M1 and M2) were identified in the bile.

The role of sulphation in bioactivation of NVP has been suggested; Atunes *et al.* (2009) demonstrated the reactivity of 12-sulphoxy NVP by formation of multiple DNA adducts in reactions with 12-mesyloxy NVP. 12-OH NVP was found to be a substrate for sulphotransferase in rats (Chen *et al.*, 2008), and it has been proposed that the sulphate ester dissociates to a form reactive quinone methide intermediate (Chen *et al.*, 2008, Uetrecht, 2006). In Chapter 6, 2, 6-dichloro-4-nitrophenol (DCNP) was used to inhibit sulphation; no inhibition of M1 formation was observed when DCNP was administered prior to NVP or 12-OH NVP (50 mg/kg *i.v.* in saline) in rats. This suggests that sulphation may not be involved in NVP bioactivation; however further studies, involving metabolite identification, would have to be conducted in order to confirm this.

In contrast to previous studies, pre-treatment with ABT decreased 12-OH NVP and M1 formation (Chapter 6). Using ABT pre-treatment in a chronic dosing experiment, similar to that described in Chapter 5, would provide more information on the role of oxidative metabolism in development of NVP-induced skin rash in female Brown Norway rats. ABT has been used previously to inhibit oxidative metabolism of NVP in rats (Chen *et al.*, 2008); authors found that urinary concentrations of all metabolites decreased, except 12-OH NVP. This finding was correlated with an increase in incidence of skin rash from 0% to 100% in female Brown Norway rats. What was more significant in this work was the fact that following a 50 mg/kg/day dosing regimen plus ABT, serum NVP concentrations increased to levels similar to those seen at a dose that was three times that (150 mg/kg/day), without ABT pre-treatment (Chen *et al.*, 2008). Uetrecht and colleagues have shown that 12-OH NVP is unable to induce an immune response; lymph nodes were removed from Brown Norway rats treated with nevirapine or 12-OH NVP, and the response of lymphocytes to NVP and 12-OH NVP by cytokine production and proliferation was measured (Chen *et al.*, 2009). Lymphocytes from animals re-challenged with NVP or 12-OH NVP proliferated on treatment with NVP, but not with 12-OH NVP (Chen *et al.*, 2009). Similarly, NVP-reactive T cells have been observed in a patient with early-onset hepatitis in the absence of any cutaneous manifestations. The patient's T cells proliferated in vitro on exposure to NVP but not its stable metabolites (Drummond *et al.*, 2006). This data suggest that NVP concentrations could be a primary determinant of whether NVP-induced skin rash is observed. Further studies analysing NVP metabolism following administration of ABT, and other inhibitors, would to provide answers to whether parent compound or a CRM(s) is responsible for NVP-induced ADRs.

7.4 IMPORTANCE OF COVALENT BINDING IN RISK ASSESSMENT

One of the few methods for looking at the downstream effects of bioactivation is measuring covalent binding. Covalent binding is known to be an important step in the development of drug-induced toxicity for some drugs. However, in some cases, a drug can be toxic without any evidence of covalent binding and covalent binding can occur without toxicity. Nevertheless, assessment of the degree of covalent binding to protein is frequently used in *in vitro* and in animal studies, as an indicator of a drug's

potential to cause toxicity. How informative covalent binding data is, in terms of predicting human hazard, depends on the systems and species employed to carry out the studies. This is referred to in section 7.2, where an example is given of the difference in retrospective predictivity between human microsomes and human hepatocytes in identifying hepatotoxic drugs from non-hepatotoxic drugs (Bauman *et al.*, 2009; Nakayama *et al.*, 2009; Obach *et al.*, 2008).

In the work conducted using FS and TPA there was certainly a disconnect between different species and systems with regard to covalent binding and glutathione depletion. FS has previously been shown to undergo covalent binding to microsomal protein in NADPH supplemented mouse, rat and human micrcosomes and in freshly isolated rat and mouse hepatocytes (Williams *et al.*, 2007). However, *in vivo*, hepatic covalent binding was only significant in mice; no covalent binding was observed in rats (Williams *et al.*, 2007). Significant covalent binding of radiolabelled TPA to microsomal protein was observed in CD-1 mouse and Wistar rat liver microsomes in the presence of NADPH. In mouse hepatocytes, TPA was shown to bind covalently to protein in a dose-dependent mannor, however, in rat hepatocytes covalent binding was not significant (although there was a non-significant increase). *In vivo*, TPA did not covalently bind to hepatic protein in either rats or mice (Butler, 2006).

The data from the experiments in microsomes and hepatocytes provide evidence that TPA can undergo bioactivation and that the reactive products of the process are able to bind covalently to hepatic protein. It was concluded, based on the metabolism data generated for TPA, that the reason for the lack of hepatotoxicity it induced in mice, compared to FS, was because of its conjugation with GSH.

In cases where covalent binding is observed but toxicity is not, a critical protein might not have been targeted by the drug reactive metabolite. This concept is best illustrated by APAP and its structural isomer 3′-hydroxyacetanilide (*N*-acetyl-*m*-aminophenol, 3-acetamidophenol; AMAP), where AMAP at the same molar dose as APAP was found to covalently bind to cellular protein and yet did not result in toxicity. The RM of APAP and AMAP, a quinone imine (NAPQI) and a quinone respectively, are chemically similar species yet there is an intrinsic difference between them, which accounts for the difference in ability to cause hepatotoxicity (Rashed and Nelson, 1989). This introduced the concept of the critical protein

hypothesis, delineating certain proteins as critical targets in hepatotoxicity (Park *et al.*, 2005; Tirmenstein and Nelson, 1989). Supporting this, the reactive metabolite of APAP, NAPQI binds to a number of proteins. In mice, one of the major targets of NAPQI is urate oxidase, an enzyme lost during primate evolution. As a result it is thought unlikely that irreversible binding to urate oxidase represents a role in APAP-induced hepatotoxicity in mice, as both humans and mice develop centrilobular necrosis with similar per kg doses (Qiu *et al.*, 1998).

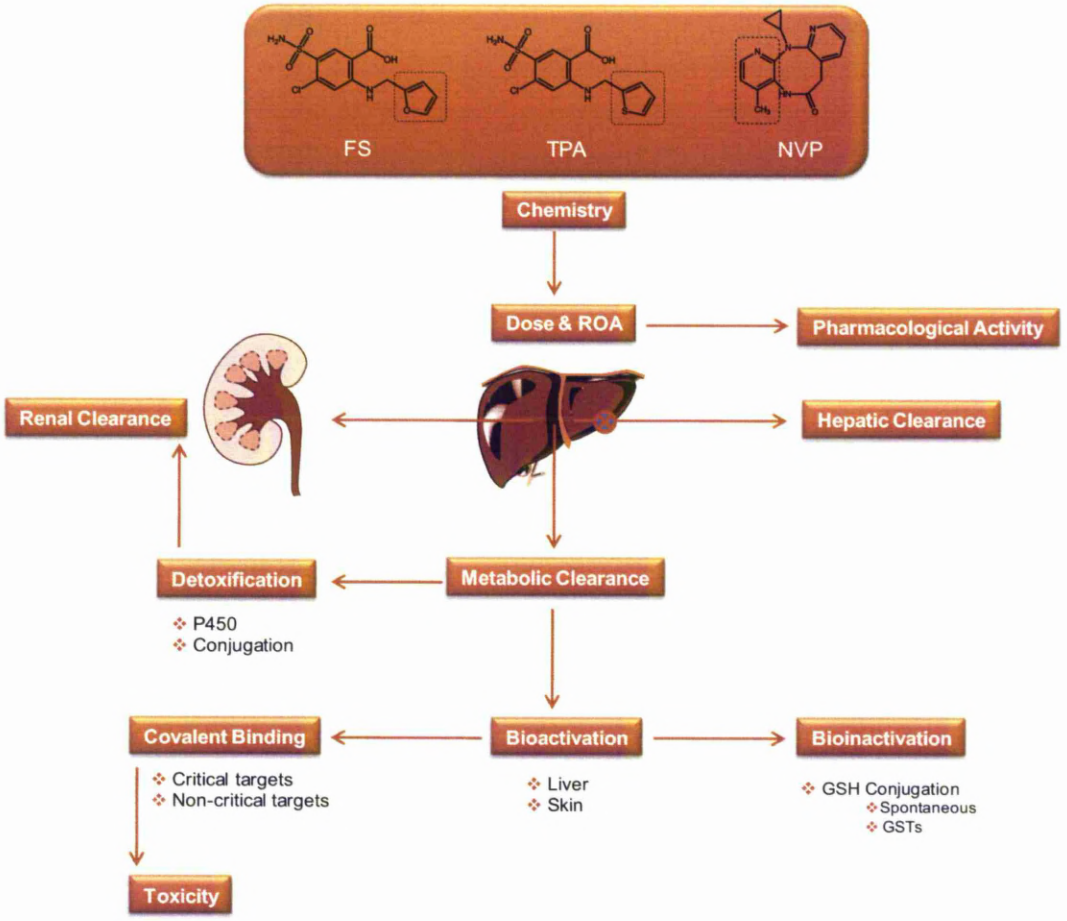

Figure 7.2: An example of a potential assessment framework that would encompass all aspects of drug disposition and metabolism, and their relationship with bioactivation and toxicity. The framework can be populated with quantitative data and could be used in the assessment of NCEs and highlight drug properties that require optimisation

7.5 CONSIDERATION FOR ADME IN RISK ASSESSMENT

Previous evidence has suggested that species differences in phase II metabolism is the reason for species differences observed in the hepatotoxicity of FS (Williams *et al.*, 2007). The reactive metabolite of FS covalently binds to murine hepatic protein; this does not occur in rats, instead the CRM is excreted in the form of a GSH conjugate, suggesting a possible safety mechanism exists in the rat to protect from FS-induced hepatotoxicity (Williams *et al.*, 2007). As well as the species differences in the balance of bioactivation and detoxification, the toxicokinetic studies conducted here also highlighted differences in the concentrations of FS in the liver. The liver exposure in the mouse was twice that in the rat, with free liver AUC values at 243 and 128 μg.h/ml respectively. It has previously been reported that with inhibition of biliary excretion of FS following a large dose of FS or pretreatment with sulfobromophthlein increases levels of covalent binding and development of liver necrosis in the mouse (Spitznagle *et al.*, 1977). It was concluded that development of FS-induced hepatotoxicity in the mouse is a function of the chemistry of FS and species characteristics in terms of detoxification and excretion, which give rise to higher levels of reactive metabolite in the liver.

7.6 CONCLUDING SUMMARY

In terms of predictivity of current methods to detect CRM and/or potential hazard of drugs to humans, there is a disconnect between *in vitro*, pre-clinical and human systems; a greater understanding of the relevance of surrogate models to the clinical situation is crucial if any real extrapolations are to be made. The work conducted in Chapter 2 and previous studies demonstrates this point, as outcomes (GSH depletion, covalent binding and toxicity) vary in the different systems (rodent hepatocytes, pre-clinical animal models and humans). Research and development of models that more accurately represent the human physiological situation is much needed. As well as a drugs propensity to form a CRM, other factors, such as dose, ROA, etc, must also be taken into consideration when determining the overall human hazard (Figure 7.2). In Chapter 3 it was shown that dose and ROA were crucial in determining whether hepatotoxicity was observed; this resonates with the wider context of drug development. One also has to evaluate the detoxicification of drug CRM; in Chapter

4 it was shown that, unlike FS, TPA forms several GSH adducts in rodent heptocytes; identification of GSH adducts in this setting suggests a successful detoxification system for CRMs of TPA highlighting the fact that identification of thioether conjugate should not be automatically assumed to be a hazard signal.

It is accepted that the probability that a drug will cause an ADR is a function of the chemistry of the drug and also a function of the biology of the individual. The chemistry of FS was a major determinant in the development of hepatotoxicity; the TPA compound had a one-atom difference from FS yet failed to induce hepatotoxicity at all. Although both compounds had the potential to undergo bioactivation to a reactive metabolite, the reactive metabolite of TPA was inferred to be a better substrate for GSH conjugation and therefore detoxification. The biology of the animals was shown to be an important factor, this was reflected in the species differences observed in their ability to detoxify the FS reactive metabolites and also in their ability to eliminate FS from the system. In the mouse, FS concentrations in the liver were twice that in the rat. The investigation conducted in this thesis regarding FS and TPA revealed that development of FS-induced hepatotoxicity in the mouse was a function of dose and ROA which was reflected in plasma and liver concentrations. The identification of drug metabolite-GSH adducts in a preclinical setting is often treated as a hazard signal (Gan *et al.*, 2009, Reese *et al.*, 2010), however, in the case presented here, it is clear that a GSH adduct is an indication of an effective detoxification system.

NVP has been shown to be bioactivated *in vitro* and *in vivo*, however, the biological implications of the products of bioactivation remain unknown. Despite evidence to suggest that the 12-OH NVP metabolic pathway gives rise to the reactive metabolite that causes skin rash in female Brown Norway rats, data in the same study point at parent compound plasma concentrations as a determinant of skin rash formation (Chen *et al.*, 2008). The immunological studies into NVP-induced hypersensitivity have also negated the 12-OH NVP metabolite as being responsible for toxicity (Chen *et al.*, 2009, Drummond *et al.*, 2006). Based on current hypotheses on the mechanisms of drug-induced hypersensitivity reactions, the reactive metabolite or parent compound could still be the responsible species (Uetrecht, 2008). The work described here presents more evidence that 12-OH NVP is a substrate for bioactivation, and, although NVP mercapturates were detected in the urine of

animals presenting rash, no mechanistic understanding could be drawn from the findings. Further investigations utilising enzyme inhibitors in the female Brown Norway rat model of NVP-induced skin rash would give more definitive answers to whether toxicity is induced by NVP itself or a reactive metabolite and whether pursuing NVP mercapturates as markers of exposure to bioactivation products is a valid endeavour.

The investigations using FS, TPA and NVP have highlighted a significant disconnect between *in vitro*, pre-clinical and human systems that make the extrapolation of data to the clinic difficult. A better understanding of current systems for detecting potential human hazard and development of improved animal models and surrogate end-points that more closely resemble the human physiological situation would improve the predictability of these systems. In a clinical setting, development of biomarker panels that can monitor hazard posed by a drug would improve safety and also be used to reduce attrition in clinical studies. Development of an assessment framework that encompasses all aspects of drug disposition and metabolism, and their relationship with bioactivation and toxicity, would be a valuable tool in drug development. Outcomes of changes or interventions to a new therapy could then be measured quantitatively and mechanisms defined.

		FS	TPA	NVP	NVP
	Toxic	Liver	Liver	Skin	Liver
	Mouse	✓	×	×	×
	Rat	×	×	✓	×
	Human	×	-	✓(idiosyncratic)	✓(idiosyncratic)
	Covalent binding				
in	Mouse	✓	×	-	×
vivo	Rat	×	×	×	✓
	Thioether conjugate				
	Mouse	×	-	-	-
	Rat	✓	✓	✓	✓
	Human	-	-	✓	✓
	Toxic				
	Mouse	✓	✓	-	-
	Rat	✓	✓	-	×
	Human	-	-	-	-
	Covalent binding				
in	Mouse	✓	✓	-	-
vitro	Rat	✓	✓/×*	-	✓
	Human	✓	-	-	×
	Thioether conjugate				
	Mouse	✓	✓	-	-
	Rat	✓	✓	✓	✓
	Human	-	-	✓	✓

Table 7.1: Summary of propensity of FS, TPA and NVP to cause toxicity, and systems in which evidence of bioactivation has been shown. Information has been compiled from data presented in this thesis, in Butler, 2006, PhD thesis, University of Liverpool and literature referenced throughout. * Covalent binding was observed in rat microsomes but not in rat hepatocytes.

BIBLIOGRAPHY

ABBOUD, G, Kaplowitz, N (2007). Drug-induced liver injury. *Drug Safety* **30**: 277-94.

ALBERTS, B, Johnson, A, Lewis, J, Raff, M, Roberts, K & Walter, P (2002). *Molecular Biology of the Cell.* Garland Science.

ALMOND, LM, Boffito, M, Hoggard, PG, Bonora, S, Raiteri, R, Reynolds, HE, *et al.* (2004). The relationship between nevirapine plasma concentrations and abnormal liver function tests. *AIDS Res Hum Retroviruses* **20**: 716-22.

AMACHER, DE (2002). A toxicologist's guide to biomarkers of hepatic response. *Human and Experimental Toxicology* **21**: 253-62.

AMORE, BM, Kalhorn, TF, Skiles, GL, Hunter, AP, Bennett, GD, Finnell, RH, *et al.* (1997). Characterization of carbamazepine metabolism in a mouse model of carbamazepine teratogenicity. *Drug Metab Disposition* **25**: 953-62.

ANDERSON, ME (1985). Determination of glutathione and glutathione disulfide in biological samples. *Methods Enzymol* **113**:548-55.

ANDREASEN, F, Christensen, CK, Jakobsen, FK & Mogensen, CE (1981). The use of HPLC to elucidate the metabolism and urinary excretion of furosemide and its metabolic products. *Acta Pharmacol Toxicol* **49**: 223-9.

ANDREASEN, F, Hansen, HE & Mikkelsen, E (1978). Pharmacokinetics of furosemide in anephric patients and in normal subjects. *Eur J Clin Pharmacol* **13**: 41-8.

ANTOINE, DJ, Mercer, AE, Williams, DP & Park, BK (2009a). Mechanism-based bioanalysis and biomarkers for hepatic chemical stress. *Xenobiotica* **39**: 565-77.

ANTOINE, DJ, Williams, DP, Jenkins, AK, Regan, SL, Sathish, JG, Kitteringham, NR, *et al.* (2009b). High-mobility group box-1 protein and keratin-18, circulating serum proteins informative of acetaminophen-induced necrosis and apoptosis in vivo. *Toxicological Sciences* **112**: 521-31.

ANTUNES, AMM, Godinho, ALA, Martins, IL, Justino, GC, Beland, FA & Marques, MM (2010). Amino acid adduct formation by the nevirapine metabolite, 12-Hydroxynevirapine- A Possible Factor in Nevirapine Toxicity. *Chem Res Toxicol* **23**: 888-99.

ASHAMISS, F, Wierzbicki, Z, Chrzanowska, A, Scibior, D, Pacholczyk, M, Kosieradzki, M, *et al.* (2004). Clinical significance of arginase after liver transplantation. *Ann Transplant* **9**: 58-60.

ATKINSON, A.J, J, Colburn, WA, DeGruttola, VG, DeMets, DL, Downing, GJ, Hoth, DF, *et al.* (2001). Biomarkers and surrogate endpoints: Preferred definitions and conceptual framework. *Clin Pharmacol Ther* **69**: 89-95.

BAER, BR, Rettie, AE & Henne, KR (2005). Bioactivation of 4-ipomeanol by CYP4B1: Adduct characterization and evidence for an enedial intermediate. *Chem Res Toxicol* **18**: 855-64.

BAKKER, J, Gommers, FJ, Nieuwenhuis, I & Wynberg, H (1979). Photoactivation of the nematicidal compound α-terthienyl from roots of marigolds (Tagetes species). A possible singlet oxygen role. *J Biol Chem* **254**: 1841-4.

BARNER, A, Myers, M (1998). Nevirapine and rashes [5]. *Lancet* **351**: 1133.

BARREIRO, P, Soriano, V, Casas, E, Estrada, V, Téllez, MJ, Hoetelmans, R, *et al.* (2000). Prevention of nevirapine-associated exanthema using slow dose escalation and/or corticosteroids. *AIDS* **14**: 2153-7.

BAUMAN, JN, Kelly, JM, Tripathy, S, Zhao, SX, Lam, WW, Kalgutkar, AS, *et al.* (2009). Can in vitro metabolism-dependent covalent binding data distinguish hepatotoxic from nonhepatotoxic drugs? An analysis using human hepatocytes and liver S-9 fraction. *Chem Res Toxicol* **22**: 332-40.

BEERMANN, B, Dalen, E & Lindstrom, B (1977). Elimination of furosemide in healthy subjects and in those with renal failure. *Clin Pharmacol Ther* **22**: 70-8.

BEERMANN, B, Dalen, E, Lindstrom, B & Rosen, A (1975). On the fate of furosemide in man. *Eur J Clin Pharmacol* **9**: 57-61.

BELGHAZI, M. Jean, P. Poli, S. Schmitter, J.-. Mansuy, D. & Dansette, P.M. (2001). Use of isotopes and LC-MS-ESI-TOF for mechanistic studies of tienilic acid metabolic activation. *Advances in Experimental Medicine and Biology,* **500**, 139-44.

BENET, LZ (1979). Pharmacokinetics/pharmacodynamics of furosemide in man: A review. *J Pharmacokinet Biopharm* **7**: 1-27.

BERGSTRÖM, MA, Ott, H, Carlsson, A, Neis, M, Zwadlo-Klarwasser, G, Jonsson, CAM, *et al.* (2007). A skin-like cytochrome P450 cocktail activates prohaptens to contact allergenic metabolites. *J Invest Dermatol* **127**: 1145-53.

BERMAN, JD (1997). Human leishmaniasis: Clinical, diagnostic, and chemotherapeutic developments in the last 10 years. *Clinical Infectious Diseases* **24**: 684-703.

BERSOFF-MATCHA, SJ, Miller, WC, Aberg, JA, Van der Horst, C, Hamrick H.J., J, Powderly, WG, *et al.* (2001). Sex differences in nevirapine rash. *Clinical Infectious Diseases* **32**: 124-9.

BIGBY, M, Jick, S, Jick, H & Arndt, K (1986). Drug-induced cutaneous reactions. A report from the Boston Collaborative Drug Surveillance Program on 15,438 consecutive inpatients, 1975 to 1982. *J Am Med Assoc* **256**: 3358-63.

BJÖRNSSON, E (2010). Review article: Drug-induced liver injury in clinical practice. *Alimentary Pharmacology and Therapeutics* **32**: 3-13.

BOELSTERLI, U (2003). *Mechanistic Toxicology: The Molecular Basis of How Chemicals Disrupt Biological Targets, Second Edition* Taylor & Francis.

BOLES PONTO, LL, Schoenwald, RD (1990). Furosemide (frusemide). A pharmacokinetic/pharmacodynamic review (Part I). *Clin Pharmacokinet* **18**: 381-408.

BOLZE, S, Bromet, N, Gay-Feutry, C, Massiere, F, Boulieu, R & Hulot, T (2002). Development of an in vitro screening model for the biosynthesis of acyl glucuronide metabolites and the assessment of their reactivity toward human serum albumin. *Drug metabolism and disposition: the biological fate of chemicals* 30: 404-13.

BONNET, F, Lawson-Ayayi, S, Thiébaut, R, Ramanampamonjy, R, Lacoste, D, Bernard, N, *et al.* (2002). A Cohort study of nevirapine tolerance in clinical practice: French Aquitaine Cohort, 1997-1999. *Clinical Infectious Diseases* **35**: 1231-7.

BOSKEN, JM, Lehner, AF, Hunsucker, A, Harkins, JD, Woods, WE, Karpiesiuk, W, *et al.* (2000). Direct MS-MS identification of isoxsuprine-glucuronide in post-administration equine urine. *Canadian Journal of Veterinary Research* 64: 107-16.

BOYD, MR, Wilson, BJ (1972). Isolation and characterization of 4-ipomeanol, a lung-toxic furanoterpenoid produced by sweet potatoes (ipomoea batatas). *J Agric Food Chem* **20**: 428-30.

BRANCH, RA, Roberts, CJC, Homeida, M & Levine, D (1977). Determinants of response to frusemide in normal subjects. *Br J Clin Pharmacol* **4**: 121-7.

BRENDLE, JJ, Outlaw, A, Kumar, A, Boykin, DW, Patrick, DA, Tidwell, RR, *et al.* (2002). Antileishmanial activities of several classes of aromatic dications. *Antimicrob Agents Chemother* **46**: 797-807.

BROGDEN, RN, Carmine, AA & Heel, RC (1982). Ranitidine: A review of its pharmacology and therapeutic use in peptic ulcer disease and other allied diseases. *Drugs* **24**: 267-303.

BRÖNNIMANN, M, Yawalkar, N (2005). Histopathology of drug-induced exanthems: Is there a role in diagnosis of drug allergy? *Current Opinion in Allergy and Clinical Immunology* **5**: 317-21.

BRÜCK, S, Witte, S, Brust, J, Schuster, D, Mosthaf, E, Procaccianti, M, *et al.* (2008). Hepatotoxicity in patients prescribed efavirenz or Nevirapine. *Eur J Med Res* **13**: 343-8.

BU, H-, Zhao, P, Dalvie, DK & Pool, WF (2007). Identification of primary and sequential bioactivation pathways of carbamazepine in human liver microsomes using liquid chromatography/tandem mass spectrometry. *Rapid Communications in Mass Spectrometry* **21**: 3317-22.

BUCKO, AD, Hunt, BJ, Kidd, SL & Hom, R (2002). Randomized, double-blind, multicenter comparison of oral cefditoren 200 or 400 mg BID with either cefuroxime 250 mg BID or cefadroxil 500 mg BID for the treatment of uncomplicated skin and skin-structure infections. *Clin Ther* **24**: 1134-47, DOI: 10.1016/S0149-2918(02)80024-8.

BUDNITZ, DS, Pollock, DA, Mendelsohn, AB, Weidenbach, KN, McDonald, AK & Annest, JL (2005). Emergency department visits for outpatient adverse drug events: Demonstration for a national surveillance system. *Ann Emerg Med* **45**: 197-206.

BURG, M, Stoner, L, Cardinal, J & Green, N (1973). Furosemide effect on isolated perfused tubules. *Am J Physiol* **225**: 119-24.

BUTLER, P.J. (2006). Toxicophores: Groups and metabolic routes associated with hepatotoxicity. Thesis (PhD). University of Liverpool.

BUYSE, S, Vibert, E, Sebagh, M, Antonini, T, Ichai, P, Castaing, D, *et al.* (2006). Liver transplantation for fulminant hepatitis related to nevirapine therapy. *Liver Transplantation* **12**: 1880-2.

CANTAROW, A, Wirts, CW (1948). Excretion of bilirubin and bromsulfalein in bile. *Am J Physiol* **154**: 211-9.

CARAKOSTAS, MC, Gossett, KA, Church, GE & Cleghorn, BL (1986). Evaluating toxin-induced hepatic injury in rats by laboratory results and discriminant analysis. *Vet Pathol* **23**: 264-9.

CARR, A, Cooper, DA (2000). Adverse effects of antiretroviral therapy. *Lancet* **356**: 1423-30.

CHAN, GFQ, Towers, GHN & Mitchell, JC (1975). Ultraviolet-mediated antibiotic activity of thiophene compounds of Tagetes. *Phytochemistry* **14**: 2295-6.

CHASSANDE, O, Frelin, C, Farahifar, D, Jean, T & Lazdunski, M (1988). The Na+/K+/Cl- cotransport in C6 glioma cells. Properties and role in volume regulation. *European Journal of Biochemistry* **171**: 425-33.

CHEN, J, Mannargudi, BM, Xu, L & Uetrecht, J (2008). Demonstration of the metabolic pathway responsible for nevirapine-induced skin rash. *Chem Res Toxicol* **21**: 1862-70.

CHEN, Q, Ngui, JS, Doss, GA, Wang, RW, Cai, X, DiNinno, FP, *et al.* (2002). Cytochrome P450 3A4-mediated bioactivation of raloxifene: Irreversible enzyme inhibition and thiol adduct formation. *Chem Res Toxicol* 15: 907-14.

CHEN, W, Caceres-Cortes, J, Zhang, H, Zhang, D, Humphreys, WG & Gan, J (2011). Bioactivation of substituted thiophenes including α-chlorothiophene- containing compounds in human liver microsomes. *Chem Res Toxicol* 24: 663-9.

CHEN, X, Tharmanathan, T, Mannargudi, B, Gou, H & Uetrecht, JP (2009). A study of the specificity of lymphocytes in nevirapine-induced skin rash. *J Pharmacol Exp Ther* **331**: 836-41.

CHU, KM, Boulle, AM, Ford, N, Goemaere, E, Asselman, V & Van Cutsem, G (2010). Nevirapine-associated early hepatotoxicity: Incidence, risk factors, and associated mortality in a primary care art programme in South Africa. *PLoS ONE* **5**.

CHUNG, W-, Park, C-, Roh, H-, Lee, W- & Cha, Y- (2000). Oxidation of ranitidine by isozymes of flavin-containing monooxygenase and cytochrome P450. *Jpn J Pharmacol* **84**: 213-20.

CICCACCI, C, Borgiani, P, Ceffa, S, Sirianni, E, Marazzi, MC, Doro Altan, AM, *et al.* (2010). Nevirapine-induced hepatotoxicity and pharmacogenetics: A retrospective study in a population from Mozambique. *Pharmacogenomics* **11**: 23-31.

CLAES, P, Wintzen, M, Allard, S, Simons, P, De Coninck, A & Lacor, P (2004). Nevirapine-induced toxic epidermal necrolysis and toxic hepatitis treated successfully with a combination of intravenous immunoglobulins and N-acetylcysteine. *Eur J Intern Med* **15**: 255-8, DOI: 10.1016/j.ejim.2004.04.007.

CLARKE, JB, Maggs, JL, Kitteringham, NR & Park, BK (1990). Immunogenicity of amodiaquine in the rat. *Int Arch Allergy Appl Immunol* **91**: 335-42.

COLBURN, WA, Keefe, DL (2003). Biomarkers in drug discovery and development: From target identification through drug marketing. *J Clin Pharmacol* **43**: 329-41.

COPPLE, IM, Goldring, CE, Kitteringham, NR & Park, BK (2008). The Nrf2-Keap1 defence pathway: Role in protection against drug-induced toxicity. *Toxicology* **246**: 24-33.

CUMMINGS, J, Ranson, M, Lacasse, E, Ganganagari, JR, St-Jean, M, Jayson, G, *et al.* (2006). Method validation and preliminary qualification of pharmacodynamic biomarkers employed to evaluate the clinical efficacy of an antisense compound (AEG35156) targeted to the X-linked inhibitor of apoptosis protein XIAP. *Br J Cancer* **95**: 42-8.

DAHLIN, DC, Miwa, GT, Lu, AYH & Nelson, SD (1984). N-acetyl-p-benzoquinone imine: A cytochrome P-450-mediated oxidation product of acetaminophen. *ISOTOPENPRAXIS* **20**: 1327-31.

DALVIE, DK, Kalgutkar, AS, Khojasteh-Bakht, SC, Obach, RS & O'Donnell, JP (2002). Biotransformation reactions of five-membered aromatic heterocyclic rings. *Chem Res Toxicol* **15**: 269-99.

DANSETTE, PM, Amar, C, Valadon, P, Pons, C, Beaune, PH & Mansuy, D (1991). Hydroxylation and formation of electrophilic metabolites of tienilic acid and its isomer by human liver microsomes: Catalysis by a cytochrome P450 IIC different from that responsible for mephenytoin hydroxylation. *Biochem Pharmacol* **41**: 553-60, DOI: 10.1016/0006-2952(91)90627-H.

DANSETTE, PM, Bertho, G & Mansuy, D (2005). First evidence that cytochrome P450 may catalyze both S-oxidation and epoxidation of thiophene derivatives. *Biochem Biophys Res Commun* **338**: 450-5.

DANSETTE, PM, Do Cao Thang, El Amri, H & Mansuy, D (1992). Evidence for thiophene-S-oxide as a primary reactive metabolite of thiophene in vivo: Formation of a dihydrothiophene sulfoxide mercapturic acid. *Biochem Biophys Res Commun* **186**: 1624-30.

DAVIS, DC, Potter, WZ, Jollow, DJ & Mitchell, JR (1974). Species differences in hepatic glutathione depletion, covalent binding and hepatic necrosis after acetaminophen. *Life Sci* **14**: 2099-109.

DE CLERCQ, E (2004). Non-nucleoside reverse transcriptase inhibitors (NNRTIs): past, present, and future. *Chemistry & biodiversity* **1**: 44-64.

DE MAAT, MMR, Matho't, RAA, Veldkamp, AI, Huitema, ADR, Mulder, JW, Meenhorst, PL, *et al.* (2002). Hepatotoxicity following nevirapine-containing regimens in HIV-1-infected individuals. *Pharmacological Research* **46**: 295-300.

DE MAAT, MMR, Ter Heine, R, Van Gorp, ECM, Mulder, JW, Mairuhu, ATA & Beijnen, JH (2003). Case series of acute hepatitis in a non-selected group of HIV-infected patients on nevirapine-containing antiretroviral treatment. *AIDS* **17**: 2209-14.

DELEVE, LD, Kaplowitz, N (1991). Glutathione metabolism and its role in hepatotoxicity. *Pharmacology and Therapeutics* **52**: 287-305.

DI MARCO, A, D'Antoni, M, Attaccalite, S, Carotenuto, P & Laufer, R (2005). Determination of drug glucuronidation and UDP-glucuronosyltransferase selectivity using a 96-well radiometric assay. *Drug Metab Disposition* 33: 812-9.

DIECKHAUS, CM, Fernández-Metzler, CL, King, R, Krolikowski, PH & Baillie, TA (2005). Negative ion tandem mass spectrometry for the detection of glutathione conjugates. *Chem Res Toxicol* 18: 630-8.

DIECKHAUS, CM, Thompson, CD, Roller, SG & Macdonald, TL (2002). Mechanisms of idiosyncratic drug reactions: The case of felbamate. *Chem Biol Interact* **142**: 99-117.

DISSE, B, Reichl, R, Speck, G, Traunecker, W, Rominger, KL & Hammer, R (1993). Ba 679 BR, a novel long-acting anticholinergic bronchodilator. *Life Sci* **52**: 537-44.

DISSE, B, Speck, GA, Rominger, KL, Witek Jr., TJ & Hammer, R (1999). Tiotropium (spiriva(TM)): Mechanistical considerations and clinical profile in obstructive lung disease. *Life Sci* **64**: 457-64.

DONATO, MT, Castell, JV & Gomez-Lechon, MJ (1994). Cytochrome P450 activities in pure and co-cultured rat hepatocytes. Effects of model inducers. *In Vitro Cellular and Developmental Biology - Animal* **30 A**: 825-32.

DONNELLY, PJ, Walker, RM & Racz, WJ (1994). Inhibition of mitochondrial respiration in vivo is an early event in acetaminophen-induced hepatotoxicity. *Arch Toxicol* **68**: 110-8.

DRUMMOND, NS, Vilar, FJ, Naisbitt, DJ, Hanson, A, Woods, A, Park, BK, *et al.* (2006). Drug-specific T cells in an HIV-positive patient with nevirapine-induced hepatitis. *Antivir Ther (Lond)* **11**: 393-5.

DU, L, Neis, MM, Ladd, PA, Lanza, DL, Yost, GS & Keeney, DS (2006). Effects of the differentiated keratinocyte phenotype on expression levels of CYP1-4 family genes in human skin cells. *Toxicol Appl Pharmacol* **213**: 135-44.

DUTCHER, JS, Boyd, MR (1979). Species and strain differences in target organ alkylation and toxicity by 4-ipomeanol. Predictive value of covalent binding in studies of target organ toxicities by reactive metabolites. *Biochem Pharmacol* **28**: 3367-72.

EDWARDS, IR, Aronson, JK (2000). Adverse drug reactions: Definitions, diagnosis, and management. *Lancet* **356**: 1255-9.

ELAUT, G, Papeleu, P, Vinken, M, Henkens, T, Snykers, S, Vanhaecke, T, *et al.* (2006). Hepatocytes in suspension. *Methods Mol Biol* **320**: 255-63.

EL-HASSAN, H, Anwar, K, Macanas-Pirard, P, Crabtree, M, Chow, SC, Johnson, VL, *et al.* (2003). Involvement of mitochondria in acetaminophen-induced apoptosis and hepatic injury: Roles of cytochrome c, Bax, Bid, and caspases. *Toxicol Appl Pharmacol* **191**: 118-29.

ERICKSON, DA, Mather, G, Trager, WF, Levy, RH & Keirns, JJ (1999). Characterization of the in vitro biotransformation of the HIV-1 reverse transcriptase inhibitor nevirapine by human hepatic cytochromes P-450. *Drug Metab Disposition* **27**: 1488-95.

EVANS, DC, Baillie, TA (2005). Minimizing the potential for metabolic activation as an integral part of drug design. *Current Opinion in Drug Discovery and Development* **8**: 44-50.

EVANS, DC, Watt, AP, Nicoll-Griffith, DA & Baillie, TA (2004). Drug-Protein Adducts: An Industry Perspective on Minimizing the Potential for Drug Bioactivation in Drug Discovery and Development. *Chem Res Toxicol* **17**: 3-16.

FAGOT, J-, Mockenhaupt, M, Bouwes-Bavinck, J-, Naldi, L, Viboud, C & Roujeau, J- (2001). Nevirapine and the risk of Stevens-Johnson syndrome or toxic epidermal necrolysis. *AIDS* **15**: 1843-8.

FESTJENS, N, Vanden Berghe, T & Vandenabeele, P (2006). Necrosis, a well-orchestrated form of cell demise: Signalling cascades, important mediators and concomitant immune response. *Biochimica et Biophysica Acta (BBA) - Bioenergetics* **1757**: 1371-87, DOI: 10.1016/j.bbabio.2006.06.014.

FISHER, MB, Campanale, K, Ackermann, BL, Vandenbranden, M & Wrighton, SA (2000). In vitro glucuronidation using human liver microsomes and the pore- forming peptide alamethicin. *Drug Metab Disposition* 28: 560-6.

FOOD AND DRUG ADMINISTRATION. (2008). Guidance for industry: Safety testing of drug metabolites.

FORGUE, ST, Allen, JR (1982). Identification of an arene oxide metabolite of 2,2',5,5'-tetrachlorobiphenyl by gas chromatography-mass spectroscopy. *Chem Biol Interact* **40**: 233-45, DOI: 10.1016/0009-2797(82)90103-X.

FOSTER, GR, Goldin, RD & Oliveira, DBG (1989). Serum F protein: A new sensitive and specific test of hepatocellular damage. *Clinica Chimica Acta* **184**: 85-92.

GAFFNEY, GR, Betzer, LK, Mow, MT & Williamson, HE (1979). Decrease in hepatic blood flow during furosemide-induced diuresis. *Arch Int Pharmacodyn Ther* **239**: 155-60.

GAN, J, Ruan, Q, He, B, Zhu, M, Shyu, WC & Humphreys, WG (2009). In vitro screening of 50 highly prescribed drugs for thiol adduct formation - Comparison of potential for drug-induced toxicity and extent of adduct formation. *Chem Res Toxicol* **22**: 690-8.

GATANAGA, H, Yazaki, H, Tanuma, J, Honda, M, Genka, I, Teruya, K, *et al.* (2007). HLA-Cw8 primarily associated with hypersensitivity to nevirapine [7]. *AIDS* **21**: 264-5.

GEBHARDT, R, Hengstler, JG, Müller, D, Glöckner, R, Buenning, P, Laube, B, *et al.* (2003). New hepatocyte in vitro systems for drug metabolism: Metabolic capacity and recommendations for application in basic research and drug development, standard operation procedures. *Drug Metab Rev* 35: 145-213.

GIBSON, G, Skett, P (2001). *Introduction to Drug Metabolism.* Nelson Thornes Publishers.

GILL, HJ, Tingle, MD & Park, BK (1995). N-Hydroxylation of dapsone by multiple enzymes of cytochrome P450: Implications for inhibition of haemotoxicity. *Br J Clin Pharmacol* **40**: 531-8.

GIULIANO, C, Fiore, F, Di Marco, A, Velazquez, JP, Bishop, A, Bonelli, F, *et al.* (2005). Preclinical pharmacokinetics and metabolism of a potent non-nucleoside inhibitor of the hepatitis C virus NS5B polymerase. *Xenobiotica* **35**: 1035-54.

GONZÁLEZ DE REQUENA, D, Jiménez-Nácher, I & Soriano, V (2005). Changes in nevirapine plasma concentrations over time and its relationship with liver enzyme elevations. *AIDS Res Hum Retroviruses* **21**: 555-9.

GONZÁLEZ DE REQUENA, D, Núñez, M, Jiménez-Nácher, I & Soriano, V (2002). Liver toxicity caused by nevirapine. *AIDS* **16**: 290-1.

GOPAUL, S, Farrell, K & Abbott, F (2003). Effects of age and polytherapy, risk factors of valproic acid (VPA) hepatotoxicity, on the excretion of thiol conjugates of (E)-2,4-diene VPA in people with epilepsy taking VPA. *Epilepsia* **44**: 322-8.

GORDI, T, Lepist, E- (2004). Artemisinin derivatives: Toxic for laboratory animals, safe for humans? *Toxicol Lett* **147**: 99-107.

GRAHAM, EE, Walsh, RJ, Hirst, CM, Maggs, JL, Martin, S, Wild, MJ, *et al.* (2008). Identification of the thiophene ring of methapyrilene as a novel bioactivation-dependent hepatic toxicophore. *J Pharmacol Exp Ther* **326**: 657-71.

GREENBERGER, PA (2006). 8. Drug allergy. *J Allergy Clin Immunol* **117**: S464,S470+S488.

GREENBLATT, DJ, Duhme, DW, Allen, MD & Koch Weser, J (1977). Clinical toxicity of furosemide in hospitalized patients. A report from the Boston Collaborative Drug Surveillance Program. *Am Heart J* **94**: 6-13.

GUENGERICH, FP (2006). Cytochrome P450s and other enzymes in drug metabolism and toxicity. *AAPS Journal* **8**: E105-11.

HAAS, DW, Bartlett, JA, Andersen, JW, Sanne, I, Wilkinson, GR, Hinkle, J, *et al.* (2006). Pharmacogenetics of nevirapine-associated hepatotoxicity: An adult AIDS Clinical Trials Group Collaboration. *Clinical Infectious Diseases* **43**: 783-6.

HAGEN, SE, Domagala, J, Gajda, C, Lovdahl, M, Tait, BD, Wise, E, *et al.* (2001). 4-Hydroxy-5,6-dihydropyrones as inhibitors of HIV protease: The effect of heterocyclic substituents at C-6 on antiviral potency and pharmacokinetic parameters. *J Med Chem* **44**: 2319-32.

HALL, DB, MacGregor, TR (2007). Case-control exploration of relationships between early rash or liver toxicity and plasma concentrations of nevirapine and primary metabolites. *HIV Clinical Trials* **8**: 391-9.

HAMMARLUND, MM, Paalzow, LK & Odlind, B (1984). Pharmacokinetics of furosemide in man after intravenous and oral administration. Application of moment analysis. *Eur J Clin Pharmacol* **26**: 197-207.

HAMMARLUND, MM, Paalzow, LK (1982). Dose-dependent pharmacokinetics of furosemide in the rat. *Biopharmaceutics and Drug Disposition* **3**: 345-59.

HAMMARLUND-UDENAES, M, Benet, LZ (1989). Furosemide pharmacokinetics and pharmacodynamics in health and disease - An update. *J Pharmacokinet Biopharm* **17**: 1-46.

HARI, Y, Urwyler, A, Hurni, M, Yawalkar, N, Dahinden, C, Wendland, T, *et al.* (1999). Distinct serum cytokine levels in drug- and measles-induced exanthema. *Int Arch Allergy Immunol* **120**: 225-9.

HART, D, Ward, M & Lifschitz, D (1987). Suprofen-related nephrotoxicity. A distinct clinical syndrome. *Ann Intern Med* **106**: 235-8.

HAVLIR, D, Cheeseman, SH, McLaughlin, M, Murphy, R, Erice, A, Spector, SA, *et al.* (1995). High-dose nevirapine: Safety, pharmacokinetics, and antiviral effect in patients with human immunodeficiency virus infection. *J Infect Dis* **171**: 537-45.

HAYES, JD, Pulford, DJ (1995). The glutathione S-transferase supergene family: Regulation of GST and the contribution of the isoenzymes to cancer chemoprotection and drug resistance. *Crit Rev Biochem Mol Biol* **30**: 445-600.

HIGAKI, J, Harada, H, Tonda, K & Hirata, M (1989). Chemical stucture and toxicity of diuretics in isolated hepatocytes. *Pharmacology and Toxicology* **65**: 21-4.

HOLT, MP, Ju, C (2006). Mechanisms of drug-induced liver injury. *AAPS Journal* **8**: E48-54.

HOMBERG, JC, Andre, C & Abuaf, N (1984). A new anti-liver-kidney microsome antibody (anti-LKM2) in tienilic acid-induced hepatitis. *Clin Exp Immunol* **55**: 561-70.

HORI, O, Brett, J, Slattery, T, Cao, R, Zhang, J, Jing Xian Chen, *et al.* (1995). The receptor for advanced glycation end products (RAGE) is a cellular binding site for amphoterin. Mediation of neurite outgrowth and co-expression of RAGE and amphoterin in the developing nervous system. *J Biol Chem* **270**: 25752-61.

HOWIE, D, Adriaenssens, PI & Prescott, LF (1977). Paracetamol metabolism following overdosage: application of high performance liquid chromatography. *J Pharm Pharmacol* **29**: 235-7.

HU, Y, Yang, S, Shilliday, FB, Heyde, BR, Mandrell, KM, Robins, RH, *et al.* (2010). Novel metabolic bioactivation mechanism for a series of anti-inflammatory agents (2,5-diaminothiophene derivatives) mediated by cytochrome P450 enzymes. *Drug Metab Disposition* 38: 1522-31.

HUDSON, JB, Graham, EA, Miki, N, Towers, GHN, Hudson, LL, Rossi, R, *et al.* (1989). Photoactive antiviral and cytotoxic activities of synthetic thiophenes and their acetylenic derivative. *Chemosphere* **19**: 1329-43.

HUTZLER, JM, Balogh, LM, Zientek, M, Kumar, V & Tracy, TS (2009). Mechanism-based inactivation of cytochrome P450 2C9 by tienilic acid and (±)-suprofen: A comparison of kinetics and probe substrate selection. *Drug Metab Disposition* **37**: 59-65.

INUI, S, Yamamoto, M, Nakae, H & Asada, S (1982). Dose dependent of loop diuretics, furosemide and piretanide in the rat. *Yakugaku Zasshi* **102**: 1053-60.

IYENGAR, S, Arnason, JT, Philogene, BJR, Morand, P, Werstiuk, NH & Timmins, G (1987). Toxicokinetics of the phototoxic allelochemical α-terthienyl in three herbivorous lepidoptera. *Pestic Biochem Physiol* **29**: 1-9.

JAESCHKE, H, Cover, C & Bajt, ML (2006). Role of caspases in acetaminophen-induced liver injury. *Life Sci* **78**: 1670-6.

JOLLOW, DJ, Mitchell, JR & Potter, WZ (1973). Acetaminophen induced hepatic necrosis. II. Role of covalent binding in vivo. *J Pharmacol Exp Ther* **187**: 195-202.

JOSHI, EM, Heasley, BH, Chordia, MD & Macdonald, TL (2004). In Vitro Metabolism of 2-Acetylbenzothiophene: Relevance to Zileuton Hepatotoxicity. *Chem Res Toxicol* **17**: 137-43.

KALGUTKAR, AS, Gardner, I, Obach, RS, Shaffer, CL, Callegari, E, Henne, KR, *et al.* (2005). A comprehensive listing of bioactivation pathways of organic functional groups. *Curr Drug Metab* **6**: 161-225.

KALGUTKAR, AS AND SOGLIA, JR (2005). Minimising the potential for metabolic activation in drug discovery. *Expert opinion on drug metabolism & toxicology* **1**: 91-142.

KAPLOWITZ, N (2004). Drug-Induced Liver Injury. *Clinical Infectious Diseases* **38**: S44-8.

KAPLOWITZ, N (2005). Idiosyncratic drug hepatotoxicity. *Nature Reviews Drug Discovery* **4**: 489-99.

KAPPELHOFF, BS, Van Leth, F, Robinson, PA, MacGregor, TR, Baraldi, E, Montella, F, *et al.* (2005). Are adverse events of nevirapine and efavirenz related to plasma concentrations? *Antivir Ther (Lond)* **10**: 489-98.

KENNY, JR, Maggs, JL, Meng, X, Sinnott, D, Clarke, SE, Park, BK, *et al.* (2004). Syntheses and characterization of the acyl glucuronide and hydroxy metabolites of diclofenac. *J Med Chem* 47: 2816-25.

KERDPIN, O, Knights, KM, Elliot, DJ & Miners, JO (2008). In vitro characterisation of human renal and hepatic frusemide glucuronidation and identification of the UDP-glucuronosyltransferase enzymes involved in this pathway. *Biochem Pharmacol* **76**: 249-57.

KERREMANS, ALM, Tan, Y, Van Ginneken, CAM & Gribnau, FWJ (1982). Specimen handling and high-performance liquid chromatographic determination of furosemide. *J Chromatogr* **229**: 129-39.

KESSELRING, AM, Wit, FW, Sabin, CA, Lundgren, JD, Gill, MJ, Gatell, JM, *et al.* (2009). Risk factors for treatment-limiting toxicities in patients starting nevirapine-containing antiretroviral therapy. *AIDS* **23**: 1689-99.

KHAYROLLAH, AA, Al-Tamer, YY, Taka, M & Skursky, L (1982). Serum alcohol dehydrogenase activity in liver diseases. *Ann Clin Biochem* **19**: 35-42.

KHOJASTEH-BAKHT, SC, Chen, W, Koenigs, LL, Peter, RM & Nelson, SD (1999). Metabolism of (R)-(+)-pulegone and (R)-(+)-menthofuran by human liver cytochrome P-450s: Evidence for formation of a furan epoxide. *Drug Metab Disposition* **27**: 574-80.

KILFORD, PJ, Stringer, R, Sohal, B, Houston, JB & Galetin, A (2009). Prediction of drug clearance by glucuronidation from in vitro data: Use of combined cytochrome P450 and UDP-glucuronosyltransferase cofactors in alamethicin-activated human liver microsomes. *Drug Metab Disposition* 37: 82-9.

KIM, EJ, Han, KS & Lee, MG (2000). Gastrointestinal first-pass effect of furosemide in rats. *J Pharm Pharmacol* **52**: 1337-43.

KIM, SH, Choi, YM & Lee, MG (1993). Pharmacokinetics and pharmacodynamics of furosemide in protein-calorie malnutrition. *J Pharmacokinet Biopharm* **21**: 1-17.

KISHIDA, T, Muto, S-, Hayashi, M, Tsutsui, M, Tanaka, S, Murakami, M, *et al.* (2008). Strain differences in hepatic cytochrome P450 1A and 3A expression between Sprague-Dawley and Wistar rats. *J Toxicol Sci* **33**: 447-57.

KITTERINGHAM, NR, Powell, H, Clement, YN, Dodd, CC, Tettey, JN, Pirmohamed, M, *et al.* (2000). Hepatocellular response to chemical stress in CD-1 mice: Induction of early genes and γ-glutamylcysteine synthetase. *Hepatology* **32**: 321-33.

KOBAYASHI, T, Sugihara, J & Harigaya, S (1987). Mechanism of metabolic cleavage of a furan ring. *Drug Metab Disposition* **15**: 877-81.

KOENIGS, LL, Peter, RM, Hunter, AP, Haining, RL, Rettie, AE, Friedberg, T, *et al.* (1999). Electrospray ionization mass spectrometric analysis of intact cytochrome P450: Identification of tienilic acid adducts to P450 2C9. *Biochemistry (N Y)* **38**: 2312-9.

KOLA, I, Landis, J (2004). Can the pharmaceutical industry reduce attrition rates? *Nature Reviews Drug Discovery* **3**: 711-5.

KONO, H, Rock, KL (2008). How dying cells alert the immune system to danger. *Nature Reviews Immunology* **8**: 279-89.

KOSTRUBSKY, SE, Sinclair, JF, Strom, SC, Wood, S, Urda, E, Stolz, DB, *et al.* (2005). Phenobarbital and phenytoin increased acetaminophen hepatotoxicity due to inhibition of UDP-glucuronosyltransferases in cultured human hepatocytes. *Toxicological Sciences* **87**: 146-55.

KOSTRUBSKY, SE, Strom, SC, Kalgutkar, AS, Kulkarni, S, Atherton, J, Mireles, R, *et al.* (2006). Inhibition of hepatobiliary transport as a predictive method for clinical hepatotoxicity of nefazodone. *Toxicological Sciences* **90**: 451-9.

KRAMER, JA, Sagartz, JE & Morris, DL (2007). The application of discovery toxicology and pathology towards the design of safer pharmaceutical lead candidates. *Nature Reviews Drug Discovery* **6**: 636-49.

KUBITZA, D, Becka, M, Voith, B, Zuehlsdorf, M & Wensing, G (2005a). Safety, pharmacodynamics, and pharmacokinetics of single doses of BAY 59-7939, an oral, direct factor Xa inhibitor. *Clin Pharmacol Ther* **78**: 412-21.

KUBITZA, D, Becka, M, Wensing, G, Voith, B & Zuehlsdorf, M (2005b). Safety, pharmacodynamics, and pharmacokinetics of BAY 59-7939 - An oral, direct Factor Xa inhibitor - After multiple dosing in healthy male subjects. *Eur J Clin Pharmacol* **61**: 873-80.

LAI, Y (2009). Identification of interspecies difference in hepatobiliary transporters to improve extrapolation of human biliary secretion. *Expert Opinion on Drug Metabolism and Toxicology* 5: 1175-87.

LAGARRIGA, J, Buenrrostro, C, Rodríguez, P & Castañeda, J (1977). Hepatinecrosis caused by furosemide. Special lesions of various species? *Revista de Gastroenterologia de Mexico* **42**: 117-25.

LAMMERT, C, Einarsson, S, Saha, C, Niklasson, A, Bjornsson, E & Chalasani, N (2008). Relationship between daily dose of oral medications and idiosyncratic drug-induced liver injury: Search for signals. *Hepatology* **47**: 2003-9.

LAPOINTE, RW, Roy, AF, Turgeon, PL, Lewis, RT & al, e (1994). Comparison of single-dose cefotetan and multidose cefoxitin as intravenous prophylaxis in elective, open biliary, tract surgery: A multicentre, double-blind, randomized study. *Canadian Journal of Surgery* **37**: 313,313-8.

LARREY, D (2002). Epidemiology and individual susceptibility to adverse drug reactions affecting the liver. *Semin Liver Dis* **22**: 145-55.

LASSER, KE, Allen, PD, Woolhandler, SJ, Himmelstein, DU, Wolfe, SM & Bor, DH (2002). Timing of new black box warnings and withdrawals for prescription medications. *J Am Med Assoc* **287**: 2215-20.

LAZAROU, J, Pomeranz, BH & Corey, PN (1998). Incidence of adverse drug reactions in hospitalized patients: A meta- analysis of prospective studies. *J Am Med Assoc* **279**: 1200-5.

LE FUR, JM, Labaune, JP (1985). Metabolic pathway by cleavage of a furan ring. *Xenobiotica* **15**: 567-77.

LEBLANC, A, Sleno, L (2011). Atrazine metabolite screening in human microsomes: Detection of novel reactive metabolites and glutathione adducts by LC-MS. *Chem Res Toxicol* 24: 329-39.

LECOEUR, S, André, C & Beaune, PH (1996). Tienilic acid-induced autoimmune hepatitis: Anti-liver and -kidney microsomal type 2 autoantibodies recognize a three-site conformational epitope on cytochrome P4502C9. *Mol Pharmacol* **50**: 326-33.

LECOEUR, S, Bonierbale, E, Challine, D, Gautier, J-, Valadon, P, Dansette, PM, *et al.* (1994). Specificity of in vitro covalent binding of tienilic acid metabolites to human liver microsomes in relationship to the type of hepatotoxicity: Comparison with two directly hepatotoxic drugs. *Chem Res Toxicol* **7**: 434-42.

LEE, MG, Chiou, WL (1983). Evaluation of potential causes for the incomplete bioavailability of furosemide: Gastric first-pass metabolism. *J Pharmacokinet Biopharm* **11**: 623-40.

LEE, WM (2003). Acute liver failure in the United States. *Semin Liver Dis* **23**: 217-26.

LERCH, M, Pichler, WJ (2004). The immunological and clinical spectrum of delayed drug-induced exanthems. *Current Opinion in Allergy and Clinical Immunology* **4**: 411-9.

LESAR, TS (2006). Medication prescribing errors involving the route of administration. *Hosp Pharm* **41**: 1053-66.

LI, Q-, Peggins, JO, Lin, AJ, Masonic, KJ, Trotman, KM & Brewer, TG (1998). Pharmacology and toxicology of artelinic acid: Preclinical investigations on pharmacokinetics, metabolism, protein and red blood cell binding, and acute and anorectic toxicities. *Trans R Soc Trop Med Hyg* **92**: 332-40.

LIEBLER, DC, Guengerich, FP (2005). Elucidating mechanisms of drug-induced toxicity. *Nature Reviews Drug Discovery* **4**: 410-20.

LIKANONSAKUL, S, Rattanatham, T, Feangvad, S, Uttayamakul, S, Prasithsirikul, W, Tunthanathip, P, *et al.* (2009). HLA-Cw*04 allele associated with nevirapine-induced rash in HIV-infected Thai patients. *AIDS Res Ther* **6**: 22, 10.1186/1742-6405-6-22.

LINDBLOM, P, Rafter, I, Copley, C, Andersson, U, Hedberg, JJ, Berg, A-, *et al.* (2007). Isoforms of alanine aminotransferases in human tissues and serum-Differential tissue expression using novel antibodies. *Arch Biochem Biophys* **466**: 66-77.

LITTERA, R, Carcassi, C, Masala, A, Piano, P, Serra, P, Ortu, F, *et al.* (2006). HLA-dependent hypersensitivity to nevirapine in Sardinian HIV patients. *AIDS* **20**: 1621-6.

LIU, ,Zhang-Xu, Kaplowitz, ,Neil. (2007). Immune Mechanisms in Drug-Induced Hepatotoxicity. : 363-74, 10.1007/978-1-59745-518-3_29.

LIU, ZC, Uetrecht, JP (2000). Metabolism of ticlopidine by activated neutrophils: Implications for ticlopidine-induced agranulocytosis. *Drug Metab Disposition* **28**: 726-30.

LÓPEZ-GARCIA, MP, Dansette, PM & Mansuy, D (1994). Thiophene derivatives as new mechanism-based inhibitors of cytochromes P-450: Inactivation of yeast-expressed human liver cytochrome P-450 2C9 by tienilic acid. *Biochemistry (N Y)* **33**: 166-75.

LOWRY, OH, Rosebrough, NJ, Farr, AL & Randall, RJ (1951). Protein Measurement with the Folin Phenol Reagent. *J Biol Chem* **193**: 265-75.

MA, L, Wen, B, Ruan, Q & Zhu, M (2008). Rapid screening of glutathione-trapped reactive metabolites by linear ion trap mass spectrometry with isotope pattern-dependent scanning and postacquisition data mining. *Chem Res Toxicol* **21**: 1477-83.

MACHINIST, JM, Mayer, MD, Shet, MS, Ferrero, JL & Rodrigues, AD (1995). Identification of the human liver cytochrome P450 enzymes involved in the metabolism of zileuton (ABT-077) and its N-dehydroxylated metabolite, Abbott- 66193. *Drug Metab Disposition* 23: 1163-74.

MADDEN, S, Maggs, JL & Park, BK (1996). Bioactivation of carbamazepine in the rat in vivo: Evidence for the formation of reactive arene oxide(s). *Drug Metab Disposition* **24**: 469-79.

MAGGS, JL, Naisbitt, DJ, Tettey, JNA, Pirmohamed, M & Park, BK (2000). Metabolism of lamotrigine to a reactive arene oxide intermediate. *Chem Res Toxicol* **13**: 1075-81.

MAGGS, JL, Williams, D, Pirmohamed, M & Park, BK (1995). The metabolic formation of reactive intermediates from clozapine, a drug associated with agranulocytosis in man. *J Pharmacol Exp Ther* 275: 1463-75.

MALLAL, S, Phillips, E, Carosi, G, Molina, J-, Workman, C, Tomažič, J, *et al.* (2008). HLA-B*5701 screening for hypersensitivity to abacavir. *N Engl J Med* **358**: 568-79.

MALMSTRÖM, J, Jonsson, M, Cotgreave, IA, Hammarström, L, Sjödin, M & Engman, L (2001). The antioxidant profile of 2,3-dihydrobenzo[b]furan-5-ol and its 1-thio, 1-seleno, and 1-telluro analogues. *J Am Chem Soc* **123**: 3434-40.

MANIAR, JK, Shah, SR, Verma, R, Kamath, R, Gupte, P & Maniar, A (2006). Nevirapine-induced fulminant hepatitis. *Journal of Association of Physicians of India* **54**: 957-8.

MANSUY, D, Valadon, P, Erdelmeier, I, Lopez-Garcia, P, Amar, C, Girault, J-, *et al.* (1991). Thiophene S-oxides as new reactive metabolites: Formation by cytochrome P450 department oxidation and reaction with nucleophiles. *J Am Chem Soc* **113**: 7825-6.

MANSUY, D (1991). Formation of reactive metabolites and appearance of antiorganelle antibodies in man. *Adv Exp Med Biol* **283**: 133-7.

MARTIN, AM, Nolan, D, James, I, Cameron, P, Keller, J, Moore, C, *et al.* (2005). Predisposition to nevirapine hypersensitivity associated with HLA-DRB1*0101 and abrogated by low CD4 T-cell counts. *AIDS* **19**: 97-9.

MARTÍNEZ, E, Blanco, JL, Arnaiz, JA, Pérez-Cuevas, JB, Mocroft, A, Cruceta, A, *et al.* (2001). Hepatotoxicity in HIV-1-infected patients receiving nevirapine-containing antiretroviral therapy. *AIDS* **15**: 1261-8.

MASUBUCHI, N, Makino, C & Murayama, N (2007). Prediction of in vivo potential for metabolic activation of drugs into chemically reactive intermediate: Correlation of in vitro and in vivo generation of reactive intermediates and in vitro glutathione conjugate formation in rats and humans. *Chem Res Toxicol* **20**: 455-64.

MASUBUCHI, Y, Saito, H & Horie, T (1998). Structural requirements for the hepatotoxicity of nonsteroidal anti- inflammatory drugs in isolated rat hepatocytes. *J Pharmacol Exp Ther* **287**: 208-13.

MATSUURA, H, Saxena, G, Farmer, SW, Hancock, REW & Towers, GHN (1996). Antibacterial and antifungal polyine compounds from Glehnia littoralis ssp. leiocarpa. *Planta Med* **62**: 256-9.

MATZINGER, P (2002). The danger model: A renewed sense of self. *Science* **296**: 301-5.

MCCLANAHAN, RH, Thomassen, D, Slattery, JT & Nelson, SD (1989). Metabolic activation of (R)-(+)-pulegone to a reactive enonal that covalently binds to mouse liver proteins. *Chem Res Toxicol* **2**: 349-55.

MEDOWER, C, Wen, L & Johnson, WW (2008). Cytochrome P450 oxidation of the thiophene-containing anticancer drug 3-[(quinolin-4-ylmethyl)-amino]-thiophene-2-carboxylic acid (4-trifluoromethoxy- phenyl)-amide to an electrophilic intermediate. *Chem Res Toxicol* **21**: 1570-7.

MEIER, Y, Cavallaro, M, Roos, M, Pauli-Magnus, C, Folkers, G, Meier, PJ, *et al.* (2005). Incidence of drug-i'nduced liver injury in medical inpatients. *Eur J Clin Pharmacol* **61**: 135-43.

MEISTER, A (1983). Transport and metabolism of glutathione and γ-glutamyl amino acids. *Biochem Soc Trans* **11**: 793-4.

MEISTER, A, Anderson, ME (1983). Glutathione. *Annu Rev Biochem* **Vol. 52**: 711-60.

MENESES-LORENTE, G, Guest, PC, Lawrence, J, Muniappa, N, Knowles, MR, Skynner, HA, *et al.* (2004). A proteomic investigation of drug-induced steatosis in rat liver. *Chem Res Toxicol* **17**: 605-12.

MEOTTI, FC, Silva, DO, Dos Santos, ARS, Zeni, G, Rocha, JBT & Nogueira, CW (2003). Thiophenes and furans derivatives: A new class of potential pharmacological agents. *Environ Toxicol Pharmacol* **15**: 37-44.

MERK, HF (2009). Drug skin metabolites and allergic drug reactions. *Current Opinion in Allergy and Clinical Immunology* **9**: 311-5.

MERK, HF, Baron, JM, Neis, MM, Obrigkeit, DH & Karlberg, A- (2007). Skin: Major target organ of allergic reactions to small molecular weight compounds. *Toxicol Appl Pharmacol* **224**: 313-7.

MICHELE, TM, Pinheiro, S & Iyasu, S (2010). The safety of tiotropium - The FDA's conclusions. *N Engl J Med* **363**: 1097-9.

MILLER, JA (1970). Carcinogenesis by chemicals: an overview--G. H. A. Clowes memorial lecture. *Cancer Res* **30**: 559-76.

MILLER, JA (1994). Brief history of chemical carcinogenesis. *Cancer Lett* **83**: 9-14.

MILLER, TJ, Knapton, A, Adeyemo, O, Noory, L, Weaver, J & Hanig, JP (2008). Cytochrome c: A non-invasive biomarker of drug-induced liver injury. *Journal of Applied Toxicology* **28**: 815-28.

MITCHELL, JR, Jollow, DJ & Potter, WZ (1973a). Acetaminophen induced hepatic necrosis. I. Role of drug metabolism. *J Pharmacol Exp Ther* **187**: 185-94.

MITCHELL, JR, Jollow, DJ & Potter, WZ (1973b). Acetaminophen induced hepatic necrosis. IV. Protective role of glutathione. *J Pharmacol Exp Ther* **187**: 211-7.

MITCHELL, JR, Nelson, WL & Potter, WZ (1976). Metabolic activation of furosemide to a chemically reactive hepatotoxic metabolite. *J Pharmacol Exp Ther* **199**: 41-52.

MITCHELL, JR, Potter, WZ, Hinson, JA & Jollow, DJ (1974). Hepatic necrosis caused by furosemide. *Nature* **251**: 508-10.

MIZUMA, T, Benet, LZ & Lin, ET (1998). High-performance liquid chromatographic determination and identification of acyl migration and photodegradation products of furosemide 1-O-acyl glucuronide. *Journal of Chromatography B: Biomedical Applications* 718: 153-62.

MOORTHY, B, Madyastha, P & Madyastha, KM (1989). Hepatotoxicity of pulegone in rats: Its effects on microsomal enzymes, in vivo. *Toxicology* **55**: 327-37, DOI: 10.1016/0300-483X(89)90022-X.

MORI, Y, Kuroda, N & Sakai, Y (1985). Species differences in the metabolism of suprofen in laboratory animals and man. *Drug Metab Disposition* **13**: 239-45.

MORI, Y, Kuroda, N, Sakai, Y, Yokoya, F, Toyoshi, K & Baba, S (1985b). Species differences in the metabolism of suprofen in laboratory animals and man. *Drug metabolism and disposition: the biological fate of chemicals* 13: 239-45.

MORI, Y, Sakai, Y & Kuroda, N (1984). Further structural analysis of urinary metabolites of suprofen in the rat. *Drug Metab Disposition* **12**: 767-71.

MULDER, GJ, Scholtens, E (1977). Phenol sulphotransferase and uridine diphosphate glucuronyltransferase from rat liver in vivo and in vitro. 2,6-dichloro-4-nitrophenol as selective inhibitor of sulphation. *Biochem J* **165**: 553-9.

MURATA, J, Abe, R & Shimizu, H (2008). Increased soluble Fas ligand levels in patients with Stevens-Johnson syndrome and toxic epidermal necrolysis preceding skin detachment. *J Allergy Clin Immunol* **122**: 992-1000.

NAKAYAMA, S, Atsumi, R, Takakusa, H, Kobayashi, Y, Kurihara, A, Nagai, Y, *et al.* (2009). A zone classification system for risk assessment of idiosyncratic drug toxicity using daily dose and covalent binding. *Drug Metab Disposition* **37**: 1970-7.

NASSIF, A, Bensussan, A, Boumsell, L, Deniaud, A, Moslehi, H, Wolkenstein, P, *et al.* (2004). Toxic epidermal necrolysis: Effector cells are drug-specific cytotoxic T cells. *J Allergy Clin Immunol* **114**: 1209-15.

NIGEN, S, Knowles, SR & Shear, NH (2003). Drug eruptions: approaching the diagnosis of drug-induced skin diseases. *J Drugs Dermatol* **2**: 278-99.

NISHIYA, T, Mori, K, Hattori, C, Kai, K, Kataoka, H, Masubuchi, N, *et al.* (2008). The crucial protective role of glutathione against tienilic acid hepatotoxicity in rats. *Toxicol Appl Pharmacol* 232: 280-91.

NOCE, R, Paredes, BE, Pichler, WJ & Krahenbuhl, S (2000). Acute generalized exanthematic pustulosis (AGEP) in a patient treated with furosemide. *The American journal of the medical sciences* **320**: 331-3.

OBACH, RS, Kalgutkar, AS, Soglia, JR & Zhao, SX (2008). Can in vitro metabolism-dependent covalent binding data in liver microsomes distinguish hepatotoxic from nonhepatotoxic drugs? An analysis of 18 drugs with consideration of intrinsic clearance and daily dose. *Chem Res Toxicol* **21**: 1814-22.

O'CALLAGHAN, CH, Sykes, RB & Ryan, DM (1976). Cefuroxime - a new cephalosporin antibiotic. *J Antibiot* **29**: 29-37.

OCHOA, AB, Wolfe, M, Lewis, P & Lenihan, DJ (1998). Ticlopidine-induced neutropenia mimicking sepsis early after intracoronary stent placement. *Clin Cardiol* **21**: 304-7.

O'DONNELL, JP, Dalvie, DK, Kalgutkar, AS & Obach, RS (2003). Mechanism-based inactivation of human recombinant P450 2C9 by the nonsteroidal anti-inflammatory drug suprofen. *Drug Metab Disposition* **31**: 1369-77.

OHUCHI, T, Tada, K & Akamatsu, K (1995). Endogenous ET-1 contributes to liver injury induced by galactosamine and endotoxin in isolated perfused rat liver. *American Journal of Physiology - Gastrointestinal and Liver Physiology* **268**: G997-G1003.

OLSON, H, Betton, G, Robinson, D, Thomas, K, Monro, A, Kolaja, G, *et al.* (2000). Concordance of the toxicity of pharmaceuticals in humans and in animals. *Regulatory Toxicology and Pharmacology* **32**: 56-67.

OMURA, T, Sato, R. (1964). The Carbon Monoxide-Binding Pigment of Liver Microsomes. Ii. Solubilization, Purification, and Properties. - *J Biol Chem.1964 Jul;239:2379-85.*

ORHAN, H, Vermeulen, NPE (2011). Conventional and novel approaches in generating and characterization of reactive intermediates from drugs/drug candidates. *Curr Drug Metab* **12**: 383-94.

OSTAPOWICZ, G, Fontana, RJ, Schiødt, FV, Larson, A, Davern, TJ, Han, SHB, *et al.* (2002). Results of a prospective study of acute liver failure at 17 tertiary care centers in the United States. *Ann Intern Med* **137**: 947-54.

OWEN, A, Pirmohamed, M, Khoo, SH & Back, DJ (2006). Pharmacogenetics of HIV therapy. *Pharmacogenetics and Genomics* **16**: 693-703.

OWENS, CWI, Belcher, RV (1965). A colorimetric micromethod for the determination of glutathione. *Biochem J* **94**: 661-5.

OZER, J, Ratner, M, Shaw, M, Bailey, W & Schomaker, S (2008). The current state of serum biomarkers of hepatotoxicity. *Toxicology* **245**: 194-205.

PARK, B.K. Kitteringham, N.R. Maggs, J.L. Pirmohamed, M. & Williams, D.P. (2005). The role of metabolic activation in drug-induced hepatotoxicity. *Annual Review of Pharmacology and Toxicology,* **45**, 177-202.

PARK, BK, Boobis, A, Clarke, S, Goldring, CEP, Jones, D, Kenna, JG, *et al.* (2011). Managing the challenge of chemically reactive metabolites in drug development. *Nature Reviews Drug Discovery* **10**: 292-306.

PARK, BK, Kitteringham, NR (1990a). Assessment of enzyme induction and enzyme inhibition in humans: toxicological implications. *Xenobiotica* **20**: 1171-85.

PARK, BK, Kitteringham, NR (1990b). Drug-protein conjugation and its immunological consequences. *Drug Metab Rev* **22**: 87-144.

PARK, BK, Kitteringham, NR, Powell, H & Pirmohamed, M (2000). Advances in molecular toxicology - Towards understanding idiosyncratic drug toxicity. *Toxicology* **153**: 39-60.

PARK, BK, Pirmohamed, M & Kitteringham, NR (1998). Role of drug disposition in drug hypersensitivity: A chemical, molecular, and clinical perspective. *Chem Res Toxicol* **11**: 969-88.

PARK, JS, Svetkauskaite, D, He, Q, Kim, J-, Strassheim, D, Ishizaka, A, *et al.* (2004). Involvement of Toll-like Receptors 2 and 4 in Cellular Activation by High Mobility Group Box 1 Protein. *J Biol Chem* **279**: 7370-7.

PARK, TH, Lee, WI, Yoon, WH, Park, Y-, Lee, J- & Lee, MG (1998). Pharmacokinetic and pharmacodynamic changes of furosemide after intravenous and oral administration to rats with alloxan-induced diabetes mellitus. *Biopharmaceutics and Drug Disposition* **19**: 357-64.

PATEL, SM, Johnson, S, Belknap, SM, Chan, J, Sha, BE & Bennett, C (2004). Serious Adverse Cutaneous and Hepatic Toxicities Associated with Nevirapine Use by Non-HIV-Infected Individuals. *J Acquir Immune Defic Syndr* **35**: 120-5.

PAULI-MAGNUS, C, Meier, PJ (2006). Hepatobiliary transporters and drug-induced cholestasis. *Hepatology* **44**: 778-87.

PELKONEN, O, Raunio, H (1997). Metabolic activation of toxins: Tissue-specific expression and metabolism in target organs. *Environ Health Perspect* **105**: 767-74.

PENZAK, SR, Kabuye, G, Mugyenyi, P, Mbamanya, F, Natarajan, V, Alfaro, RM, *et al.* (2007). Cytochrome P450 2B6 (CYP2B6) G516T influences nevirapine plasma concentrations in HIV-infected patients in Uganda. *HIV Medicine* **8**: 86-91.

PEREZ, J, Sitar, DS & Ogilvie, RI (1979). Biotransformation of furosemide in patients with acute pulmonary edema. *Drug Metab Disposition* **7**: 383-7.

PERZBORN, E, Roehrig, S, Straub, A, Kubitza, D & Misselwitz, F (2011). The discovery and development of rivaroxaban, an oral, direct factor Xa inhibitor. *Nature Reviews Drug Discovery* **10**: 61-75.

PETERS, TS (2005). Do preclinical testing strategies help predict human hepatotoxic potentials? *Toxicol Pathol* **33**: 146-54.

PHANUPHAK, N, Apornpong, T, Teeratakulpisarn, S, Chaithongwongwatthana, S, Taweepolcharoen, C, Mangclaviraj, S, *et al.* (2007). Nevirapine-associated toxicity in HIV-infected Thai men and women, including pregnant women. *HIV Medicine* 8: 357-66.

PICHLER, WJ (2002). Pharmacological interaction of drugs with antigen-specific immune receptors: The p-i concept. *Current Opinion in Allergy and Clinical Immunology* **2**: 301-5.

PIRMOHAMED, M, Drummond, NS, Naisbitt, DJ & Park, BK (2007). Drug hypersensitivity reactions in patients with HIV disease. *Expert Review of Clinical Immunology* **3**: 395-410.

PIRMOHAMED, M, James, S, Meakin, S, Green, C, Scott, AK, Walley, TJ, *et al.* (2004). Adverse drug reactions as cause of admission to hospital: Prospective analysis of 18 820 patients. *Br Med J* **329**: 15-9.

PIRMOHAMED, M, Williams, D, Madden, S, Templeton, E & Park, BK (1995). Metabolism and bioactivation of clozapine by human liver in vitro. *J Pharmacol Exp Ther* **272**: 984-90.

POLLARD, RB, Robinson, P & Dransfield, K (1998). Safety profile of nevirapine, a nonnucleoside reverse transcriptase inhibitor for the treatment of human immunodeficiency virus infection. *Clin Ther* **20**: 1071-92.

POPOVIC, M, Caswell, JL, Mannargudi, B, Shenton, JM & Uetrecht, JP (2006). Study of the sequence of events involved in nevirapine-induced skin rash in Brown Norway rats. *Chem Res Toxicol* **19**: 1205-14.

POSADAS, SJ, Leyva, L, Torres, MJ, Rodriguez, JL, Bravo, I, Rosal, M, *et al.* (2000). Subjects with allergic reactions to drugs show in vivo polarized patterns of cytokine expression depending on the chronology of the clinical reaction. *J Allergy Clin Immunol* **106**: 769-76.

POSADAS, SJ, Torres, MJ, Mayorga, C, Juarez, C & Blanca, M (2002). Gene expression levels of cytokine profile and cytotoxic markers in non-immediate reactions to drugs. *Blood Cells Mol Dis* **29**: 179-89.

POTTER, WZ, Davis, DC & Mitchell, JR (1973). Acetaminophen induced hepatic necrosis. III. Cytochrome P 450 mediated covalent binding in vitro. *J Pharmacol Exp Ther* **187**: 203-10.

PRANDOTA, J, Pruitt, AW (1975). Furosemide binding to human albumin and plasma of nephrotic children. *Clin Pharmacol Ther* **17**: 159-66.

PRANDOTA, J, Pruitt, AW (1991). Pharmacokinetic, biliary excretion, and metabolic studies of 14C-furosemide in the rat. *Xenobiotica* **21**: 725-36.

PRICE, D, Sharma, A & Cerasoli, F (2009). Biochemical properties, pharmacokinetics and pharmacological response of tiotropium in chronic obstructive pulmonary disease patients. *Expert Opinion on Drug Metabolism and Toxicology* **5**: 417-24.

PUJARI, SN, Patel, AK, Naik, E, Patel, KK, Dravid, A, Patel, JK, *et al.* (2004). Effectiveness of generic fixed-dose combinations of highly active antiretroviral therapy for treatment of HIV infection in India. *J Acquir Immune Defic Syndr* **37**: 1566-9.

RANDLE, LE, Goldring, CEP, Benson, CA, Metcalfe, PN, Kitteringham, NR, Park, BK, *et al.* (2008). Investigation of the effect of a panel of model hepatotoxins on the Nrf2-Keap1 defence response pathway in CD-1 mice. *Toxicology* **243**: 249-60.

QIU, Y, Benet, LZ & Burlingame, AL (1998). Identification of the hepatic protein targets of reactive metabolites of acetaminophen in vivo in mice using two-dimensional gel electrophoresis and mass spectrometry. *J Biol Chem* **273**: 17940-53.

RASHED, MS, Nelson, SD (1989). Characterization of glutathione conjugates of reactive metabolites of 3′-hydroxyacetanilide, a nonhepatotoxic positional isomer of acetaminophen. *Chem Res Toxicol* **2**: 41-5.

REESE, M, Sakatis, M, Ambroso, J, Harrell, A, Yang, E, Chen, L, *et al.* (2010). An integrated reactive metabolite evaluation approach to assess and reduce safety risk during drug discovery and development. *Chem Biol Interact.*

REGAN, SL, Maggs, JL, Hammond, TG, Lambert, C, Williams, DP & Park, BK (2010). Acyl glucuronides: The good, the bad and the ugly. *Biopharmaceutics and Drug Disposition* 31: 367-95.

REID, AB, Kurten, RC, McCullough, SS, Brock, RW & Hinson, JA (2005). Mechanisms of acetaminophen-induced hepatotoxicity: Role of oxidative stress and mitochondrial permeability transition in freshly isolated mouse hepatocytes. *J Pharmacol Exp Ther* **312**: 509-16.

RISKA, P, Lamson, M, Macgregor, T, Sabo, J, Hattox, S, Pav, J, *et al.* (1999). Disposition and biotransformation of the antiretroviral drug nevirapine in humans. *Drug Metab Disposition* **27**: 895-901.

ROTGER, M, Colombo, S, Furrer, H, Bleiber, G, Buclin, T, Lee, BL, *et al.* (2005). Influence of CYP2B6 polymorphism on plasma and intracellular concentrations and toxicity of efavirenz and nevirapine in HIV-infected patients. *Pharmacogenetics and Genomics* **15**: 1-5.

ROTH, RA, Luyendyk, JP, Maddox, JF & Ganey, PE (2003). Inflammation and drug idiosyncrasy - Is there a connection? *J Pharmacol Exp Ther* **307**: 1-8.

ROTH, T, Zammit, GK, Scharf, MB & Farber, R (2007). Efficacy and safety of as-needed, post bedtime dosing with indiplon in insomnia patients with chronic difficulty maintaining sleep. *Sleep* **30**: 1731-8.

ROUJEAU, JC, Stern, RS (1994). Severe adverse cutaneous reactions to drugs. *N Engl J Med* **331**: 1272-85.

ROUSU, T, Pelkonen, O & Tolonen, A (2009). Rapid detection and characterization of reactive drug metabolites in vitro using several isotope-labeled trapping agents and ultra-performance liquid chromatography/time-of-flight mass spectrometry. *Rapid Communications in Mass Spectrometry* **23**: 843-55.

SAITOH, A, Spector, SA (2008). Effect of Host Genetic Variation on the Pharmacokinetics and Clinical Response of Non-nucleoside Reverse Transcriptase Inhibitors. *Futur HIV Ther* **2**: 69-81, 10.2217/17469600.2.1.69.

SALTIEL, E, Ward, A (1987). Ticlopidine. A review of its pharmacodynamic and pharmacokinetic properties, and therapeutic efficacy in platelet-dependent disease states. *Drugs* **34**: 222-62.

SANNE, I, Mommeja-Marin, H, Hinkle, J, Bartlett, JA, Lederman, MM, Maartens, G, *et al.* (2005). Severe hepatotoxicity associated with nevirapine use in HIV-infected subjects. *J Infect Dis* **191**: 825-9.

SCAFFIDI, P, Misteli, T & Bianchi, ME (2002). Release of chromatin protein HMGB1 by necrotic cells triggers inflammation. *Nature* **418**: 191-5.

SCHUTTE, B, Henfling, M, Kölgen, W, Bouman, M, Meex, S, Leers, MPG, *et al.* (2004). Keratin 8/18 breakdown and reorganization during apoptosis. *Exp Cell Res* **297**: 11-26.

SEGLEN, PO (1976). Preparation of isolated rat liver cells. *Methods Cell Biol* **Vol. 13**: 29-83.

SEUTTER BERLAGE, F, Van Dorp, HL, Kosse, HGJ & Henderson Th., P (1977). Urinary mercapturic acid excretion as a biological parameter of exposure to alkylating agents. *Int Arch Occup Environ Health* **39**: 45-51.

SGRO, C, Clinard, F, Ouazir, K, Chanay, H, Allard, C, Guilleminet, C, *et al.* (2002). Incidence of drug-induced hepatic injuries: A French population-based study. *Hepatology* **36**: 451-5.

SHENTON, JM, Chen, J & Uetrecht, JP (2004). Animal models of idiosyncratic drug reactions. *Chem Biol Interact* **150**: 53-70.

SHENTON, JM, Popovic, M, Chen, J, Masson, MJ & Uetrecht, JP (2005). Evidence of an immune-mediated mechanism for an idiosyncratic nevirapine-induced reaction in the female brown Norway rat. *Chem Res Toxicol* **18**: 1799-813.

SHENTON, JM, Teranishi, M, Abu-Asab, MS, Yager, JA & Uetrecht, JP (2003). Characterization of a potential animal model of an idiosyncratic drug reaction: Nevirapine-induced skin rash in the rat. *Chem Res Toxicol* **16**: 1078-89.

SHIMIZU, S, Atsumi, R, Nakazawa, T, Fujimaki, Y, Sudo, K & Okazaki, O (2009). Metabolism of ticlopidine in rats: Identification of the main biliary metabolite as a glutathione conjugate of ticlopidine S-oxide. *Drug Metab Disposition* **37**: 1904-15.

SHIMIZU, S, Atsumi, R, Nakazawa, T, Izumi, T, Sudo, K, Okazaki, O, *et al.* (2011). Ticlopidine-induced hepatotoxicity in a GSH-depleted rat model. *Arch Toxicol* 85: 347-53.

SIEGERS, CP, Loeser, W, Gieselmann, J & Oltmanns, D (1984). Biliary and renal excretion of paracetamol in man. *Pharmacology* **29**: 301-3.

SMITH, DA, Obach, RS (2006). Metabolites and safety: What are the concerns, and how should we address them? *Chem Res Toxicol* **19**: 1570-9.

SMITH, DE, Benet, LZ (1983). Biotransformation of furosemide in kidney transplant patients. *Eur J Clin Pharmacol* **24**: 787-90.

SMITH, DE, Lin, ET & Benet, LZ (1980). Absorption and disposition of furosemide in healthy volunteers, measured with a metabolite-specific assay. *Drug Metab Disposition* **8**: 337-42.

SMITH, PC, Liu, JH (1993). Covalent binding of suprofen acyl glucuronide to albumin in vitro. *Xenobiotica* **23**: 337-48.

SOGA, T, Baran, R, Suematsu, M, Ueno, Y, Ikeda, S, Sakurakawa, T, *et al.* (2006). Differential metabolomics reveals ophthalmic acid as an oxidative stress biomarker indicating hepatic glutathione consumption. *J Biol Chem* **281**: 16768-76.

SPITZNAGLE, LA, Wirth, PJ & Boobis, SW (1977). The role of biliary excretion in the hepatotoxicity of furosemide in the mouse. *Toxicol Appl Pharmacol* **39**: 283-94.

SRIVASTAVA, A, Lian, L-, Maggs, JL, Chaponda, M, Pirmohamed, M, Williams, DP, *et al.* (2010). Quantifying the metabolic activation of nevirapine in patients by integrated applications of NMR and mass spectrometries. *Drug Metab Disposition* **38**: 122-32.

STAACK, RF, Hopfgartner, G (2007). New analytical strategies in studying drug metabolism. *Analytical and Bioanalytical Chemistry* **388**: 1365-80.

STACHULSKI, AV, Harding, JR, Lindon, JC, Maggs, JL, Park, BK & Wilson, ID (2006). Acyl glucuronides: biological activity, chemical reactivity, and chemical synthesis. *Journal of medicinal chemistry* 49: 6931-45.

STERN, JO, Robinson, PA, Love, J, Lanes, S, Imperiale, MS & Mayers, DL (2003). A comprehensive hepatic safety analysis of nevirapine in different populations of HIV infected patients. *J Acquir Immune Defic Syndr* **34**: S21-33.

STEVENS, JL (2006). Future of toxicology - Mechanisms of toxicity and drug safety: Where do we go from here? *Chem Res Toxicol* **19**: 1393-401.

STEVENS, JL, Baker, TK (2009). The future of drug safety testing: expanding the view and narrowing the focus. *Drug Discov Today* **14**: 162-7.

SUBRAMANIAN, R, Fang, X & Prueksaritanont, T (2002). Structural characterization of in vivo rat glutathione adducts and a hydroxylated metabolite of simvastatin hydroxy acid. *Drug Metab Disposition* 30: 225-30.

SUNDAR, S, Makharia, A, More, DK, Agrawal, G, Voss, A, Fischer, C, *et al.* (2000). Short-course of oral miltefosine for treatment of visceral leishmaniasis. *Clinical Infectious Diseases* **31**: 1110-3.

SYMEONIDIS, A, Kouraklis-Symeonidis, A, Seimeni, U, Galani, A, Giannakoulas, N, Fragopanagou, E, *et al.* (2002). Ticlopidine-induced aplastic anemia: Two new case reports, review, and meta-analysis of 55 additional cases. *Am J Hematol* **71**: 24-32.

TAFAZOLI, S, O'Brien, PJ (2009). Amodiaquine-induced oxidative stress in a hepatocyte inflammation model. *Toxicology* **256**: 101-9.

TAKAKUSA, H, Masumoto, H, Yukinaga, H, Makino, C, Nakayama, S, Okazaki, O, *et al.* (2008). Covalent binding and tissue distribution/retention assessment of drugs associated with idiosyncratic drug toxicity. *Drug Metab Disposition* **36**: 1770-9.

TEMPLE, RJ, Himmel, MH (2002). Safety of newly approved drugs: Implications for prescribing. *J Am Med Assoc* **287**: 2273-5.

TESTA, B, Krämer, SD (2009). The biochemistry of drug metabolism - An introduction part 5. Metabolism and bioactivity. *Chemistry and Biodiversity* **6**: 591-684.

TETTEY, JN, Maggs, JL, Rapeport, WG, Pirmohamed, M & Park, BK (2001). Enzyme-induction dependent bioactivation of troglitazone and troglitazone quinone in vivo. *Chem Res Toxicol* **14**: 965-74.

THOMPSON, RA, Isin, EM, Li, Y, Weaver, R, Weidolf, L, Wilson, I, *et al.* (2011). Risk assessment and mitigation strategies for reactive metabolites in drug discovery and development. *Chem Biol Interact* **192**: 65-71.

TIRMENSTEIN, MA, Nelson, SD (1989). Subcellular binding and effects on calcium homeostasis produced by acetaminophen and a nonhepatotoxic regioisomer, 3'-hydroxyacetanilide, in mouse liver. *J Biol Chem* **264**: 9814-9.

TREIBER, A, Dansette, PM, El Amri, H, Girault, J-, Ginderow, D, Mornon, J-, *et al.* (1997). Chemical and biological oxidation of thiophene: Preparation and complete characterization

of thiophene S-oxide dimers and evidence for thiophene S-oxide as an intermediate in thiophene metabolism in vivo and in vitro. *J Am Chem Soc* **119**: 1565-71.

TULAYAKUL, P, Sakuda, S, Dong, KS & Kumagai, S (2005). Comparative activities of glutathione-S-transferase and dialdehyde reductase toward aflatoxin B1 in livers of experimental and farm animals. *Toxicon* **46**: 204-9.

TURNER, SR, Strohbach, JW, Tommasi, RA, Aristoff, PA, Johnson, PD, Skulnick, HI, *et al.* (1998). Tipranavir (PNU-140690): A potent, orally bioavailable nonpeptidic HIV protease inhibitor of the 5,6-dihydro-4-hydroxy-2-pyrone sulfonamide class. *J Med Chem* **41**: 3467-76.

UETRECHT, J (2003). Screening for the potential of a drug candidate to cause idiosyncratic drug reactions. *Drug Discov Today* **8**: 832-7.

UETRECHT, J (2006). Evaluation of which reactive metabolite, if any, is responsible for a specific idiosyncratic reaction. *Drug Metab Rev* **38**: 745-53.

UETRECHT, J (2008). Idiosyncratic drug reactions: Past, present, and future. *Chem Res Toxicol* **21**: 84-92.

UETRECHT, J (2009). Immune-mediated adverse drug reactions. *Chem Res Toxicol* **22**: 24-34.

UETRECHT, J. (2007). Idiosyncratic drug reactions: Current understanding. *Annual Review of Pharmacology and Toxicology,* **47**, 513-39.

UETRECHT, J.P. Popovic, M. Shenton, J.M. Chen, J. Baban, A. Tharmanathan, T., *et al.* (2010). Nevirapine hypersensitivity. *Handbook of Experimental Pharmacology,* **196**, 437-51.

UETRECHT, JP (1999). New concepts in immunology relevant to idiosyncratic drug reactions: The 'danger hypothesis' and innate immune system. *Chem Res Toxicol* **12**: 387-95.

VALADON, P, Dansette, PM, Girault, J-, Amar, C & Mansuy, D (1996). Thiophene sulfoxides as reactive metabolites: Formation upon microsomal oxidation of a 3-aroylthiophene and fate in the presence of nucleophiles in vitro and in vivo. *Chem Res Toxicol* 9: 1403-13.

VANDEPUTTE, C, Guizon, I, Genestie-Denis, I, Vannier, B & Lorenzon, G (1994). A microtiter plate assay for total glutathione and glutathione disulfide contents in cultured/isolated cells: Performance study of a new miniaturized protocol. *Cell Biol Toxicol* **10**: 415-21.

VELAYUDHAM, LS, Farrell, GC (2003). Drug-induced cholestasis. *Expert Opin Drug Saf* **2**: 287-304.

VERBEECK, RK, Patwardhan, RV & Villeneuve, JP (1982). Furosemide disposition in cirrhosis. *Clin Pharmacol Ther* **31**: 719-25.

VERONESE, ME, McLean, S, D'Souza, CA & Davies, NW (1985). Formation of reactive metabolites of phenacetin in humans and rats. *Xenobiotica* **15**: 929-40.

VITEZICA, ZG, Milpied, B, Lonjou, C, Borot, N, Ledger, TN, Lefebvre, A, *et al.* (2008). HLA-DRB1*01 associated with cutaneous hypersensitivity induced by nevirapine and efavirenz. *AIDS* **22**: 540-1.

VOGEL, M, Bertram, N, Wasmuth, J-, Wyen, C, Voigt, E, Schwarze-Zander, C, *et al.* (2009). Nevirapine pharmacokinetics in HIV-infected and HIV/HCV-coinfected individuals. *J Antimicrob Chemother* **63**: 988-91.

VREE, TB, Van Der Ven, AJAM (1999). Clinical consequences of the biphasic elimination kinetics for the diuretic effect of furosemide and its acyl glucuronide in humans. *J Pharm Pharmacol* **51**: 239-48.

WAGNER, S, Scholz, K, Sieber, M, Kellert, M & Voelkel, W (2007). Tools in metabonomics: An integrated validation approach for LC-MS metabolic profiling of mercapturic acids in human urine. *Anal Chem* **79**: 2918-26.

WALLER, ES, Hamilton, SF & Massarella, JW (1982). Disposition and absolute bioavailability of furosemide in healthy males. *J Pharm Sci* **71**: 1105-8.

WANG, H, Bloom, O, Zhang, M, Vishnubhakat, JM, Ombrellino, M, Che, J, *et al.* (1999). HMG-1 as a late mediator of endotoxin lethality in mice. *Science* **285**: 248-51.

WANG, Y, Zhong, D, Chen, X & Zheng, J (2009a). Identification of quinone methide metabolites of dauricine in human liver microsomes and in rat bile. *Chem Res Toxicol* **22**: 824-34.

WANG, K, Zhang, S, Marzolf, B, Troisch, P, Brightman, A, Hu, Z, *et al.* (2009b). Circulating microRNAs, potential biomarkers for drug-induced liver injury. *Proc Natl Acad Sci U S A* **106**: 4402-7.

WEN, B, Chen, Y & Fitch, WL (2009). Metabolic activation of nevirapine in human liver microsomes: Dehydrogenation and inactivation of cytochrome P450 3A4. *Drug Metab Disposition* **37**: 1557-62.

WEN, B, Fitch, WL (2009a). Screening and characterization of reactive metabolites using glutathione ethyl ester in combination with Q-trap mass spectrometry. *Journal of Mass Spectrometry* 44: 90-100.

WEN, B, Fitch, WL (2009b). Analytical strategies for the screening and evaluation of chemically reactive drug metabolites. *Expert Opinion on Drug Metabolism and Toxicology* **5**: 39-55.

WEN, B, Ma, L, Nelson, SD & Zhu, M (2008). High-throughput screening and characterization of reactive metabolites using polarity switching of hybrid triple quadrupole linear ion trap mass spectrometry. *Anal Chem* 80: 1788-99.

WILLIAMS, DP, Antoine, DJ, Butler, PJ, Jones, R, Randle, L, Payne, A, *et al.* (2007). The metabolism and toxicity of furosemide in the wistar rat and CD-1 mouse: A chemical and biochemical definition of the toxicophore. *J Pharmacol Exp Ther* **322**: 1208-20.

WILLIAMS, DP, Kitteringham, NR, Naisbitt, DJ, Pirmohamed, M, Smith, DA & Park, BK (2002). Are chemically reactive metabolites responsible for adverse reactions to drugs? *Curr Drug Metab* **3**: 351-66.

WILLIAMS, DP, Naisbitt, DJ (2002). Toxicophores: Groups and metabolic routes associated with increased safety risk. *Current Opinion in Drug Discovery and Development* **5**: 104-15.

WILLIAMS, DP, Park, BK (2003). Idiosyncratic toxicity: The role of toxicophores and bioactivation. *Drug Discov Today* **8**: 1044-50.

WINTERSTEIN, AG, Hatton, RC, Gonzalez-Rothi, R, Johns, TE & Segal, R (2002). Identifying clinically significant preventable adverse drug events through a hospital's database of adverse drug reaction reports. *American Journal of Health-System Pharmacy* **59**: 1742-9.

WIRTH, PJ, Bettis, CJ & Nelson, WL (1976). Microsomal metabolism of furosemide. Evidence for the nature of the reactive intermediate involved in covalent binding. *Mol Pharmacol* **12**: 759-68.

WONG, SGW, Card, JW & Racz, WJ (2000). The role of mitochondrial injury in bromobenzene and furosemide induced hepatotoxicity. *Toxicol Lett* **116**: 171-81.

WU, G, Vashishtha, SC & Erve, JCL (2010). Characterization of glutathione conjugates of duloxetine by mass spectrometry and evaluation of in silico approaches to rationalize the site of conjugation for thiophene containing drugs. *Chem Res Toxicol* **23**: 1393-404.

YAKATAN, GJ, Maness, DD & Scholler, J (1976). Absorption, distribution, metabolism, and excretion of furosemide in dogs and monkeys. I. Analytical methodology, metabolism, and urinary excretion. *J Pharm Sci* **65**: 1456-60.

YAN, Z, Caldwell, GW (2005). Stable-isotope trapping and high-throughput screenings of reactive metabolites using the isotope MS signature. *Anal Chem* 76: 6835-47.

YAWALKAR, N, Egli, F, Hari, Y, Nievergelt, H, Braathen, LR & Pichler, WJ (2000). Infiltration of cytotoxic T cells in drug-induced cutaneous eruptions. *Clinical and Experimental Allergy* **30**: 847-55.

YIM, HB, Lieu, PK & Choo, PWJ (1997). Ticlopidine induced cholestatic jaundice. *Singapore Med J* **38**: 132-3.

YTRESTØYL, T, Bjerkeng, B (2007). Intraperitoneal and dietary administration of astaxanthin in rainbow trout (Oncorhynchus mykiss) - Plasma uptake and tissue distribution of geometrical E/Z isomers. *Comparative Biochemistry and Physiology - B Biochemistry and Molecular Biology* **147**: 250-9.

YUAN, L, Kaplowitz, N (2009). Glutathione in liver diseases and hepatotoxicity. *Mol Aspects Med* **30**: 29-41.

ZANGER, UM, Klein, K, Saussele, T, Blievernicht, J, Hofmann, MH & Schwab, M (2007). Polymorphic CYP2B6: Molecular mechanisms and emerging clinical significance. *Pharmacogenomics* **8**: 743-59.

ZHENG, J, Ma, L, Xin, B, Olah, T, Humphreys, WG & Zhu, M (2007). Screening and identification of GSH-trapped reactive metabolites using hybrid triple quadruple linear ion trap mass spectrometry. *Chem Res Toxicol* 20: 757-66.

ZIEVE, L, Anderson, WR & Dozeman, R (1985). Acetaminophen liver injury: Sequential changes in two biochemical indices of regeneration and their relationship to histologic alterations. *J Lab Clin Med* **105**: 619-24. Zimmerman, HJ (1999). *Hepatotoxicity: The Adverse Effects of Drugs and Other Chemicals on the Liver.*

ZIMMERMAN, HJ, Lewis, JH, Ishak, KG & Maddrey, WC (1984). Ticrynafen-Associated Hepatic Injury: Analysis of 340 Cases. *Hepatology* **4**: 315-23, 10.1002/hep.1840040223. Lagarriga, J, Buenrrostro, C, Rodríguez, P & Castañeda, J (1977). Hepatinecrosis caused by furosemide. Special lesions of various species? *Revista de Gastroenterologia de Mexico* **42**: 117-25.